FLEXURAL PERFORMANCE AND BOND CHARACTERISTICS OF

FRP STRENGTHENING TECHNIQUES FOR CONCRETE

STRUCTURES

By

Tarek Kamal Hassan Mohamed

A Dissertation
Submitted to the Faculty of Graduate Studies
In Partial Fulfilment of the Requirements for the Degree of

DOCTOR OF PHILOSOPHY

Structural Engineering Division
Department of Civil and Geological Engineering
The University of Manitoba
Winnipeg, Manitoba, Canada

© **May 2002**

THE UNIVERSITY OF MANITOBA

FACULTY OF GRADUATE STUDIES
*****
COPYRIGHT PERMISSION

FLEXURAL PERFORMANCE AND BOND CHARACTERISTICS OF FRP STRENGTHENING

TECHNIQUES FOR CONCRETE STRUCTURES

BY

TAREK KAMAL HASSAN MOHAMED

A Thesis/Practicum submitted to the Faculty of Graduate Studies of The University of

Manitoba in partial fulfillment of the requirement of the degree

of

DOCTOR OF PHILOSOPHY

TAREK KAMAL HASSAN MOHAMED © 2002

Acknowledgments

The author would like to express his deepest gratitude to his supervisor Dr. Sami Rizkalla. In addition to his support and friendship over the past three years, he has provided the unwavering source of inspiration, determination, and leadership that was so essential for the successful execution of this research project.

The author would like to thank Dr. Aftab Mufti, Dr. Dimos Polyzois and Dr. Christine Wu for their constructive comments and encouragements throughout the research. The support provided by the Network of Centres of Excellence on the Intelligent Sensing of Innovative Structures (ISIS Canada) is greatly acknowledged.

The author also expresses his thanks to Mr. M. McVey, Mr. G. Whiteside and Mr. S. Sparrow for their valuable assistance during the fabrication and testing of the specimens. Special thanks are extended to Dr. A. Kamiharako, Dr. A. Sultan, Dr. M. Mohamedien and Dr. N. Hassan for their assistance during the experimental phase of this study. The support provided by Vector Construction Group and Concrete Restoration Services is greatly appreciated.

Finally, the love, patience and support of my parents, my wife and my daughter cannot be praised enough; to them this thesis is dedicated.

Abstract

Strengthening of reinforced concrete structures using FRPs has emerged as a potential solution to the problems associated with civil infrastructure. Many researchers have reported significant increases in strength and stiffness of FRP retrofitted concrete structures. Nevertheless, possible brittle failures of the retrofitted system could limit the use of the full efficiency of the FRP system. These brittle failures include premature debonding of the FRP, which could occur at load levels significantly less than the strength of the FRP material used in the retrofitted system. Therefore, there is a need for an improved understanding of various failure mechanisms of FRP strengthened concrete structures as a basis for a reliable retrofit design. Innovative structural detailing is also needed to utilize the FRP system more effectively.

The work reported in this thesis deals with the development of a comprehensive approach towards understanding the flexural behaviour of FRP strengthened concrete structures. This study presents a comparison among various FRP strengthening techniques and develops fundamental criteria governing the choice of a specific technique. The applicability of cracked section analysis as well as non-linear finite element simulations for the analysis of concrete structures strengthened with FRP reinforcement is enumerated. Design guidelines regarding the use of FRP in retrofitting applications are provided. Mathematical models are proposed to quantify the bond characteristics and load transfer mechanisms of various FRP strengthening schemes using bars and strips for near surface mounted configurations as well as externally bonded sheets and strips.

A two-phase experimental program was conducted at the University of Manitoba to examine the structural performance of concrete structures strengthened with various FRP systems. The experimental program was designed to ensure full utilization of the strengthening schemes and to avoid possible premature failure of the retrofitted system. Three half-scale models of a typical concrete bridge slab were constructed and tested in the first phase of the investigation. The performance of near surface mounted FRP bars and strips as well as externally bonded FRP sheets and strips was evaluated. The three specimens were used to perform a total of nine tests in this phase. A cost analysis for each of the FRP strengthening techniques considered in this investigation was performed. Complementary to the experimental program, numerical simulations were performed using finite element analysis to predict the behaviour of concrete members strengthened with near surface mounted FRP reinforcement. Based on test results, the investigation was extended to a second stage to provide fundamental data for the bond characteristics of efficient FRP techniques. A total of 24 concrete T-beams were tested to characterize the load transfer mechanisms between FRP and concrete. Three different strengthening techniques were investigated. For each technique, different bond lengths were considered. Based on the experimental results, development lengths for various FRP strengthening techniques are proposed.

The thesis also presents three analytical models, proposed to predict the behaviour of concrete structures strengthened with near surface mounted FRP bars, near surface mounted FRP strips and externally bonded FRP sheets. New methodologies are introduced as a basis for design. With the formulae proposed in this thesis, the risk of

premature failure of concrete structures strengthened with various FRP systems can be estimated. The entire investigation leads to simple design rules, with a profound theoretical basis, to allow an economical, safe and reliable FRP retrofit design for concrete structures and bridges.

Table of Contents

Chapter 3. Experimental Program

Chapter 5. Experimental Results & Analytical Modelling: Bond Specimens

Chapter 6. Summary & Conclusions

Notation

$a_{1,2,3}$ = Coefficients used to determine the applied moment on a concrete beam

A = Cross-sectional area of a concrete section

A_c = Area of concrete in compression

A_p = Area of prestressed steel reinforcement

A_f = Area of CFRP reinforcement

A_s = Area of tension steel reinforcement

A_s' = Area of compression steel reinforcement

b = Width of concrete section

$b_{1,2,3}$ = Coefficients defined by Equation 2.7.

b_f = Width of externally bonded FRP sheets/strips

b_s = Width of externally bonded steel plates

c = Depth of the neutral axis from the extreme compression fibres

c_{cr} = Neutral axis depth for the cracked transformed section;

c_{eff} = Effective neutral axis depth for the transformed section;

c_g = Neutral axis depth for the gross transformed section;

C_1, C_2 = Parameters in the solution of differential equation;

C = Clear cover of reinforcing bars

C_s' = Compression force in steel reinforcement

d = Depth from extreme compression fibre to the flexural reinforcement; diameter of near surface mounted FRP bar

d_f = Depth of near surface mounted CFRP strips from compression fibre

d_p = Depth of the prestressing steel from compression fibre

d_s	=	Depth of the internal steel reinforcement from compression fibre
D	=	Deformability index
e	=	Eccentricity of tendons; edge distance
E	=	Efficiency of FRP strengthening techniques
E_a	=	Modulus of elasticity of the adhesive
E_c	=	Modulus of elasticity of concrete
E_f	=	Modulus of elasticity of FRP reinforcement
E_p	=	Modulus of elasticity of the steel strands
E_s	=	Modulus of elasticity of steel reinforcement
f_{Bottom}	=	Concrete stress at bottom fibres
f_c	=	Concrete stress in compression
f_{ct}	=	Splitting tensile strength of concrete
f'_c	=	Compressive strength of concrete after 28 days
f_{FRP}	=	Maximum tensile stress in near surface mounted FRP bars
f_{ps}	=	Stress in steel strands
f_f	=	Stress in CFRP reinforcement
f_{pu}	=	Ultimate stress in steel strands
f_s	=	Stress in tension steel reinforcement
$f_{s'}$	=	Stress in compression steel reinforcement
f_t	=	Tensile stress in concrete after cracking
f_{Top}	=	Concrete stress at top fibres
f_y	=	Yield stress of steel reinforcement
$G_{1,2,2'}$	=	Coefficients for near surface mounted FRP bars

G_a	=	Shear modulus of the adhesive
G_f	=	Fracture energy
h	=	Total height of a concrete section
$I_{cr\ (transformed)}$	=	Cracked moment of inertia of the transformed strengthened section
I_{eff}	=	Effective moment of inertia of the transformed strengthened section
I_f	=	Moment of inertia of the FRP sheets
$I_{g\ (transformed)}$	=	Gross moment of inertia of the transformed strengthened section
k_n	=	Parameter defined by Equation 5.48
L	=	Embedment/bond length of FRP reinforcement, length of tendons
L'	=	Total span of the simply supported beam
L_d	=	Development length of reinforcement
L_e	=	Effective bond length
L_g	=	Gauge length
l_o	=	Unbonded length of the CFRP reinforcement
M_a	=	Applied moment on a concrete section
M_{cr}	=	Cracking moment of a concrete section
M_{live}	=	Moment due to specified live load
M_p	=	Applied moment at peeling failure
M_u	=	Ultimate moment capacity of a concrete section
M_s	=	Moment corresponding to a concrete compressive strain of 0.001
M_{sw}	=	Moment due to self weight
N	=	Normal force acting on the FRP at the two ends of a segment
n	=	Number of cracks passing through a PI gauge; modular ratio; number of

FRP layers

P $\quad=\quad$ Applied load

P_{cr} $\quad=\quad$ Cracking load

P_d $\quad=\quad$ Debonding/delamination load

P_e $\quad=\quad$ Effective prestressing force after loses

P_o $\quad=\quad$ Required prestressing force in the tendons

P_j $\quad=\quad$ Jacking force

P_u $\quad=\quad$ Failure load of the specimen

q $\quad=\quad$ Applied uniform load

s $\quad=\quad$ Clear spacing between grooves

S $\quad=\quad$ Section modulus of the concrete

t_a $\quad=\quad$ Thickness of the adhesive layer

t_c $\quad=\quad$ Thickness of concrete in shear-type specimens

t_f $\quad=\quad$ Thickness of CFRP strip/sheet

T_f $\quad=\quad$ Tensile force in CFRP reinforcement

T_p $\quad=\quad$ Tensile force in prestressing reinforcement

T_s $\quad=\quad$ Tensile force in steel reinforcement

u $\quad=\quad$ Longitudinal displacement in the adhesive layer

U_e $\quad=\quad$ Elastic energy of the system

v $\quad=\quad$ Vertical displacement in the adhesive layer

V_c $\quad=\quad$ Shear force in the concrete at cutoff points due to interfacial shear stresses

V_f $\quad=\quad$ Shear force in the FRP sheets at cutoff points due to interfacial shear

stresses

V_o	=	Shear force in the concrete beam at cutoff points due to externally applied loads
V_p	=	Peeling shear force
V_u	=	Ultimate shear capacity of a beam
w	=	Groove width; transverse displacement in the adhesive layer
W	=	Work done by external force
w_{avg}	=	Average crack width
x	=	Longitudinal coordinate starting from the cut-off point of the CFRP strip/sheet
y	=	Distance from the FRP laminate to the section neutral axis
y_{eff}	=	Effective distance from the CFRP strip/sheet to the neutral axis
α	=	Curve fitting parameter less than 1.0
α_1	=	An empirical constant, depends on the concrete compressive strength; factor accounts for the bond characteristics of reinforcement
α_2	=	Factor accounts for the type of loading
β	=	Angle of inclination of the resultant of bond forces to the bar axis, parameter defined by Equation 5.49
β_1	=	An empirical constant, depends on the concrete compressive strength
δ	=	Slip of the FRP reinforcement
δ_f	=	Maximum slip
δ_i	=	Slip at maximum bond stress
Δ	=	Tendon elongation
Δ_{cr}	=	Deflection at cracking

Δ_h	=	Horizontal displacement measured by the PI gauge
Δ_s	=	Deflection corresponding to a concrete compressive strain of 0.001
Δ_u	=	Deflection at failure
ε_c	=	Concrete strain at the extreme compression fibre; interfacial strain of concrete
ε_{ce}	=	Concrete strain at the level of the prestressing steel due to prestressing
ε_{cr}	=	Maximum tensile strain in the concrete at cracking
ε_{ct}	=	Average tensile strain in concrete after cracking
ε_e	=	Effective strain in the prestressing steel after losses
ε_f	=	Interfacial strain of CFRP strips
ε_{fu}	=	Rupture tensile strain of the FRP reinforcement
ε_o	=	Initial strain in the concrete at the time of strengthening
ε_{ps}	=	Strain in the steel strands
ε_u	=	Maximum tensile strain of the FRP reinforcement at failure
ϕ	=	Curvature at a given strain increment
γ	=	Shear strain in the adhesive
κ_m	=	Reduction factor for the tensile strain in externally bonded FRP reinforcement
μ	=	Coefficient of friction between near surface mounted FRP bars and epoxy
ρ_f	=	Reinforcement ratio of FRP
ρ_s	=	Reinforcement ratio of steel
σ_c	=	Normal stress in the concrete

$\sigma_{con\text{-}epoxy} =$ Tensile stress at the concrete-epoxy interface

$\sigma_f \quad =$ Normal stress in the CFRP strip

$\sigma_{FRP\text{-}epoxy} =$ Tensile stress at the FRP-epoxy interface

$\sigma_n \quad =$ Normal stress at sheets cutoff points

$\sigma_{nmax} \quad =$ Normal strength at sheets cutoff points

$\sigma_{radial} \quad =$ Radial stresses around a near surface mounted FRP bar

$\tau \quad =$ Interfacial shear stress; average bond stress

$\tau_f \quad =$ Peak bond stress

$\tau_{max} \quad =$ shear strength

$\omega, \omega' \quad =$ Parameters defined by Equations 5.22 and 5.47, respectively

Chapter 1

Introduction

This chapter gives an introduction to the main topic of this doctoral thesis and highlights the needs for strengthening using innovative FRP techniques. Background information and lack of knowledge concerning various strengthening techniques are discussed. Research objectives as well as the research approach are enumerated. Finally, the aims and the outline of this doctoral thesis are clarified.

1.1 General

The need for repair and strengthening of deteriorated, damaged and substandard civil infrastructure has become an important challenge confronting the repair and rehabilitation industries worldwide. Deterioration of structures begins shortly after completion of construction due to environmental influences and/or due to the structures' routine use. Deficiency of structures may be the result of insufficient reinforcement, excessive deflections, poor concrete quality, reinforcement corrosion, or insufficient bearing capacity. In some cases, strengthening and repairing are necessary to account for human mistakes at the designing stage or to solve execution errors during the construction. For these purposes, various strengthening techniques have been developed to satisfy the demand to increase the load carrying capacity and/or to fulfill certain serviceability

requirements. Some of the traditional strengthening techniques for concrete structures are:

- introducing extra supports to shorten the span of flexural members;

- adding reinforcement by subsequently removing and casting concrete;

- applying additional internal or external prestressing;

- bonding external steel plates; and

- using advanced composite materials.

Continuous development of Fiber Reinforced Polymer (FRP) materials in various forms and configurations offers an alternative design approach for the construction of new structures and rehabilitation of existing civil engineering infrastructure. Nevertheless, their applications to bridges and structures are still relatively few. FRPs offer designers an excellent combination of properties not available for other materials and present a potential solution to civil infrastructure's crisis. High strength-to-weight ratio, ease of installation and corrosion resistance characteristics make FRPs ideal for strengthening applications. Externally bonded FRP sheets and strips are currently the most commonly used techniques for strengthening bridges and concrete structures. In spite of the significant research being reported on their structural mechanism and performance, there are still heightened concerns regarding possible premature failure due to debonding, especially in zones of combined high flexural and shear stresses. In addition, externally bonded FRP reinforcements are relatively unprotected against wear and impact loads. Thus, their structural performance could be greatly affected by harsh environmental conditions.

The work presented in this doctoral thesis demonstrates an alternative use of FRPs for strengthening concrete bridges. It was conducted in response to the heightened demand towards increasing the flexural capacity of bridges to accommodate new truck loads. Theoretical knowledge and design guidelines are provided to ensure a safe, reliable and cost-efficient use of FRP materials. It is expected that the use of FRPs will lead to radical changes in construction methods, final forms and maintenance regimes for structures. Innovative strengthening techniques are becoming increasingly important to enable the extension of service life of deteriorated civil infrastructure.

1.2 Research Objective

The main objective of this research is to study and examine the structural performance of various FRP strengthening techniques for concrete structures and bridges. The study focuses also on fundamental research to evaluate and characterize the bond and load transfer mechanisms between FRP materials and concrete. The analytical phase attempts to provide mathematical models describing the interaction between the flexure, shear and debonding failure mechanisms of the FRP reinforcement from the strengthened zones. The research utilizes a non-linear finite element analysis to model the response of concrete structures strengthened with FRPs. The thesis provides some references to the cost-effectiveness of each of the strengthening techniques considered in the study. The study includes five different strengthening techniques: near surface mounted Leadline CFRP bars, C-Bars, CFRP strips and externally bonded CFRP sheets and strips. The specific objectives of this research study could be summarized as follows:

a) study the various flexural limit states behaviour of concrete members strengthened with near surface mounted FRP bars and strips as well as externally bonded FRP sheets and strips, including behaviour after cracking and modes of failure;

b) investigate the load-deformation response, as well as the cracking behaviour of concrete members strengthened with different FRP systems;

c) present an overview of the cost-effectiveness of each of the strengthening techniques considered in this study;

d) determine experimentally the development length of near surface mounted FRP bars, strips and externally bonded FRP sheets;

e) propose analytical models to predict the interfacial shear stresses and the minimum anchorage length needed for near surface mounted FRP bars, strips as well as externally bonded FRP sheets;

f) develop fundamental criteria governing the failure behaviour of concrete beams strengthened with near surface mounted FRP bars, strips and externally bonded FRP sheets.

g) investigate the influence of various geometric parameters such as groove width, spacing between near surface mounted bars and minimum edge distance on the debonding process; and

h) provide design guidelines and establish a general methodology for the strengthening of concrete structures with various FRP systems.

1.3 Research Approach

The research approach followed in this study consisted of a literature survey, extensive experimental program, numerical simulations using finite element analysis and theoretical analysis using rational models. Fig. 1.1 shows a schematic representation of the research approach adopted in this study.
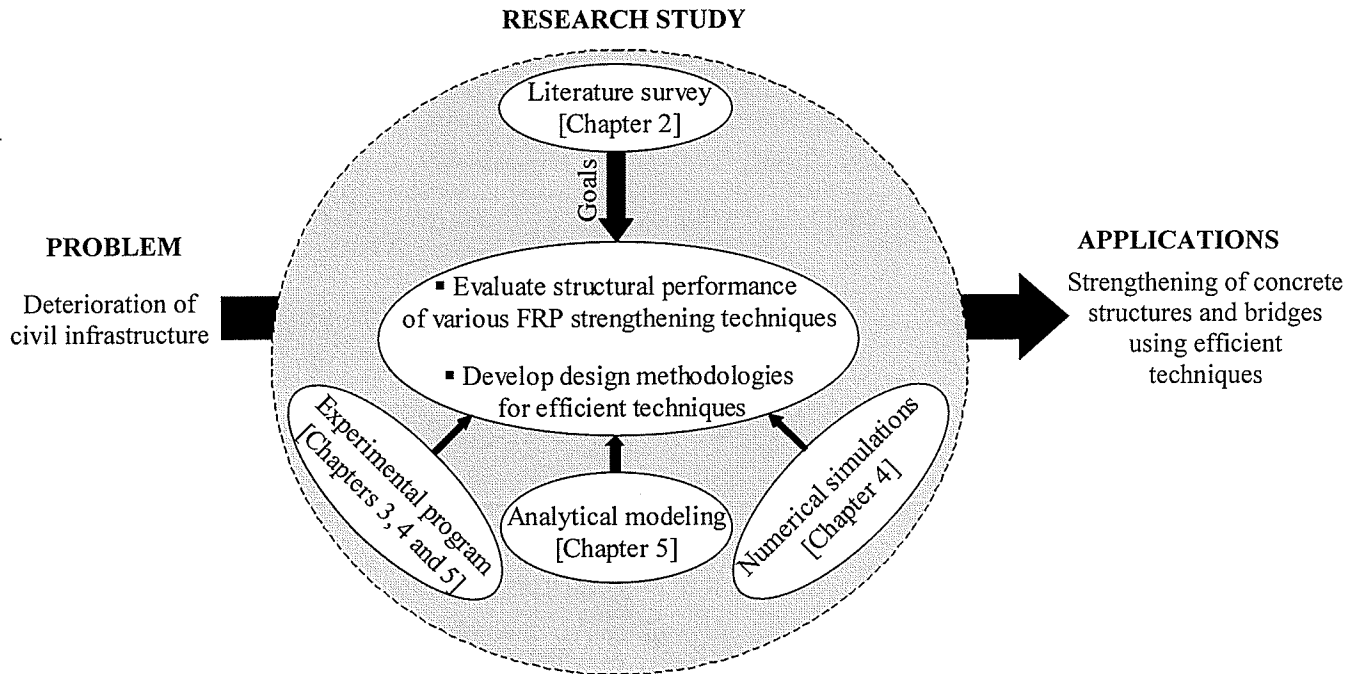
Fig. 1.1 Schematic representation of research approach

A state-of-the-art literature survey was carried out to collect information on various strengthening schemes. Research gaps and limitations of different techniques were categorized. The necessity for innovative strengthening techniques to overcome current problems was recognized. The experimental program consisted of testing three large-scale specimens to failure to examine the performance of various FRP strengthening techniques and to determine the efficiency of each technique. Bond characteristics of the most efficient techniques were investigated by testing 24 concrete beams. Test results

were used to introduce analytical models developed to predict the interfacial shear stresses and the minimum anchorage length needed for various FRP strengthening techniques. The models were validated also by non-linear finite element modelling. Finally, design guidelines for retrofitting damaged concrete beams using near surface mounted FRP bars, strips and externally bonded sheets are provided. The effectiveness of these techniques, as influenced by debonding/delamination of FRP reinforcement is presented. Each phase of this study is discussed briefly in the following subsections:

Experimental Investigation: The experimental program was designed to provide fundamental understanding of the behaviour of concrete members strengthened in flexure with different FRP strengthening techniques. The experimental program included two phases.

The first phase, Phase I, consisted of three half-scale models of a typical prestressed concrete bridge slab. The post-tensioned solid slabs represented typical bridge slabs over intermediate pier columns. The specimens were tested in simple span with a double cantilever configuration. The specimens represented also a portion of continuous bridges between the inflection points beyond two adjacent supports. Each specimen was tested three times using loads applied at different locations in each test. The first and second tests were performed on the two cantilevers where the load was applied at the edge of each cantilever. The third test was conducted using a load applied at the mid-span. Prior to the third test of the mid-span, the cracks resulted from testing the two cantilevers were sealed entirely by injecting a high strength epoxy resin adhesive into the concrete. The

simply supported span was then strengthened using FRPs and tested. Five different strengthening techniques were investigated including near surface mounted Leadline bars, C-Bars, CFRP strips and externally bonded CFRP sheets and strips.

The second phase, Phase II, was designed to evaluate the bond characteristics and load transfer mechanism between the FRP and concrete for the most efficient techniques. A total of 24 concrete beams were constructed and tested under monotonic loading. The bond specimens were designed to fail either due to rupture or debonding of the FRP reinforcement. Variables considered in this phase were the bond length and the strengthening technique.

Analytical Modelling: The analytical modeling included two phases:

The first phase, focused on the behaviour of the concrete specimens tested in the first phase of the experimental program. The analysis included both rational and non-linear finite element analysis to predict the behaviour of concrete members strengthened with FRPs. The rational analysis is based on a strain compatibility approach. The analysis used the mechanical properties of the FRP materials to predict the moment-curvature and the load-deflection behaviour of concrete specimens strengthened with near surface mounted FRP reinforcement.

The second phase, introduced three different design methodologies to evaluate the bond strength of near surface mounted FRP bars, strips and externally bonded FRP sheets,

respectively. The analytical models were calibrated by comparing the predicted values with test results as well as non-linear finite element modelling.

Design Guidelines: Based on the experimental results of the tested specimens and the proposed analytical models, the efficiency of various FRP strengthening techniques is quantified. Design recommendations for flexural strengthening of concrete structures using near surface mounted FRP reinforcement are introduced. The influence of various parameters including material properties, groove dimensions and internal steel configuration is discussed.

1.4 Outline of the Thesis

The following is a brief description of the contents of each chapter in the thesis:

Chapter 2 reviews the use of advanced composite materials to strengthen concrete structures through a literature survey and evaluates the commonly used retrofit materials, properties and application procedures. The content is placed within the framework of the knowledge and the aim of this doctoral thesis.

Chapter 3 describes the experimental program conducted at the University of Manitoba including Phases I and II. The mechanical properties of the FRP materials, steel, epoxy and concrete are presented.

Chapter 4 presents the results of the first phase of the experimental program including the effects of various parameters as well as different failure modes. The overall behaviour of concrete members strengthened with various FRP techniques is discussed. A cost-effective analysis for each of the strengthening techniques considered in this study is enumerated. The chapter also describes the numerical simulations carried out using non-linear finite element analysis. The flexural behaviour of the large-scale specimens tested in the first phase of the experimental program is predicted.

Chapter 5 presents both experimental and analytical investigations undertaken to evaluate bond characteristics of various FRP strengthening techniques. This chapter provides detailed steps of the proposed analytical models introduced to predict the interfacial shear stresses for near surface mounted FRP bars, strips and externally bonded FRP sheets. The models are calibrated by comparing the predicted behaviour to test results as well as non-linear finite element modelling.

Chapter 6 summarizes the thesis with a retrospective view on the research study and draws conclusions from the work. Recommendations for future research are also highlighted in this chapter.

Chapter 2

Strengthening of Reinforced Concrete Structures with FRPs

This chapter presents a state-of-the-art overview of various FRP strengthening techniques. Different aspects and specific considerations of externally bonded reinforcement are discussed. Materials' choice and the corresponding advantages and disadvantages are highlighted. Failure modes of FRP strengthened concrete structures are reviewed with equations governing their behaviour. Mechanical characteristics of FRPs are examined and various applications for strengthening reinforced concrete structures with FRP materials are presented. Existing design procedures for delamination failures are enumerated. Finally, environmental concerns of various FRP strengthening techniques are reviewed.

2.1 Introduction

In an aggressive environment, concrete may be vulnerable to chemical attacks such as carbonation and chloride contamination which breaks down the alkaline barrier in the cement matrix. Consequently, the steel reinforcement in concrete structures becomes susceptible to corrosion. Such a phenomenon leads to delamination of the concrete at the reinforcement level, cracking and spalling of the concrete under more severe conditions due to the volume increase of the steel reinforcement. In the United States, nearly one-

third of the nation's 581,000 bridges are structurally deficient or functionally obsolete [US DOT, 1997]. A large number of these deficient bridges are reinforced or prestressed concrete structures, and are in urgent need of repair and strengthening. In the United Kingdom, over 10,000 concrete bridges need structural attention. In Europe, it is estimated that the repair of reinforced concrete structures due to corrosion of reinforcing bars costs over $600 million annually [Tann and Delpark, 1999]. In Canada, it is estimated that the required repair costs for parking garages alone is in the range of $6 billion [Benmokrane and Wang, 2001].

A possible solution to combat reinforcement corrosion for new construction is the use of non-corrosive materials to replace conventional steel bars. High tensile strength, lightweight and corrosion resistance characteristics make FRPs ideal for such applications. FRPs also provide cost effectiveness and a practical technique for the repair and strengthening of structures and bridges using externally bonded sheets or prefabricated laminates. FRP tendons can also be used to strengthen old prestressed concrete girders as well as to prevent corrosion from occurring in tendons in salty regions [Corry and Dolan, 2001].

2.2 Strengthening of Concrete Structures

2.2.1 Historical Background

During the last decades, several strengthening techniques have been investigated to discover new ways towards extending the service life of existing concrete structures. This situation confronts the construction industry with a distinctive challenge, along with

increasingly economical constraints. A study by Klaiber et al. (1987) identified the most popular techniques for strengthening concrete structures. These techniques included external prestressing, hand-applied repairs with concrete mortar, shot concrete, injection techniques, and different kinds of concrete castings. One of the most remarkable techniques developed during the mid 1960's was bonding of steel plates, which could be glued by epoxy and/or anchored. Strengthening through the attachment of external materials has become popular because it is often the most economical choice. In Europe, records indicate that the use of epoxy to glue steel plates for the last 30 years still remains and functions very well even with the limited manufacturing technology available at that time [Beber et al., 2001].

The use of externally bonded steel plates started in France, where L'Hermite and Bressson (1967) carried out tests on strengthened concrete beams. Nevertheless, the method has been used all over the world since then, in places such as Israel [Lerchental, 1967], Switzerland [Lander, 1983], Japan [Raithby, 1980], United Kingdom [Jones et al., 1988], Australia [Palmer, 1979], Sweden [Taljsten, 1994], Germany [Kaiser, 1989] and the United States [Klaiber et al., 1987]. Small-scale on site applications using externally bonded steel plates were executed in Belgium [Van Gemert, 1980]. The first large-scale application was the strengthening of a concrete bridge over the Nete Canal at Lier, Belgium [Brosens and Van Gemert, 2001].

The method performs quite well technically. However, it has some drawbacks such as the self-weight of the steel plates, which are quite heavy and require costly erection

equipment for field installation. It has been demonstrated that steel plates are vulnerable to corrosion, especially at the steel-epoxy interface [He et al., 1997]. It is also necessary to apply an outer pressure to the plate during the erection until hardening of the epoxy is achieved. Furthermore, use of the steel plate method is inflexible, expensive and difficult to apply to curved surfaces. Due to the foregoing reasons, researchers worldwide have been seeking alternative materials. Their attention has been drawn to the use of non-metallic composite materials as a substitute to steel plates.

In the early nineties of the last century, a real explosion of research and development took place through the use of FRPs for strengthening applications. FRPs offer an excellent alternative to steel plates because of their high tensile capacity, non-corrosive nature and light weight. Commercially available FRP products are made of continuous fibres of Aramid (AFRP), Carbon (CFRP), or Glass (GFRP) impregnated in a resin matrix. The most imperative characteristic of FRPs in repair/strengthening applications is the speed and ease of installation. FRPs may be bonded to the tension side of concrete beams, girders and slabs to provide additional flexural strength, and/or on the sides of beams and girders to provide additional shear strength. For seismic zones, FRPs may also be used to wrap columns to enhance the ductility due to the induced confinement of the concrete. FRP material's selection should be based on strength, stiffness and durability required for a specific application. Resins are selected based on the environment to which the FRP will be exposed, as well as the method by which the FRP is manufactured. FRP plate bonding technology was first investigated at the Swiss Federal Laboratory for Materials Testing and Research (EMPA) [Meier, 1992]. FRP composites have been used in other

areas such as the aerospace industry for many years and their superior properties are well known [Teng et al., 2002].

2.2.2 Concrete Beams Strengthened with Steel Plates

Since the early work in South Africa by Fleming and King (1967) and in France in the mid 1960's [L'Hermite and Bresson, 1967], the technique of strengthening reinforced concrete members by bonding thin steel plates to their surfaces has been used worldwide. This technique extended to FRPs as they became economically feasible. Consequently, the research into the use of bonded steel plates is very relevant to the use of bonded FRP sheets/strips and for this reason a literature survey on the research in this area was conducted.

For thirty years, strengthening with externally bonded steel plates was investigated both experimentally and analytically. The prime objective of various investigations was to focus on understanding different failure mechanisms, safety measures and detailing provisions. MacDonald and Calder (1982) studied the behaviour of reinforced concrete I-beams strengthened with externally bonded steel plates. The concrete beams were tested under four-point bending. Full composite action between the concrete and the steel plate was achieved. Significant improvement in performance was observed in terms of crack control, stiffness and strength. Exposure tests were carried out on 0.5 m long unreinforced concrete beams, with steel plates bonded to one face. Considerable corrosion of the steel plate was observed. As a result, loss of bond strength at the steel-

epoxy interface was detected. The reduction in the overall strength of the beams was attributed to corrosion.

Van Gemert and Vanden Bosch (1985) reported durability test results on concrete beams strengthened with epoxy-bonded external steel plates. The effects of long-term exposure, fatigue, and temperature loading were investigated. Cyclic loading tests were performed on two 6.0 m long simply supported beams. The beams were reinforced with a double layer of glued steel plates. The cross-section of the beams was 300 mm deep by 250 mm wide. The steel plates were 5 mm thick by 200 mm wide. The beams were tested under four-point bending and were subjected to cyclic loading resulting in a maximum tensile stress of 40 MPa in the steel plates. Test results showed that no redistribution of stresses took place by deformation in the glue or by any failure in the glued connection. Full-scale temperature loading tests in a temperature ranged between $-20^{\circ}C$ to $+90^{\circ}C$ were conducted on beam specimens. It was found that the cold-hardening epoxy glue had a poor thermal resistance. There was no decrease in the ultimate load for lower temperatures. However, at higher temperatures, the behaviour was quite different. The epoxy joint was not able to transfer the shearing stresses from the steel plate to the concrete surface, and a crack propagated from the plate end into the concrete beam. The performance of the cold-hardening epoxy was considerably reduced at high temperatures.

Swamy et al. (1987, 1989) investigated the influence of glued steel plates on the first cracking load, cracking behaviour, deformation, serviceability, and ultimate strength of reinforced concrete beams. Forty beams were tested. All test beams had a rectangular

cross-section of 225 mm deep by 155 mm wide. The beams were 2.5 m long. The beams were strengthened by bonding steel plates of 1.5 mm, 3 mm and 6 mm thick. In addition, the thickness of the epoxy resin bed was varied from 1.5 mm to 6 mm thick. Test results indicated that the presence of the steel plates substantially increased the flexural stiffness, strength and reduced the crack width and deflections at all load levels. Due to the significant increase in the sectional stiffness, the service load of the strengthened beams was increased. At the plate cut-off region, the local bond stresses were considerably higher than those predicted by simple elastic theory and could result in premature debonding of the plates. Different techniques were studied to prevent premature plate debonding. Test results showed that by providing a mechanical anchorage to the plate ends, the ultimate load capacity and mode of failure of the plated beam could be positively improved. Simple design guidelines were provided by restricting the width-to-thickness ratios of the plates and neutral axis depth of the concrete sections, both to maintain ductility and to avoid premature debonding of the plates.

Oehlers (1988, 1990, 1998) conducted a series of detailed studies on the failure mechanism of steel plated beams. Different identified failure mechanisms rationally categorized by the author are illustrated in Fig. 2.1.
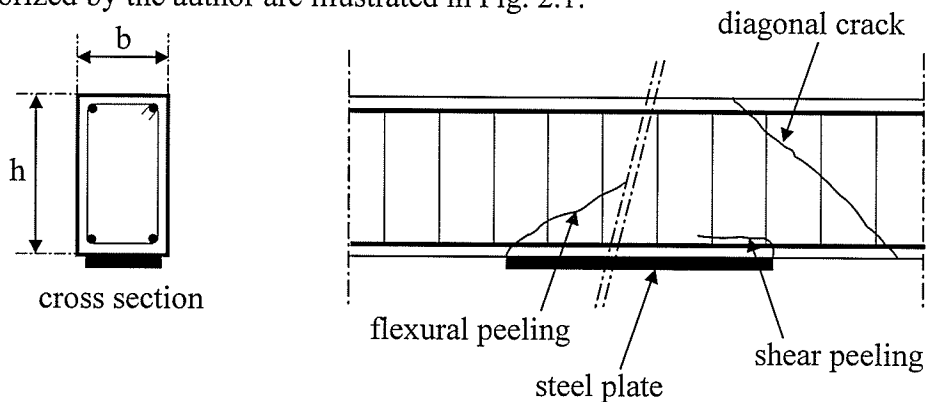
Fig.2.1 Failure modes in steel-plated reinforced concrete beams [Oehlers, 1988]

Test results on concrete beams strengthened with steel plates in the constant moment region showed that the increase in the applied load resulted in a corresponding increase in the curvature of the beam, which could induce *flexural peeling*. In this mode of failure, separation of the steel plate occurred gradually. The formation of diagonal shear cracks induced *shear peeling* as the steel plates terminated close to the support where high shear stresses were located. This type of peeling failure occurred rapidly and was very brittle. If a shear span was partially plated, a combined *shear flexural peeling* occurred. Peeling failure modes for concrete beams strengthened with externally bonded steel plates are illustrated in Fig. 2.2. All peeling failure modes occurred at the level of the internal steel reinforcement.
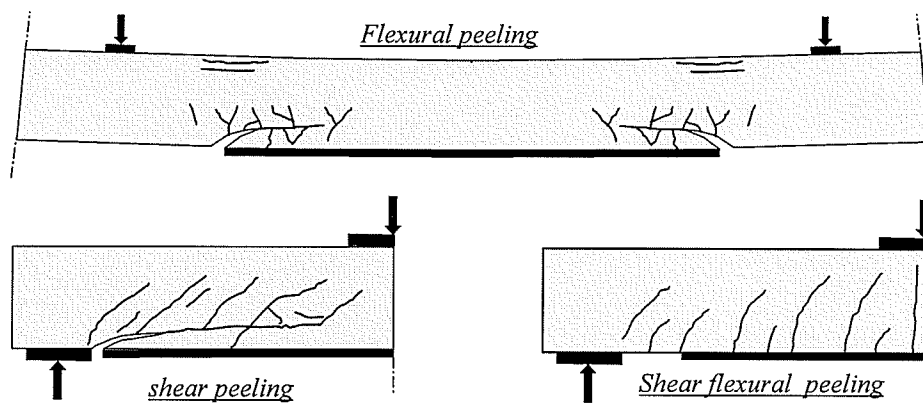
Fig. 2.2 Peeling failure modes [Oehlers 1988, 1990, 1998]

According to test results, the stress concentration at the ends of the steel plate depended not only on the externally applied forces, but also on the non-linear behaviour of the three material components of steel, adhesive, and concrete. The effects of flexural cracks and the tension-stiffening induced by these cracks at plate cut-off points created a complex region that was difficult to simulate on a computer. Oehlers concluded that flexural and

shear cracks, bond stress along the bottom reinforcement, and aggregate interlock forces across peeling cracks played a major role in the failure mechanism.

The efficiency of various anchorage details was investigated to overcome anchorage problems due to high shear stress concentration at the plate ends [Jones et al, 1988]. Tests by Roberts and Haji-Kazemi (1989) on concrete beams strengthened with mechanically connected steel plates showed that a significant improvement in stiffness and strength was achieved by fixing the steel plates with bolts. However, full composite action was not accomplished due to excessive slip of the steel plate at the bolted connections.

Hussain et al. (1995) investigated the influence of a bolted end anchorage on ductility and strength. Bolts were installed to 50 percent of the beam depth. Tests results showed that bolted anchorages could not prevent premature debonding failure. However, the ductility was significantly improved. It was concluded that an additional anchorage had a marginal effect on improving the ultimate strength.

Rutz (1995) studied the structural performance of concrete structures strengthened with externally bonded steel plates and subjected to high temperatures. Test results showed that at ambient temperatures higher than 50°C, the contribution of the stiffness of the adhesive became negligible. Rutz concluded that fire protection provisions should be provided for steel plated concrete beams.

Hankers (1997) investigated various failure mechanisms that might occur under repeated loading conditions for concrete members strengthened with externally bonded steel plates. The failure mechanisms were categorized as follows:

- *plate separation by concrete failure*: failure occurred in the concrete above the epoxy layer;

- *plate separation by interface failure*: failure was initiated at the root of a flexural crack and subsequently propagated to the end of the steel plate;

- *plate separation by epoxy failure*: failure occurred at the epoxy when the steel plate was highly stressed;

- *fatigue failure of steel plate*; and

- *plate separation at the level of the internal reinforcement.*

Hankers (1997) concluded that members strengthened in flexure with externally bonded steel plates are not sensitive to repeated loading conditions if the plates are properly bonded to the concrete.

From the above discussion, it is concluded that most studies focused on the flexural behaviour, anchorage capacity and shear strengthening. Accordingly, the basic mechanism of shear failure without shear reinforcement was hardly investigated. Various research projects are currently focusing on plate-end shear and its influence on plate separation [Jansze, 1997 ; Hearing and Buyukozturk, 2000].

2.2.3 Concrete Beams Strengthened with FRPs

Externally bonded FRP systems come in a variety of forms, including wet lay-up systems and precured systems. Wet lay-up FRP systems consist of dry unidirectional or multidirectional fibre sheets or fabrics impregnated with a saturating resin on-site. Precured FRP systems consist of a wide variety of composite shapes manufactured off-site. Typically, an adhesive along with the primer and putty is normally used to bond the precured shapes to the concrete surface. Precured FRP systems include unidirectional laminates, multi directional grid and precured shells.

Since 1982, externally bonded FRP sheets/strips have been successfully applied to reinforced concrete beams [Meier et al., 1995]. Meier et al. suggested that CFRP laminates could replace steel plates with overall cost savings emanating from the simplicity of the strengthening method because:

- FRPs do not corrode;

- FRPs are easy to handle in the construction site and can be bonded to structure without expensive scaffolding; and

- FRPs are available in long lengths, therefore no joints are necessary.

Most of the failure modes observed in the beam tests carried out by Meier (1995) are illustrated in Fig. 2.3.
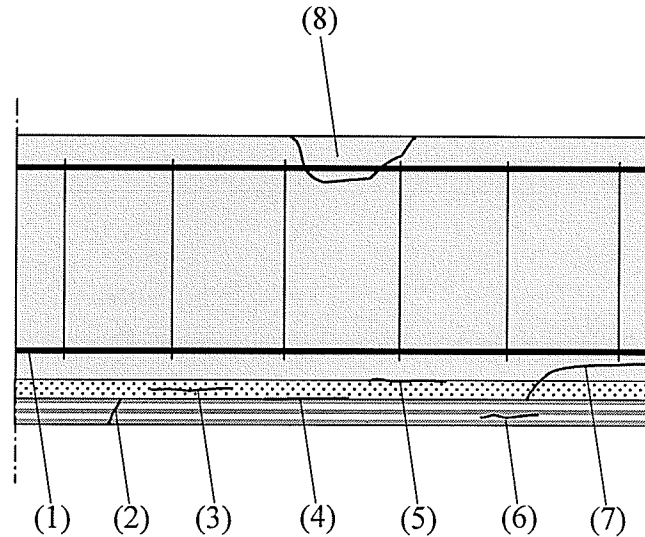
(1) Failure of steel bars   (5) Adhesive failure at the concrete/adhesive interface
(2) Tensile failure of FRP   (6) Interlaminar shear within the FRP
(3) Cohesive failure within the adhesive   (7) Continuous peeling of FRP sheets/strips
(4) Adhesive failure at the FRP/adhesive interface   (8) Crushing of concrete

Fig. 2.3 Failure modes in reinforced concrete beams strengthened with FRPs

Externally bonded FRP sheets were used for strengthening concrete beams by Kaiser (1989). The experimental program consisted of testing a series of rectangular beams, 300 mm wide by 250 mm deep and 2.0 m long. The beams were strengthened with different thicknesses of externally bonded CFRP strips. Test results confirmed the validity of the strain compatibility hypothesis in the cross-section analysis. Kaiser also investigated the fatigue behaviour of a beam strengthened with CFRP laminates. The beam with the same dimensions as the previous static loading test specimens was strengthened with a strip of 0.3x200 mm of glass/carbon hybrid sheet without end laminate anchoring. The results depicted that the hybrid sheet could still withstand after the fatigue failure of the steel reinforcement. Kaiser studied the temperature effect over 100 freeze-thaw cycles from +25°C to -25°C on concrete beams strengthened with CFRP laminates and found no adverse influence on the flexural capacity.

Ritchie et al. (1991) used iterative analysis procedures to predict the flexural stiffness and strength of FRP laminated concrete beams. The analytical model was not verified completely by experimental testing due to lack of failures within the constant moment region. However, for those beams that failed in flexure, the model appeared to predict the flexural behaviour fairly accurately.

Saadatmanesh and Ehsani (1991) studied the structural behaviour of reinforced concrete beams strengthened with GFRP laminates. Test results showed that concrete surface preparation and selection of the adhesive were of primary importance. Furthermore, strengthening with externally bonded FRP laminates was particularly effective for beams with relatively low internal steel reinforcement ratios.

Meier et al. (1995) performed a fatigue test on a reinforced concrete beam strengthened with CFRP laminates applied to its soffit. The beam was tested under six point loading using a realistic fatigue load range (130 MPa to 260 MPa in steel bars) up to 10.7 million loading cycles to verify the excellent performance of CFRP laminates in fatigue resistance. A method for prestressing the laminates to increase the service load of the structure was also proposed. Meier et al. pointed out that shear deformations between cracks in reinforced concrete members could initiate premature debonding of the laminates as shown in Fig. 2.4.
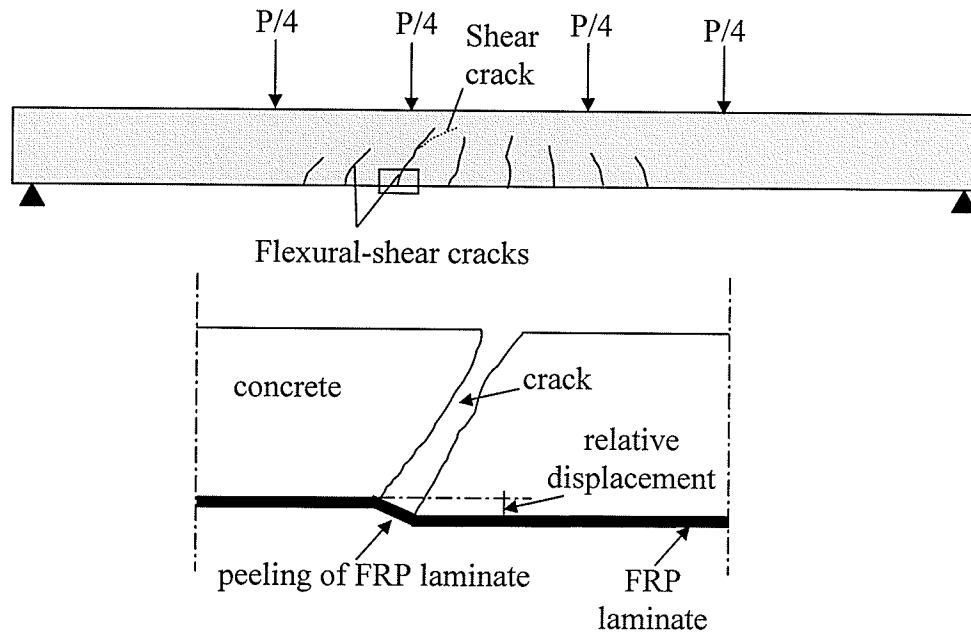
Fig. 2.4 Peeling of FRP laminate due to shear cracks [Meier et al., 1995]

Meier et al. (1995) suggested ways to use FRP sheets to act as shear reinforcement and to effectively clamp the ends of the laminate as shown in Fig. 2.5.
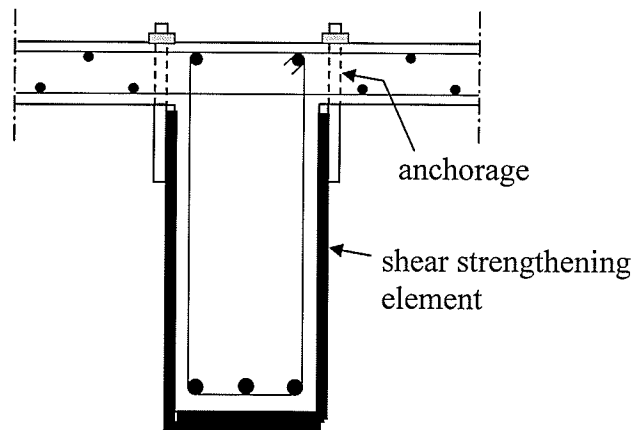
Fig. 2.5 Cross-section of a beam with shear strengthening arrangement [Meier et al., 1995]

2.3 Concrete — Steel/FRP Interface Bond Strength

In the design of retrofit schemes incorporating externally bonded reinforcement, the concrete-to-steel/FRP interface bond strength is an imperative design variable that needs to be evaluated. Experiments have been carried out using several test-setups, including single shear tests as shown in Fig. 2.6a. [Taljsten, 1994, 1997; Chajes et al. 1995, 1996; Bizindavji and Neale, 1999], double shear tests as shown in Fig. 2.6b [Van Gemert, 1980; Swamy et al., 1986; Kobatake et al., 1993; Maeda et al., 1997; Neubauer and Rostasy, 1997; Brosens and Van Gemert, 2001] and modified beam tests [Van Gemert 1980; Ziraba et al., 1995]. A literature survey of the research work conducted up to date is reviewed in this section.
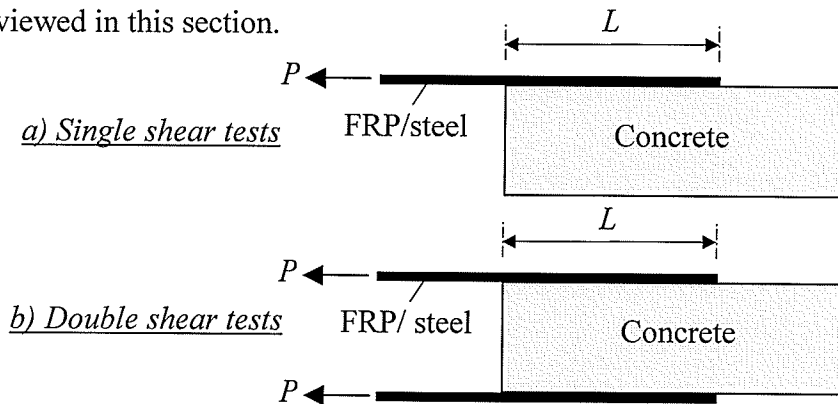
Fig. 2.6 Single and double shear tests

The earliest study on normal and shear stress distributions in glued joints was published by Goland and Reissner (1944). The analysis led to a more general form of the differential equations describing the normal and shear stresses in glued joints in an elastic medium.

Research on the force transfer mechanism in epoxy bonded steel-to-concrete joints was started by Bresson (1971). A mathematical model was proposed to describe the behaviour

of joints loaded in the elastic region. Ladner (1983) derived a mathematical model, which coincided with experimental test results. According to Ladner's study, a relatively small amount of the total anchorage length was efficient for load transfer, when all the materials behaved elastically. Using linear material properties, a hyperbolic distribution of the shear stresses along the interface was obtained as shown in Fig. 2.7. The total anchorage length would only be needed when the peak value of the bond stress moved towards the unloaded end of the sheet and a redistribution of the bond stresses took place as shown in Fig. 2.7.
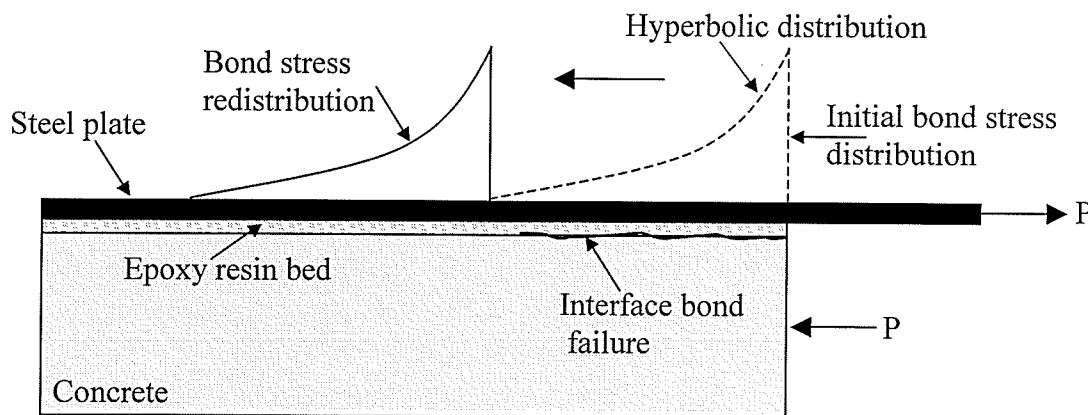
Fig.2.7 Bond stress redistribution [Ladner 1983]

For practical design procedures, the hyperbolic stress distribution was simplified by a triangular approximation [Van Gemert, 1990]. Based on an extensive experimental program, Van Gemert concluded that the bond strength at the concrete-steel interface was equivalent to the tensile strength of the concrete.

Swamy and Jones (1987, 1989) used the elastic theory to study the bond stress concentration at plate cut-off point. Based on the analysis, the bond strength was related to the concrete cube strength, proposing that it varied from 6 to 8 MPa for cube strengths

varying between 25 to 70 MPa. In a later study using full-scale beams, Swamy et al. related the bond strength to the splitting tensile strength of the concrete, claiming that the bond strength is equal to $\sqrt{2}$ times the tensile strength of concrete. Since the tensile strength of concrete is unlikely to exceed 4 to 5 MPa, the bond strength was estimated to be about 6 to 7 MPa. Test results indicated that the peak interface bond stress had a value of 2τ, where τ is the bond stress derived using elastic theory.

Roberts (1988) proposed an analytical model using practical interaction theory to predict shear and normal stress concentrations in adhesive joints. Roberts concluded that the shear and normal stress concentrations in the adhesive layer at plate cut-off point could be reduced significantly by:

- using a more flexible adhesive;
- reducing the thickness of the steel plate; and
- terminating the steel plate as close as possible to the beam supports.

Test Results showed that failure of the epoxy-bonded steel plates was likely to occur at bond stresses ranged from 3 to 5 MPa.

Kaiser (1989) modified Ladner's model and accounted for the non-linearity in the bond stress distribution for CFRP laminates as shown in Fig. 2.8. The study focused on finding an analytical model to calculate the anchorage length of CFRP laminates used for increasing the flexural capacity of reinforced concrete beams. A bond strength of 8 MPa was proposed based on theoretical and experimental investigations. However, the

influence of the concrete strength was neglected in the analytical model. The concrete cube strength adopted in the model was 40 MPa.
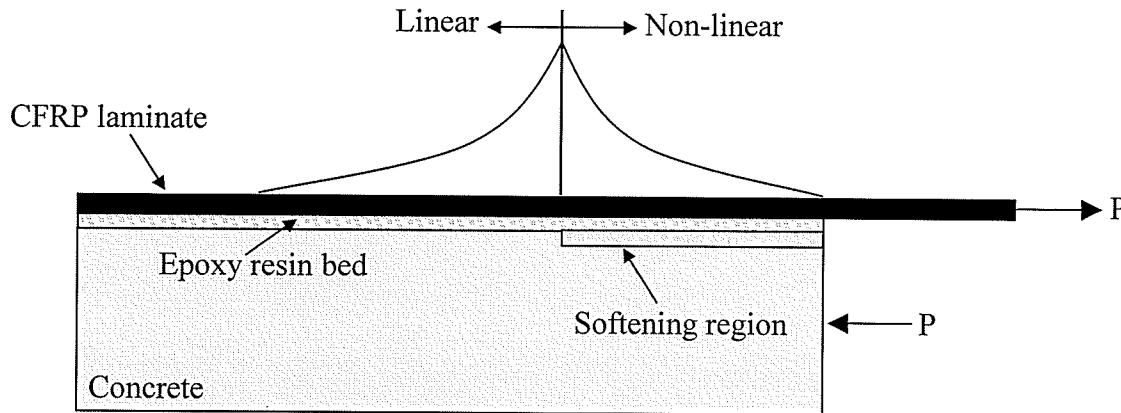
Fig.2.8 Bond stress distribution on CFRP laminate [Kaiser, 1989]

Sharif et al. (1994) carried out double shear tests on FRP laminates bonded to concrete specimens. Test results showed that the maximum sustainable interface shear stress ranged from 3.5 to 4 MPa, with failure occurring in the concrete in all cases.

Arduini et al. (1997) concluded that the bond strength of the FRP-to-adhesive interface was about three times the bond strength of concrete-to-adhesive interface. As a result, FRP-to-concrete bond strength was controlled by failure at the concrete-to-adhesive interface. A recommended bond strength of 5 MPa was proposed for concrete of compressive strength of 30 MPa.

Quantrill et al. (1996) performed shear pull-off tests using GFRP laminates, bonded with 1 mm thick adhesive to a concrete prism of 65 MPa cube compressive strength. Test results indicated an average bond strength of 6.4 MPa. Doubling the thickness of the

adhesive layer, the average bond strength was reduced by 10 percent. In all cases, failure occurred within the concrete adjacent to the GFRP laminates.

2.3.1 Effect of Surface Preparation on Bond Performance

In order to achieve a good bond, the surface of the concrete must be clean, dry and free of all loose materials. Typical methods for concrete surface preparation prior to the application of externally bonded FRP systems are: grinding; mechanical abrasion with a wire wheel; sand-blasting; or hydro-blasting with high pressure water. In separate bond tests, Chajes et al. (1996) concluded that mechanical abrasion with a wire wheel resulted in better bond performance than the grinding technique. Yoshizawa et al. (1996) found that high pressure hydro-blasting increased the bond strength by a factor of two when compared to grinding. For applications using FRP sheets, a primer is applied to strengthen the clean concrete surface. The primer is usually chemically similar to the impregnation resin to provide good adhesion to the concrete, but less viscous for good penetration into the concrete. In bond tests conducted by Yoshizawa et al. (1996), the use of different primers had no noticeable influence on the bond performance.

2.3.2 Effect of Adhesive on Bond Performance

Load is transferred from the FRP sheet/strip to the concrete through shear flow, and the relative stiffness of the FRP and the adhesive influence how the load is transferred [Chajes et al., 1996]. Hamada et al. (1997) conducted bond tests to compare the performance of flexible and rigid adhesives using beam specimens. The flexible adhesive had a modulus of elasticity of 1.0 GPa and an ultimate strain of 3 percent, while the rigid

adhesive had a modulus of elasticity of 3.15 GPa and an ultimate strain of 0.8 percent. According to test results of specimens fabricated with the rigid adhesive, the maximum load increased with increasing the stiffness of the FRP. By comparison, no such relationship was observed for the specimens with the flexible adhesive.

2.3.3 Effect of FRP Stiffness on Bond Performance

Maeda et al. (1997) observed a significant increase in the average bond strength with increasing the stiffness of the FRP sheets. The increase in average bond strength was not directly proportional to the increase in the stiffness of FRP. An increase in the FRP stiffness by a factor of three resulted in an increase in bond strength that was less than two. Yoshizawa et al. (1996) also reported an increase in bond strength with higher modulus FRP sheets and increased layers of sheets.

2.3.4 Effect of Concrete Strength on Bond Performance

Horiguchi and Saeki (1997) tested three different types of bond specimens with three different concrete compressive strengths, 11 MPa, 31 MPa and 46 MPa, for each type of specimen. An increase in bond strength with increased concrete compressive strength was observed for all types of specimens. However, the effect of concrete strength on the bond performance was less for the shear type test compared with the bending test and the tensile test as shown in Fig. 2.9.
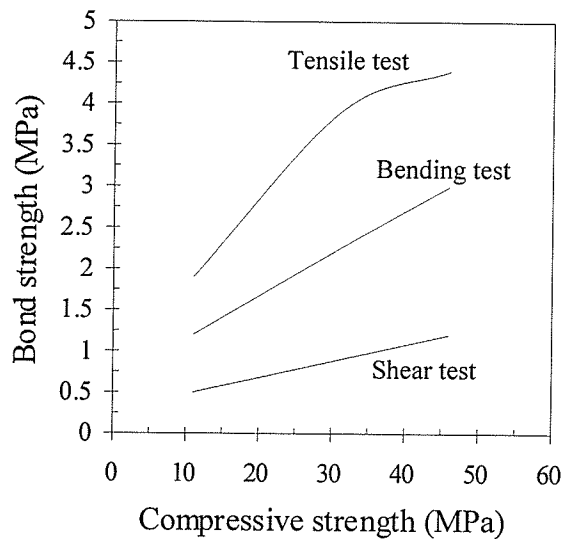
Fig. 2.9 Bond strength vs. concrete compressive strength for three types of
bond specimens [Horiguchi and Saeki, 1997]

Substrate strength is an important parameter for bond-critical applications, including flexure or shear strengthening. The existing concrete substrate should possess the necessary strength to develop the design stresses of the FRP system through bond. The substrate, including all bond surfaces between repaired areas and the original concrete, should have sufficient direct tensile and shear strength to transfer force to the FRP system. The tensile strength of the concrete should not be less than 1.4 MPa as recommended by the draft report of the ACI-440 (2002).

2.4 Failure Mechanisms of Concrete Beams Strengthened with FRPs

2.4.1 General

This section reviews the behaviour of FRP retrofitted concrete beams at the ultimate limit state to describe the state beyond which a structure no longer satisfies the design performance requirements. Flexural failures are reviewed first, including both FRP

rupture and concrete crushing modes. Then shear failures are examined, including new types of shear failure observed in plated structures. Finally, debonding failures involving separation of the FRP from the concrete substrate are discussed. Various failure modes in FRP retrofitted concrete beams are illustrated in Fig. 2.10.

Rupture of FRP laminate

Crushing of concrete

Shear failure

Delamination of FRP

Peeling due to shear crack
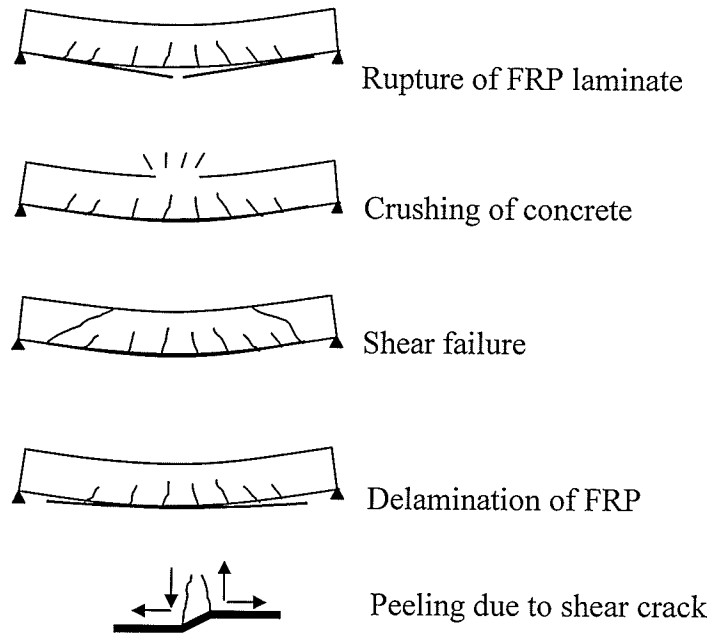
Fig. 2.10 Failure modes in FRP retrofitted concrete beams

2.4.2 Flexural Failures

Reinforced concrete beams strengthened with FRPs have been observed to fail in flexural failure modes similar to traditional reinforced concrete beams. Flexural failures of retrofitted beams include either rupture of the FRP or compression failure in the concrete. To assure adequate ductility, Meier and Kaiser (1991) recommended that failure of concrete beams strengthened with FRPs should occur with yielding of the steel and ultimately rupture of the FRP before compression failure.

Many researchers have investigated flexural failures of retrofitted concrete systems and have observed a variety of strength increases. Typically, the strength increase percentage reported is the ratio of the ultimate load after strengthening to the yielding load of the unretrofitted system. Experimental studies of Jones et al. (1988) showed that the strength of under reinforced concrete beams could be increased up to 96 percent while maintaining failure modes of rupture of the FRP. Strength increases up to 26 percent were also observed with rupture failures in GFRP retrofitted concrete beams [Sharif et al., 1994]. Other research programs have reported concrete crushing failures in beams with increased yield loads of 33 percent [Saadatmanesh and Ehsani, 1990]. Therefore, the flexural failure modes of the retrofitted system can vary depending on many factors of the retrofit scenario.

The American Concrete Institute, [ACI 440, 2002], proclaims that flexural behvaiour of strengthened systems can be analyzed using the following assumptions:

- FRPs have a linear elastic stress-strain relationship up to failure;
- strain compatibility and equilibrium;
- maximum concrete strain of 0.003; and
- tensile strength of concrete could be ignored.

The stress in each material is calculated based on strain compatibility, force equilibrium, and the governing failure mode. The strain in the FRP has been shown to exhibit three distinct stages of beam behaviour corresponding to: uncracked section of the beam, cracked section with elastic steel, and finally the section with plastic steel ending with rupture of the FRP [Meier and Kaiser, 1991]. Consequently, flexural failures are highly

governed by the amount of FRP relative to the amount of the existing steel and beam dimensions.

Many researchers have presented analyses of the flexural behaviour of concrete beams strengthened with FRPs [Ziraba et al., 1994; Plevris et al., 1995; Malek et al., 1998]. A compilation of these analyses is presented herein.

A typical cross-section of a concrete beam strengthened with FRP is shown in Fig. 2.11.
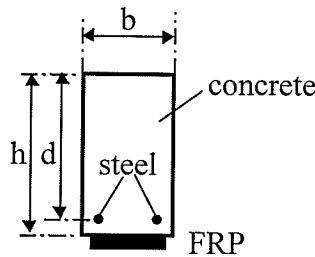
Fig. 2.11 Cross section of a reinforced concrete beam strengthened with FRP laminate

The FRP has a reinforcement ratio of ρ_f (defined as the cross-section area of the FRP divided by the effective area of the concrete section); Young's modulus E_f and tensile failure strain ε_{fu}. The concrete has a compressive strength fc' and Young's modulus E_c; and the steel has a reinforcement ratio ρ_s; Young's modulus E_s; and yield stress f_y.

Plevris et al. (1995) showed that properly designed CFRP strengthened concrete beams might fail in bending according to one of the following failure mode sequences: steel yielding—CFRP rupture or steel yielding—concrete crushing. If the total area of steel and CFRP reinforcement were relatively high, a third failure mode occurred, in which the concrete crushed in a catastrophic manner. The ultimate moment capacity M_u corresponding to these failures can be expressed by:

Steel yielding — CFRP rupture

$$\frac{M_u}{bd^2 f_c{}'} = \frac{f_y}{f_c{}'}\rho_s\left(1 - \frac{\overline{y}}{d}\right) + \frac{E_f \varepsilon_{fu}}{f_c{}'}\rho_f\left(\frac{h}{d} - \frac{\overline{y}}{d}\right) \qquad (2.1)$$

Steel yielding — Concrete crushing

$$\frac{M_u}{bd^2 f_c{}'} = 0.85\beta_1\frac{c}{d}\left(\frac{h}{d} - \frac{\beta_1 c}{2d}\right) - \frac{f_y}{f_c{}'}\rho_s\left(\frac{h}{d} - 1\right) \qquad (2.2)$$

Concrete crushing —Steel in the elastic range, same as in (2.2) with f_y replaced by

$$\frac{0.003\left(1 - \dfrac{c}{d}\right)}{\dfrac{c}{d}}E_s$$

where c is the depth of the neutral axis from the top section; h is the total height of the section; d is the distance from the steel reinforcement to the maximum compression fibres; $\overline{y}$ is the distance from the centroid of the concrete stress block to the FRP given in terms of ε_{fu}, h/d, ε_o (the initial strain at the concrete bottom fibre resulting from loads carried by the member at the time when strengthening was applied); and c/d (described in terms of ε_{fu}, h/d, ε_o, ρ_s, ρ_f, f_y, fc', and E_f); and β_1 is an empirical constant which depends on the concrete compressive strength. Debonding of the FRP was not considered in this analysis, as the failure load for such mechanism is highly dependent on quality control during strengthening and on the properties of the adhesive employed.

2.4.3 Shear Failures

Shear failure is typically brittle and should be avoided as a failure mode of the retrofitted system (ACI 440, 2002). Many types of failures have been attributed to shear such as peeling due to the shear force at the plate end. Traditional shear failures similar to that of unstrengthened reinforced concrete beams have been observed by researchers. These failures are termed *flexural-shear failure* and *diagonal tension failure*. Reports on flexural shear failure in plated members date back to 1967 [L'Hermite and Bresson, 1967]. Shear failures have also been attributed to the presence of the retrofit plate; these types of failures are termed *plate-end shear failures*. Failures must be distinguished between those that appear to originate at the end of the plate and propagate into debonding-type failures and shear failure of the section. Plate-end shear was clearly defined and studied in depth with steel plated reinforced concrete beams [Jansze, 1997]. The basis for Jansze's model was the formulae for shear capacity given by CEB-FIB MC90. The model was verified with an extensive experimental program and by numerical simulations using non-linear finite element modelling. Recently, Jansze's model was extended to FRP retrofitted concrete members by Ahmed (2000). Empirical parameters were introduced based on the ACI code, 1992 and calibrated with experimental data.

Recently, many shear-strengthening configurations have been proposed to increase the shear capacity of reinforced concrete beams through FRP retrofit. Multiple options exist for shear strengthening as shown in Fig. 2.12, including laminate bonding to the sides of the beam, U-jacketing around the bottom, and total wrapping of the beam. The shear

resisting system can be in the form of continuous sheet or laminates with spacing. Fibres can be oriented either perpendicular to the axis of the beam or perpendicular to the potential shear cracks, or a combination of both orientations. Sufficient development length must be provided to assure anchorage of the shear reinforcement.
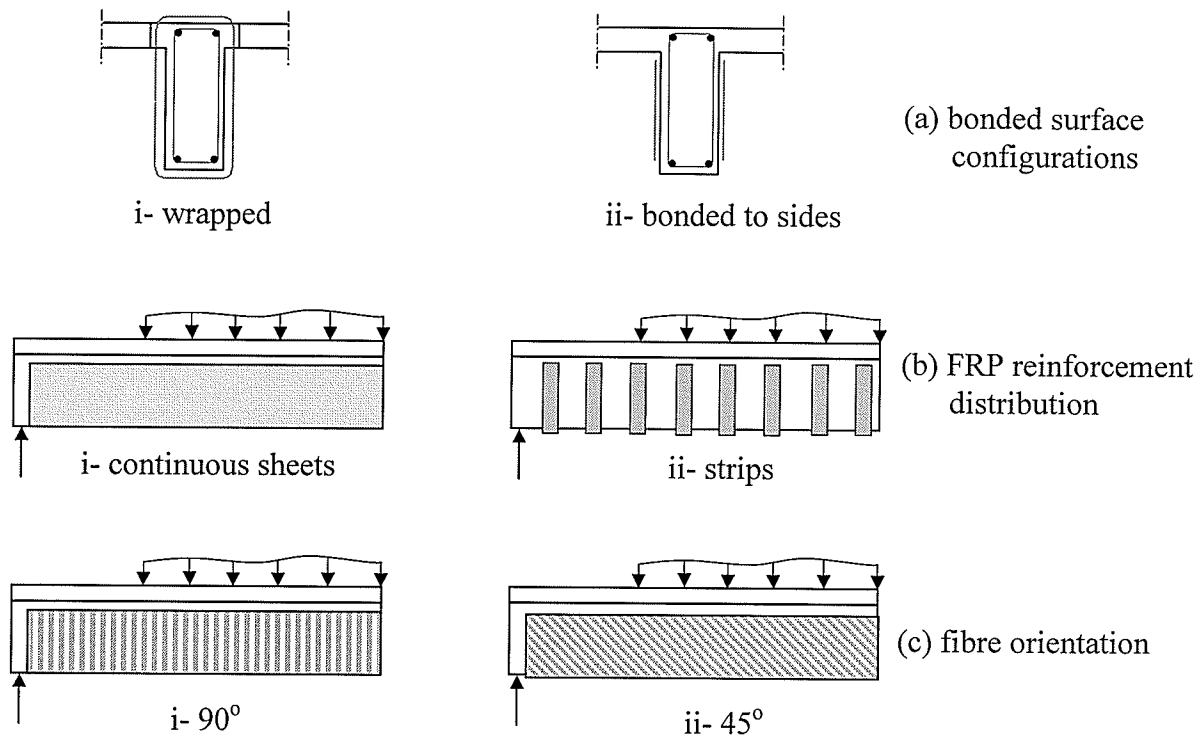

(a) bonded surface configurations

i- wrapped   ii- bonded to sides

(b) FRP reinforcement distribution

i- continuous sheets   ii- strips

(c) fibre orientation

i- 90°   ii- 45°

Fig. 2.12 Various shear strengthening configurations using FRP

2.4.4 Debonding Failures

Debonding failures are often brittle, occur with little or no visible warnings, and take place at load levels significantly lower than the flexural or shear strength of the retrofitted system. This mode of failure starts in the form of a horizontal crack at one of the edges of the bonded strip/plate below the internal steel reinforcement level and propagates toward mid-span, leading eventually to a complete separation of the strip/plate with the adjacent concrete cover layer. This brittle mode of failure is a result of high shear and normal

(peeling) stress concentrations arising at the edges of the bonded strip/plate. This limited area in the close vicinity of the bonded strip edge, proves to be among the most critical regions of the strengthened beam. Debonding failures are characterized by propagation of the failure process parallel to the plane of the laminate, while other failures such as flexural or shear failures propagate perpendicular to this plane. Debonding includes failure of the concrete layer between the FRP and flexural steel followed by delamination or peeling of the FRP from the concrete as shown in Fig. 2.13.
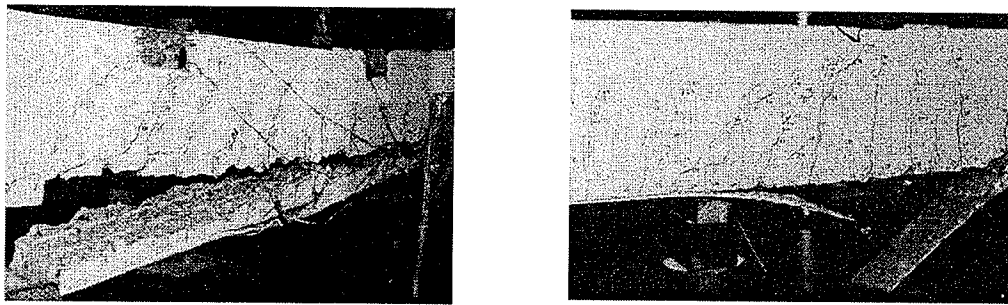

Fig. 2.13 Peeling of the FRP from the concrete beams [Ritchie et al., 1991]

Debonding failures have been observed and reported by many researchers [Saadatmanesh and Ehsani, 1989; Ritchie et al., 1991; Sharif et al., 1994]. It has been concluded that peeling failures can occur in different modes, including failure in the concrete substrate, adhesive shear failure, interlaminar shear failure, and interfacial failure at the concrete-adhesive interface or at the adhesive-FRP interface. Shear crack peeling is characterized by differential vertical displacements at crack tips in the retrofitted concrete beam that cause a stress intensity in the local bond region, as illustrated in Fig. 2.14. This stress intensity can initiate fracture and results in delamination propagation under increased loading [Neubauer and Rostasy, 1997].
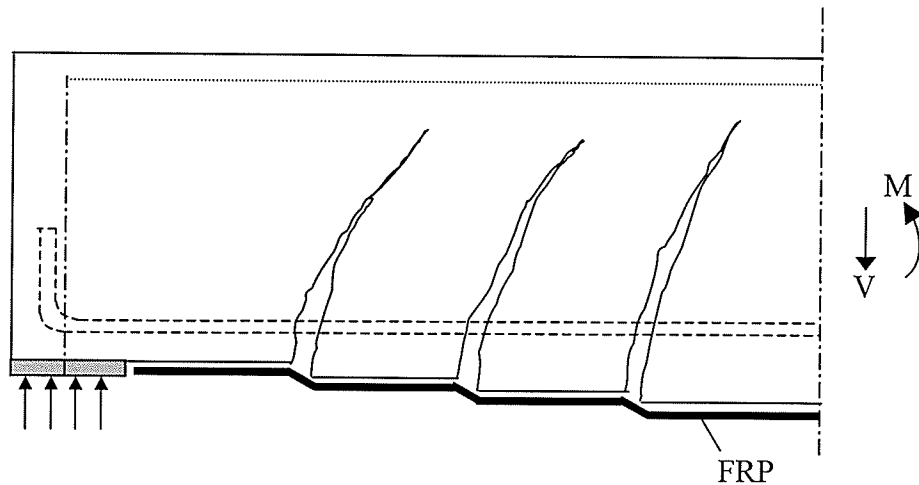
Fig. 2.14 Differential crack mouth opening displacements [Neubauer and Rostasy, 1997]

Peeling failures in the concrete substrate were first observed in an experimental investigation involving concrete beams strengthened with steel plates [Johnson and Tait, 1981]. To investigate the delamination process, strains in the retrofitted plate around the cracks in the shear span of concrete beam specimens were measured. It was shown that delamination could be monitored with strain gauges.

Other research programs studied the premature failure due to separation between the steel plate and concrete. The research took many forms that could be categorized in terms of the forces that were present near the ends of the plates where separation or peeling always commenced. Ong and Cusens (1982) tested specimens in which the plates were terminated in regions of bearing stresses; Van Gemert (1981) in regions of pure shear; Jones et al. (1988) in regions of shear and flexure.

One of the first large-scale research programs involving the use of FRP to retrofit concrete members concluded that shear peeling significantly influenced the capacity of

the retrofit system [Kaiser, 1989]. Although delamination was not the focus of the investigation, peeling failures from shear cracks were reported. Strains in the laminates were monitored in the vicinity of the crack tips in the concrete beams. Peak strains relative to the mean laminate strains were found to be similar among all specimens that failed through delamination. Peak strains were used to develop a criterion governing delamination in the tested specimens. The experimental program was limited to one retrofit scenario with a fixed laminate length and shear capacity, so conclusions regarding peeling process were limited.

Deuring (1993) reported peeling failure in concrete substrates of FRP retrofitted concrete beams. Acoustic emission results were used to evaluate delamination activity at various load stages. Strains in the laminate as well as crack tip displacements were also monitored, but because delamination was not the focus of the program many beams were tested with clamps to prevent peeling. Delamination in actual rehabilitated structures was reported by Karbhari et al. (1997), as well as in research programs involving slabs, beams, joints and columns [Meier, 1991; Arduini et al., 1997].

<u>Basis of Adhesion</u>: In bonding FRP materials to concrete, mechanical interlocking is the dominant mechanism of adhesion. Mechanical interlocking assumes that the major source of adhesion is the interlocking of the resin into the irregularities of the concrete surface. A rougher surface topography, created through surface abrasion, allows the resin to penetrate into the irregularities of the concrete and increases the adhesion. In general, the use of FRP composites although attractive, makes this mode even more critical due to

the anisotropy of the material and the sensitivity of most resin systems to moisture uptake and plasticization. The concern is further heightened through debonding and peeling seen in some existing structures [Karabhari et al., 1997]. Interfacial crack propagation can actually proceed due to a number of reasons including imperfect bonding between the FRP and concrete, flexural cracking in the concrete, peel stresses due to non-uniformity of the concrete surface, cyclic loading, environmental degradation, and the presence of large resin-rich zones. The presence of any of these flaws obviously can lead to further degradation and deterioration including ease of vandalism at loose edges.

Stress intensities can initiate mircocracking in laminated concrete beams. Microcracks can form in any of the constituent materials or their interfaces as shown in Fig. 2.15. Upon further loading these microcracks can ultimately form macrocracks causing delamination failure [Hankers, 1997].
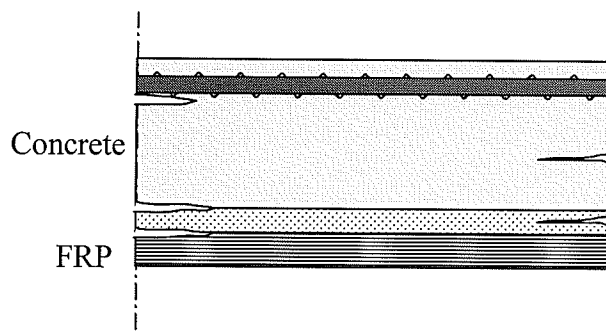
Concrete

FRP

Fig. 2.15 Possible microcrack locations

Adhesives: In recent years, adhesives have found many applications in civil engineering. The growing demand for the use of FRP composites in repair and strengthening applications created a great need of understanding both the short- and long-term behaviour of these materials. Generally, adhesives used in retrofitting applications

display similar characteristics as the FRP composites. The mechanical properties of the adhesives are significantly affected by service temperature, relative humidity and sustained loadings. Most adhesives display higher compressive and shear capacities than tensile and peeling capacities [Mosallam and Dutta, 2001].

There is very limited published research regarding suitable adhesives for concrete-composite joints. Saadatmanseh and Ehsani (1990) conducted an experimental study to evaluate the performance of four different adhesives used to bond composite plates to the tension surface of reinforced concrete beams. It was concluded that the success of such a strengthening technique strongly depends on the suitability of the epoxy bonding agent. The epoxy should have sufficient stiffness and strength to transfer the shear force between the concrete beam and the composite material. The epoxy should also be tough enough to prevent brittle failure caused by cracking of the concrete. Ritchie et al. (1991) reported that a two-part, rubber-toughened epoxy would be the most appropriate selection. Other researchers such as Meier et al. (1992) used epoxies that were developed for purposes such as bonding steel reinforcement to concrete.

2.4.4.1 Delamination Models

Theoretical work on the bond strength and delamination models can be roughly classified into three main categories:

- Empirical models, based directly on regression of test data [Tanaka, 1996; Hiroyuki and Wu, 1997];

- Mechanics of materials approach [Neubauer and Rostasy, 1997; Malek et al. 1998]; and

- Fracture mechanics approach [Holzenkampfer, 1994; Taljsten, 1996; Wu and Niu, 2000, Hearing and Buyukozturk, 2000].

Many experimental programs reporting debonding failures in the literature do not have provisions for detecting the exact origin, propagation, and secondary mechanisms involved with the debonding process. Thus an improved experimental technique for monitoring debonding failure is enormously required. This section presents a review of various models and an assessment of their performance.

(a) Empirical Models

Hiroyuki and Wu (1997) conducted a set of double shear tests on reinforced concrete members strengthened with CFRP sheets. An empirical relationship was proposed relating the bond length, L (cm), and the average bond strength, τ_{max} (MPa), as follows:

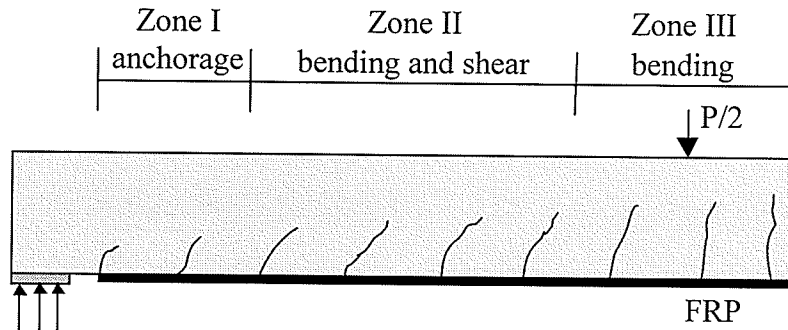$$\tau_{max} = 5.88 \left(L^{-0.669} \right) \tag{2.3}$$

Tanaka (1996) presented another simple expression for the bond strength

$$\tau_{max} = 6.13 - \ln L \tag{2.4}$$

where L is the bond length in mm and τ_{max} is the bond strength in MPa.

(b) Mechanics of Materials Approach

Neubauer and Rostasy (1997) classified bonding mechanisms into three different types as illustrated in Fig. 2.16.

2.16 Bonding zones in retrofitted concrete beams [Neubauer and Rostasy, 1997]

The first zone corresponded to anchorage bonding at the end of the plate, the second zone described regions of mixed shear force and moderate bending, and the last zone was used to describe regions of primarily high bending moments with low shear forces.

Zone I: Anchorage Bonding: Within the zone of anchorage bonding, the plate receives its share of the tensile force through high bond stresses in the adhesive line, as shown in Fig. 2.17. These stresses can initiate debonding from the end of the plate, which propagates parallel to the plane of the laminate, typically near the adhesive-concrete interface or along the flexural rebar layer.
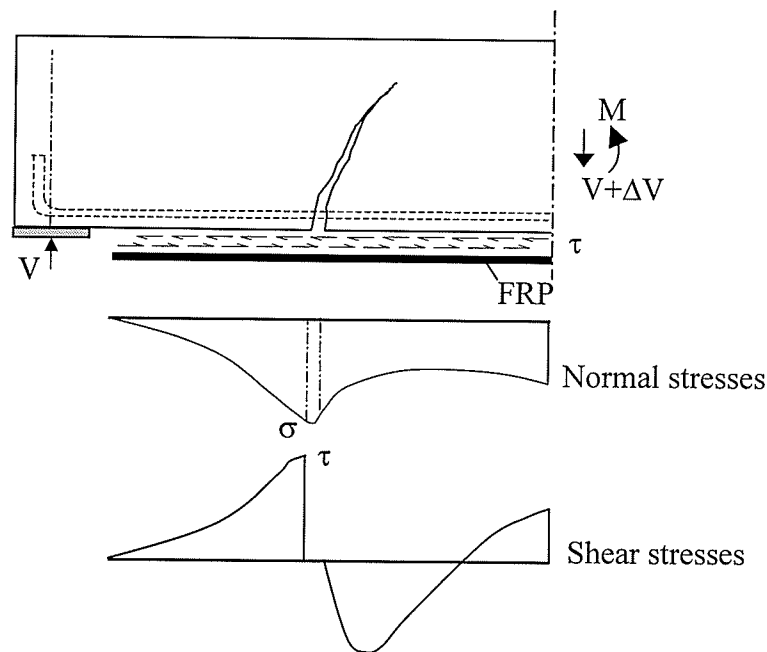
Fig. 2.17 Zone I: anchorage of plate end [Neubauer and Rostasy, 1997]

Anchorage debonding was the failure mode of beams strengthened with GFRP, even after external clamps were added in the anchorage zone [Saadatmanesh and Ehsani, 1990]. Anchorage failures were also observed in retrofitted concrete beams made with steel-fibre reinforced concrete [Arduini et al., 1994]. A major study of anchorage failures was conducted where a high-speed camera captured frames of the anchorage failure process, as shown in Fig. 2.18 [Hankers, 1997].
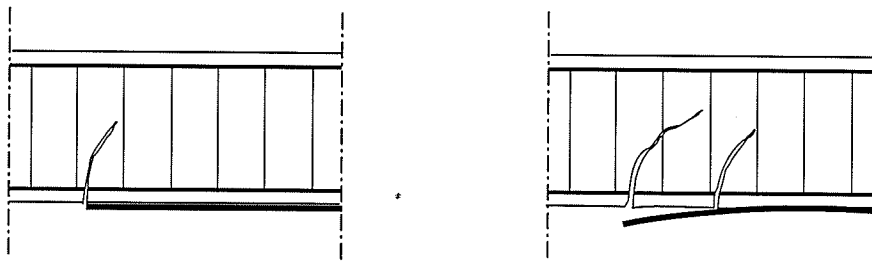

Fig. 2.18 High speed video clips of plate end zone failures [Hankers, 1997]

The elastic stress field at the termination point of the FRP material was analyzed by many researchers [Roberts, 1989; Ziraba et al., 1994; Malek et al., 1998]. The interfacial shear stresses between the FRP plate and adhesive were calculated by considering the equilibrium of an infinitesimal portion of the plate as shown in Fig. 2.19.
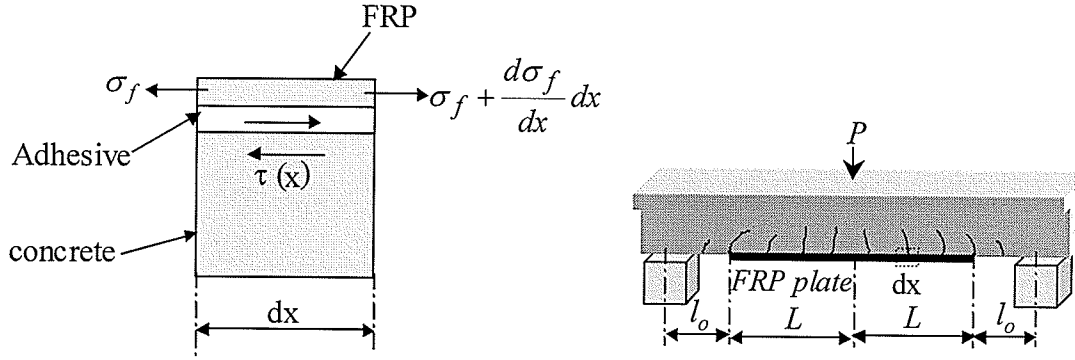

Fig. 2.19 Equilibrium of an infinitesimal portion of FRP strip/sheet

$$\frac{d\sigma_f(x)}{dx} = \frac{G_a}{t_f}\left(\frac{\partial u}{\partial y} + \frac{\partial v}{\partial x}\right) \qquad (2.5)$$

where u and v are horizontal and vertical displacements in the adhesive layer, σ_f is the longitudinal stress in the FRP plate, t_f is the thickness of the FRP plate and G_a is the shear modulus of the adhesive. Differentiating Equation 2.5 with respect to x and expressing $\partial^2 u/\partial x \partial y$ in terms of interfacial strains results in:

$$\frac{d^2\sigma_f(x)}{dx^2} = \frac{G_a}{t_a t_f}\left(\varepsilon_f - \varepsilon_c\right) \qquad (2.6)$$

where $\varepsilon_f = \sigma_f/E_f$ and $\varepsilon_c = f_c/E_c$ assuming uncracked section for concrete, E_f and E_c are the elastic modulus of the FRP plate and concrete, respectively, f_c is the tensile stress in the bottom of the concrete beam and t_a is the thickness of the adhesive. The solution of Equation 2.6 is given by:

$$\sigma_f(x) = c_1 \sinh(\omega'x) + c_2 \cosh(\omega'x) + b_1 x^2 + b_2 x + b_3 \qquad (2.7)$$

where:

$$\omega'^2 = \frac{G_a}{t_a t_f E_f}$$

$$b_1 = \frac{\overline{y} a_1 E_f}{I_{tr} E_c}$$

$$b_2 = \frac{\overline{y} E_f}{I_{tr} E_c}(2a_1 l_o + a_2)$$

$$b_3 = \left(\frac{\overline{y} E_f}{I_{tr} E_c}(a_1 l_o^2 + a_2 l_o + a_3) + 2b_1 \frac{E_f t_f t_a}{G_a}\right)$$

$c_{1,2}$ are constants solved for given boundary conditions, $\overline{y}$ is the distance from the FRP plate to the section neutral axis, I_{tr} is the transformed moment of inertia of the strengthened section, the variables a_i are used to express the applied moment by $M(x) = a_1 x^2 + a_2 x + a_3$ and l_o is the unplated length as shown in Fig. 2.19. The derivative of Equation 2.7 gives the interfacial shear stress, which reaches its maximum intensity at the termination of the plate.

$$\tau(x) = \frac{d\sigma_f(x)}{dx} t_f = t_f\left[c_1 \omega' \cosh(\omega'x) + c_2 \omega' \sinh(\omega'x) + 2b_1 x + b_2\right] \qquad (2.8)$$

These types of solution assume linear elastic behaviour of both concrete and adhesive and a linear strain distribution over the full depth of the section. Consequently, such type of analysis is limited to regions of low damage, such as inflection points or areas of zero moment where the normal stresses are generally low. Furthermore, the analysis can only be used to evaluate the initiation of constituent failure; in non-linear softening materials such as concrete this may not coincide with failure of the entire system, which is

influenced by size effects of the structure. Moreover, the elastic solution can not be used to represent scenarios with crack tips, such as peeling from existing cracks in a concrete beam. Other analyses of anchorage zone behaviour were concentrated on a shear-lap type specimens, shown in Fig. 2.20, where the bond was subjected to pure shear loading [Chajes et al., 1996; Maeda et al., 1997].
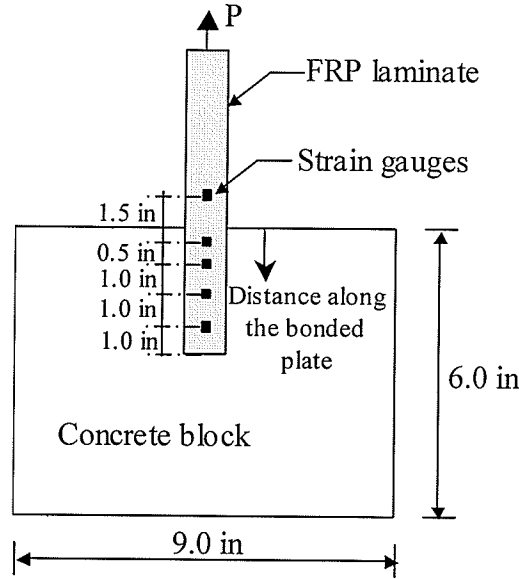

Fig. 2.20 Investigation techniques of bond integrity through shear-lap type specimens
[Chajes et al., 1996]

In this type of analysis, concrete prisms were bonded with a lap joint. During the action of the load P, the load joint displaced a distance δ, and the crack increased by an amount da. The work done by the external force, W, is given by:

$$W = \frac{1}{b_f}\left(P\frac{d\delta}{da} - \frac{dU_e}{da} \right) \tag{2.9}$$

where b_f is the width of the FRP plate and U_e is the elastic energy.

$$U_e = \frac{1}{2}P\delta = \frac{1}{2}P^2 C \tag{2.10}$$

Using the chain rule and solving for the load P results in:

$$P = \sqrt{2 \; b_f \; W \; \frac{\partial a}{\partial C}} \qquad (2.11)$$

Using simple beam theory, the compliance $C = \dfrac{a}{2 \; b_f E_f \; t_f}$ is inserted into Equation

2.11, results in:

$$P = 2 \; b_f \sqrt{E_f \; t_f \; W} \qquad (2.12)$$

where t_f and E_f are the thickness and modulus of elasticity of the FRP plate, respectively. This approach was used to derive maximum plate forces and anchorage lengths, which were compared to experimental results. The analysis provided a maximum allowable force in the laminate at a certain distance from the end of the laminate known as the development length. Lap-shear analysis also assumed that the materials were homogeneous, isotropic and linear elastic. Therefore, these approaches are also applicable to regions of low damage. Furthermore, the geometry subjected the adhesive to shearing force only. As a result, the analysis is limited to regions of constant forces where uniform force transfer is possible over the length of anchorage.

Zone II: Mixed Bending and Shear: The second zone describes regions of mixed shear force and moderate bending. In this region, bond stresses are caused by variation of bending moments along the strengthened member and by force transfer at cracks. Less experimental work is available on this type of debonding failure. Kaiser (1989) concluded that vertical crack opening displacements in this region could initiate debonding. This process was studied more in depth with relation to shear capacity by Deuring (1993). Shear peeling and interaction between shear peeling and flexural peeling

with steel plated members was studied with simply supported reinforced concrete beams [Oehlers, 1992]. Interaction between debonding due to shear forces and moment forces was quantified by a moment-shear interaction equation for design and was given by Oehlers and Moran (1990) as:

$$\frac{M_p}{M_u} + \frac{V_p}{V_u} \leq 1.17 \tag{2.13}$$

where $M_p < M_u$ is the ratio of the applied moment to peeling moment and $V_p < V_u$ is the ratio of the applied shear to the ultimate shear capacity of the beam. This type of approach did not incorporate any capabilities for analysis of different peeling failures, where the interaction of these processes with flexural behaviour might differ from the type of failures observed in the experimental program used to derive this empirical value. Thus, this analysis is limited to retrofit scenarios with parameters similar to that of the tested specimens.

Zone III: Bending zone: This zone describes areas of high bending moments and relatively low shear forces. Bonding stresses are mainly caused by force transfer at flexural cracks. Meier et al. (1992) concluded that cracks in this region do not have a significant influence on the delamination process. Analysis of pure flexure-type cracks was conducted by Hankers (1997), where the stress distribution around the crack was derived for delamination originating from the crack. The influence of bonded laminates on the development of flexural cracks was studied by Kaiser (1989) and was concluded to not significantly affect the carrying capacity of the system.

Arduini et al. (1997) performed a discrete element analysis to predict the flexural behaviour of reinforced concrete members. The proposed model took into account the mechanical properties of the constituent materials and the characteristics of the concrete-to-FRP interface. At the concrete-adhesive interface of each segment, the shear stress τ, was generated from the difference between the normal forces N acting on the FRP reinforcement at the two ends of the segment. The distribution of the shear stress was considered to be triangular in shape. The shear stress, τ, for the generic segment was equal to:

$$\tau = \frac{2\left(\Delta N_{j+1} - \Delta N_j\right)}{b\,dx} \tag{2.14}$$

where b is the beam width and dx is the length of the segment.

In this model, the failure mechanisms that can be detected are:

- FRP rupture when the ultimate tensile strain of the material is reached;

- shear failure in concrete when the shear stress τ reaches τ_{max};

- tensile fracture of concrete when the maximum tensile stress reaches the tensile strength of the concrete; and

The analysis carried out by Arduini et al. was also compared to a numerical solution using non-linear finite element analysis and showed good agreement with the experimental results. Arduini et al. concluded that changing the thickness of the FRP, changing the bonded length, or adding shear reinforcement significantly modifies the crack distribution along the beam and changes the failure mechanism. A simple solution to model the behaviour of the retrofitted system was provided. However, the model did

not consider the effect of diagonal shear cracking, which would affect the realistic bond stress distribution of the retrofitted system.

Finite element models of strengthened concrete beams were performed by Quantrill et al. (1995). The adhesive layer and the FRP strip were each represented only by one element through the thickness. Although the overall behaviour of the member was well predicted by the model, it could not provide a suitable description of the edge stresses. It should be noted that an accurate analysis of the edge zone using the finite element method could be problematic due to the singular character of the stress distribution at that edge as shown in Fig. 2.21.
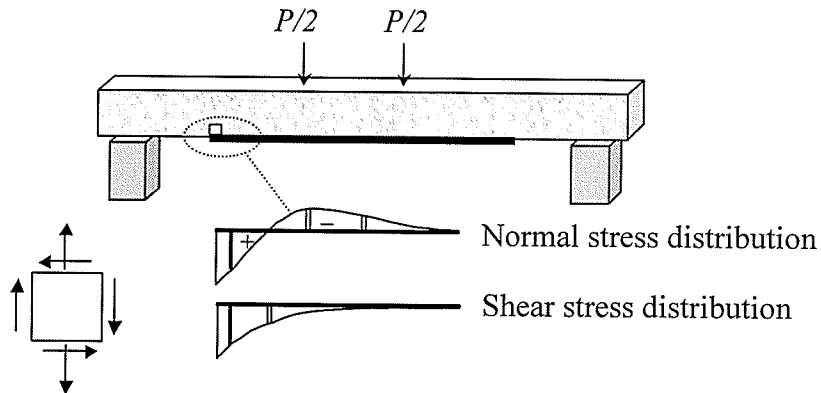
Fig. 2.21 Interlaminar shear and normal stress concentration at edges

This singularity might lead to divergence of the numerical solution with refinement of the finite element mesh. Various analytical models of strengthened concrete beams used the elastic foundation concept in which the adhesive was modelled as continuously distributed horizontal and vertical springs. Karam (1992) used a one-parameter elastic foundation model consisted of shear springs only, thus neglecting vertical peeling stresses and bending effects in the FRP strip.

Models based on the elastic foundation approach have two inherent inefficiencies. First is the lack of fulfillment of point equilibrium within the thickness of the adhesive layer, because no interaction between the distributed shear and vertical springs exist. Second is the inability to control the fulfillment of the boundary and continuity conditions concerning the shear stress within the adhesive layer and at edges. These two obstacles, accompanied with the presumed linear deformations pattern through the thickness of the adhesive layer and the uniform shear and peeling stresses distribution through the thickness, yields solutions that roughly approximate the edge stresses and in many cases conservative.

A different approach that overcame these obstacles was developed by Rabinovich and Frostig (2000) in which a closed-form high-order analytical solution for the analysis of concrete beams strengthened with externally bonded FRP strips was proposed. The model was based on equilibrium and deformation compatibility requirements in and between all parts of the strengthened beam, i.e., concrete beam, FRP strip and the adhesive layer. The governing equations representing the behaviour of the strengthened beam along with the appropriate boundary and continuity conditions were derived and solved with closed form analytical solutions. In the mathematical formulation of the model, the concrete member was described by an elastic linear beam element governed by the classical beam theory (Bernoulli-Euler assumption). The FRP strip was modelled as an ordinary laminated beam using the lamination theory. The adhesive layer was assumed to be homogeneous, linear elastic and orthotropic with negligible longitudinal stiffness. The composite infinitesimal element is shown in Fig. 2.22.
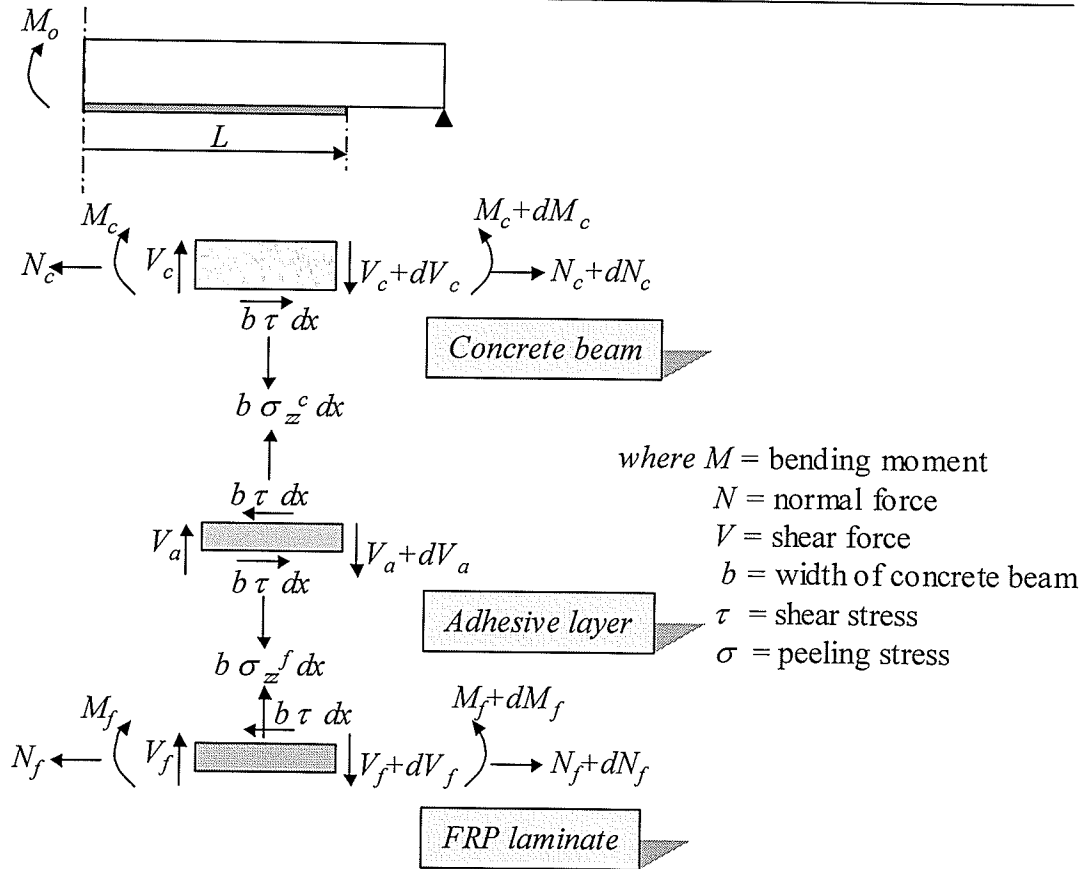
M_o

L

M_c N_c V_c V_c+dV_c M_c+dM_c N_c+dN_c

$b\,\tau\,dx$

$b\,\sigma_z^c\,dx$

$b\,\tau\,dx$

V_a $b\,\tau\,dx$ V_a+dV_a

$b\,\sigma_z^f\,dx$

M_f N_f V_f $b\,\tau\,dx$ V_f+dV_f M_f+dM_f N_f+dN_f

Concrete beam

Adhesive layer

FRP laminate

where M = bending moment
N = normal force
V = shear force
b = width of concrete beam
τ = shear stress
σ = peeling stress

Fig. 2.22 Infinitesimal subelements of concrete, adhesive and FRP
[Rabinovich and Frostig, 2000]

The material denoted by c represented the concrete beam, whereas the material denoted by a represented the adhesive and, finally f denoted the FRP laminate. The mathematical formulation of the strengthened beam was derived using the principle of virtual work and compatibility of deformations. The shear was assumed to be constant through the thickness of the adhesive. The vertical and longitudinal displacements were assumed to have quadratic and cubic patterns, respectively. The closed-form solution consisted of a third order polynomial and eight exponential functions. Due to the exponential character of the solution, the algebraic set of equations solved for the unknown constants involved

extremely large and small numbers, which were far beyond the ability of ordinary computer codes and hardware floating point accuracy [Rabinovich and Frostig, 2000].

(c) Fracture Mechanics Approach

Quantitative studies of FRP delamination through fracture mechanics concepts offer great potential in understanding the role of relative materials and design properties on the overall failure process through delamination. Interfacial fracture mechanics can be used to characterize bimaterial notches, crack tip stresses, crack propagation, and crack path evaluation, as illustrated in Fig. 2.23. However, the use of interfacial fracture mechanics with laminated concrete structures has remained relatively limited.

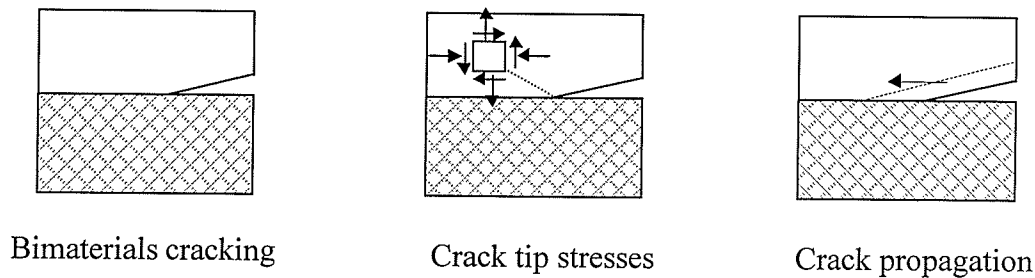Bimaterials cracking   Crack tip stresses   Crack propagation

Fig. 2.23 Functions of interfacial fracture mechanics

Hamoush and Ahmad (1990) used a fracture mechanics approach to investigate strain energy release rates for interfacial cracks in unreinforced, steel-plated reinforced concrete beams. The thickness of the adhesive had a little influence on the debonding process. A finite element fracture-based investigation was also used by Wu et al. (1997) to model initially notched concrete specimens retrofitted with FRP laminates. It was concluded that the strength of retrofitted concrete structures could be governed by interfacial fracture. Additionally, bimaterial elasticity at the interface between the constituent materials could

2. Strengthening of Reinforced Concrete Structures with FRPs

be characterized to describe the singularity of the stress field at the interfacial notches in the system.

Holzenkampfer (1994) investigated the bond between externally bonded steel plates and concrete using non-linear fracture mechanics (NLFM), The modified expression proposed by Niedermeier (1996) calculated the debonding load, P_{max}, using:

$$P_{max} = \begin{cases} 0.78\,b_s\,\sqrt{2G_f E_s t_s} & \text{if } L \ge L_e \\[2ex] 0.78\,b_s\,\sqrt{2G_f E_s t_s}\,\dfrac{l}{L_e}\left(2 - \dfrac{l}{L_e}\right) & \text{if } L < L_e \end{cases}$$

(2.15)

where L is the bonding length; E_s and t_s are the modulus of elasticity and the cross-sectional thickness of the externally bonded steel plate, respectively; G_f is the fracture energy; b_s is the width of the steel plate; and L_e is the effective bond length and can be expressed by:

$$L_e = \sqrt{\frac{E_s t_s}{4 f_{ct}}} \quad (mm)$$

(2.16)

where f_{ct} is the splitting tensile strength of concrete in MPa.

Taljsten (1996) applied a linear and non-linear fracture mechanics to the plate bonding technique and derived a series of formulae based on linear shear stress-slip relationship and linear elastic assumption of the materials as shown in Fig. 2.24a.
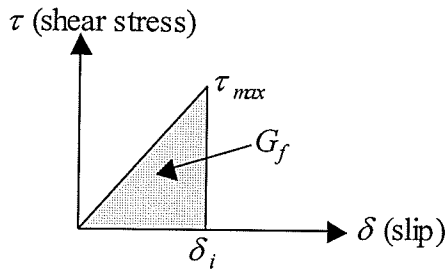
τ (shear stress)

Fig. 2.24a Linear shear stress-slip relationship [Taljsten, 1996]
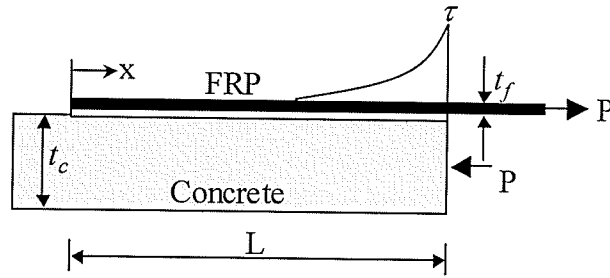
Fig. 2.24b Shear stress transfer in a simple shear test [Taljsten, 1996]

The derived expression for the interfacial shear stress was given as:

$$\tau(x) = \frac{P\varpi \cosh(\varpi x)}{b_f \sinh(\varpi l)}, \quad 0 \le x \le L \tag{2.17}$$

where L is the bonding length; $\varpi^2 = \dfrac{Ga}{t_a}\left(\dfrac{1}{E_c t_c} + \dfrac{1}{E_f t_f}\right)$; $E_c t_c$ and $E_f t_f$ are the stiffnesses of

concrete and FRP, respectively; G_a is the shear modulus of the adhesive; t_a is the thickness of the adhesive; and b_f is the width of the FRP plate. A graphical representation of the shear stress distribution is shown in Fig. 2.24b. The shear stress at the end of the specimen where the force was introduced can be obtained from Equation 2.17 as:

$$\tau = \sqrt{\frac{G_a}{t_a E_f t_f}} \frac{P}{b_f} \tag{2.18}$$

Using a bilinear shear stress-slip relationship as shown in Fig. 2.25a, Brosens and Van Gemert (1998) derived the expression for calculating the maximum load as a function of the bonded length:

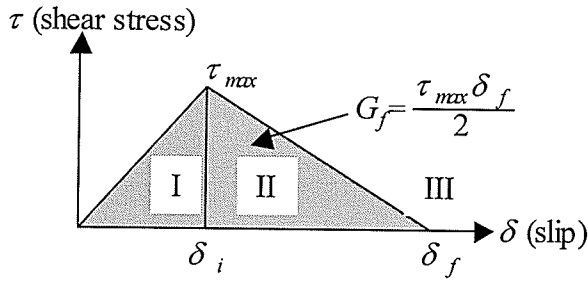$$P = \frac{E_f A_f \lambda \omega \delta_f \sin[\lambda \omega(1-x)]}{1+n\gamma} \tag{2.19}$$

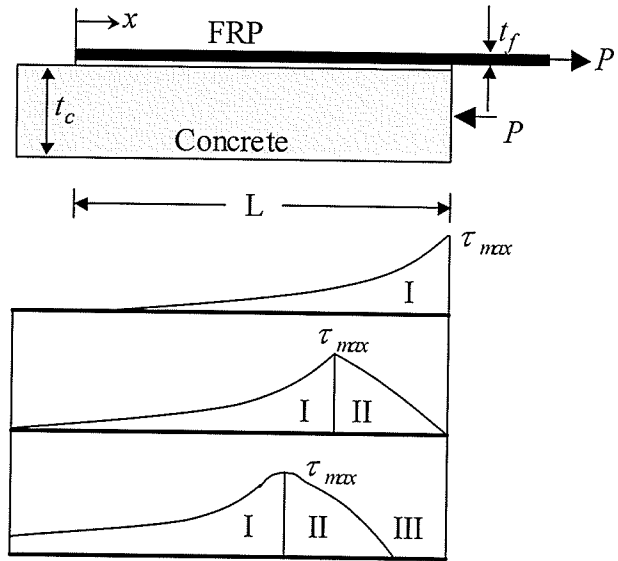Fig.2.25a Bi-linear shear stress-slip relationship [Brosens and Van Gemert, 1998]

Fig.2.25b Shear stress transfer for different stages in a simple shear test [Brosens and Van Gemert, 1998]

where:

$$\lambda = \sqrt{\frac{\delta_i}{\delta_f - \delta_i}} \; ; \; \omega = \sqrt{\frac{\tau_{max}(1+n\,\gamma)}{\delta_i E_f b_f}} \; ; \; tanh(\omega x) = \lambda tan\left[\lambda \omega (1-x)\right] \; ; \; n = \frac{E_f}{E_c} \, and \, \gamma = \frac{A_f}{A_c} \; ;$$

δ_i is the slip at τ_{max} ; δ_f is the maximum slip; E_f, A_f and b_f are elastic modulus, cross-sectional area, and width of FRP plate, respectively; E_c and A_c are the modulus of elasticity and cross-sectional area of concrete, respectively. The shear stress transfer for different stages is illustrated in Fig. 2.25b. Provided that the bonded length was larger than the effective bond length, the equations for determining the maximum load in both linear and bilinear stress-slip relationships was expressed in the terms of the fracture energy, G_f:

$$P_{max} = b_f \sqrt{2 G_f E_f t_f} \qquad (2.20)$$

where G_f is the area under the τ-δ curve for the linear relationship as illustrated in Fig. 2.24a or the area of the complete τ-δ curve for the bilinear relationship as illustrated in Fig. 2.25a.

Neubauer and Rostasy (1997) conducted a series of double shear tests on CFRP-to-concrete bonded joints. Test results indicated that for both concrete fracture and FRP delamination, the shear stress-slip relationship could be expressed by the triangular model shown in Fig. 2.25a. A modified model to Holzenkampfer (1994) was proposed. The model was applicable to both steel and FRP plates.

Wu and Niu (2000) pointed out that the bond strength is responsible for the initiation of debonding fracture and that propagation of debonding is governed by the interfacial fracture energy through a numerical simulation with non-linear fracture mechanics. Wu and Niu assumed that the interfacial fracture energy consumed for ultimate debonding failure should be a characteristic material parameter concerned with interfacial behaviour along the FRP-concrete interface, concrete strength and debonding position. When a flexural crack occurs in the concrete, a high shear stress concentration will be induced and subsequently an interfacial crack will be initiated. Whether the interfacial crack propagates or not is mainly dependent on the fracture energy. Once the crack propagates to a certain distance, an unstable propagation occurs and the ultimate debonding failure results. Wu and Niu (2000) observed that many flexural cracks were distributed along the FRP strengthened beams before the occurrence of the debonding failure.

Yuan et al. (2001) studied the bond strength between FRP and concrete using linear and non-linear fracture mechanics. The same equation as proposed by Taljsten (1996) was derived but accounted for the influence of the widths of the FRP plate and the concrete

member. Yuan et al. solved the NLFM equations for five different shear stress-slip relationships shown in Fig. 2.26.
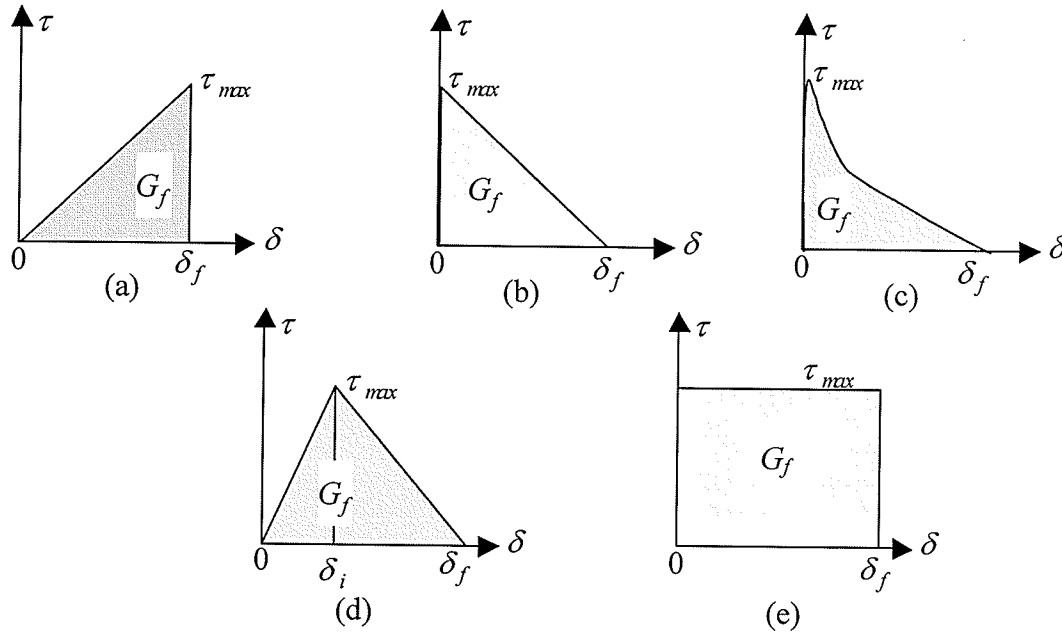

Fig. 2.26 Shear-slip models used in Yuan et al. (2001)

Yuan et al. concluded that the linearly ascending and then descending relationship, shown in Fig. 2.26d is the closet to reality.

2.4.4.2 Applicability of Delamination Models

Chen and Teng (2001) assessed the performance of some of the existing delamination models, reviewed in the previous section. Fracture mechanics based models were not included in the assessment. Empirical models proposed by Hiroyuki and Wu (1997) and Tanaka (1996) were found not to fit the experimental data statistically. The models extremely underestimated the bond strength and led to a very large scatter. The poor performance of the models was attributed by Chen and Teng to the effective bond length, which was not considered in the analysis. The model proposed by Neubauer and Rostasy

(1997) showed a reasonable performance. On average, the model overestimated the experimental results by 22 percent.

2.5 Existing Design Procedures for Delamination

2.5.1 General

Following the successes of many projects involved strengthening with FRP materials, infrastructure owners, regulators, contractors, and professional organizations began to consider FRPs in more retrofitting projects. However, widespread use is restrained by the lack of design codes. This section reviews the most widely available design procedures and identifies the merits and deficiencies of each publication.

2.5.2 Professional Organizations

2.5.2.1 American Concrete Institute

The technical committee 440 of the American Concrete Institute is currently preparing a design guideline document "Guide for the Design and Construction of Externally Bonded FRP Systems for Strengthening Concrete Structures". Sections of the guidelines cover properties of the retrofit systems, evaluation of existing structures, structural design, shipping, storage, handling, quality control and maintenance. The evaluation of existing structures section covers important criteria for field inspection and assessment of existing load capacity. The recommendations for design of columns, flexural members and walls are based on ACI-318 requirements. Failure design recommendations state to avoid brittle failures such as anchorage, delamination, and shear failure. To avoid delamination failures, the guidelines recommend that the ultimate design tensile strain of the FRP at

failure should be less than $\kappa_m \varepsilon_{fu}$ where κ_m is a modification factor less than 0.9 and ε_{fu} is the rupture strain of the FRP. The term κ_m is expressed in Equation 2.21.

$$\kappa_m = \begin{cases} 1 - \dfrac{nE_f t_f}{428,000} & for \quad nE_f t_f \leq 214,000 \\ \dfrac{107,000}{nE_f t_f} & for \quad nE_f t_f > 214,000 \end{cases} \qquad (2.21)$$

where n is the number of FRP layers, E_f (MPa) and t_f (mm), are the modulus of elasticity and thickness of the FRP, respectively. Equation 2.21 term recognizes that laminates with greater stiffness are more prone to delamination. Consequently, as the stiffness of the laminate increases, the strain limitation becomes more severe. The term κ_m is based on a general recognized trend and on the experience of engineers practicing the design of externally bonded FRP systems. Research work is currently in progress at the Centre for Infrastructure Engineering Studies (CIES) at the University of Missouri-Rolla to develop construction specifications and a process control manual for FRP bonded to concrete structures.

2.5.2.2 The Canadian Network of Centres of Excellence

The Canadian Network of Centres of Excellence on Intelligent Sensing for Innovative Structures, ISIS Canada, published "Strengthening Reinforced Concrete Structures with Externally-Bonded Fibre Reinforced Polymers" [ISIS Canada Design Manuals, 2001]. The document presents the design procedures that have been developed and validated for strengthening of concrete structures with FRPs. The basic equations and methodology are presented and examples of applications are given to illustrate the various design

procedures. Anchorage provisions are provided. The anchorage length is evaluated using a maximum allowable bonding stress.

$$L_d = \frac{b_f}{b} \frac{E_f \varepsilon_{fu} t_f}{\tau_{max}} \tag{2.22}$$

$$\tau_{max} = k\sqrt{f'_c} \tag{2.23}$$

where L_d is the development length of the FRP reinforcement; b_f is the width of the externally bonded FRP reinforcement; b is the width of the concrete section; E_f is the modulus of elasticity of the FRP reinforcement; t_f is the thickness of the FRP sheets and/or strips; ε_{fu} is the rupture tensile strain of the FRP reinforcement; τ_{max} is the bond strength of the FRP reinforcement; f'_c is the compressive strength of the concrete; k is a proportionality factor depends on the type of the FRP reinforcement, modulus of rupture of concrete and the type of the joint application (bending or shear). A typical value of k of 0.184 is recommended in the manual based on test results of Bizindavyi and Neale, 1999. FRP specific issues such as peeling are not addressed.

2.5.2.3 German Institute for Construction Technology

The German Institute for Construction Technology published a document in 1998, which acted as a certification for FRP products and their applications in Germany [Deutches Insitut fur Bautechnik, 1998]. General provisions for flexure, shear, and anchorage were provided. Anchorage was computed through an allowable anchorage force along a critical development length. The code also recommended shear strengthening through steel stirrups in cases of insufficient shear capacity. Delamination failures were not addressed.

2.5.2.4 Japan Concrete Institute and Japan Society of Civil Engineers

The Japanese Concrete Institute published "Technical Report on Fibre Reinforced Concrete, 1997". The publication provided guidelines for evaluating the contribution of external FRP reinforcement to the shear capacity of retrofitted concrete systems. The Japanese Society of Civil Engineers published JSCE 307 Subcommittee on retrofitting design. Unfortunately, the publication is available in Japanese only.

2.5.2.5 International Conference of Building Officials

The International Conference of Building Officials published AC125 "Acceptance Criteria for Reinforced Concrete and Unreinforced Masonry Strengthened using Fibre Reinforced Composite Systems" [ICBO ES, 1997]. In this publication, FRPs were treated as additional steel reinforcement; specific design equations were provided for flexural strength, shear strength and anchorage. Anchorage was evaluated through a maximum allowable bonding stress, which was used to evaluate a minimum laminate length. However, FRP specific issues such as peeling were not addressed.

2.5.3 Retrofit System Manufacturers

2.5.3.1 Sika

Sika manufactures the Sika Carbodur systems and published the Sika Carbodur manual "Sika Corporation, 1997". The design guidelines provided detailed equations for flexural strengthening of beams and slabs. A computational spreadsheet was provided to aid the designer. No provisions were provided for shear strengthening. However, the procedures considered both delamination and anchorage. Delamination was considered through a

critical shear force that caused vertical slip at concrete crack tips. The manual assumed that the ratio of vertical to horizontal displacements remained constant. The provided equation did not take into account local fracture mechanisms at the crack tip. Also the use of laminate strains relative to a crack opening displacement for evaluation of dowel action did not account for other processes where delamination could occur due to degradation or incompatible materials. Consequently, based on the empirical nature of this approach, its application in the field is limited.

2.5.3.2 MBrace Composite Strengthening Systems

MBrace manufactures high strength unidirectional CFRP and GFRP sheets and published "MBrace Composite Strengthening System Design Guide, 1998". The guide addressed strengthening of concrete structures using externally bonded CFRP and GFRP reinforcement. The guide was made to cover various types of strengthening that were developed and tested for use in construction. This included flexural strengthening, shear strengthening and guidelines for improving the ductility of compression members. Design provisions for using the system to strengthen unreinforced, conventionally reinforced, and prestressed concrete structures were also provided. However, the guide did not provide any information regarding the delamination process.

2.5.3.3 S&P Composite Reinforcing Systems

S&P Composite Reinforcing Systems manufactures CFRP laminates and sheets as well as GFRP sheets. The design guidelines published by the company evaluated the contribution of external FRP reinforcement to the flexural capacity of retrofitted concrete

systems. The maximum elongation limit for design of CFRP laminates was restricted to 0.6-0.8 percent to avoid peeling of the FRP reinforcement based on experimental results conducted by other researchers.

2.5.4 Independent Researchers

Many researchers proposed design guidelines in addition to the professional organizations and manufacturers reviewed above. The majority of the guidelines followed certain procedures along the lines of flexural and shear evaluation based on the ACI recommendations. Differences were often found in addressing anchorage and delamination issues [Malek et al., 1998]. Anchorage evaluation was addressed through a critical plate-epoxy-concrete interfacial stress value [Ziraba et al., 1994]. Furthermore, factors of safety involved in the design procedures were proposed by Kelly et al. (2000). However, a document outlining the use of available design and evaluation techniques including quantitative provisions for both delamination and anchorage is yet not available.

2.6 Bond Characteristics of FRP Rebars

2.6.1 General

Most of the early design guidelines have extended the methodologies developed for steel reinforced concrete structures to those reinforced with FRP rebars. However, many experimental studies have demonstrated that some key properties of the physical and mechanical behaviour of FRP rebars are qualitatively and quantitatively different from the well-known properties of steel bars [Cosenza et al., 1997; Katz, 2001]. Such

differences arise from the significant variations in the material properties as well as from the remarkable changes in the interaction mechanism between the reinforcement and the concrete matrix. This section presents an overview of the bond characteristics of FRP rebars, various parameters affecting the bond performance and different models proposed for the bond behaviour of FRP rebars.

2.6.2 Bond Mechanism

A first attempt to classify the bond mechanism of FRP rebars was conducted by Kanakubo et al. (1993). Two types of bond mechanisms were identified. The first mechanism was a friction-resistant type, while the second mechanism was a bearing-resistant type. According to Kanakubo et al., smooth bars exhibited the friction-resistant mechanism while ribbed FRP bars developed the bearing-resistant bond mechanism. Larralde and Silva (1993) tested GFRP bars with a spiral indentation. A friction-type bond mechanism was observed in all specimens. Larralde and Silva concluded that adhesion and friction were the primary components of the bond of FRP rebars to concrete. The same findings were reported by Benmokrane et al. (1996) from bond tests on GFRP bars. A bond mechanism involving both friction and mechanical interlock was proposed by Malvar (1994) based on testing two types of GFRP bars. The same observations were reported by Hattori et al. (1995). Based on analyzing extensive experimental results published in the literature, two different bond mechanisms were identified by Katz (2001):

- mechanical interlocking; and
- friction due to surface roughness.

2.6.3 Factors Affecting Bond Performance

Achillides et al. (1997) and Wang et al. (1999) studied the influence of various parameters, believed to affect the bond performance of FRP rebars. Their main findings are summarized below.

Rebar diameter: The average bond strength decreased as the diameter increased. Such a phenomenon was explained by the development of high shear stresses around the surface of the rod, which was more pronounced in large diameters.

Embedment length: The average bond strength decreased as the embedment length increased.

Modulus of elasticity: The comparison between FRP bars having different modulli of elasticity was difficult due to differences in the surface configuration. However, there was a trend for higher bond strength with higher modulus.

Concrete compressive strength: Bond strength was found to be slightly affected by the concrete compressive strength.

2.6.4 Bond-Slip Models

Several models have been developed to describe the bond behaviour of FRP rebars to concrete and its effect on the bond-slip relationship. The first modelling of the bond-slip relationship was given by Malvar (1994). Based on an extensive experimental research, Malvar proposed a refined model of the overall bond behaviour, depending on two empirical constants to be determined by curve fitting of the experimental data. The model is represented by Equation 2.24

$$\frac{\tau}{\tau_f} = \frac{F\left(\delta/\delta_f\right) + (G-1)\left(\delta/\delta_f\right)^2}{1 + (F-2)\left(\delta/\delta_f\right) + G\left(\delta/\delta_f\right)^2} \qquad (2.24)$$

where τ_f is the peak bond stress, δ_f is the slip at peak bond stress and F, G are empirical constants determined for each bar type. The well-known bond-slip model proposed by Eligehausen et al. (1983) for deformed steel rods was successfully applied to FRP bars by Faoro (1992) and Cosenza et al. (1997). The model represented the ascending branch of the bond-slip relation ship as follows:

$$\frac{\tau}{\tau_f} = \left(\frac{\delta}{\delta_f}\right)^{\alpha} \qquad (2.25)$$

where τ_f is the peak bond stress, δ_f is the slip at peak bond stress, τ is the average bond stress, δ is the slip at free end and α is a curve fitting parameter less than 1.0. The value of α proposed by Eligehausen et al. (1983) for steel bars was equal to 0.4. Cosenza et al. (1997) proposed an alternative analytical model and accounted for both ascending and descending branches in the bond-slip relationship. The model was extended later by Cosenza et al. (1999) and Focacci et al. (2000) for further applications. Achillides et al. (1997) used the finite element method to predict the bond-slip behaviour. The ascending branch of the bond-slip relationship was predicted quite well for both loaded and unloaded ends. Based on the above discussion, bond-slip models are beneficial to predict the structural behaviour of concrete members reinforced with particular types of FRP rebars. Bond behaviour of a new bar needs to be determined experimentally to establish the bond-slip relationship.

2.7 Strengthening of Reinforced Concrete Structures Using Near Surface Mounted FRP Reinforcement

The use of near surface mounted FRP rods/strips is a promising technology for increasing the flexural and shear capacity of deficient reinforced concrete members. Advantages of using near surface mounted FRP rods with respect to externally bonded FRP laminates/sheets are the possibility of anchoring the rods into adjacent members, and minimal installation time. Furthermore, this technique becomes particularly attractive for flexural strengthening in the negative moment regions of slabs and decks, where external reinforcement would be subjected to mechanical and environmental damage and would require protective cover which could interfere with the presence of floor finishes. The method used in applying the near surface mounted rods/strips is as follows: a groove is cut in the desired direction into the concrete surface. The groove is then filled half-way with epoxy paste. The FRP rod is then placed in the groove and lightly pressed. This forces the paste to flow around the rod and fill completely the space between the rod and the sides of the groove. The groove is then filled with more paste and the surface is leveled [De Lorenzis and Nanni, 2001].

In spite of the fact that the use of near surface mounted FRP rods for strengthening applications is very recent, near surface mounted steel bars have been used in Europe since 1947 [Asplund, 1949]. In 1947 while constructing a concrete bridge deck in Lapland, Finland, upper reinforcement bars were mounted on wooded chairs. Immediately after the concrete was poured, the foreman pulled these chairs out of the concrete and finished the surface to the exact height demanded by the drawings.

Increasing the negative moment capacity was accomplished by grouting additional bars in grooves cut with the aid of a diamond saw. Asplund (1949) carried out tests on concrete beams reinforced with steel bars and others with steel bars grouted into diamond-sawed grooves as shown in Fig. 2.27. Test results showed identical behaviour for both sets of specimens.

The same technique was used in strengthening the bridge deck slab as shown in Figs. 2.28a and 2.28b.
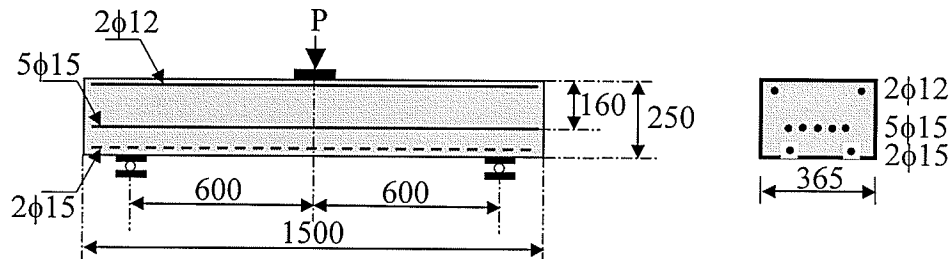
Fig. 2.27 Test specimens [Asplund, 1949]
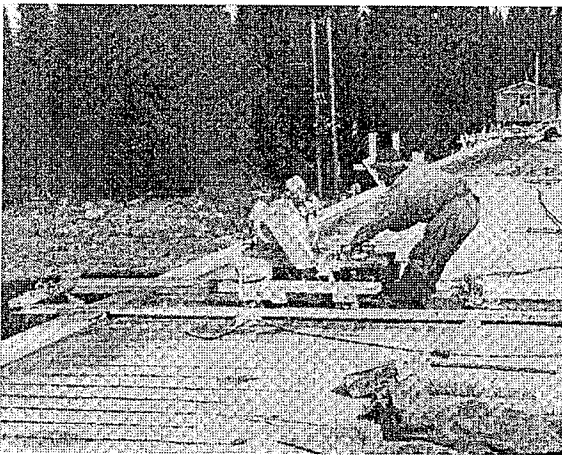
Fig. 2.28a Diamond sawing of bridge floor, Finland [Asplund, 1949]
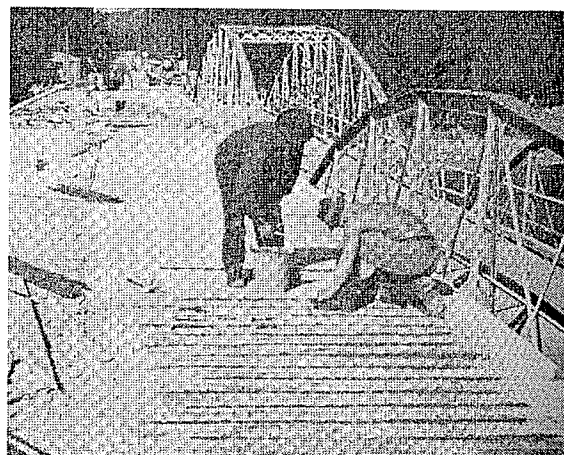
Fig. 2.28b Grouting of deformed bars [Asplund, 1949]

Currently FRPs can replace steel and adhesives can substitute cement mortar used in 1949. Very limited literature is available to date on the use of near surface mounted FRP rods/strips for structural strengthening. Blaschko (1999) carried out bond tests on CFRP

strips inserted inside grooves. The specimens consisted of a concrete block with a cross section of 200 mm by 200 mm and a total length of 900 mm. The concrete specimens consisted of CFRP strips inserted inside grooves and others with externally bonded CFRP strips to compare both techniques. The bond tests were conducted on double shear specimens as shown in Fig. 2.29. A gauged crack was implemented in the middle of the concrete block.
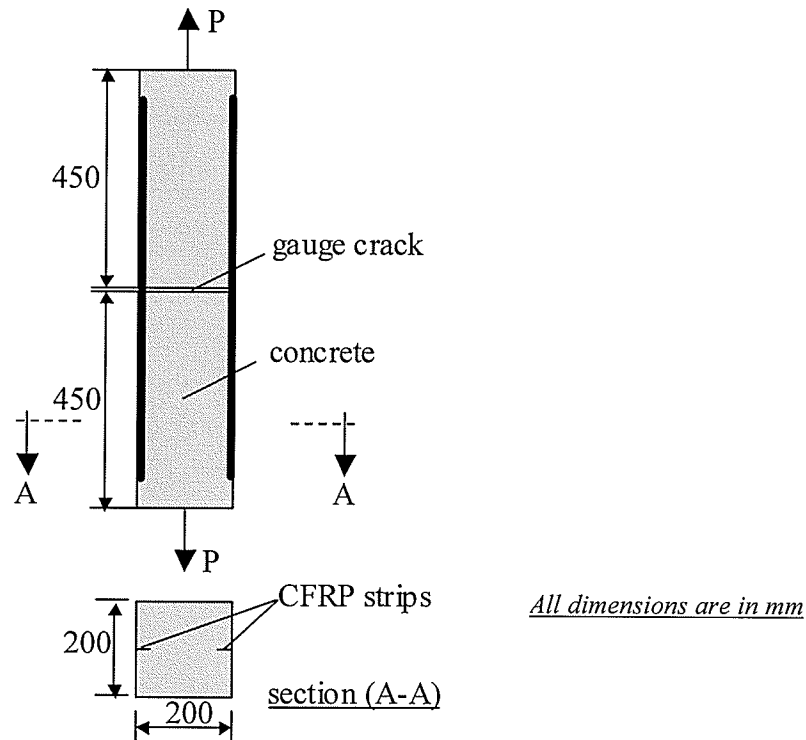
Fig. 2.29 Double shear specimens for bond test [Blaschko, 1999]

Test results showed that strengthening using near surface mounted CFRP strips had a greater anchoring capacity compared to externally bonded CFRP strips.

Gentile and Rizkalla (1999) conducted an extensive experimental program to investigate the feasibility of using near surface mounted GFRP bars for the flexural strengthening of timber bridge stringers. Based on test results, the Tourond Creek bridge constructed 39

years ago in Manitoba, Canada, was strengthened using GFRP bars. The bars were inserted longitudinally in specially constructed grooves in the stringers and adhered to the wood beams with an epoxy resin. Using this technology, the bridge is capable now to carry the current AASHTO design loads for less than 15 percent of the cost estimated to replace the bridge. The general layout of the bridge is illustrated in Fig. 2.30a. Installation procedures for near surface mounted GFRP bars are illustrated in Figs. 2.30b and 2.30c.
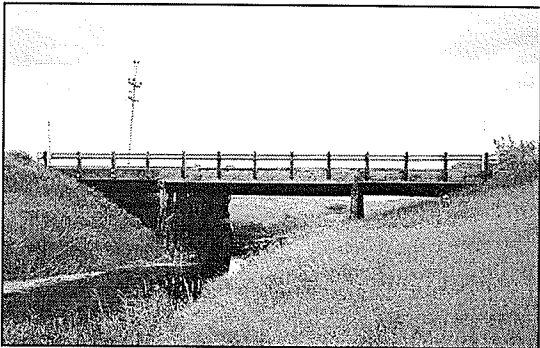
Fig. 2.30a The Tourond Creek bridge, Manitoba, Canada
[Gentile and Rizkalla, 1999]
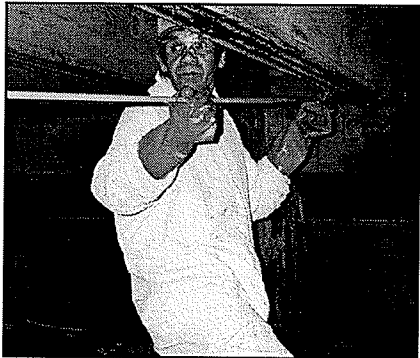
Fig. 2.30b Placing the bars inside the grooves
[Gentile and Rizkalla, 1999]

Fig. 2.30c Filling the grooves with epoxy
[Gentile and Rizkalla, 1999]

De Lorenzis and Nanni (2001) investigated the structural performance of simply supported reinforced concrete beams strengthened with near surface mounted GFRP and CFRP rods. Both flexural and shear strengthening were examined. Test results showed that the use of near surface mounted FRP rods is an effective technique to enhance the flexural and shear capacity of reinforced concrete beams. The beams strengthened in

bending showed an increase in capacity ranging from 26 percent to 44 percent over the control beam. For the beams strengthened in shear, an increase in capacity as high as 106 percent was achieved.

Nordin et al. (2001) conducted a pilot study on concrete beams strengthened with prestressed near surface mounted CFRP strips. Slots were sawn up in the concrete cover of the beams and the strips were bonded with epoxy as shown in Fig. 2.31.
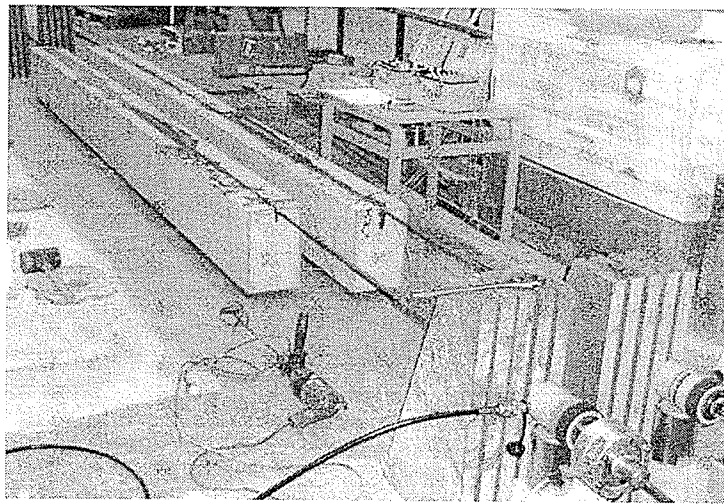
Fig. 2.31 Prestressing of near surface mounted strips [Nordin et al., 2001]

The strips were prestressed prior to bonding. The initial tensile strain in the strips was 0.2 percent with a loss of 2 percent during prestressing and 5 percent at the release of the prestress. Test results showed a substantial increase in cracking and failure loads for the strengthened specimens. Prestressing the strips did not influence the mode of failure. Compared to unstrengthened specimens, the prestressed beams had considerably smaller deflections at failure.

Recently, De Lorenzis and Nanni (2002) investigated the bond characteristics between near surface mounted FRP rods and concrete. The influence of the bond length, diameter and surface configurations of the rods was examined. Based on test results, the efficiency of using near surface mounted FRP rods was affected primarily by bond performance. The maximum measured tensile strain in the near surface mounted CFRP and GFRP bars at failure did not exceed 33 percent and 60 percent of the rupture strain of the bars, respectively. Three different failure modes were observed during testing, namely, pull-out of the FRP rod, cracking of the concrete surrounding the groove and splitting of the epoxy cover as shown in Fig. 2.32.
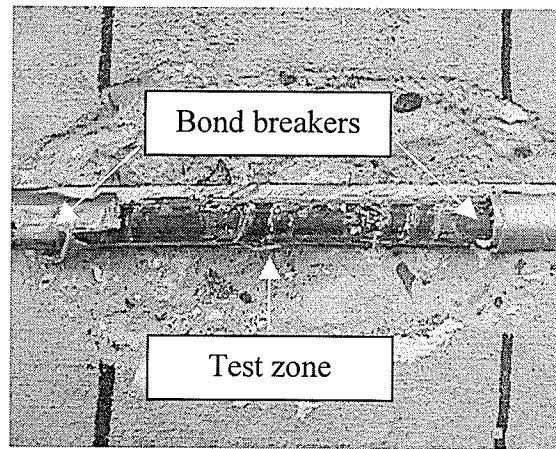
Fig. 2.32 Splitting of the epoxy cover [De Lorenzis and Nanni, 2002]

As the technology of near surface mounting emerges, the structural behaviour as well as bond characteristics of reinforced concrete members strengthened with near surface mounted FRP rods/strips needs to be investigated.

2.8 Field Applications

Strengthening of concrete structures using externally bonded FRP strips/sheets has been studied and has found its way to several field applications in the United States, Europe, Japan and Canada.

<u>United States</u>: The United States has had a long and continuous interest in fibre-based reinforcement for concrete structures since the 1930's. However, actual development and research activities into the use of these materials for retrofitting concrete structures started in the 1980's through the initiatives and the vision of the National Science Foundation (NSF) and the Federal Highway Administration (FHWA) who supported research at different universities and research institutions. Several companies are currently involved in the manufacturing, design and installation of different FRP strengthening systems in construction projects. FRP materials have quickly moved from the state-of-the-art to mainstream technology. New York's first use of FRPs for bridge repair consisted of strengthening a cracked cap-beam, which resulted in initial savings of $100,000 and was completed in two weeks. In 1994, carbon tow sheets were used on the Folk Road Bridge in Delware, Ohio to restrain transverse cracking in the prestressed box girders as shown in Fig. 2.33.
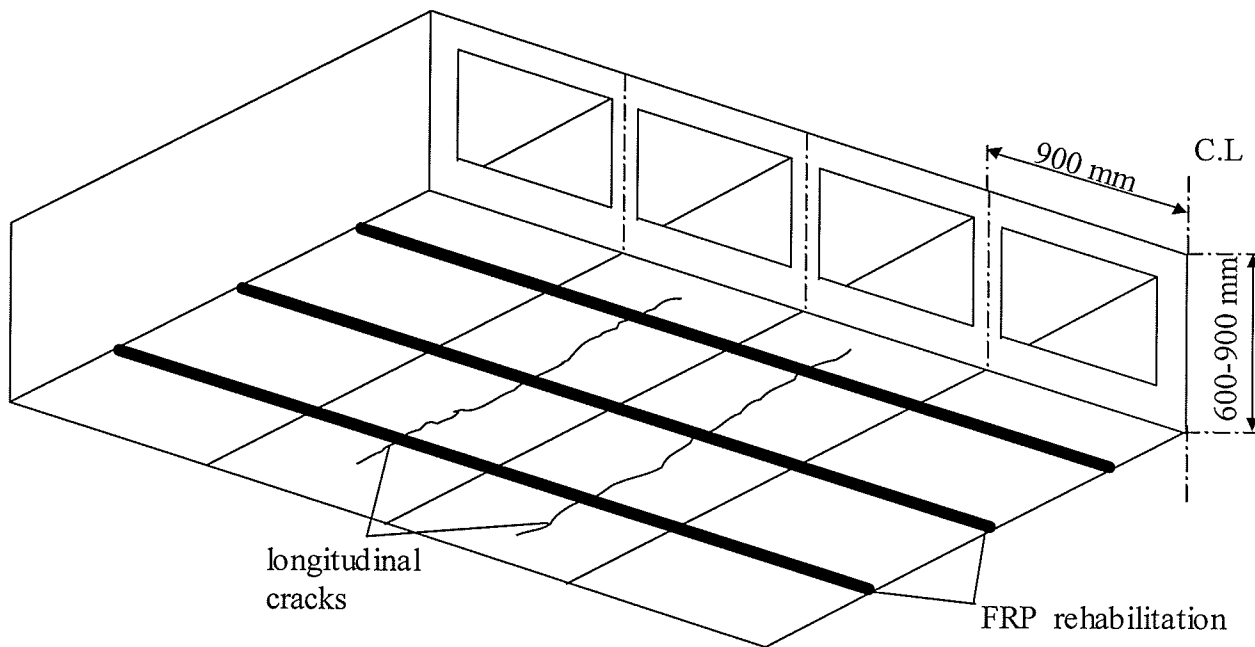
Fig. 2.33 Repair of prestressed box girders using FRP [Finch et al., 1994]

The Center of Infrastructure Engineering Studies (CIES) is currently investigating the possibility of strengthening and monitoring a structurally deficient reinforced concrete slab bridge and a prestressing concrete girder damaged by a vehicular impact at an interstate highway intersection. In Florida, several bridges have been retrofitted to increase their flexural and shear capacity, some of which were damaged due to impact, which caused failure of the prestressing tendons of the AASHTO girders.

Europe: Research on the use of FRPs in concrete structures began in Europe in the 1960's [Rubinsky, 1954; Wines et al., 1966]. In the field of strengthening with FRPs, pioneering work took place in the 1980's in Switzerland and resulted in successful practical applications [Meier, 1987; Meier and Kaiser, 1991]. Since the first FRP reinforced highway bridge in 1986, programs have been implemented to increase research and the use of FRP reinforcement in Europe. In Switzerland, studies at the Swiss

Federal Materials Testing and Research Laboratory (EMPA) concentrated on the use of CFRP for strengthening of beams. In Germany, the Technical University of Braunschweig concentrated on the use of GFRP for retrofitting beams and one-way slabs. One of the first field applications of FRP strengthening in Europe was performed in 1991 on the Ibach Bridge, a concrete box girder in Lucerne, Switzerland. GFRP was used to retrofit the Kattenbusch Roadway Bridge in Germany to reduce the steel stresses in the tendon couplers [Rostasy et al., 1992]. A pan-European collaborative research program {EUROCRETE} was established in 1993 and ended in 1997. The program was aimed at developing FRP reinforcement for concrete and included partners from the United Kingdom, Switzerland, France, Norway and the Netherlands.

Near surface mounted CFRP strips were used to rehabilitate the "Tobel Bridge" in Southern Germany in 1999. The bridge consists of prestressed, precast T-girders with a cast in place concrete deck. One of the girders was damaged by a truck, which crashed the web of that girder. A crack width of 0.5 mm was also observed. Experts demanded that shear reinforcement should be added to bridge the diagonal cracks. The company Bilfinger+Berger, Munich, Germany suggested embedding CFRP strips inside grooves for rehabilitating the bridge. CFRP strips of 20 mm by 1.2 mm were inserted inside 23 mm grooves. In total, 60 m of CFRP strips were used. The work was finished within two days [Blaschko, 1999].

Japan: Together with Europe, Japan developed the first FRP application for construction in the early 1980's. A sudden increase in the use of FRPs was attained after the 1995

Hyogoken Nanbu earthquake. Several field applications of externally bonded FRP reinforcement were executed in Japan including GFRP tow sheets used on the Hata Bridge to increase the transverse bending capacity as shown in Fig. 2.34a [Nanni 1995]. The application of the undercoat by means of roller brushing, followed by the adhesion of CFRP sheets is shown in Fig. 2.34b.
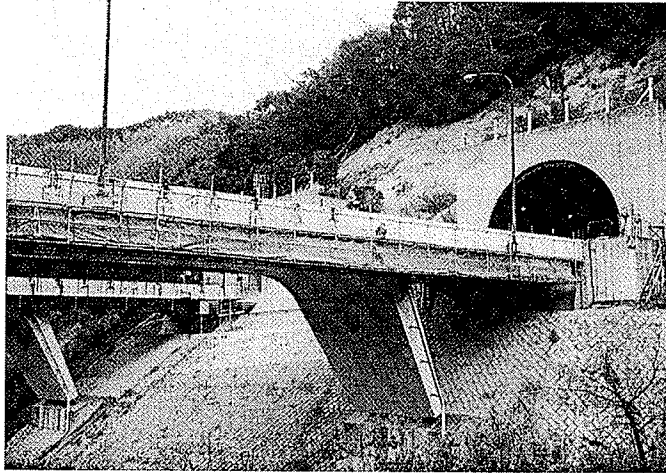

Fig. 2.34a Hata Bridge, Japan
[Nanni, 1995]

Fig. 2.34b Application of the resin coat
[Nanni, 1995]

The effectiveness of the strengthening method was demonstrated by conducting an on-site loading test that showed considerable reduction in the strain for the steel reinforcing bars. In the summer of 1994, the concrete lining of twin tunnels along the Yoshino Route on Kyushu Island were strengthened using externally bonded CFRP sheets. Cracking of the lining resulted from unexpected fluctuations in the underground water pressure. The purpose of the repair was to strengthen and stiffen the lining. It has been demonstrated that the use of externally bonded CFRP sheets is a viable method to improve the low rigidity shown by the tunnel lining against lateral pressure. No loss in tunnel cross-section area results from this type of repair. As of 1997, the Japanese led in FRP

reinforcement usage with 1,000 demonstration/commercial projects and FRP design provisions in their standard specifications of the Japan Society of Civil Engineers (JSCE 1997).

<u>Canada</u>: The use of FRPs for the repair and strengthening of concrete structures began in earnest in the late 1980's when the Canadian Society for Civil Engineering (CSCE) created a technical committee on the use of advanced composite materials in bridges and structures. In 1995, a national Network of Centres of Excellence on the use of advanced composite materials for bridges and structures was established (ISIS Canada). The following rehabilitation projects have been completed since then: Center Street Bridge (Alberta, 1999), Country Hills Boulevard (Alberta, 1999), Maryland Bridge (Manitoba, 2000), Riviere Noire Bridge (Quebec, 1998), Webster parkade (Quebec, 1996), Clement Bridge (Quebec, 1996) and John Hart Bridge (British Columbia, 2000). Most of these projects are being monitored to provide long-term data to evaluate the performance of the strengthening technique and to gain confidence in the design and overall quality assurance of the construction methods used for installation of the FRP.

2.9 Durability of FRP Strengthening Techniques

2.9.1 General

Although FRP composites perform extremely well in practice, there are heightened concerns related to their durability in the field as related to civil infrastructure applications. In these cases, FRP composites are exposed to harsh environmental conditions ranging from wide temperature fluctuations and humidity levels to rain and

snow. It is therefore imperative to examine the effects of these conditions, which could influence the performance of FRP materials and the bond between FRP and concrete. This section summarizes recent representative studies on durability of FRP rehabilitation techniques.

2.9.2 Wet—Dry Exposure

Chajes et al. (1995) tested 24 reinforced concrete beams strengthened with externally bonded AFRP, GFRP and CFRP sheets. The beams were 38 mm wide by 28 mm deep with a total length of 330 mm. A wet-dry cycle was completed by immersing the beams into a 4 percent CaCl solution for 18 hours, followed by 8 hours of drying at room temperature. Test results showed that AFRP and GFRP strengthened beams lost 36 percent of the unexposed strength, while CFRP strengthened beams lost 19 percent after 100 wet-dry cycles. Toutanji and Ortiz (1997) tested reinforced concrete beams strengthened with externally bonded GFRP and CFRP plates in a wet-dry environment. The beams were 50 mm wide by 50 mm deep with a total length of 300 mm. A wet-dry cycle involved immersion of the specimens into a 3.5 percent salt solution for 4 hours followed by 2 hours of drying at 35°C and 90 percent relative humidity. After 300 wet-dry cycles, failure was due to debonding of the FRP plates. The strength of the exposed specimens ranged from 3 to 33 percent of the unexposed strength. Ferrier et al. (1998) concluded that the shear modulus of the adhesive at the FRP-concrete interface is more critical for obtaining durable FRP retrofitted concrete members. With an exposure to 20°C dry environment, 80 percent decrease in shear modulus was observed. Mukhopadhyaya et al. (1998) reported that wet-dry cycles exposures had a significant

effect on the bond length, shear stress distribution and differential strain between the FRP and concrete.

Adhesives are generally sensitive to water [Mays and Hutchinson, 1992]. Deterioration of bonded joints is characterized by absorption of water by the adhesive and by moisture diffusion to the adhered interface. Voids can be created in the adhesive layer and at the interface. The presence of voids implies less area of contact. Water can also replace the adhesive by capillary transmission and awakens the bond [Leung et al., 2001].

2.9.3 Freeze—Thaw Exposure

Kaiser (1989) performed a series of freeze-thaw cycles on concrete beams strengthened with CFRP plates. Kaiser found no detrimental effects on the overall structural performance of the beams after 100 cycles from -25°C to +25°C. Baumert et al. (1996) investigated the influence of extreme cold on the structural performance of FRP plated beams. Test results showed that, for CFRP plated beams exposed to a temperature range of -27°C to +21°C, there were no adverse effects on the structural behaviour of the beam when subjected to static tests. Green et al. (1998 and 2000) conducted a series of tests to investigate the freeze-thaw durability of concrete beams strengthened with CFRP sheets. The beams were subjected to 50, 150 and 300 freeze-thaw cycles from -18°C to +15°C. It was concluded that the freeze-thaw action did not degrade the bond of CFRP strengthened beams. Tysl et al. (1998) studied the effect of surface delamination on the freeze-thaw durability of CFRP plated reinforced concrete beams. It was found that neither the freeze-thaw cycling nor partial surface delamination had a diminishing effect

on the overall load-deflection response of the strengthened beams. Very limited research has been reported on the effects of freeze-thaw cycling on FRPs. Tests conducted by Dutta (1988) where the FRPs were subjected to 150 freeze-thaw cycles from -40°C to +23°C showed that the tensile strength of glass-epoxy FRP was reduced by about 10 percent. Deterioration due to freeze-thaw cycles in concrete is caused primarily by freezing of pore water inside the concrete. If the pores are too small, the expansion caused by freezing can exert tensile stresses on the concrete and cause cracking and further deterioration [Neville, 1995].

2.9.4 Thermal Exposure

High temperatures showed detrimental effects on the bond characteristics of FRP rebars [Honma and Maruyama 1989]. Tsuji et al. (1991) conducted pull-out tests on CFRP, AFRP and GFRP bars exposed to 80, 140, 200 and 260°C. The reported residual bond strength was in the range of 56 to 86 percent of the initial values. Kumahara et al. (1993) studied the effects of high temperatures on the mechanical properties of FRP rebars. A reduction of 20 percent in the tensile strength of GFRP and CFRP bars was observed at 250°C. Matthys et al. (1996) conducted numerical simulations to predict thermally induced transverse cracking in concrete reinforced with AFRP bars and strips. Katz et al. (1999) studied the bond properties of FRP rebars with different surface treatments at temperatures ranging from 20 to 250°C. Test results showed a reduction of 80 to 90 percent in the bond strength. In comparison, steel rebars showed a reduction of 38 percent. Mosallam and Dutta (2001) examined the strength of various adhesives under extreme temperature environments. Test results showed that the strength of adhesives

were entirely dependent on cure time and temperature with temperature playing the significant role. A temperature-strength relationship was established for various adhesives. In general, as the temperature increased, the epoxy bond strength increased.

2.9.5 Fatigue

Fatigue of concrete beams strengthened with externally bonded CFRP sheets was first studied by Kaiser (1989). Fatigue failure was observed to occur in the internal steel bars at 4.8×10^5 cycles. The first external damage occurred at 7.5×10^5 cycles and complete failure of the strengthened beams occurred at 8.05×10^5 cycles. Grace and Abdel-sayed (1996) tested a T-bridge girder externally prestressed with CFRP cables and internally reinforced with GFRP bars. The girder was loaded up to 60 percent of the ultimate load. No significant changes were observed in the static or dynamic characteristics of the specimens after 7 million cycles. Shahawy and Beitlman (1998) investigated the fatigue behaviour of concrete beams strengthened with externally bonded CFRP sheets. All the specimens were subjected to four point bending and the fatigue load ranged from 25 to 50 percent of the ultimate capacity of the control sample, with a frequency of 1 Hz. The increase in fatigue life of the strengthened specimens was considerable. Ferrier et al. (1999) studied the fatigue behaviour of various adhesives. Test results showed that the average shear strength was 0.8 MPa for a double lap joint with a fatigue life of one million cycles.

Based on the above discussion, there are limited theoretical and experimental studies on the durability of bond between FRPs and concrete. Investigations by different researchers

are focusing on the durability of externally bonded FRP reinforcement. No literature is currently available on the durability of near surface mounted FRP reinforcement. The author expects that the performance of near surface mounted FRP reinforcement will be superior under severe environmental conditions as the reinforcement is protected inside the concrete. However, the durability of bonding adhesives needs to be investigated. Further studies are still needed to establish accurate reduction factors to be used in bond strength models for design purposes.

Chapter 3

Experimental Program

This chapter presents the details of the experimental program undertaken in this study. The main goal of the experimental program is highlighted. The fabrication process, specimen configurations, test setup, instrumentation, and testing procedures for Phases I and II of the experimental program are provided. Finally, material characteristics are identified.

3.1 General

The research program that was performed was triggered by the needs to identify the most appropriate strengthening technique for concrete bridges to upgrade a thirty-year old concrete bridge in Winnipeg, Manitoba, Canada. A bridge rating analysis conducted using the current AASHTO specifications indicated that the flexural strength of the bridge deck was not sufficient to withstand modern truck loads. To accommodate the AASHTO HSS30 truck design load, the analysis indicated a need to increase the flexural strength by approximately 10 percent at the negative moment zone, over the pier columns, where the maximum shear is also located.

Lack of information on the use of near surface mounted FRP reinforcement, for flexural strengthening in regions of combined bending and high shear stresses, identified the

nature of the test setup and its configuration in the experimental program undertaken in this investigation. The significance of the experimental and analytical research work is the location of the strengthened region where maximum shear and flexural stresses are combined. Such a configuration can typically occur at the negative moment section of cantilevers and continuous beams.

The first phase of the experimental program investigated the feasibility of using near surface mounted CFRP reinforcement to strengthen typical prestressed concrete bridges. Three half-scale models of a typical prestressed concrete bridge slab were cast and post-tensioned. The specimens were tested in a simple span with a double cantilever configuration. The dimensions of the specimens were 8.5 x 1.2 x 0.4 meters and consisted of one simple span and two overhanging cantilevers. Special arrangements were made to test each specimen three times at three different locations. The first and second tests were performed on the two cantilevers with the load applied at the edge of each cantilever, while the third test was conducted using the mid-span in a simply supported configuration. The study included different strengthening techniques using near surface mounted CFRP bars and strips as well as externally bonded CFRP sheets and strips. Based on the test results, the most efficient strengthening techniques are identified.

The second phase of the investigation was designed to evaluate bond characteristics of near surface mounted bars and strips as well as externally bonded sheets. Test results of the experimental program and the proposed analytical models were used to develop design guidelines for flexural strengthening of concrete structures using FRPs. A total of

24 concrete beams were tested under monotonic static loading. Variables considered in this study were the bond length and the strengthening technique adopted.

3.2 Phase I of the Experimental Program

This section describes the first phase of the experimental program undertaken to evaluate the flexural behaviour of concrete members retrofitted with different FRP strengthening techniques. The fabrication process, instrumentation, and testing of the specimens are also discussed.

3.2.1 Large-Scale Slab Specimens

The test specimens considered in this investigation simulate a typical post-tensioned solid slab over intermediate pier columns of a bridge similar to the bridge constructed in the early 1970s in Winnipeg, Manitoba, Canada. The bridge consisted of four spans, as shown in Fig. 3.1 and was designed for AASHTO HSS20 truck design load. The thickness of the bridge slab along the spans was 800 mm, cast in place, partially voided and post-tensioned. The solid slab over the intermediate pier columns was post-tensioned transversely to resist the negative moments at the columns and the positive moment at mid-span. An overview of the bridge is given in Fig. 3.2.
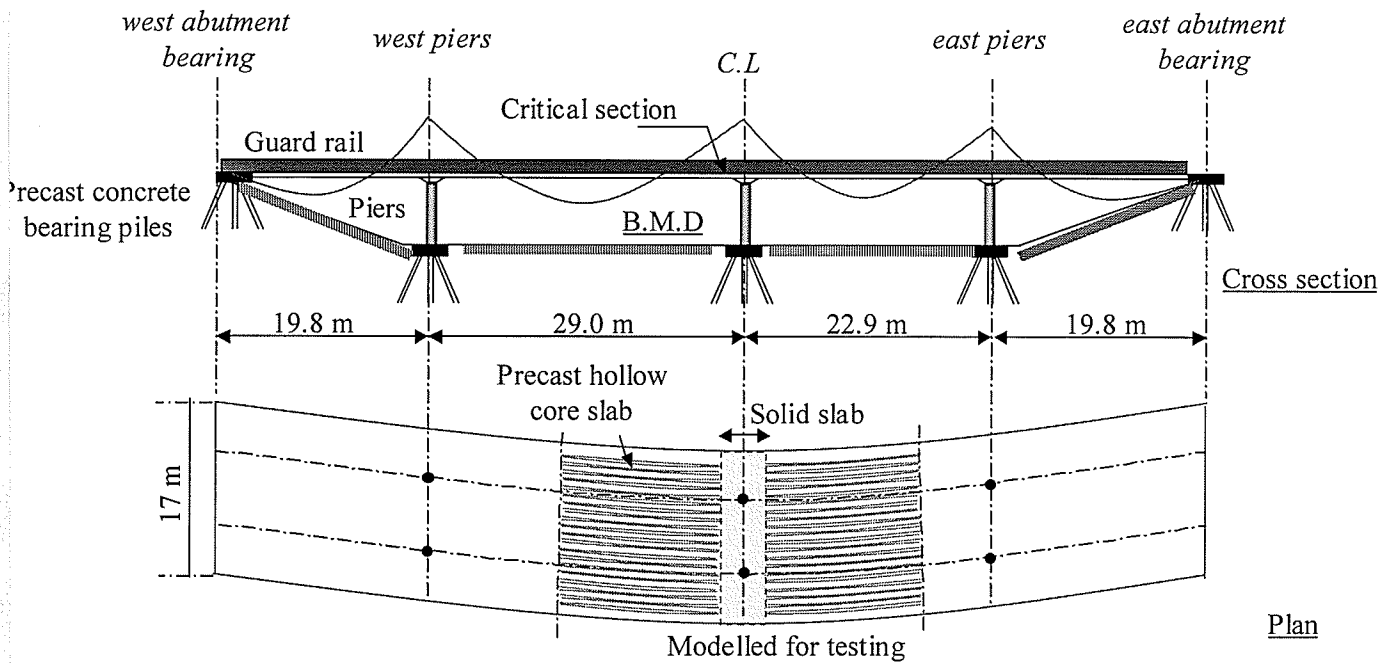
Fig. 3.1 Schematic of bridge No. 444 in Winnipeg – Manitoba - Canada
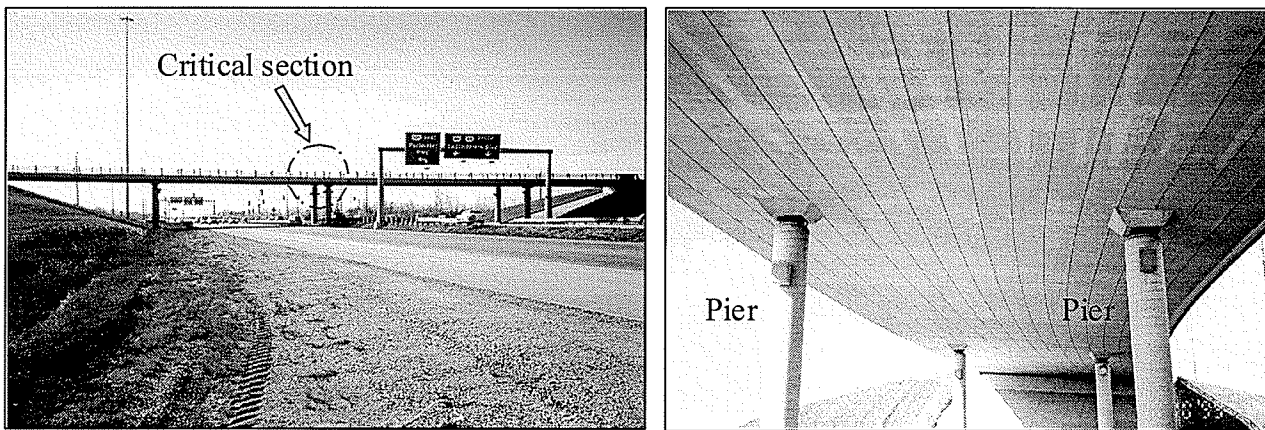
Fig. 3.2 General layout of bridge No.444 in Winnipeg - Manitoba - Canada

To simulate the combined effect of high flexural and shear stresses at the intermediate supports of the bridge, three half-scale models of the solid slab designated as S1, S2 and S3 were constructed. The support configuration of the specimens was designed to examine the FRP repair system at the zones of maximum negative moment at the support,

which coincides with the maximum shear. The number and layout of the tendons were selected to have the same stress level of the bridge under service loading conditions. The critical bending moments for the bridge were evaluated based on a linear elastic finite element analysis using a commercial computer program, SAP2000. The loss of the prestressing force was calculated according to the current AASHTO specifications. The stress profiles at mid-span and support sections of the bridge under service loading conditions are given in Fig. 3.3.
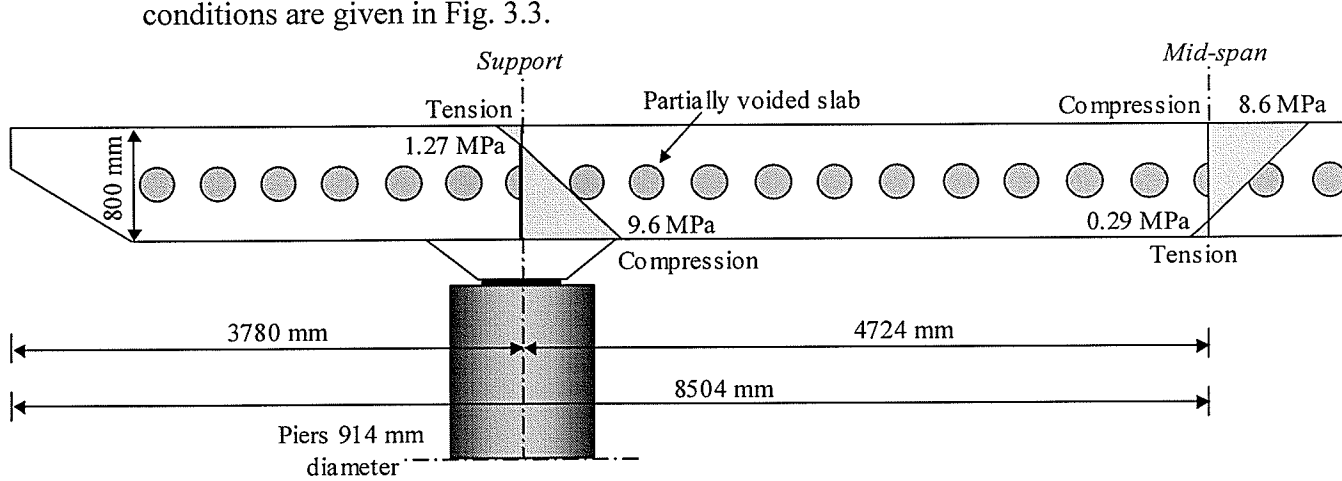
Fig. 3.3 Stress profile at support and mid-span sections for bridge No.444 under service loading conditions

$$f_{\substack{Top \\ Bottom}} = -\frac{P}{A} \mp \frac{Pe}{S} \pm \frac{M_{sw}}{S} \pm \frac{M_{Live}}{S} \qquad \text{for the support section} \qquad (3.1)$$

$$f_{\substack{Top \\ Bottom}} = -\frac{P}{A} \pm \frac{Pe}{S} \mp \frac{M_{sw}}{S} \mp \frac{M_{Live}}{S} \qquad \text{for the mid-span section} \qquad (3.2)$$

where:

f =   concrete stress at top or bottom fibres (MPa);

P =   effective prestressing force after all losses (N);

A =   cross-sectional area of concrete (mm^2);

e =   eccentricity of tendons (mm);

S = section modulus of the concrete (mm^3);

M_{sw} = moment due to self-weight (N.mm); and

M_{live} = moment due to specified live load [AASHTO HSS30] (N.mm).

The specimens were reinforced with four 15M mild steel bars as top reinforcement and five 15M mild steel bars as bottom reinforcement. The number of bars of the top reinforcement was selected to represent the same reinforcement ratio in the cantilever portion of the bridge. Shear reinforcement consisted of 10M U-shaped stirrups. The stirrups were spaced at 125 mm centre to centre in the cantilever span and 250 mm centre to centre in the simply supported span. Reinforcement details of the specimens are shown in Fig. 3.4.
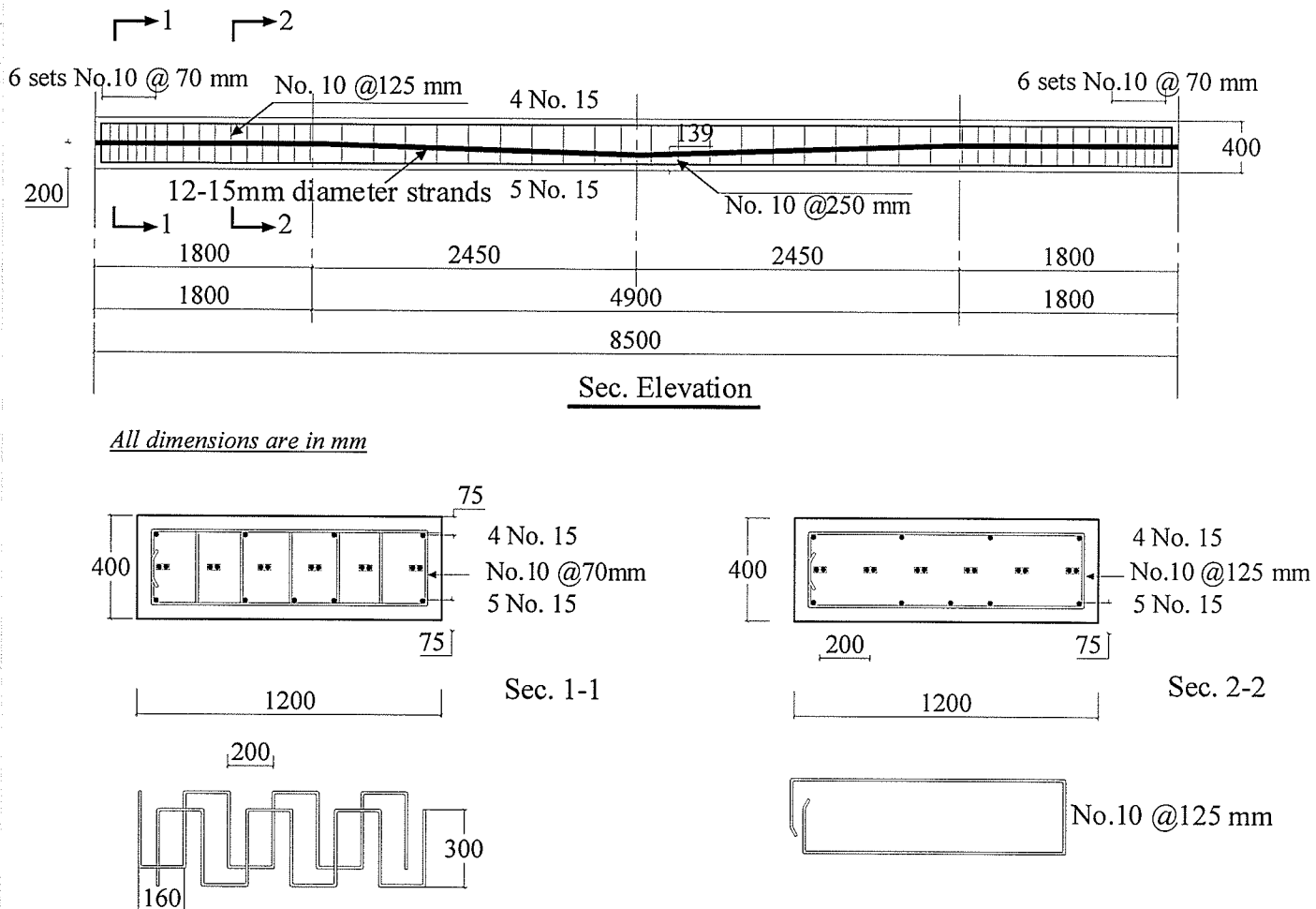
Fig. 3.4 Reinforcement details of test specimens in phase I

90

Bursting reinforcement was provided using six pairs of 10M looped bars spaced at 70 mm. Twelve 15 mm 7-wire strands were used for post-tensioning the specimens. Section properties, prestressing forces, eccentricities and design moments used for both the bridge slab and the model are summarized in Table 3.1.

Table 3.1 Design parameters of the bridge and the model

Parameter	Bridge	Model
Cantilever length (m)	3.47	1.80
Full length (m)	17.0	8.50
Cross-sectional area (m^2)	3.47	0.48
Moment of Inertia (m^4)	0.1912	0.0064
Self weight moment, M_{sw} at support (kN.m)	3436	16.94
Self weight moment, M_{sw} at mid-span (kN.m)	3383	19.21
Live load moment, M_L at support (kN.m)	939.4 *	171.5
Live load moment, M_L at mid-span (kN.m)	888.2 *	253.5
Eccentricity at support (m)	0.127	0.0
Eccentricity at mid-span (m)	0.0508	0.066
Prestressing force, (kN)	14400	2000

* Based on linear elastic finite element analysis (SAP2000)

3.2.2 Fabrication of the Specimens

3.2.2.1 Preparation of the Forms

The specimens were fabricated by a local precast concrete company, Lafarge Inc., Winnipeg, Manitoba. A special form was constructed using wooden sections to account

3. Experimental Program

for the shape and the size of the specimens. The form was cleaned and lubricated and the

steel cage was assembled and tied in place as illustrated in Fig. 3.5.
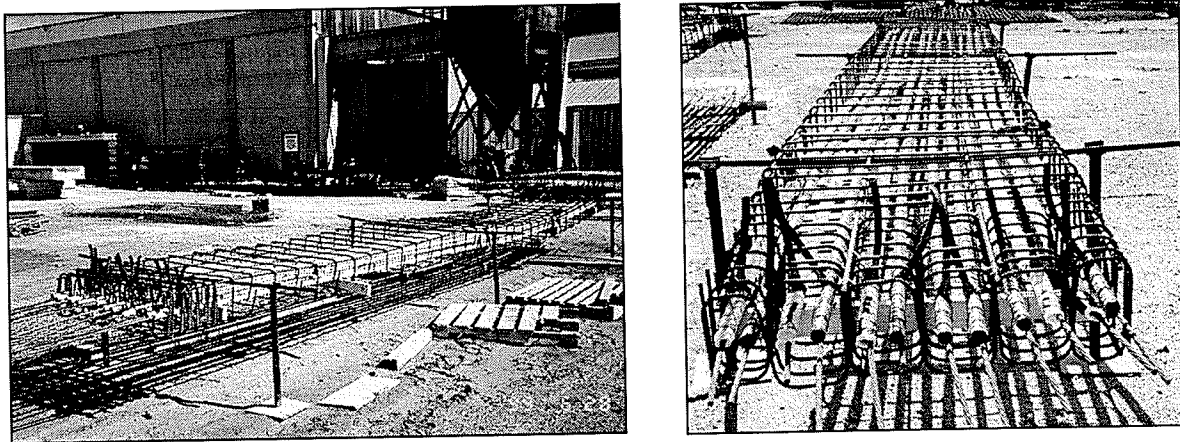
Fig. 3.5 Reinforcement cage

Casting of the test specimens is shown in Fig. 3.6.
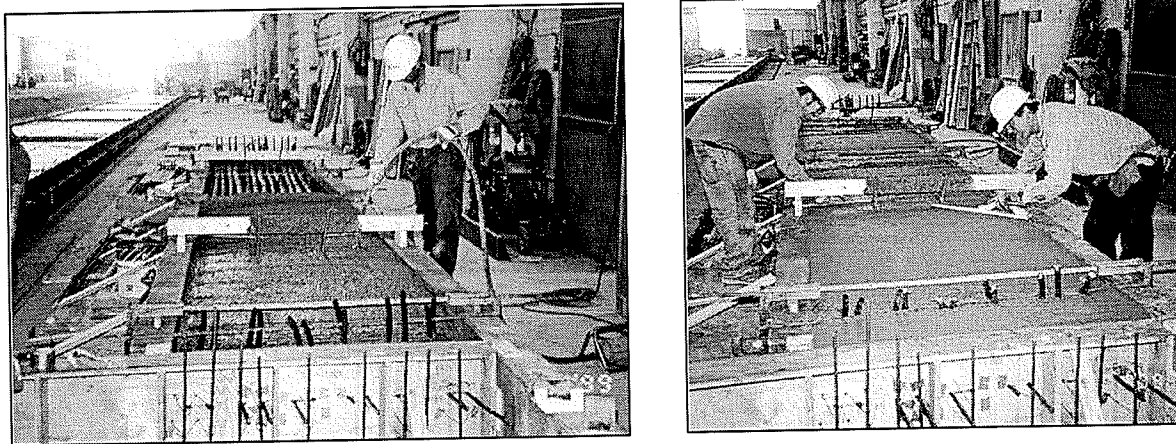
Fig. 3.6 Casting of test specimens of phase I

3.2.2.2 Stressing of the Tendons

The slabs were post-tensioned after 28 days from casting using hydraulic screw jacks,

with locking nuts to maintain the force constant after jacking as shown in Fig. 3.7. The

tendons were anchored from one end and stressed from the other end.
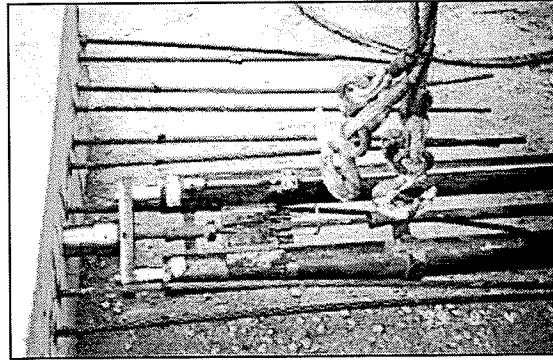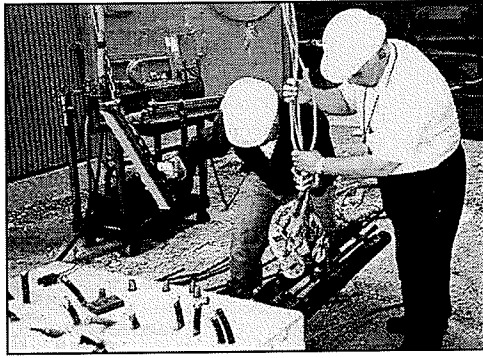
Fig. 3.7 Post-tensioning of specimens of phase I

The load was applied in increments using a hydraulic air pump. Each strand was tensioned individually in the sequence starting in the centre of the slab and continued symmetrically towards the sides. The strain and the elongation of the tendons were monitored for each load increment.

$$\Delta = \frac{P_o L}{A_{ps} E_p}$$
(3.3)

where

Δ =   expected tendon elongation;

P_o =   required prestressing force in the tendon;

L =   total length of tendon;

A_{ps} =   cross-sectional area of tendon; and

E_p =   modulus of elasticity of prestressing tendons.

The tendons were stressed to $0.78 f_{pu}$ (204 kN/tendon). After the required force was recorded based on the strain gauge reading and the elongation of the tendons, the jacks were locked with nuts.

Completed slabs are shown in Fig. 3.8.

Fig. 3.8 Completed specimens (phase I)

The jacking, effective prestressing forces and prestress losses for specimens S1, S2 and S3 are summarized in Table 3.2.

Table 3.2 Prestressed forces in test specimens

Specimen	Jacking force, P_j (kN)	Effective prestressing force, P_e (kN)	Prestress loss (%)
S1*	194.6	160.8	17.3
S2*	180.82	142.85	20.6
S3*	194.76	167.55	13.97

* Based on measured strains

3.2.2.3 Grouting

The ducts were grouted one week after stressing the tendons. The objective of the grouting process was to fill the ducts completely with material that provides an alkaline environment for corrosion protection of the prestressing steel and has sufficient strength to bond the tendons to the surrounding concrete. Cement grout of suitable consistency was injected under pressure into the sheath by a diaphragm pump as illustrated in Fig.3.9
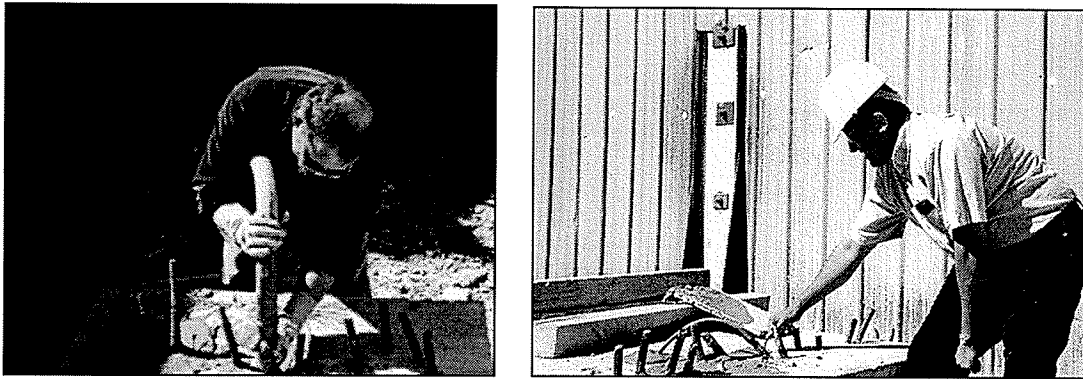
Fig. 3.9 Grouting of the specimens of phase I

3.2.3 Strengthening Techniques

Slab S1:

One cantilever of the slab S1 was strengthened using near surface mounted Leadline bars while the other cantilever remained unstrengthened. The Leadline bars are produced by Mitsubishi Chemicals Corporation, Japan. Based on equilibrium and compatibility conditions, six 10 mm diameter Leadline bars were used to achieve a 30 percent increase in the ultimate load carrying capacity of the slab. In the preliminary analysis, the concrete is assumed to be subjected to uniform uniaxial strains over the entire width of the slab. Strains are assumed to vary linearly over the depth of the section. The stress-strain relationship of the concrete was modelled using a parabolic relationship in compression. The internal compression force in the concrete was evaluated using the stress-block parameters introduced by Collins and Mitchell (1991). The stress-strain behaviour of the CFRP reinforcement is assumed to be linearly elastic up to failure [Hassan and Rizkalla, 2002].

To strengthen the cantilever slab using near surface mounted bars, grooves were cut at the top surface of the concrete. The location of the grooves was first marked using a chalk line. The grooves were 200 mm apart. A concrete saw was used to cut six grooves of approximately 18 mm wide and 30 mm deep at the tension surface of the cantilever as shown in Fig. 3.10.
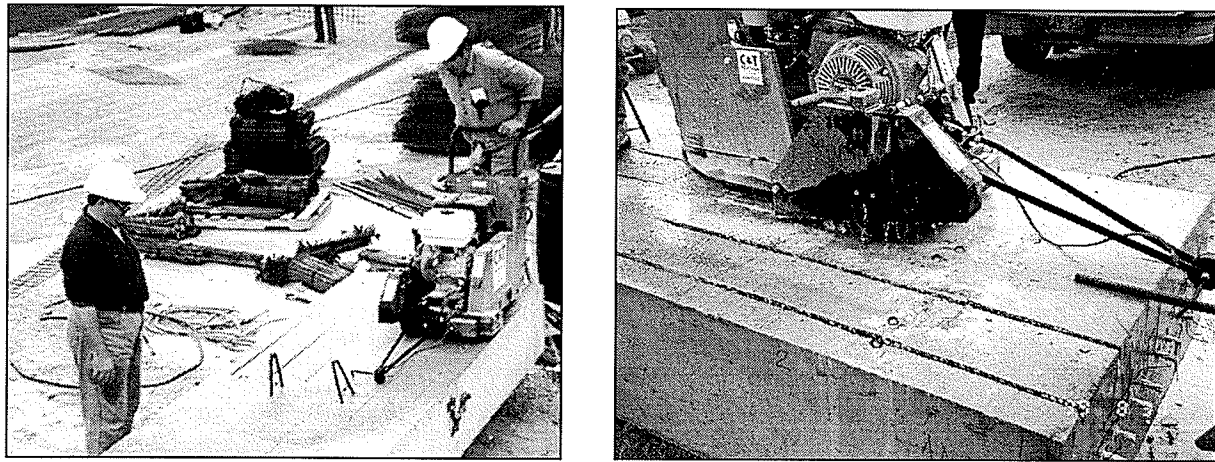
Fig. 3.10 Cutting grooves for near surface mounted CFRP bars

The groove ends were widened to provide wedge action and to prevent possible slip of the bars. Tapering the ends of the grooves was intended to induce inclined friction forces at the concrete-epoxy interface. These inclined forces provided radial confining forces on the bars and consequently, increased the pullout resistance.

Kemko 040 was used for bonding the CFRP bars to the surrounding concrete. The epoxy was produced by ChemCo Systems, Inc., USA. The adhesive is commonly used for grouting bolts, dowels and steel bars in concrete. The adhesive has a modulus of elasticity of 1200 MPa and an ultimate tensile strength of 48 MPa as reported by the manufacturer. The epoxy was pressure injected into the grooves to cover 2/3 of the groove height. The

bars were placed in the grooves and gently pressed to displace the bonding agent as shown in Fig. 3.11. The grooves were then filled completely with the epoxy. Quality control was achieved through continuous inspections and measurements during the installation procedures.
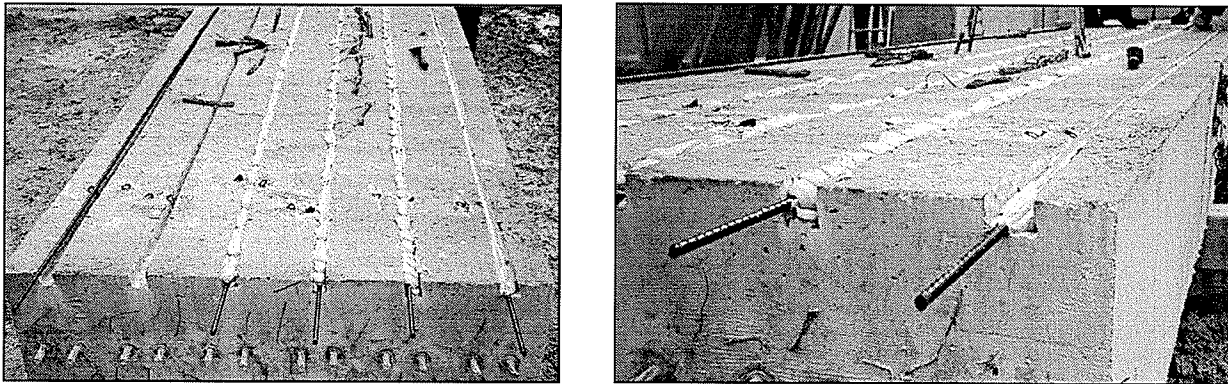
Fig. 3.11 CFRP bars inserted in epoxy

After completion of the two tests for both cantilevers, the resulting cracks were injected with epoxy. A temporary seal [SCB Concresive 1446] was applied at the backside of the slab to prevent the injecting adhesive from running out. Entry ports were placed at the cracked surfaces as shown in Fig. 3.12. Two metering pumps were used to drive the two components (resin and hardener) of a fast-setting epoxy adhesive [SCB Concresive 1360] to a special mixing head. The adhesive was mixed at the nozzle and injected through a special gasket, which prevented leakage on the face of the concrete. The tensile strength of the cured adhesive is 55 MPa after 7 days as reported by the manufacturer. The adhesive was pumped into the first entry port until it began to flow at the next adjacent port. The first injected port was then plugged and injection was resumed at the second port. These procedures were followed until all major cracks were filled as shown in Fig. 3.13.
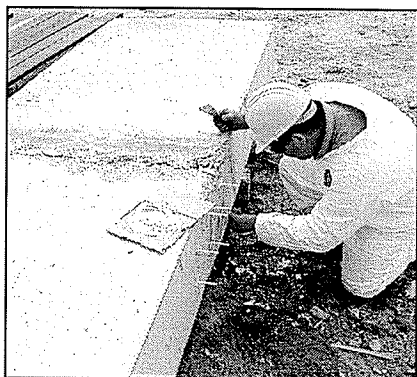
Fig. 3.12 Placing entry ports   Fig. 3.13 Injecting the cracks

Based on the equilibrium and compatibility design approach, ten 10 mm diameter Leadline bars were found to be needed to increase the flexural capacity by 30 percent at the mid-span section of the simply supported slab. The same procedures as described in section 3.2.3 were applied to cut the grooves and to place the Leadline bars. To enable further testing of the slab, a fast setting epoxy resin was used to level the crushed areas at both ends of the simply supported span. It should be noted that the compressive strength of the added epoxy was 45 MPa as reported by the manufacturer, which matched that of the concrete [Hassan et al., 2000].

Slab S2:

The second slab, S2, was used to investigate the performance of both near surface mounted and externally bonded CFRP strips in the strengthening of concrete bridges. Rational analysis of the cantilever specimens indicated a need for six CFRP strips, 50 mm wide and 1.4 mm thick to achieve a 30 percent increase in the ultimate capacity of the cantilever slab. The first cantilever was strengthened using six externally bonded CFRP strips. The concrete substrate was prepared by grinding of the surface at the locations of the strips as shown in Fig. 3.14. The epoxy was then placed over the strips and on the concrete surface as shown in Fig. 3.15.

Fig. 3.14 Grinding the surface

Fig. 3.15 Placing the epoxy on the strip

Finally, the strips were placed on the concrete surface and gently pressed into the epoxy using a ribbed roller as shown in Fig. 3.16.
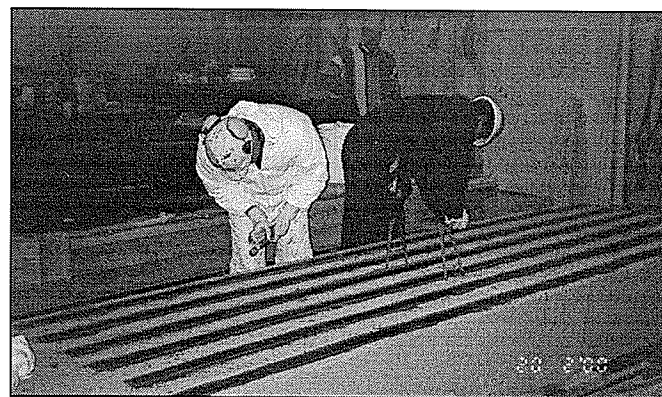
Fig. 3.16 Bonding the CFRP strips to the surface

The second cantilever was strengthened also using six CFRP strips inserted into grooves cut at the top surface of the concrete. In order to insert the strips within the concrete cover layer, the strips were cut into two halves each, 25 mm wide as shown in Fig. 3.17.
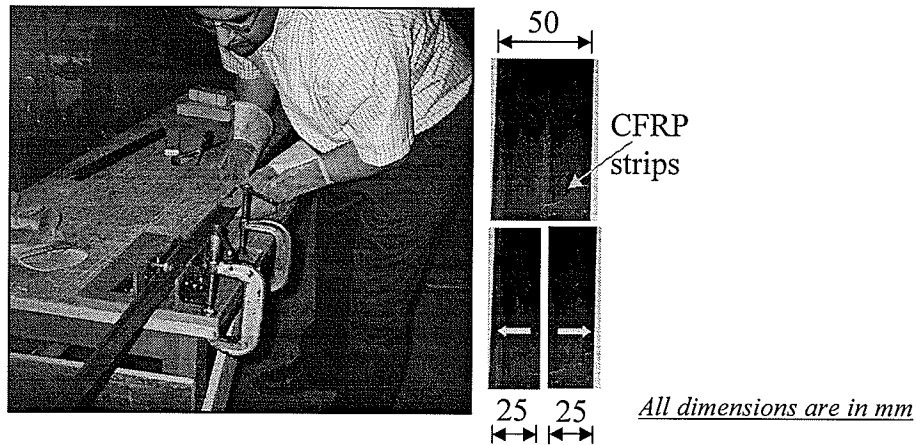
Fig. 3.17 Splitting the CFRP strips into two halves

Using a concrete saw, 12 grooves of approximately 5 mm wide and 25 mm deep were cut at the tension surface of the second cantilever. The grooves were then injected with the epoxy adhesive to provide the necessary bond with the surrounding concrete as shown in Fig. 3.18. The strips were then placed in the grooves ensuring that they were completely covered with the epoxy as shown in Fig. 3.19.
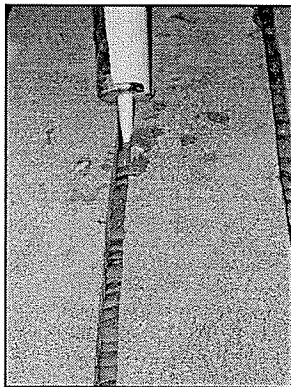
Fig. 3.18 Filling the grooves with epoxy

Fig. 3.19 Inserting the CFRP strips inside grooves

The CFRP strips are produced by S&P Clever Reinforcement Company, Switzerland. After testing both cantilevers, the areas above the supports were substantially cracked. To enable further testing of the mid-span, the cracks were injected similar to slab S1. Eighteen near surface mounted CFRP strips, 25 mm wide and 1.4 mm thick spaced by 66 mm centre to centre were used to achieve a 30 percent increase of the ultimate capacity of the simply supported slab. EN-Force CFL was used in bonding both near surface mounted and externally bonded CFRP strips to the concrete. The epoxy is produced by Structural Composites, Inc, USA. The adhesive has a modulus of elasticity of 3500 MPa and an ultimate tensile strength of 70 MPa as reported by the manufacturer.

Slab S3:

Externally bonded FRP sheets are currently the most commonly used technique for strengthening bridges and concrete structures. This method can be seen as the state-of-the-art technique in spite of some detailing problems and design aspects, which could influence the failure modes. To investigate the effectiveness of this strengthening method in comparison to the three previously prescribed techniques, one cantilever of Slab S3, as well as the simply supported span, were strengthened using externally bonded CFRP sheets. The sheets are manufactured by Master Builders Technologies, Ltd., Ohio, USA. The required area of the CFRP sheets was calculated to achieve a 30 percent increase in the flexural capacity of the cantilever slab.

For the first cantilever, the sheets were applied in two plies. The first ply covered the entire width of the slab while the second ply covered 480 mm and was centred along the width of the slab. Installation procedures are illustrated in Fig. 3.20.

a) grinding of the surface   b) applying the MBrace saturant   c) bonding the CFRP sheets
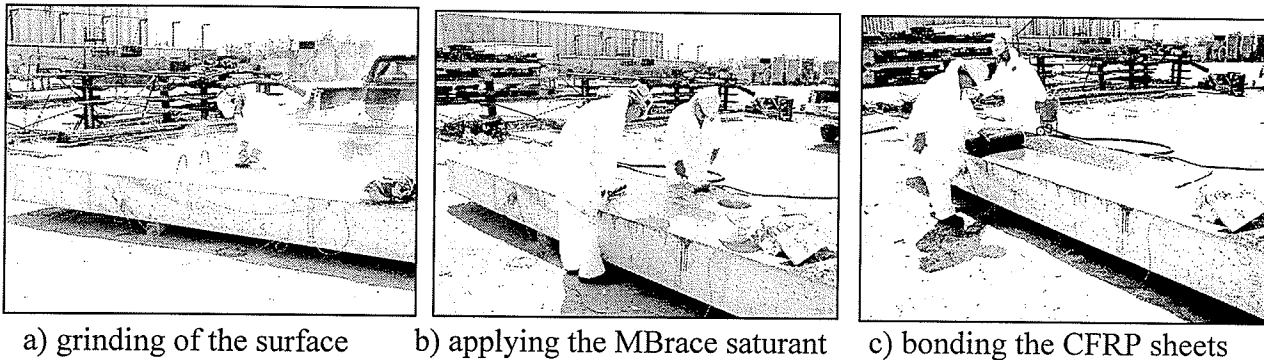
Fig. 3.20 Installation procedures for CFRP sheets

The second cantilever was strengthened using eight 10 mm diameter, near surface mounted C-Bars. The bars are manufactured by Marshall Industries Composites Inc., USA. The bars were sandblasted to enhance their bond to the epoxy adhesive as shown in Fig. 3.21. The bars were then inserted inside grooves cut at the top surface of the concrete as illustrated in Fig. 3.22. The grooves were 150 mm apart. The groove dimensions were 18 mm wide and 30 mm deep.

The simply supported span was strengthened with externally bonded CFRP sheets after injecting the cracks resulting from cantilever tests. Three plies of CFRP sheets were used to achieve a 30 percent increase in flexural capacity. The first two plies covered the entire width of the slab, while the third ply covered 400 mm and was centred along the width of the slab [Hassan and Rizkalla, 2002].
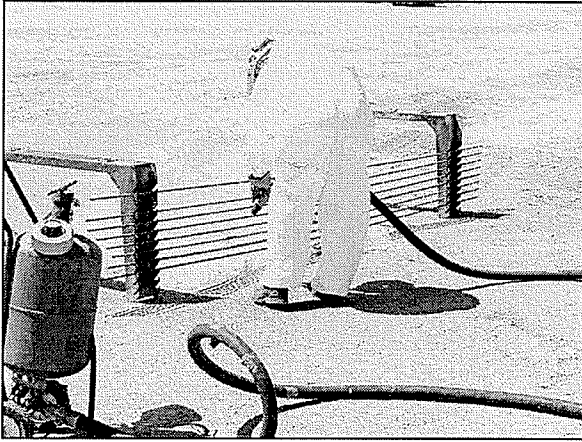
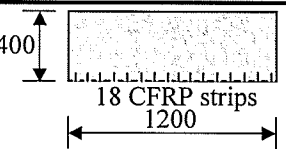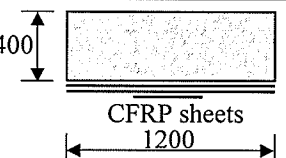Fig. 3.21 Sandblasting of C-Bars
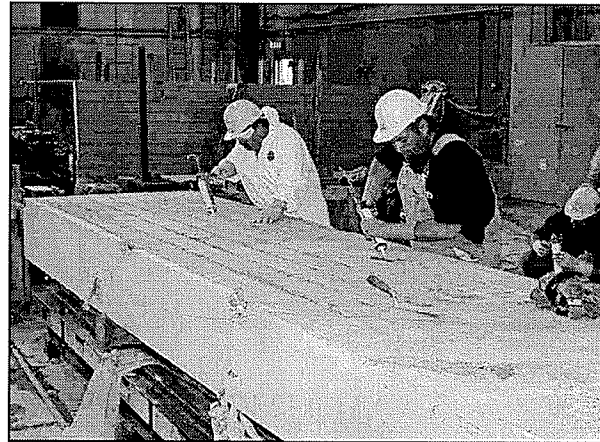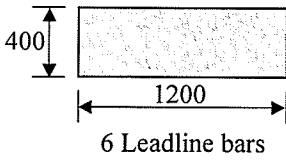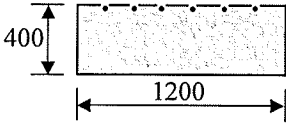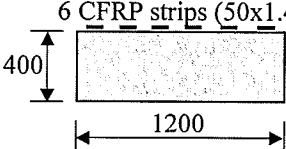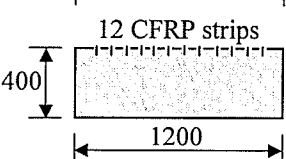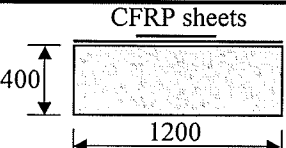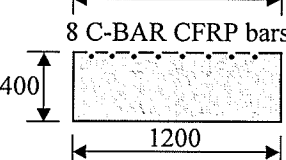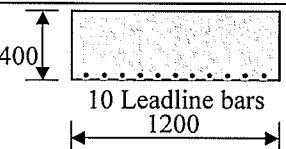
Fig. 3.22 Inserting C-Bars inside grooves

Strengthening procedures for all the slabs were performed by Vector Construction Ltd., Winnipeg, Canada. Detailed information about the tested specimens is provided in Table 3.3. The designation of the tested specimens has the first letters either C, or SS refers to Cantilever or Simply Supported specimens, respectively.

Table 3.3 Details of large-scale slab specimens

Slab #	CANTILEVER TESTS		
	Cross-section configuration	Specimen	Strengthening method
S1	400 / 1200	C1	Control specimen (unstrengthened)
	6 Leadline bars / 400 / 1200	C2	Near surface mounted Leadline bars
S2	6 CFRP strips (50x1.4) / 400 / 1200	C3	Externally bonded CFRP strips (50 x 1.4 mm)
	12 CFRP strips / 400 / 1200	C4	Near surface mounted CFRP strips (25 x 1.4 mm)
S3	CFRP sheets / 400 / 1200	C5	Externally bonded CFRP sheets
	8 C-BAR CFRP bars / 400 / 1200	C6	Near surface mounted C-BAR CFRP bars
	SIMPLY SUPPORTED TESTS		
S1	400 / 10 Leadline bars / 1200	SS1	Near surface mounted Leadline bars
S2	400 / 18 CFRP strips / 1200	SS2	Near surface mounted CFRP strips
S3	400 / CFRP sheets / 1200	SS3	Externally bonded CFRP sheets

104

3.2.4 Instrumentation

The instrumentation used to monitor the behaviour of the slabs during testing consisted of a combination of electrical strain gauges, linear variable differential transducers (LVDTs), demec points, and PI gauges.

Reinforcement strains: Thirteen electrical strain gauges produced by Showa Measuring Instruments Co. Ltd., Tokyo, Japan, of the type of N11-FA-5-120-11 were installed at the top and bottom mild steel reinforcement. Nine strain gauges were installed on the prestressing steel strands. The gauge length was 5 mm and the resistance of the gauge was 120 ohms. The strain gauges were glued to the smoothened part on the surface of the bars using M-Bond 200. The strain gauges were covered by a waterproof coating to protect them from water and damage during casting the concrete. The strain gauges were permanently attached to a strain-indicator device to monitor the loss of the prestressing force until the day of testing.

Crack width monitoring: A microscope of a magnification factor of ten was used to measure the crack width development during testing. The crack width measurements were taken every 50 kN up to failure.

3.2.4.1 Cantilever Tests

Deflections: The deflection at the free end of the cantilever was monitored using two LVDTs. The deformation of the neoprene pads placed between the concrete slab and the support was also monitored using two LVDTs. Two LVDTs located at the centre of the

cantilever span were used to monitor the deflection distribution along the cantilever length.

Concrete strains: Four PI gauges, located on one side of the cantilever slab over the support and four demec point stations, located on the other side were used to measure the strain profile of the concrete during the test. Two demec point rosettes on one side of the specimen, located at a height of 200 mm from the bottom surface of the slab were used to monitor the shear behaviour of the cantilever. Loading of the specimen was paused every 50 kN to manually record the strain. On the top of the slab, five PI gauges were used to identify the cracking load and measure the crack width. Three PFL-30-11-3L strain gauges were installed on the bottom surface of the slab to measure concrete compressive strain. The gauge length was 30 mm and the resistance of the gauges was 120 ohms.

Slip monitoring: One LVDT was attached to the FRP to monitor any possible slip of the reinforcement.

The instrumentation used for cantilever tests, location of strain gauges, PI gauges and LVDTs are illustrated in Figs 3.23, 3.24 and 3.25.

Cross-section   *Side -2-*

Location of strain gauges on top mild steel reinforcement

Location of strain gauges on bottom mild steel reinforcement

Location of strain gauges on prestressing steel

All dimensions are in mm

Cross-section   *Side -1-*

Location of PI gauges on top concrete surface

Location of strain gauges on bottom concrete surface
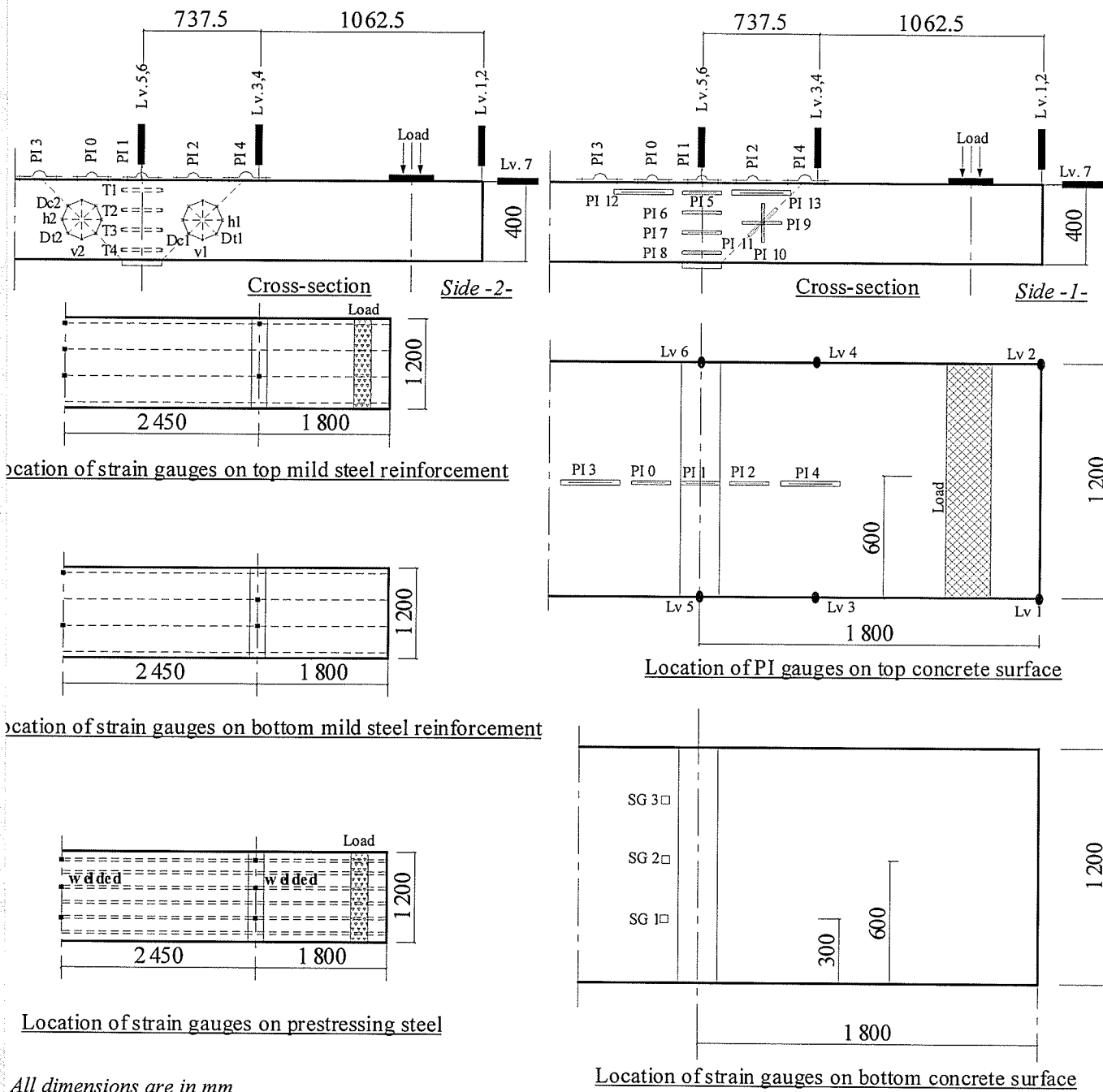
Fig. 3.23 Schematic of the instrumentation for cantilever tests

Fig. 3.24 Instrumentation for cantilever tests

Location of strain gauges on Leadline CFRP bars (C2)

Location of strain gauges on CFRP sheets (C5)

Location of strain gauges on externally bonded CFRP strips (C3)

Location of strain gauges on C-BAR CFRP bars (C6)

Location of strain gauges on near surface mounted CFRP strips (C4)
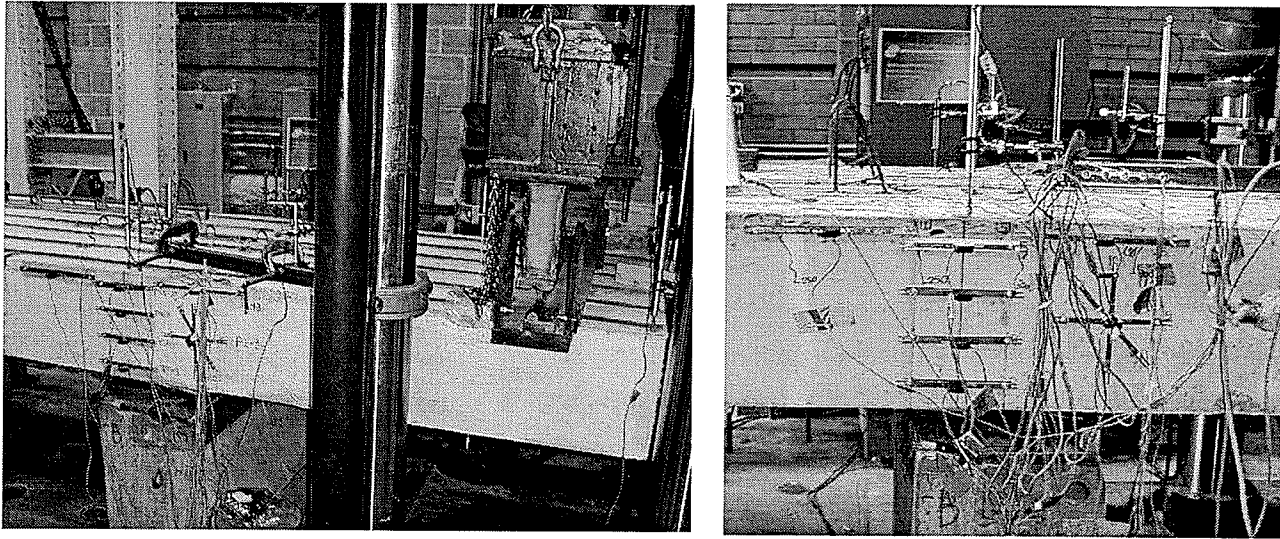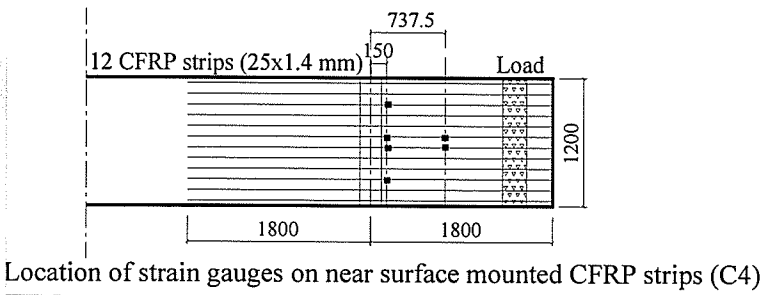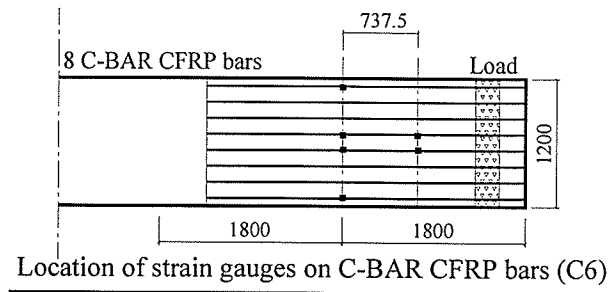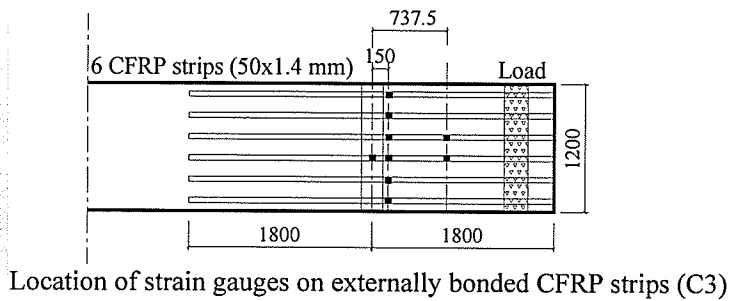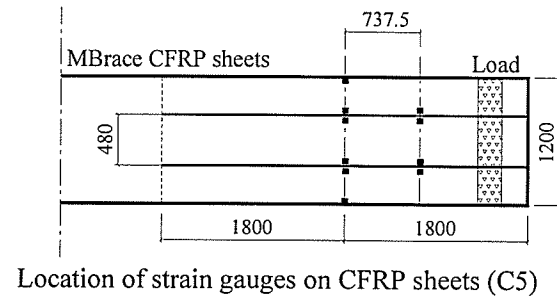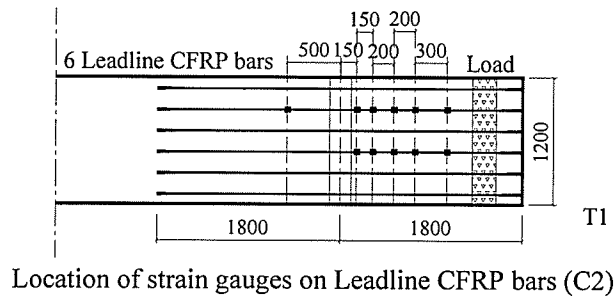
All dimensions are in mm

Fig. 3.25 Location of strain gauges on FRP reinforcement for cantilever specimens

3.2.4.2 Simply Supported Tests

Deflections: The deflection at mid-span was monitored using two LVDTs. The deformation of the neoprene pads placed between the concrete slab and the support was also monitored using four LVDTs located over the supports at the edges of the slab. Four LVDTs were located also along the length of the slab to monitor the deflection distribution along the span.
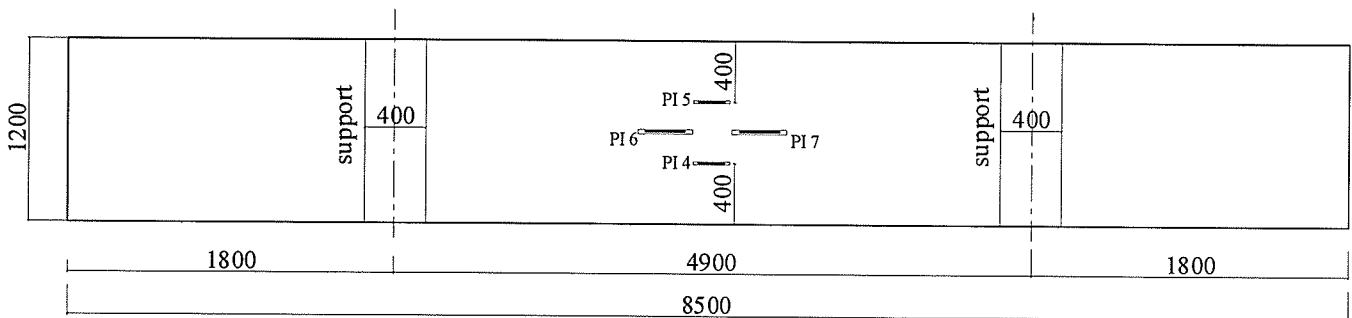
Concrete strains: Four PI gauges were placed along the depth of the slab at mid-span to measure the strain profile of the concrete during the test. Two demec point rosettes, on one side of the specimen located at a height of 200 mm from the bottom surface of the slab, were used to monitor the strain in three directions to determine the shear behaviour of the slab. The specimen was loaded manually in increments of 50 kN to record the strain. On the bottom of the slab, four PI gauges were used to identify the cracking load and measure the crack width. Three electrical strain gauges were installed on the top surface of the concrete under the load and at the face of loading to measure the compressive strain of the concrete. The instrumentation used for the simply supported tests, location of strain gauges, PI gauges and LVDTs are shown in Figs. 3.26 and 3.27.

All the LVDTs, PI gauges, strain gauges, applied load, and stroke readings were recorded continuously using a computerized data acquisition system. During testing, the measured data was stored and viewed using the data acquisition software LABVIEW. The applied load, stroke, readings of the PI gauges and LVDTs were displayed graphically during the test.

Side -1-

Lv. 1,6   Lv. 2,7   Load   Lv. 4,9   Lv. 5,10

PI 8   PI 0   PI 1   PI 2   PI 3   PI 9

PI 6   Lv. 3,8   PI 4,5   PI 7

1225   1225   1225   1225

1800   4900   1800

8500

Side -2-

Lv. 1,6   Lv. 2,7   Load   Lv. 4,9   Lv. 5,10

Left rosette   Right rosette

1225   1225   1225   1225

1800   4900   1800

8500

Lv 6   Lv 7   Lv 8   Lv 9   Lv 10

support   400   600   SG1 SG2 SG3   support   400

600   Load

Lv 1   Lv 2   Lv 3   Lv 4   Lv 5

1800   4900   1800

8500
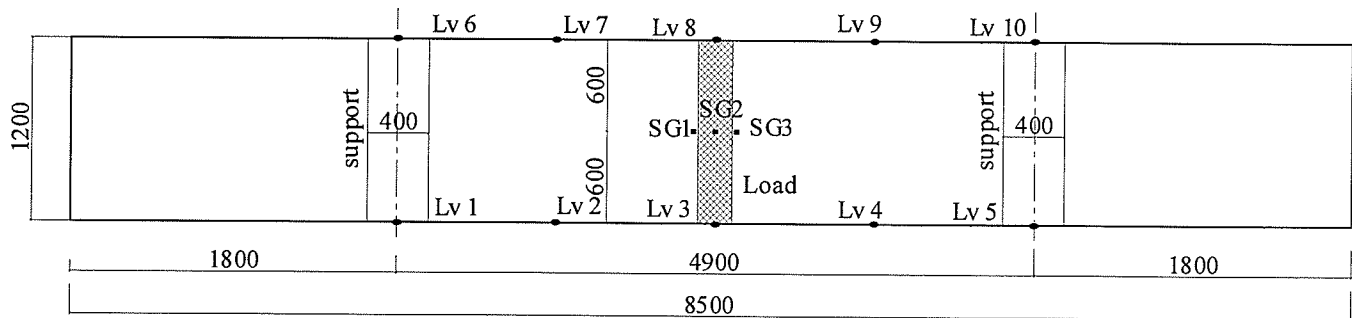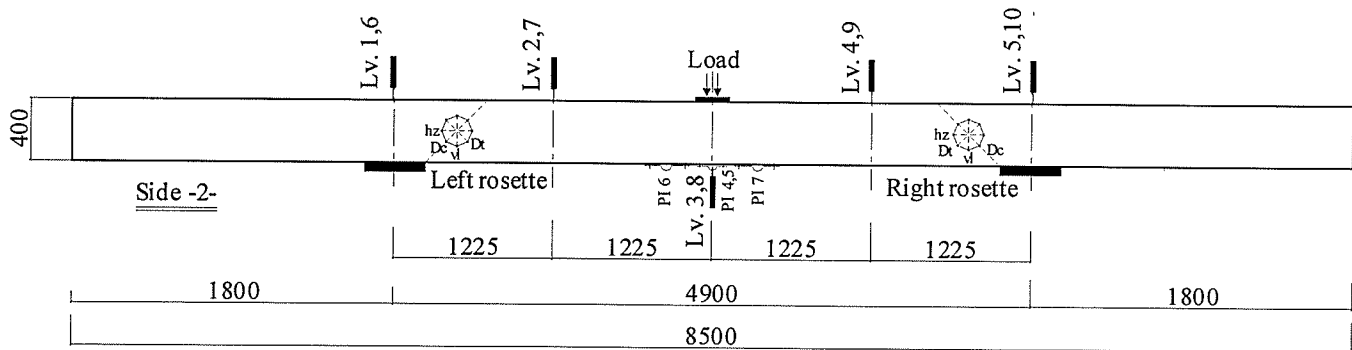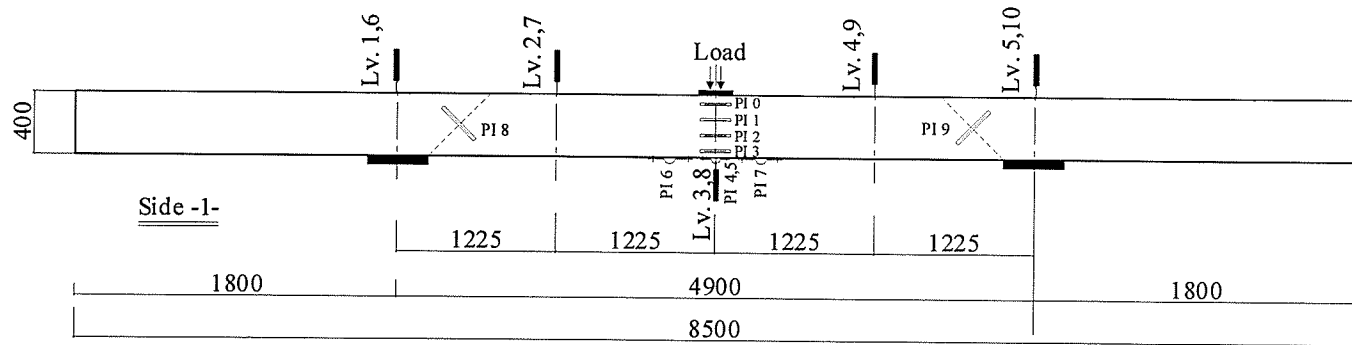
Instrumentation used at the top of the concrete slab

support   400   PI 5   400   support   400

PI 6   PI 7

PI 4   400

1800   4900   1800

8500

All dimensions are in mm   Instrumentation used at the bottom of the concrete slab
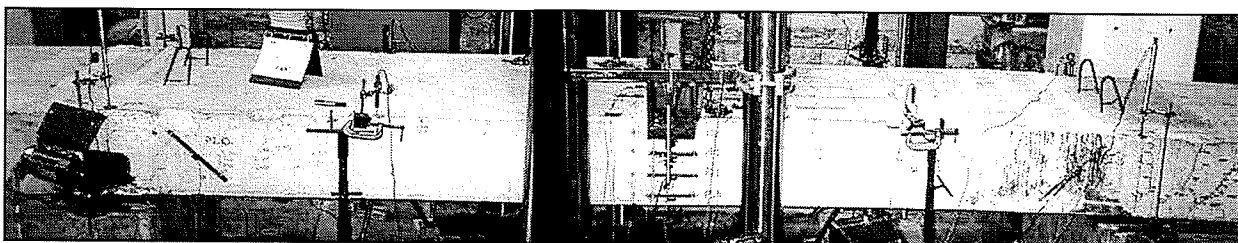
Fig. 3.26 Instrumentation of simply supported tests

110

Location of strain gauges on Leadline CFRP bars (SS1)

Location of strain gauges on externally bonded CFRP sheets (SS3)

Location of strain gauges on near surface mounted CFRP strips (SS2)

All dimensions are in mm
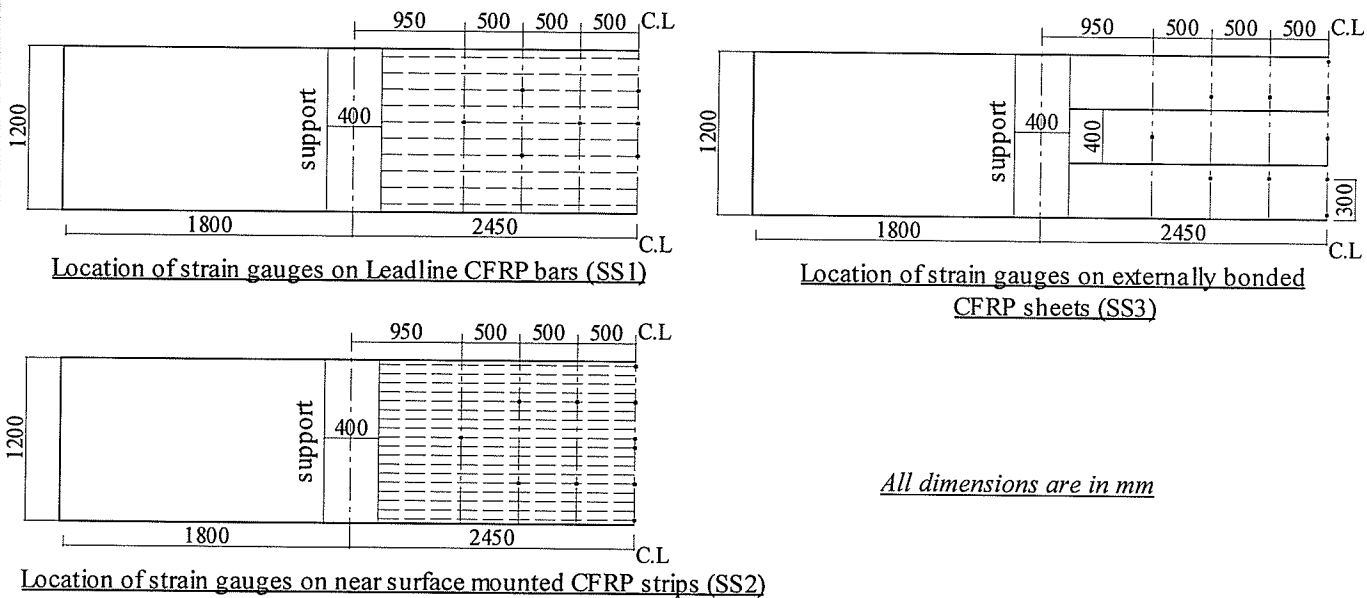
Fig. 3.27 Location of strain gauges on FRP reinforcement for simply supported tests

3.2.5 Testing Scheme

The slabs were tested under static loading conditions using a uniform line-load acting on a width equivalent to the width of a tire contact patch according to the AASHTO HSS30 design vehicle. A closed-loop MTS, 5000 kN, testing machine was used to apply the load using the stroke control mode with a rate of 0.5 mm/min for each load increment up to failure. Neoprene pads were placed between the steel beam and the slab to simulate the contact surface of a truck tire and to avoid local crushing of the concrete.

3.2.5.1 Cantilever Tests

The load was applied at a distance of 325 mm from the cantilever edge. The range cards used in the testing machine were 1000 kN for load and 200 mm for stroke. To prevent possible damage of the other cantilever during the test, an intermediate support was

provided in the simply supported span. Two channels back-to-back were placed at the top

of the slab at the location of the intermediate support. Two DYWIDAG bars, connected

to the floor, were used to prevent the upward movement of channels. The bars were pre-

tensioned before the test using a hydraulic pump as shown in Fig.3.28.
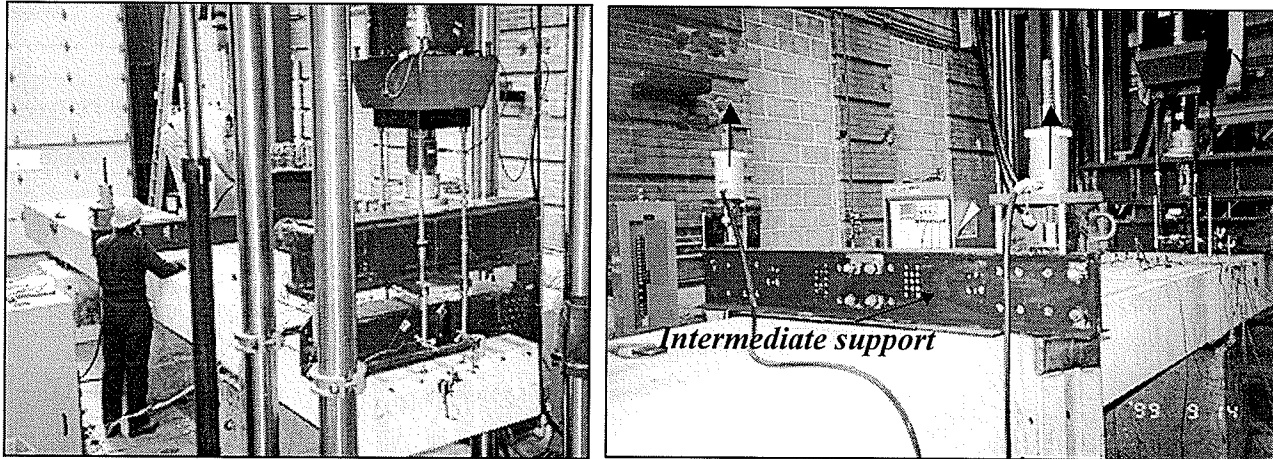

Fig. 3.28 Pre-tensioning the DYWIDAG bars at the intermediate support

The pre-tensioning force simulated the maximum expected upward force at the support.

Pre-tensioning the DYWIDAG bars applied compression in the slab and prevented any

possible upward movement. The test set-up for the cantilever tests, including the MTS

machine is shown in Figs. 3.29a and 3.29b.

Notes

(1) *Elastomeric bearings (Neoprene pads) 400x400x4*
(2) *Steel plate 200x20 (Length=1200 mm)*
(3) *HSS 76X50X5 (Length=250mm)*
(4) *HSS 100x100x5 (Length=1270mm)*
(5) *Prestressed DYWIDAG bar (Diameter = 25.4mm, Prestressing force=178 kN)*
(6) *HSS 100x100x5 (Length=1200mm)*
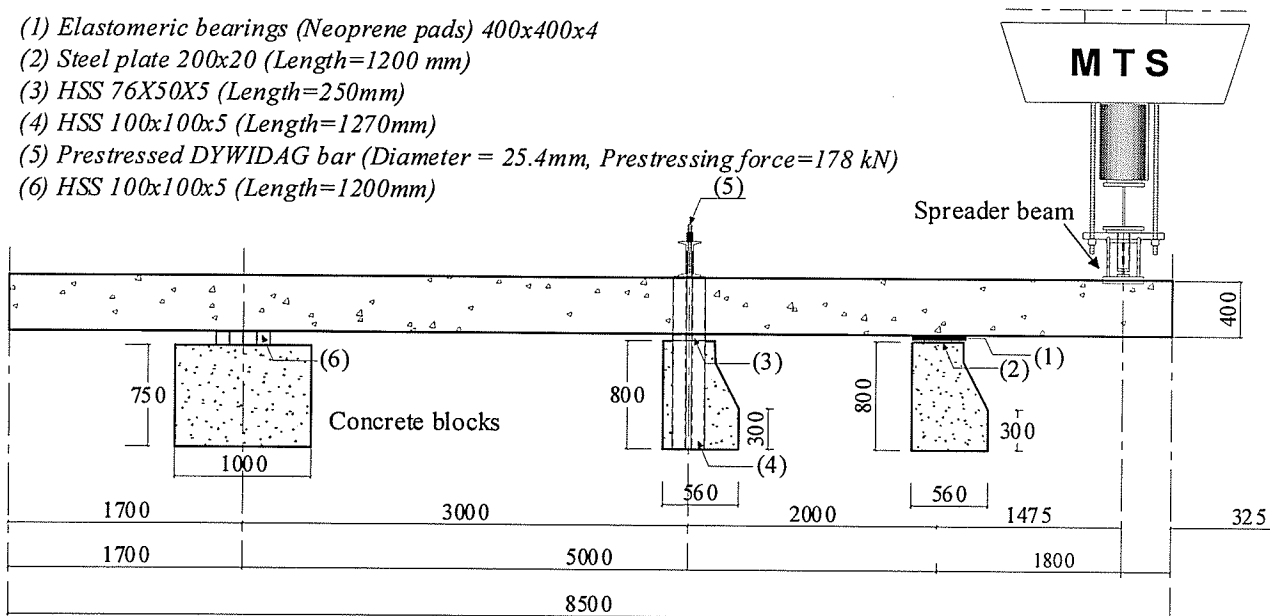
Fig. 3.29a Schematic of test set-up for cantilever tests, phase I
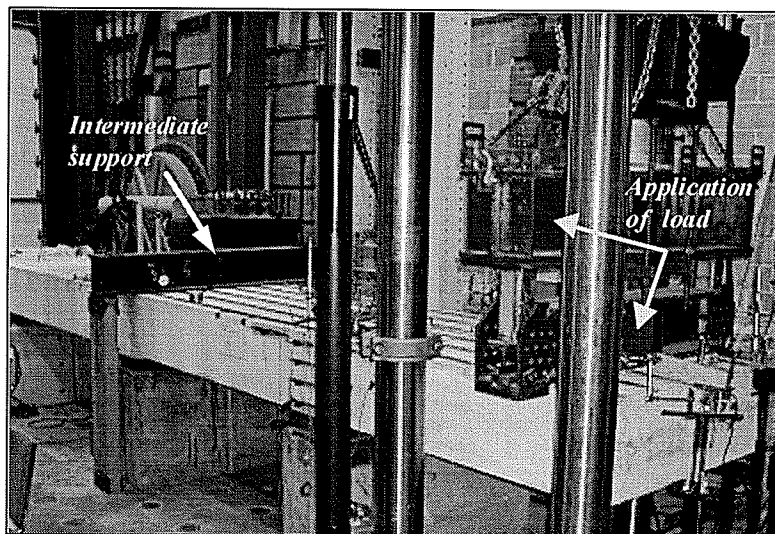
All dimensions are in mm

Fig. 3.29b Test set-up for cantilever tests, phase I

3.2.5.2 Simply Supported Tests

The slab was simply supported with a 4.90 m span and a 1.80 m projection from each end with the line load applied at the centre of the slab. The slab was supported using concrete blocks as shown in Figs. 3.30a and 3.30b. The load was applied using the stroke control

mode of the testing machine with a rate of 0.5 mm/min up to failure. Neoprene pads were

placed at the loading location and at the bearings to distribute the load evenly. The range

cards used in the testing machine were 2500 kN for load and 200 mm for stroke.
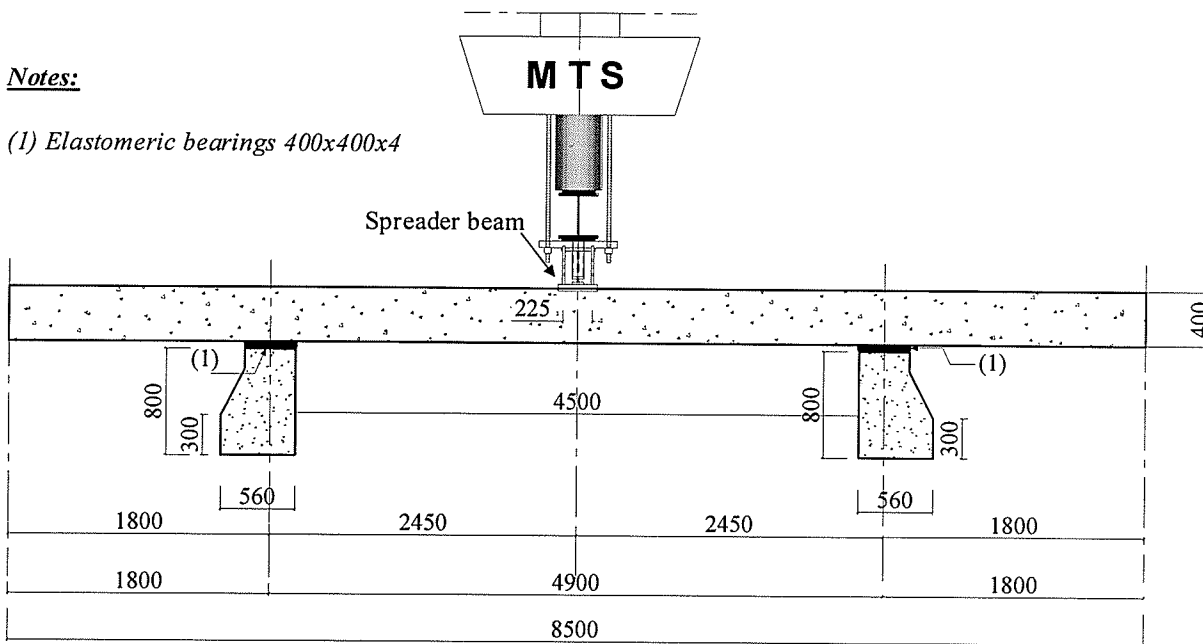

Fig. 3.30a Schematic of test set-up for simply supported tests, phase I

All dimensions are in mm
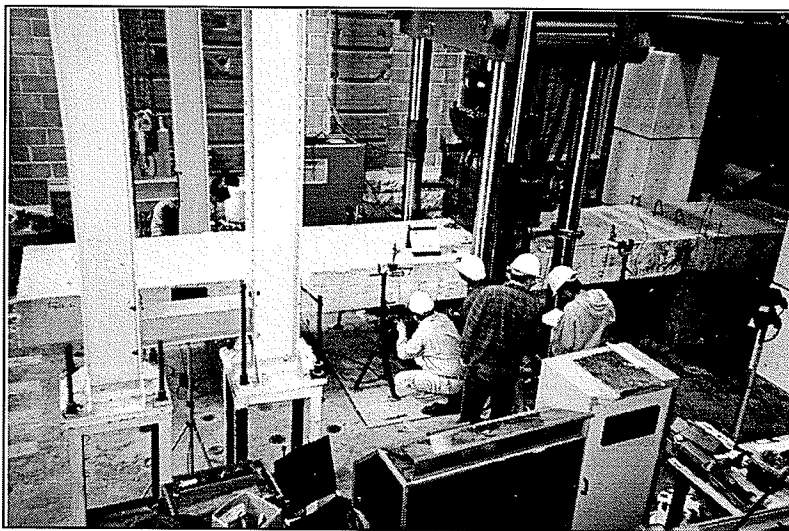
Fig. 3.30b Test set-up for simply supported tests, phase I

3.3 Phase II of the Experimental Program

This section describes the second phase of the experimental program undertaken to evaluate bond characteristics of various FRP strengthening systems tested in the first phase of the experimental program. The fabrication process, instrumentation, and testing of the specimens are discussed.

3.3.1 Bond Specimens

A total of 39 simply supported T-beams with a span of 2.5 m and a depth of 300 mm were constructed. Shear reinforcement consisted of double-legged 10M steel stirrups, uniformly spaced at 100 mm. The top flange was reinforced with welded wire fabric (WWF) 51x51 MW5.6 x MW5.6. The top reinforcement consisted of two 10M steel bars. The bottom reinforcement consisted of two 10M steel bars running along the full length of the beam and two 15M steel bars placed at 100 mm from the mid-span section of the beam on both sides as shown in Fig. 3.31.
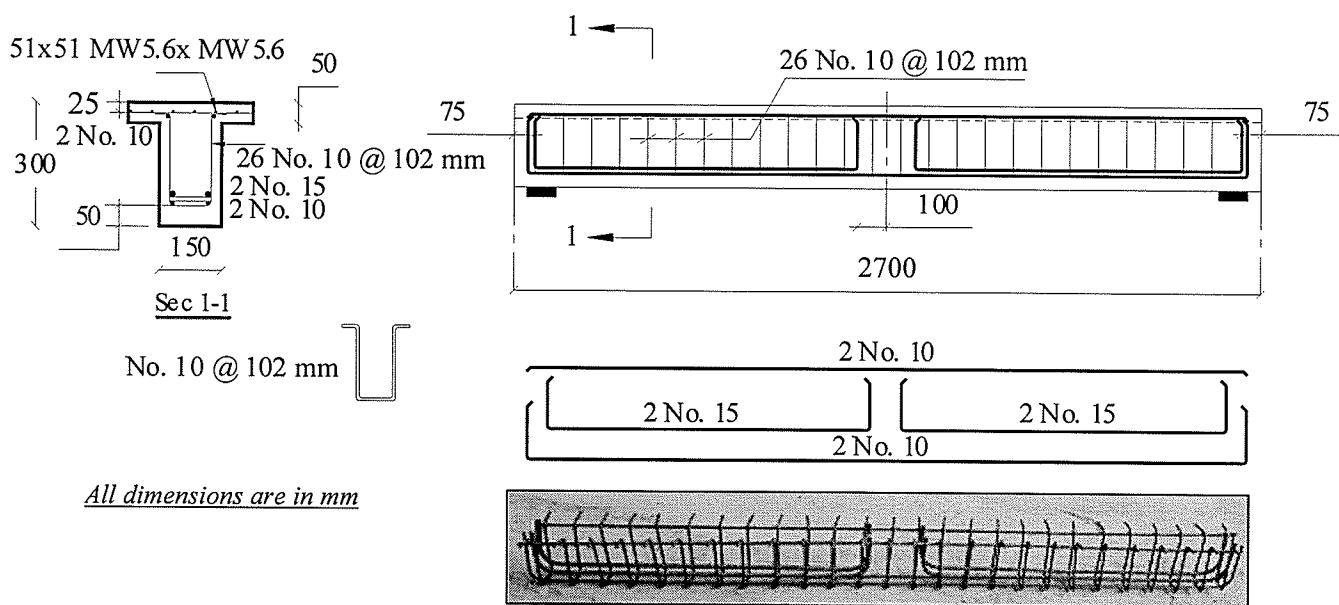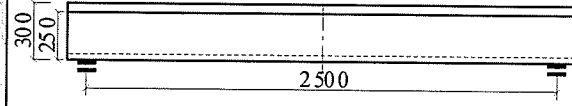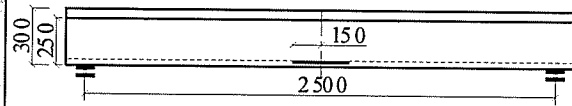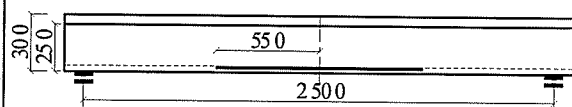
51x51 MW5.6x MW5.6   50

25
2 No. 10
300   26 No. 10 @ 102 mm
2 No. 15
50   2 No. 10
150

Sec 1-1

No. 10 @ 102 mm

All dimensions are in mm

1
26 No. 10 @ 102 mm   75   75

1   100
2700

2 No. 10
2 No. 15   2 No. 15
2 No. 10
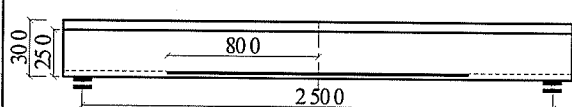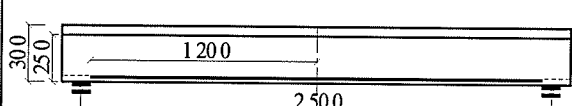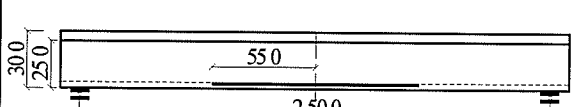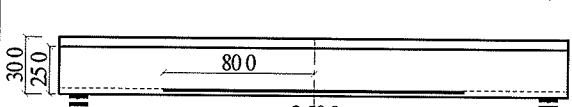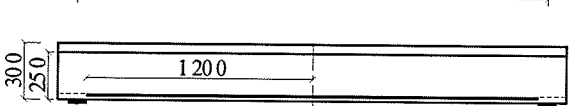
Fig. 3.31 Reinforcement details of bond specimens

115

This arrangement of the bottom reinforcement was selected to identify the location of flexural failure of the strengthened specimens. The T-section configuration was selected to avoid compression failure due to crushing of the concrete. Selection of the specimens' dimensions was finalized after testing six pilot sp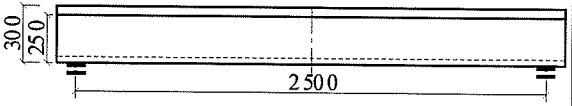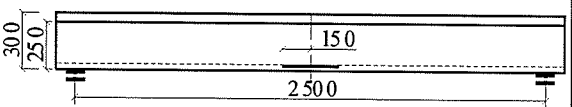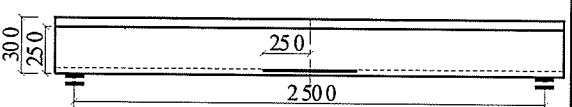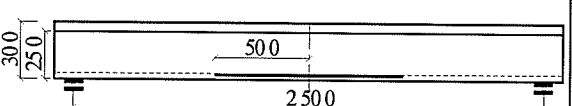ecimens. Three series of beam specimens designated as A, B and C were used, respectively. Thirteen beams were constructed for each series. In series A, the beams were strengthened using near surface mounted C-Bars. The performance of two different epoxy adhesives used for bonding the bars was investigated. In series B, the beams were strengthened using near surface mounted CFRP strips, while in series C, the beams were strengthened using externally bonded CFRP sheets. The variables considered in this phase of the experimental program were the bond length of FRP and the method of strengthening. Bond characteristics of the three strengthening techniques were evaluated based on testing a total of 24 specimens. The remaining specimens will be used in a future research project to examine the durability aspect of various FRP strengthening systems under severe environmental conditions. With the maximum moment occurring at the mid-span section of the beam, failure could be due to either debonding or rupture of the CFRP reinforcement. The specimens were adequately designed to avoid concrete crushing and premature failure due to shear. In the case of bond failure, the bond length of the CFRP reinforcement was increased in the subsequent specimens. In the case of flexural failure, the bond length was decreased in the subsequent specimens. This scheme was applied until an accurate development length for each strengthening technique was evaluated. Complete details for the bond specimens are given in Table 3.4.
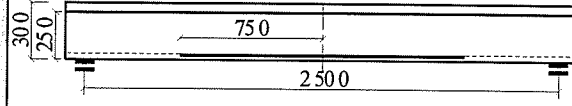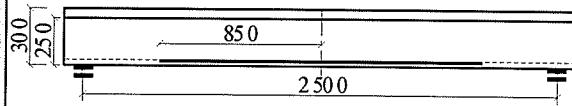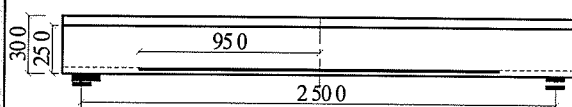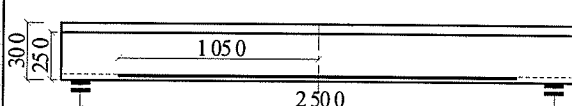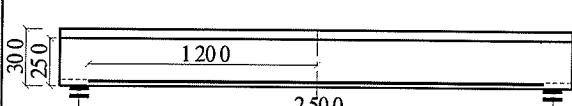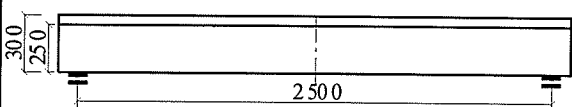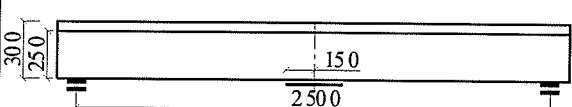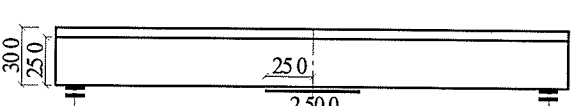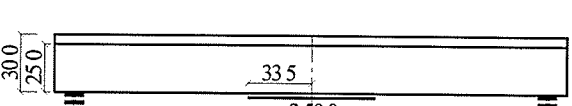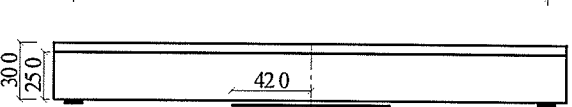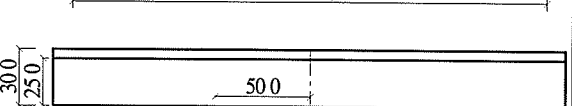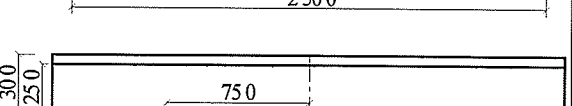
Table 3.4 Summary of bond specimens

Series	Description of specimen	Beam #	Epoxy	Strengthened with
SERIES A		A0	-	Control specimen
		A1	Duralith gel	Near surface mounted C-BAR CFRP bars
		A2	Duralith gel	Near surface mounted C-BAR CFRP bars
		A3	Duralith gel	Near surface mounted C-BAR CFRP bars
		A4	Duralith gel	Near surface mounted C-BAR CFRP bars
		A5	Kemko 040	Near surface mounted C-BAR CFRP bars
		A6	Kemko 040	Near surface mounted C-BAR CFRP bars
		A7	Kemko 040	Near surface mounted C-BAR CFRP bars
SERIES B		B0	-	Control specimen
		B1	EN-Force CFL	Near surface mounted CFRP Strips (25x1.2mm)
		B2	EN-Force CFL	Near surface mounted CFRP Strips (25x1.2mm)
		B3	EN-Force CFL	Near surface mounted CFRP Strips (25x1.2mm)

Table 3.4 Summary of bond specimens *(cont'd)*

Series	Description of specimen	Beam #	Epoxy	Strengthened with
SERIES B (cont'd)	300 250 — 750 — 2500	B4	EN-Force CFL	Near surface mounted CFRP Strips (25x1.2mm)
	300 250 — 850 — 2500	B5	EN-Force CFL	Near surface mounted CFRP Strips (25x1.2mm)
	300 250 — 950 — 2500	B6	EN-Force CFL	Near surface mounted CFRP Strips (25x1.2mm)
	300 250 — 1050 — 2500	B7	EN-Force CFL	Near surface mounted CFRP Strips (25x1.2mm)
	300 250 — 1200 — 2500	B8	EN-Force CFL	Near surafec mounted CFRP Strips (25x1.2mm)
SERIES C	300 250 — 2500	C0	-	Control specimen
	300 250 — 150 — 2500	C1	MBrace system	Externally bonded CFRP sheets
	300 250 — 250 — 2500	C2	MBrace system	Externally bonded CFRP sheets
	300 250 — 335 — 2500	C3	MBrace system	Externally bonded CFRP sheets
	300 250 — 420 — 2500	C4	MBrace system	Externally bonded CFRP sheets
	300 250 — 500 — 2500	C5	MBrace system	Externally bonded CFRP sheets
	300 250 — 750 — 2500	C6	MBrace system	Externally bonded CFRP sheets

3.3.2 Fabrication of the Specimens

The specimens were fabricated by Lafarge, Canada. Wooden forms were constructed to account for the shape and size of the specimens. The forms were cleaned and lubricated and the steel cages were assembled and tied in place, as illustrated in Fig. 3.32. The concrete was vibrated using pin vibrator, lightly trawled, and covered with polyethylene sheet. The surface of the specimens was kept wet to prevent the occurrence of any shrinkage cracks, which could affect the behaviour. Casting of the specimens is shown in Fig. 3.33.
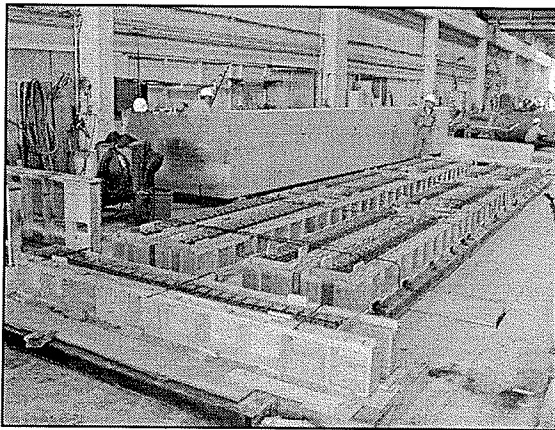
Fig. 3.32 Reinforcement cage placed in formwork   Fig. 3.33 Casting of bond specimens
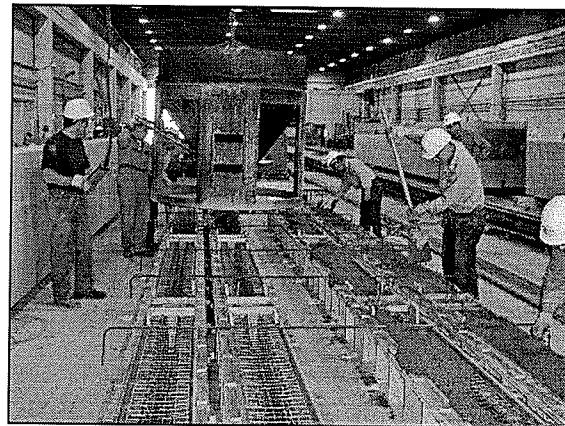
3.3.3 Strengthening Procedures

Series A:

A total of eight beams were tested from series A. One beam was tested as a control specimen, A0, while the other seven beams were strengthened with near surface mounted C-Bars. Each beam was strengthened using one 10 mm diameter bar inserted into a grove cut at the bottom surface of the beam. Beams A1, A2, A3, and A4 with embedment lengths of 150, 550, 800, and 1200 mm, respectively were tested using Duralith-gel as an epoxy adhesive for bonding the bars. The adhesive is produced by Tamms Industries,

USA and is commonly used as a mortar binder for vertical and overhead repairs of structural concrete. To investigate the suitability of the epoxy adhesive, beams A5, A6 and A7 with embedment lengths of 550, 800, and 1200 mm, respectively were tested using Kemko 040 as an alternative epoxy adhesive. Kemko 040 is produced by ChemCo Systems, Inc., USA and is designed specifically for grouting bolts, dowels and steel rebars in concrete.

A special concrete saw was used to cut a groove of approximately 18 mm wide and 30 mm deep at the bottom surface of the beam. The process of cutting the groove, filling the groove with epoxy, and inserting the bar inside the groove is illustrated in Fig. 3.34.
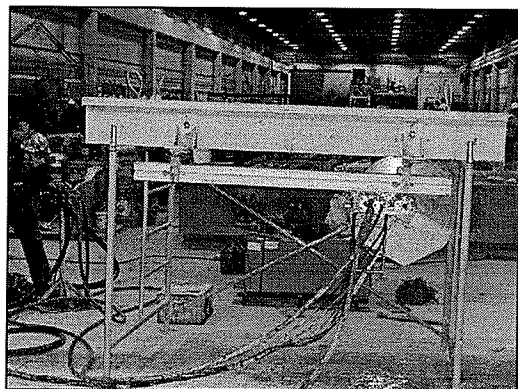
a) cutting the groove

b) filling the groove with epoxy
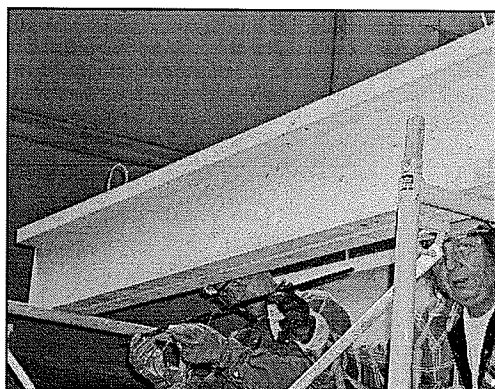
c) inserting the bar inside the groove

Fig. 3.34 Strengthening procedures for series A beams

Series B:

A total of nine concrete beams were tested from series B. Beam B0 was tested as a control specimen. The remaining beams were strengthened using near surface mounted CFRP strips (25x1.2mm). Each beam was strengthened using one strip inserted into a groove cut at the bottom surface of the beam. Eight different embedment lengths of 150, 250, 500, 750, 850, 950, 1050, and 1200 mm were investigated to evaluate the minimum embedment length required to develop the ultimate force of the strip (development length). The installation procedures of the strips at the bottom surface of the beams are illustrated in Fig. 3.35.
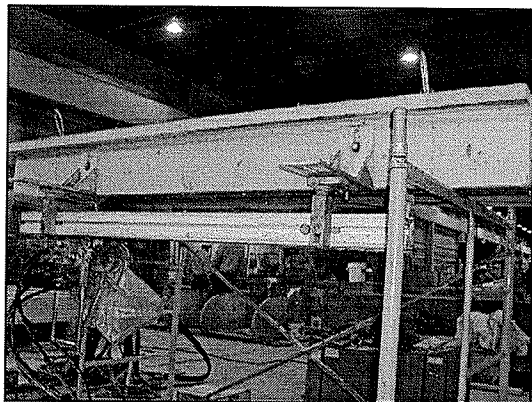
a) cutting the groove

b) filling the groove with epoxy
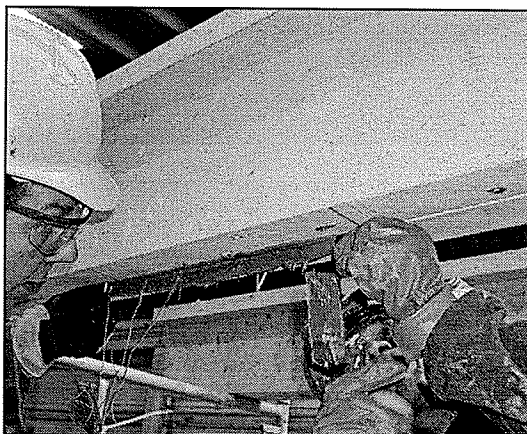
c) inserting the CFRP strip inside the groove

Fig. 3.35 Strengthening procedures for series B beams

Series C:

A total of seven concrete beams were tested from series C. Beam C0 was tested as a control specimen. The remaining beams were strengthened using one ply of an externally bonded CFRP sheet. Six different bond lengths of 150, 250, 335, 420, 500 and 750 mm were investigated. The concrete surface was prepared by grinding and sandblasting. Two coats of MBrace primer and putty were applied to the surface with a paintbrush. A coat of MBrace saturant was applied using a nap roller. Following these procedures, a sheet of CFRP was applied. The fibre sheet was again covered with a final coat of MBrace saturant. The procedures for applying the CFRP sheets are given in Fig. 3.36.
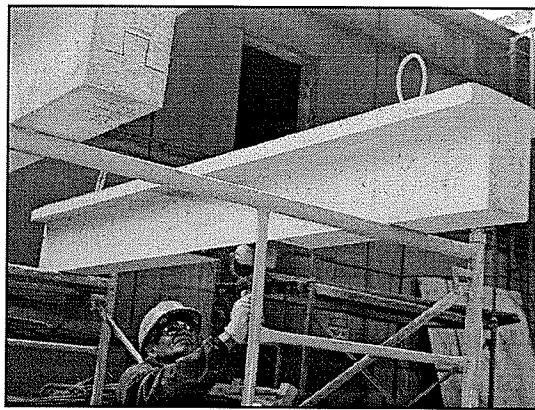
a) applying MBrace primer
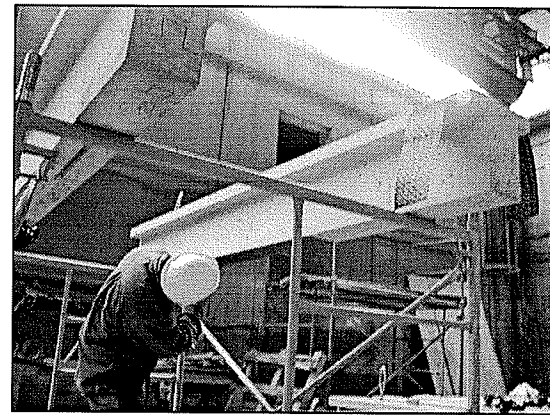
b) applying MBrace saturant

Fig. 3.36 Strengthening procedures for series C beams

Strengthening procedures for the bond specimens were performed by Concrete Restoration Services, Ltd., Winnipeg, Canada.

3.3.4 Instrumentation

Strains: The concrete strains in the compression zone at the top surface of the beam was measured using two PI gauges. The strain in the FRP reinforcement was monitored using three electrical strain gauges.

Slip monitoring: The slip at the free ends of the FRP reinforcement was measured using two LVDTs.

Deflections: The deflection at mid-span was monitored on both sides of the beam using two LVDTs.

The instrumentation used to monitor the behaviour of the bond specimens during testing is shown in Fig. 3.37
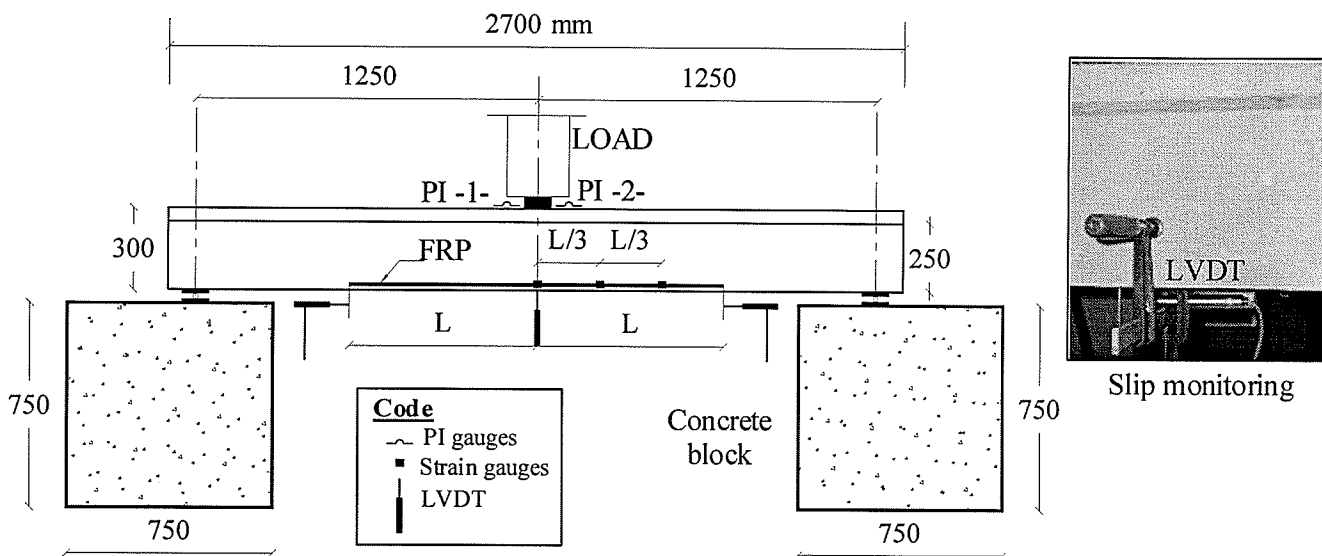
Fig. 3.37 Instrumentation used for bond specimens

3.3.5 Testing Scheme

The beams were tested under a concentrated load applied at mid-span. A closed-loop MTS, 1000 kN testing machine was used to apply the load using the stroke control mode. The rate of loading was 1.0 mm/min up to yielding of the internal steel reinforcement, beyond which the rate was increased to 3.0 mm/min up to failure. Plaster pads were used at the loading location and at the supports to provide even distribution of the load and the reactions. Fig. 3.38 shows the test set-up in the lab.
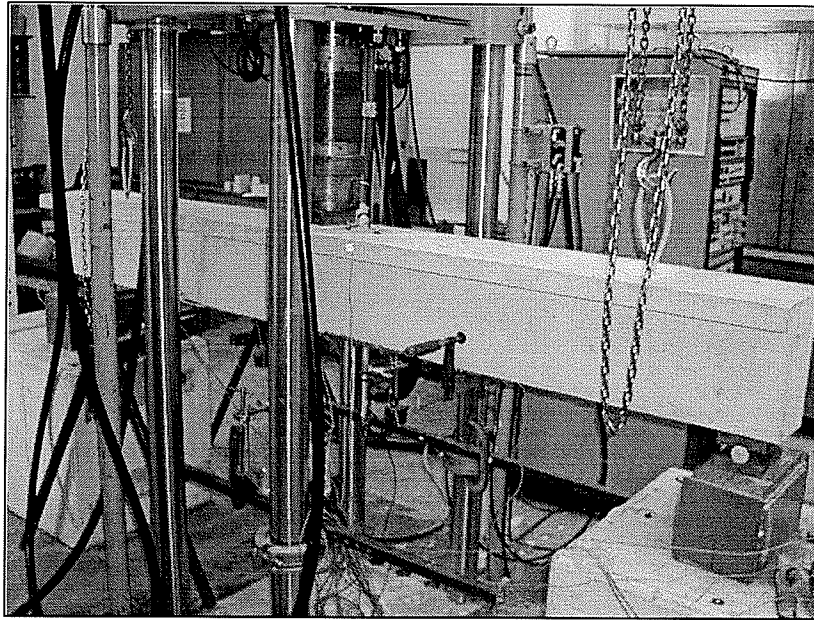
Fig. 3.38 Test set-up for bond specimens

3.4 Materials

3.4.1 Concrete

Phase I: The concrete was designed for a nominal strength of 31 MPa at release and 35 MPa at 28 days. The concrete had a 20 mm maximum aggregate size and a 130 mm slump. Twelve cylinders were cast together with each concrete slab to determine the compressive and the tensile strength of concrete. A total of nine cylinders were tested in

compression and three cylinders were tested in tension. The average compressive strength of the concrete at the time of testing ranged between 45 to 51 MPa. The average tensile strength, based on the split-cylinder test ranged between 3.25 MPa and 3.50 MPa.

Phase II: The concrete was designed for a compressive strength of 45 MPa after 28 days. A total of 27 cylinders were cast together with the beams to determine the compressive and the tensile strength of concrete. The average compressive strength of concrete after 28 days ranged between 48 to 57 MPa. All tests were conducted according to the ASTM C39-86 standard.

3.4.2 Prestressing Steel

Twelve 15 mm diameter, 7-wire strands were used for post-tensioning each slab tested in phase I. The strands were stress-relieved of grade 1860 and conformed to CSA-G279 Standard. The tensile properties of the prestressing steel strands were evaluated based on tension tests of two 15 mm diameter steel strands using conventional steel wedge anchorages in a 60,000 pound testing machine. The stress-strain relationships for both tests are shown in Fig. 3.39. Test results indicated that the average modulus of elasticity and ultimate strength were 209 GPa and 1843 MPa, respectively.
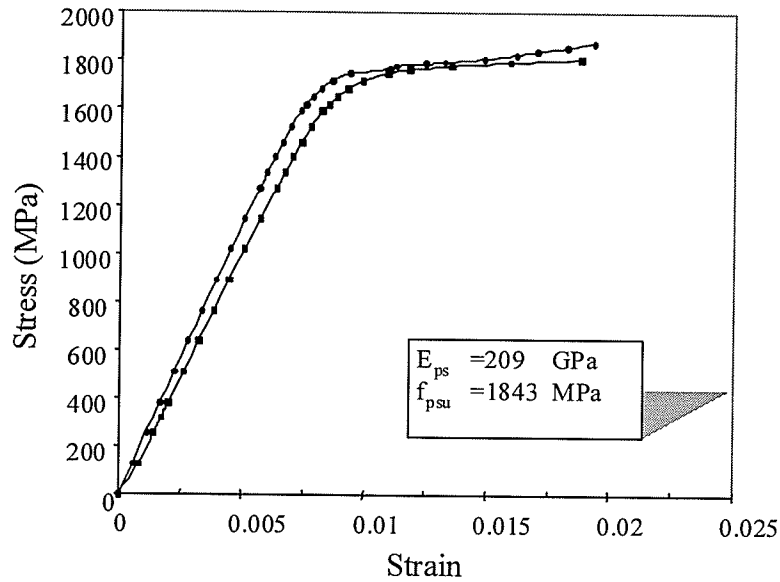
Fig. 3.39 Stress-strain behaviour of prestressing steel strands

The modified Ramberg-Osgood function [Mattock, 1979] for the prestressing steel strands is given by Equation 3.4

$$f_{ps} = E_p \, \varepsilon_{ps} \left[A + \frac{1-A}{\left(1 + \left(B \, \varepsilon_{ps}\right)^C\right)^{1/C}} \right] \leq f_{pu} \tag{3.4}$$

where:

f_{ps} =   stress in the steel strand;

E_p =   modulus of elasticity of the steel strands;

ε_{ps} =   strain in the steel strand;

A,B,C =   coefficients depending on the stress-strain behaviour of the strand; and

f_{pu} =   ultimate stress in the steel strand

Coefficients A, B, and C were evaluated from the measured stress-strain relationship. The modified Ramberg-Osgood function for the prestressed steel strands can be expressed as:

$$f_{ps} = 209,000\, \varepsilon_{ps} \left[0.063 + \frac{0.937}{\left(1 + \left(121.4\, \varepsilon_{ps}\right)^{10}\right)^{1/10}} \right] \leq f_{pu} = 1843\ MPa \qquad (3.5)$$

3.4.3 Sheathing

Both steel and plastic sheathings were used for placing the prestressing steel strands. Six steel sheaths were used to provide the bond between the concrete outside the sheath and the grout inside the sheath. Steel sheaths were galvanzied, 30 mm diameter with 3 mm corrugations. Based on the limited availability of the steel sheaths, plastic sheaths were used for placing the rest of the strands. Plastic sheaths were 20 mm by 60 mm with 10 mm corrugations. Inside the sheath, the post-tensioned strand was lubricated with a non-corrosive grease for additional corrosion protection.

3.4.4 Mild Steel

All mild steel rebars were grade 400W. The mild steel reinforcement was provided by Cowin Steel Co. of Winnipeg, Manitoba, and conformed to CSA G30.18 Standard. The reported minimum yield strength and modulus of elasticity of the bars were 400 MPa and 200 GPa, respectively.

3.4.5 Leadline

In general, CFRP reinforcement is characterized by having the highest modulus of elasticity, compared to other commercially available FRP bars. However, it has the smallest ultimate tensile strain. CFRP reinforcement is characterized by excellent fatigue

properties and a low coefficient of thermal expansion [Mufti et al., 1991]. Leadline bars, having an indented shape and 10 mm nominal diameter, were used to strengthen one cantilever of specimen S1 in the first phase of the experimental program. The Leadline bars are produced by Mitsubishi Chemicals Corporation, Japan. The bars are pultruded using linearly oriented dialead coal-tar-pitch-based continuous fibre and epoxy resin. The stress-strain relationship of the Leadline bars is linearly elastic up to failure with an ultimate guaranteed strength of 1970 MPa and a modulus of elasticity of 147 GPa. The fibre content by volume is 65 percent [Abdelrahman, 1995].

3.4.6 S&P CFRP Strips

The CFRP strips used for flexural strengthening are produced by S&P Clever Reinforcement Company, Switzerland and are provided by BK International, USA. The stress-strain relationship of the strips is linear-elastic up to failure. As reported by the manufacturer, the minimum tensile strength and modulus of elasticity are 2000 MPa and 150 GPa, respectively. However, the manufacturer did not provide a definite value for either the tensile strength or the modulus of elasticity. Three unidirectional coupons of CFRP strips were tested in tension. The coupons were cut from a flat portion of a CFRP strip, 50 mm wide. The dimensions of the coupons were selected according to the ASTM Standard D 3039-76 (1990). The width and the thickness of each coupon were measured using a digital caliber of accuracy of 0.01 mm. A typical stress-strain curve of a CFRP coupon is shown in Fig. 3.40. This behaviour is typical for all tested coupons, which showed a linear stress-strain relationship up to failure. Test results revealed an average

value of the tensile strength and the modulus of elasticity of 2120 MPa and 163 GPa, respectively.
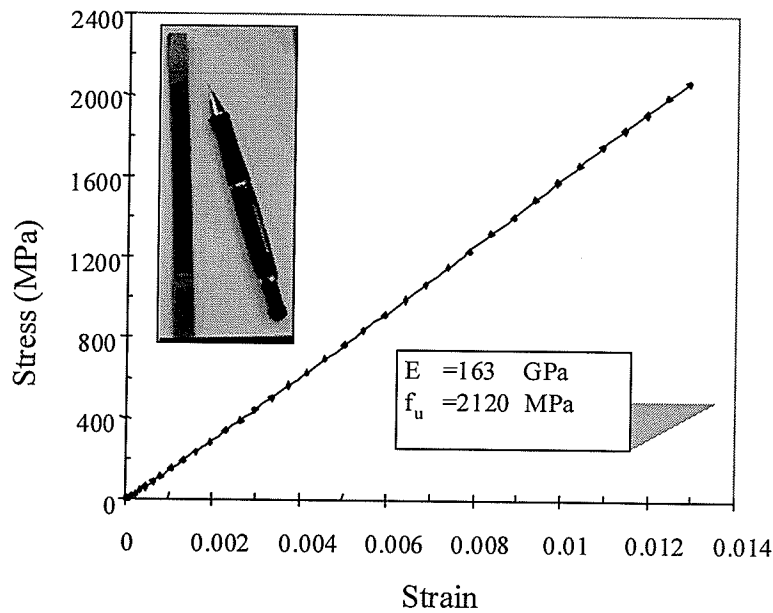
Fig. 3.40 Stress-strain behaviour of S&P CFRP strips

The test set-up and failure mode of the unidirectional CFRP coupons are shown in Figs. 3.41a and 3.41b, respectively. The CFRP strips were bonded to the concrete surface using the manufacturer recommended epoxy adhesive, EN-force CFL.
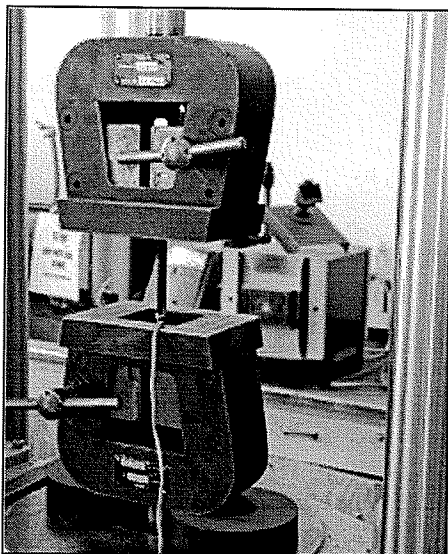
Fig. 3.41a Test set-up for unidirectional CFRP strips
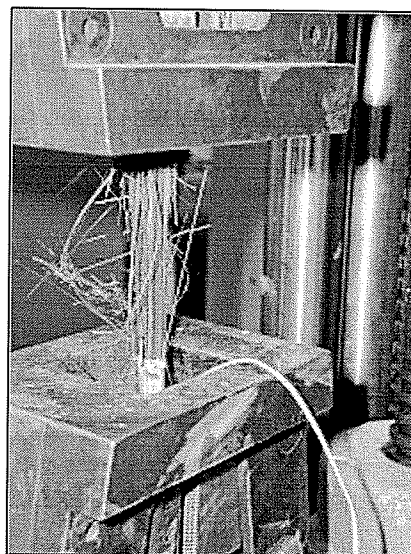
Fig. 3.41b Tension coupon after failure in the testing machine

3.4.7 MBrace CFRP Sheets

The sheets are manufactured by Master Builders Technologies, Ltd., Ohio, USA. MBrace carbon fibres are manufactured by pyrolizing polyacrylonitrile (PAN) based fibres at temperatures at approximately 1500 °C. The result of the pyrolization process is a highly aligned carbon fibre chain. The carbon fibre filaments are assembled into untwisted tows that are then used to create a continuous unidirectional sheet. The ultimate tensile strength and the modulus of elasticity are 4275 MPa and 228 GPa, respectively as reported by the manufacturer. The thickness of the sheets is 0.165 mm.

3.4.8 C-BAR

The bars are manufactured by Marshall Industries Composites Inc., USA. Based on tension tests conducted at W.R. McQuade Structural Laboratory at the University of Manitoba, the stress-strain relationship is linearly elastic up to failure with an ultimate tensile strength and modulus of elasticity of 1918 MPa and 111 GPa, respectively.

Chapter 4

Experimental Results & Analytical Modelling:

Large-Scale Slab Specimens

This chapter presents test results of the first phase of the experimental program. Three half-scale models of a typical prestressed concrete bridge slab were constructed and tested to failure. The effectiveness of various FRP strengthening schemes is investigated. The ultimate capacity, failure mechanism and cost analysis of the various strengthening techniques for concrete bridges are presented. The applicability of the non-linear finite element simulation and cracked section analysis for post-tensioned bridge slabs strengthened with near surface mounted FRP reinforcement is discussed.

4.1 Introduction

Rehabilitation and strengthening of deteriorated reinforced or prestressed concrete structures using externally bonded FRP reinforcement have received great attention in recent years. Extensive research and laboratory testing have been conducted all over the world to examine the short-term and long-term behaviour of the externally bonded FRP system. Many research studies have demonstrated the effectiveness of this technique and showed that considerable improvement in strength can be achieved using externally

bonded sheets or prefabricated laminates [Nordin et al., 2001]. Nevertheless, in-depth understanding of the bond mechanism between FRPs and concrete is still a challenging issue and needs to be investigated. Furthermore, externally bonded FRP reinforcements are sensitive to impact loads and require protection covers. The use of near surface mounted FRP rods and strips can preclude delamination-type failures, frequently observed by using externally bonded reinforcement [Hassan and Rizkalla, 2002].

In response to an increasing demand towards increasing the flexural capacity of concrete bridges to accommodate new truck loads, an experimental program was undertaken at the University of Manitoba. The main goal of the experimental program was to obtain experimental data and in-depth understanding of the structural performance of various FRP strengthening techniques and to develop fundamental criteria governing the choice of a specific technique. These techniques included near surface mounted bars and strips as well as externally bonded sheets and strips. Based on the research findings, recommendations for the most efficient techniques were developed including design guidelines for their uses in different retrofitting scenarios.

To achieve the objectives of this research program, a two-phase experimental program was conducted. The first phase presented a comparison among various FRP strengthening techniques. A total of nine tests were conducted using large–scale slab specimens to examine the structural performance and load sharing mechanisms that are encountered in typical concrete bridges. Based on the test results, the efficiency of each FRP strengthening system is identified. The applicability of a non-linear finite element

simulation and cracked section analysis for typical bridge slabs strengthened with near surface mounted FRP reinforcement is discussed. The research was extended further to evaluate bond characteristics of each FRP strengthening technique. A total of 24 concrete beams were constructed and tested in the second phase of the investigation. Mathematical models for near surface mounted bars, strips and externally bonded FRP sheets are proposed and presented in Chapter 5.

4.2 Experimental Results

4.2.1 General

This section summarizes test results of the three half-scale models of a typical prestressed concrete bridge slab, reported in Chapter 3, section 3.2. The specimens had dimensions of 8.5x1.2x0.4 m. The specimens were tested in a simple span with a double cantilever configuration. Each specimen was tested three times using loads applied at different locations in each test. The first and second tests were performed on the two cantilevers where the load was applied at the edge of each cantilever as shown in Fig. 4.1. The third test was conducted using a load applied at the mid-span as shown schematically in Fig. 4.2.
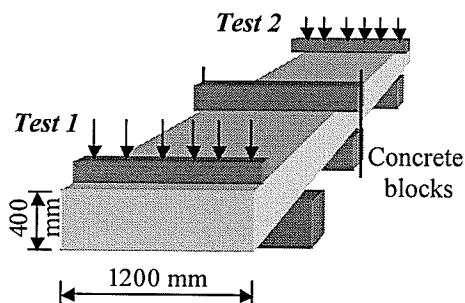
Fig. 4.1 Schematic representation
of cantilever tests
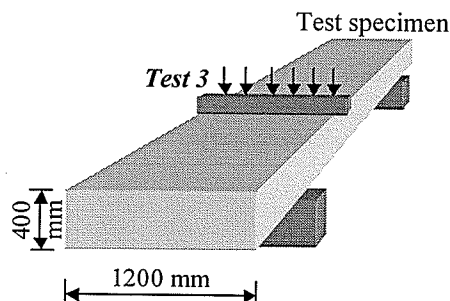
Fig. 4.2 Schematic representation
of simply supported tests

Five different strengthening techniques were investigated including near surface mounted Leadline bars, C-Bars, CFRP strips and externally bonded CFRP sheets and strips. The CFRP reinforcement was designed based on strain compatibility and internal force equilibrium procedures to achieve a 30 percent increase in the ultimate strength of the slabs as described in Chapter 3, section 3.2.3.

Since the specimens were fully prestressed, the slabs were uncracked under service loading conditions. Consequently, the effectiveness of different strengthening schemes with regard to stiffness was negligible. Therefore, serviceability could not be used as a criterion in comparing the efficiency of the various strengthening schemes used in this investigation. The focus of the current research was to examine the ultimate limit state using the various FRP strengthening schemes. It should be mentioned also that the pronounced problem for the bridge under consideration lies in the ultimate limit state rather than the serviceability limit state.

The following sections present the behaviour and test results of both cantilevers and the simply supported specimen of each slab.

4.2.2 Cantilever Test Results

4.2.2.1 Deflection

The load-deflection behaviour of the cantilever specimens strengthened with near surface mounted Leadline bars (C2), CFRP strips (C4) and C-Bars (C6) is compared to the unstrengthened specimen (C1) in Fig. 4.3.
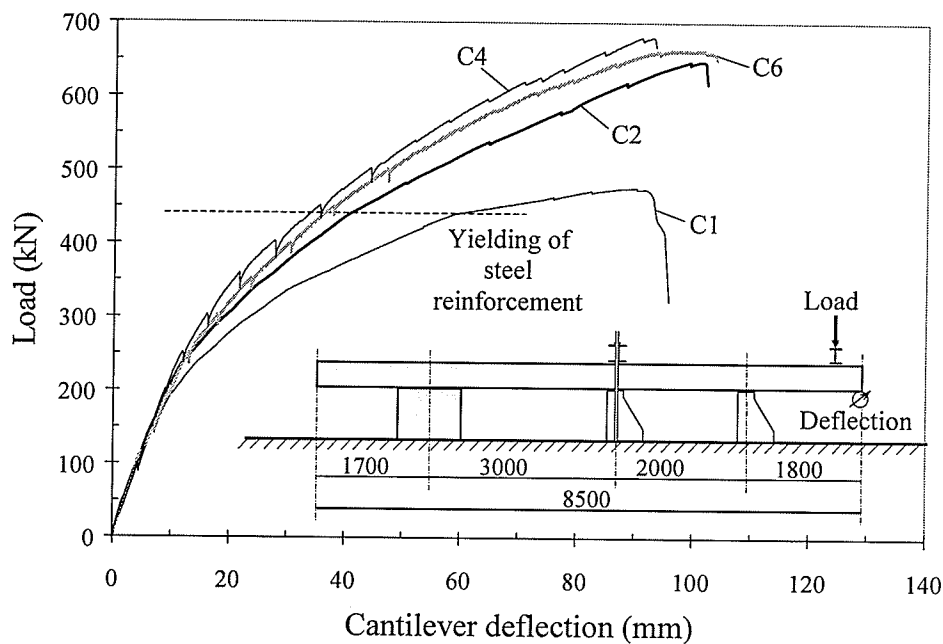
Fig. 4.3 Load-deflection behaviour of cantilever specimens strengthened with near surface mounted CFRP reinforcement

Test results indicated identical behaviour for all the specimens prior to cracking at a load level of 180 kN for the unstrengthened cantilever and 190 kN for the strengthened cantilevers. After cracking, a nonlinear behaviour was observed up to failure. The measured stiffnesses for the strengthened specimens (*expressed by the slope of the load-deflection curves*) are higher due to the addition of the CFRP reinforcement.

The presence of CFRP reinforcement precluded the flattening of the load-deflection curve, which was clear in the control specimen at the load range of 440 kN to 466 kN. Prior to yielding of the steel reinforcement, at a load level of 440 kN, the stiffnesses of all strengthened cantilevers were almost the same and were 1.5 times higher than the stiffness of the unstrengthened cantilever. Such a phenomenon was accompanied with a considerable reduction in crack width and deflections of the strengthened specimens in comparison to the control specimen. The presence of the CFRP reinforcement provided constraints to opening of the cracks. Therefore, the deflections were reduced and consequently increased the stiffness. After yielding of the tension steel reinforcement, the stiffness of the cantilever specimen strengthened with Leadline bars, specimen C2, was three times higher than that of the control specimen.

Reducing the spacing between the near surface mounted CFRP reinforcement resulted in a more uniform distribution of stresses and additional constraints to opening of the cracks along the cantilever width. Such a phenomenon reduced the curvature of the slab and resulted in a considerable increase in stiffness. This was evident by using eight C-Bars instead of six Leadline bars, the observed increase in stiffness was 20 percent. However, using 12 near surface mounted CFRP strips yielded a stiffness increase of 35 percent compared to the Leadline bars. For the control specimen, the increase in the applied load was negligible after yielding of the steel reinforcement. For the strengthened cantilevers, the load resistance and deflection increased until the concrete crushed in the compression zone. This is due to the additional strength and stiffness provided by the CFRP reinforcement.

Fig. 4.4 shows the load-deflection behaviour of cantilever specimens, C3 and C5, strengthened with externally bonded CFRP strips and sheets, respectively. The behaviour of the control specimen, C1, is also shown for comparison.
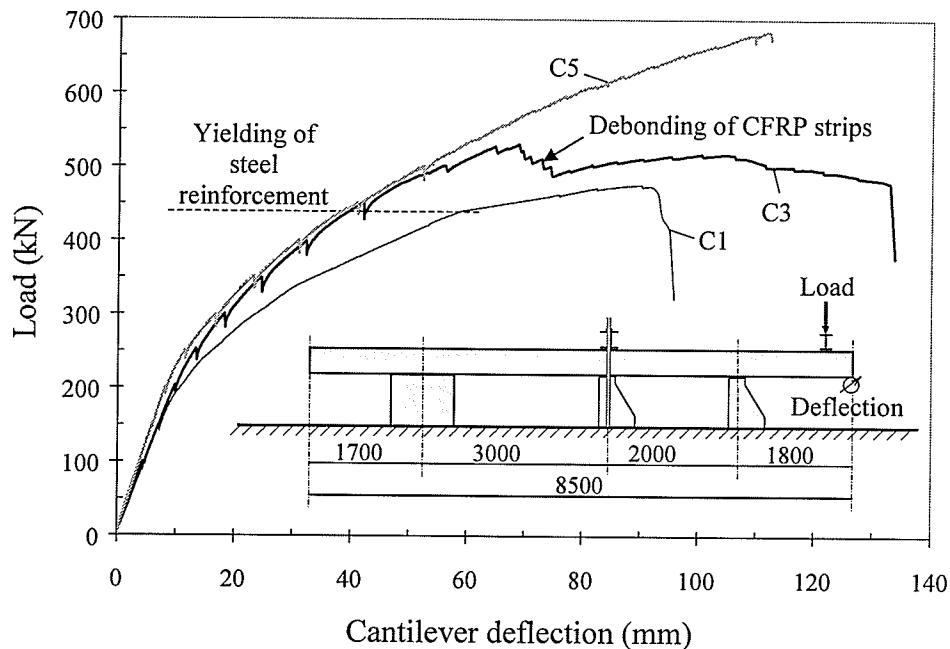
Fig. 4.4 Load-deflection behaviour of cantilever specimens strengthened with externally bonded CFRP reinforcement

The figure clearly indicates that the strength, stiffness and ductility of the specimens were greatly improved with the addition of the CFRP reinforcement. An identical behaviour was observed for specimens C3 and C5 up to a load level of 500 kN. After yielding of the steel reinforcement, the stiffness of specimen C5 was about 3.3 times higher than that of the unstrengthened cantilever. The cantilever specimens were loaded in increments of 50 kN to manually record the strain in demec points attached to the concrete surface. Since the load was applied in the stoke control mode, a drop of the load was observed at each increment of 50 kN as shown in Figs 4.3 and 4.4. According to classical beam theory (Bernoulli-Euler assumptions) and using the same axial stiffness for the CFRP

reinforcement, $(AE)_{CFRP}$, the load-deflection behaviour for all strengthened cantilevers was anticipated to be identical, where E and A are the modulus of elasticity and cross-sectional area of the CFRP reinforcement, respectively. Test results confirmed the anticipated behaviour by observing the same failure mode for most of the strengthened cantilevers, namely crushing of the concrete at the face of the support. Since, the ultimate strain of the concrete controlled the failure mode for all the tested specimens, the curvature and consequently the deflection at ultimate for all the strengthened specimens were fairly identical.

4.2.2.2 Failure Modes

The observed mode of failure for specimens C1, C2, C4, C5 and C6 was due to crushing of the concrete in the compression zone at the face of the support. At the onset of failure, the bottom steel bars and the steel stirrups were exposed, followed by buckling of the bottom steel bars. Typical failure due to crushing of concrete is shown in Fig. 4.5.
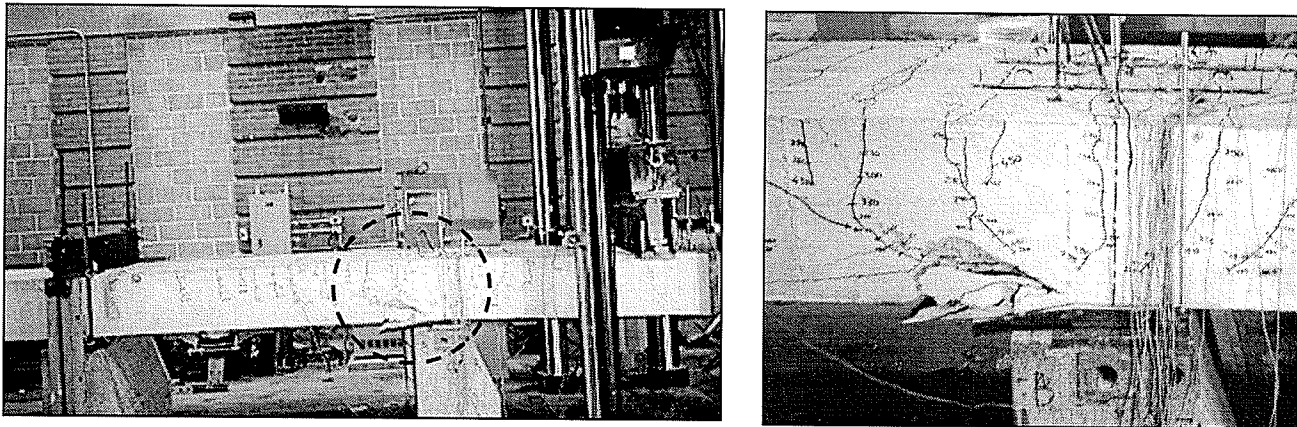
Fig. 4.5 Typical failure due to crushing of concrete

The failure extended throughout the entire width of the slab as shown in Fig. 4.6
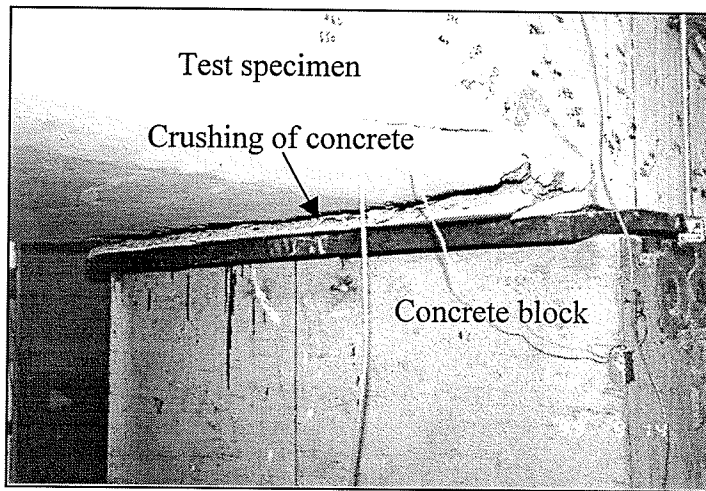
Fig. 4.6 View of failure from the bottom of the slab

In specimen C3, cracking in the concrete substrate at the anchorage zone was observed at a load level of 400 kN as shown in Fig. 4.7.
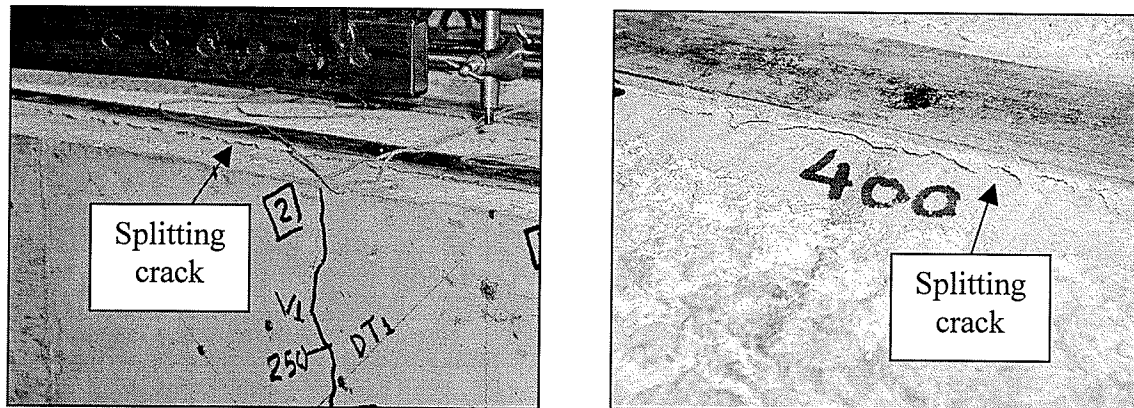
Fig. 4.7 Initial cracking in the concrete substrate of specimen C3 at 400 kN

Upon additional loading, the cracks continued to widen up to a load level of 530 kN where unstable delamination occurred resulting in peeling of the strips as shown in Fig. 4.8. At this stage, the load dropped to a level corresponding to the yield strength of the cross-section until crushing of concrete occurred, as shown in Fig. 4.5.
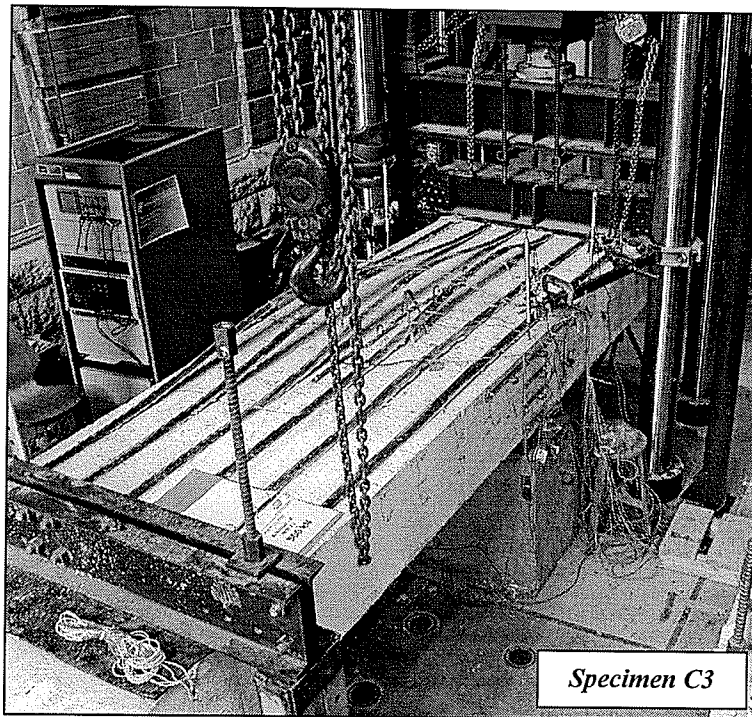
Fig. 4.8 Delamination of externally bonded CFRP strips

In general, CFRP-strengthened cantilever specimens showed considerable improvement in strength. The control specimen exhibited plastic failure with concrete failing in compression and steel yielding. The failure load of the control specimen was 476 kN. Strengthening the specimen using near surface mounted Leadline bars increased the strength by 36 percent in comparison to the design value of 30 percent. Using C-Bars instead of Leadline bars increased the strength by 39 percent. The cantilever specimen strengthened with near surface mounted CFRP strips showed the highest increase in strength by 43 percent. Using the same area of CFRP strips as externally bonded reinforcement increased the strength by only 11 percent due to the premature peeling failure of the strips [Hassan and Rizkalla, 2002].

4.2.2.3 Tensile Strains

The tensile strain in the CFRP reinforcement for all cantilever specimens was measured using electrical strain gauges. The measured load versus the maximum measured tensile strain for the three near surface mounted specimens using Leadline bars (C2), CFRP strips (C4) and C-Bars (C6) is shown in Fig. 4.9.
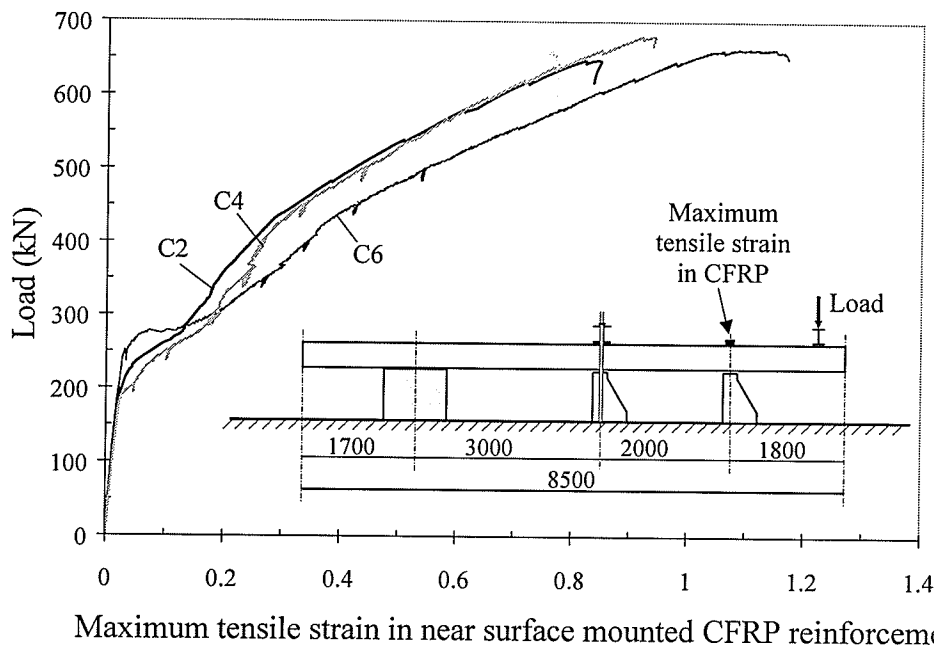
Fig. 4.9 Load-tensile strain behaviour of CFRP for cantilever specimens strengthened with near surface mounted reinforcement

Similar to the load-deflection behaviour, the load-tensile strain behaviour of the CFRP reinforcement is linear up to cracking of the concrete at the face of the support. Due to analogous values of the elastic modulus of the Leadline bars and CFRP strips, identical tensile strains were observed for specimens C2 and C4 up to failure. The measured tensile strain in the C-Bars was 35 percent higher than those measured in the Leadline bars and the CFRP strips. This is attributed to the relatively low modulus of elasticity of

the C-Bars in comparison to Leadline bars and CFRP strips ($E_{leadline}$ / $E_{C-Bar}=1.32$; E_{strips}/ $E_{C-Bar}=1.35$).

Since the governing mode of failure for specimens C2, C4 and C6 was crushing of the concrete, the strength of the CFRP reinforcement was not fully utilized in tension. The maximum measured tensile strain in the Leadline bars at failure was 0.85 percent indicating that 57 percent of the ultimate strain of the bars was utilized. Test results showed that approximately 65 percent of the ultimate strain of the CFRP strips and C-Bars was developed in specimens C4 and C6, respectively. No slip was observed in any of the three specimens during testing indicating that full composite action between near surface mounted CFRP reinforcement and concrete was developed. Fig. 4.10 shows the load-tensile behaviour of the cantilever specimens, C3 and C5, strengthened with externally bonded CFRP strips and sheets, respectively. Strain gauge readings showed identical behaviour for specimens C3 and C5 until delamination of the CFRP strips occurred.
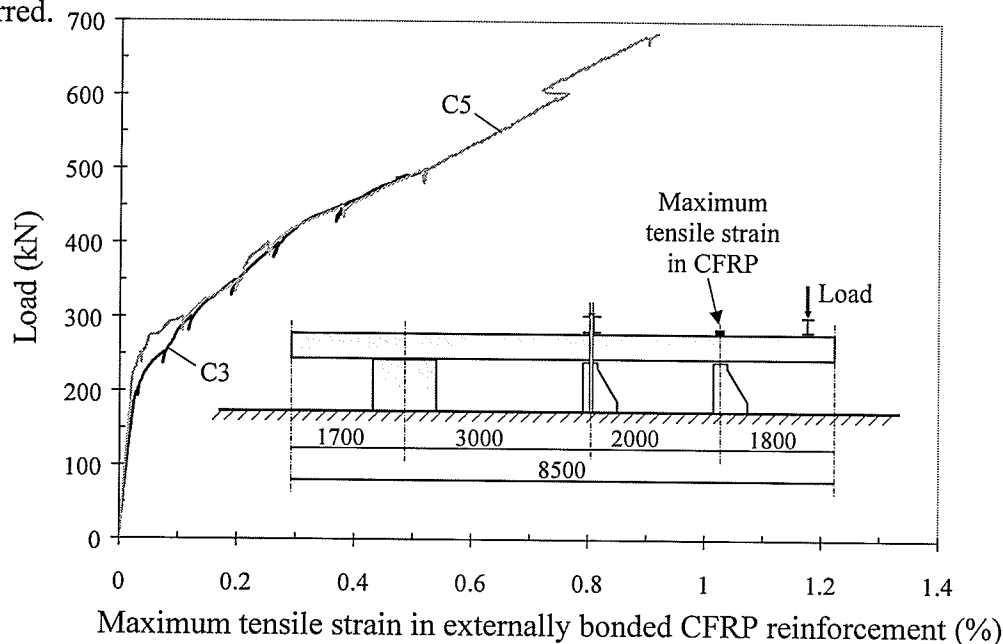
Fig. 4.10 Load-tensile strain behaviour of CFRP for cantilever specimens strengthened with externally bonded reinforcement

142

The maximum tensile strain in the externally bonded CFRP strips is given up to a load level of 500 kN, beyond which the strain gauges measured compressive strains. This is attributed to the negative curvature of the strips at the onset of delamination as shown in Fig. 4.11a. At failure, the CFRP strips slipped instantaneously from the free end of the cantilever as shown in Fig. 4.11b.
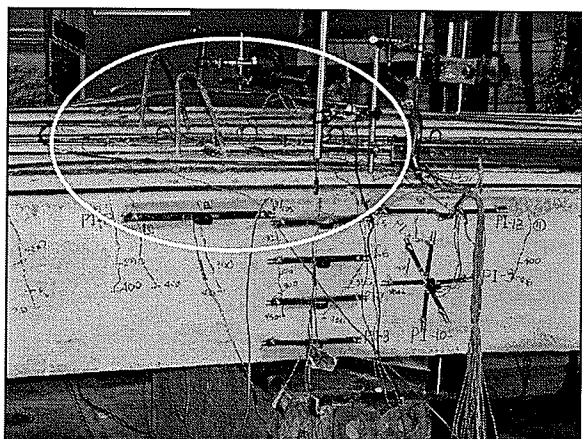
Fig. 4.11a Negative curvature of externally bonded CFRP strips at the onset of delamination
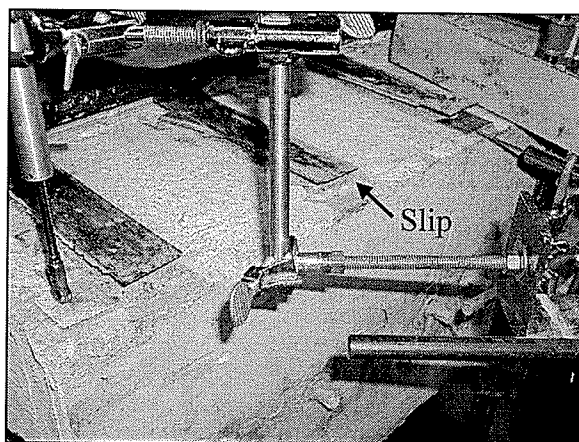
Fig. 4.11b Slip of externally bonded CFRP strips at the onset of delamination

The maximum measured tensile strain in the externally bonded CFRP strips, at the onset of delamination, was 0.54 percent, which represented only 41 percent of the ultimate strain of the strips. The measured delamination strain is 18 percent less than the value recommended by the draft of the ACI-Committee 440 (2002), which is equal to 0.66 percent (0.5 times the rupture strain). It should be mentioned that the maximum tensile strain specified by the manufacturer to avoid delamination failure is 0.65 percent. The maximum tensile strain in the CFRP sheets at failure was 0.9 percent, which is significantly higher than the limit specified and observed for externally bonded strips. The premature failure of specimen C3 is believed to be due to the large thickness of the externally bonded strips, which is four times the thickness of the externally bonded sheets

used for specimen C5. No delamination was observed between externally bonded CFRP sheets and concrete throughout the test.

From the above discussion, it is concluded that strengthening using near surface mounted CFRP strips has a greater anchoring capacity compared to externally bonded CFRP strips It should be noted also that near surface mounted strips have double the bond area compared to externally bonded strips [Hassan and Rizkalla, 2002].

4.2.2.4 Crack Patterns

Concrete cracks when the induced tensile stress exceeds the tensile strength of concrete. Increasing the applied load beyond the cracking load results in the initiation of additional cracks away from the vicinity of the first crack. Further loading may result in one of two developments:

- cracks increase in depth and the tensile stresses in the concrete between the cracks are significantly reduced; or
- cracks spread at an angle from the original crack.

At a certain crack pattern, known as the "stabilized crack pattern", increasing the applied loading may not cause the formation of new cracks [Leonhardt, 1977].

Test results in the present study indicated that stabilization of flexural cracks occurred at an applied load of 350 kN for the unstrengthened cantilever, specimen C1. This load is equivalent to 2.5 times the AASHTO HSS30 truck design load. For the strengthened cantilevers, stabilization of the cracks occurred at load values ranged from 3.2 to 3.6

times the ASSHTO HSS30 truck design load, depending on the strengthening technique adopted. Fig. 4.12 shows the typical crack pattern development for strengthened cantilevers at two loading stages. A typical load-deflection diagram is shown on the same figure.
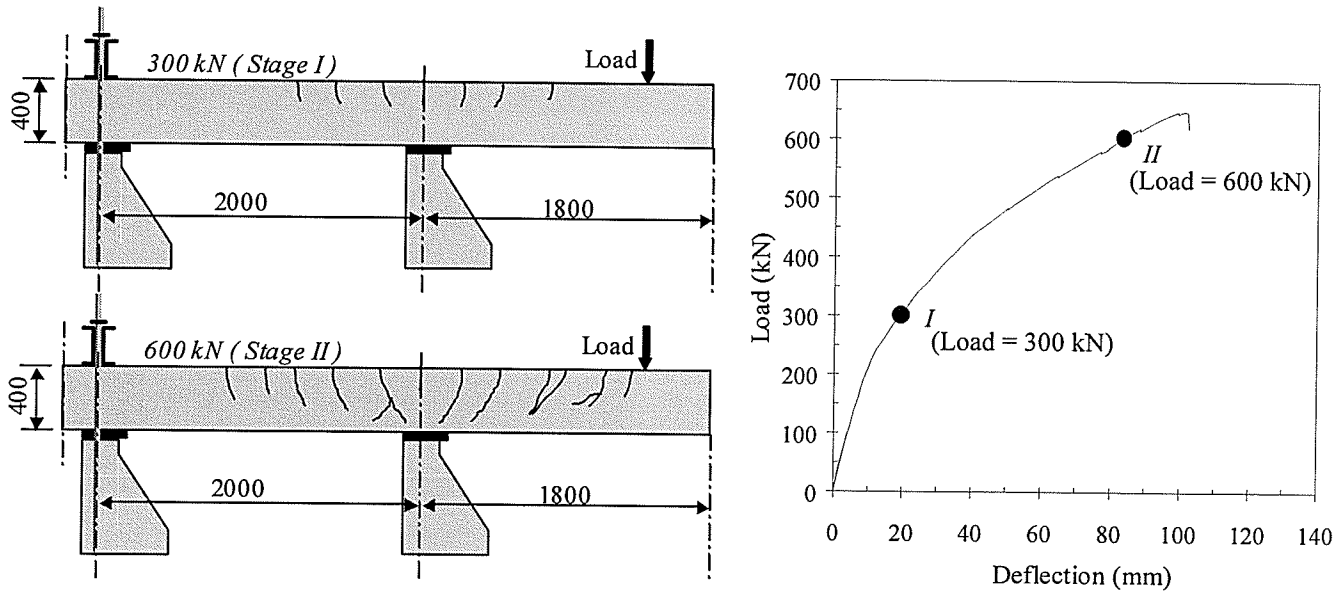
Fig. 4.12 Typical crack pattern development for strengthened cantilevers

In general, flexural cracks were evenly distributed. Cracks started perpendicular to the centre line of the slab and extended towards the bottom surface. It was observed that steel stirrups acted as crack initiators for all specimens regardless of the strengthening technique. During the tests, cracks were marked on both sides of the specimens at various loading stages.

Initiation of the first group of cracks occurred over the support section where maximum tensile stresses were developed (see stage I in Fig. 4.12). At high load levels, the neutral axis became almost stationary as shown in Fig. 4.13 and the cracks did not propagate vertically due to the presence of an almost constant compression zone depth.
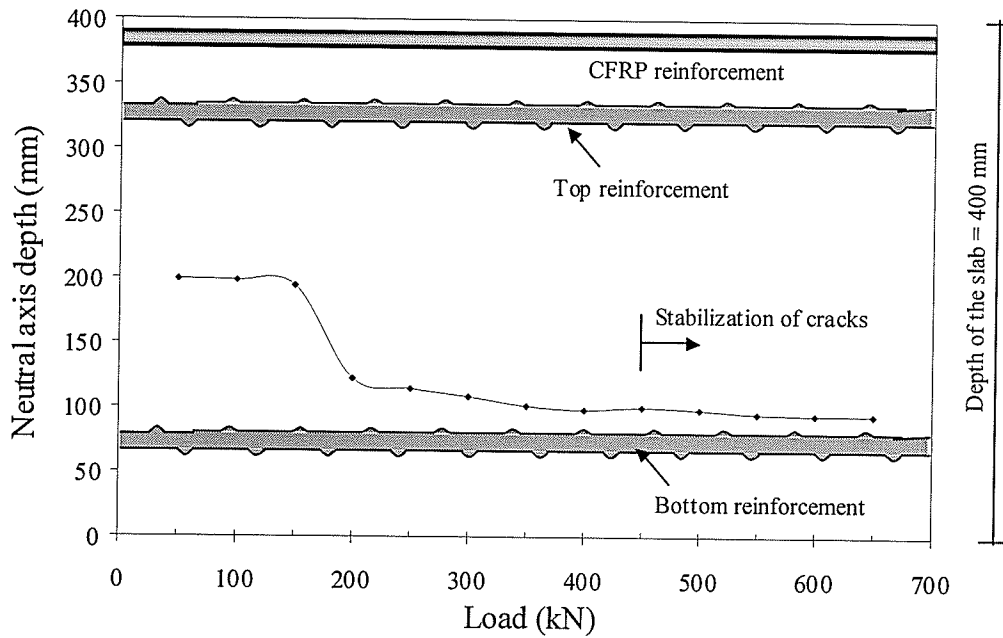
Fig. 4.13 Typical neutral axis depth vs. applied load for strengthened cantilevers

At this stage, the cracks extended laterally in a forked configuration as shown in stage II of Fig. 4.12 to reduce the tensile stresses at the tip of the cracks with an increase of the applied load. Crack patterns for both unstrengthened and strengthened cantilevers are illustrated in Fig. 4.14a and 4.14b, respectively.
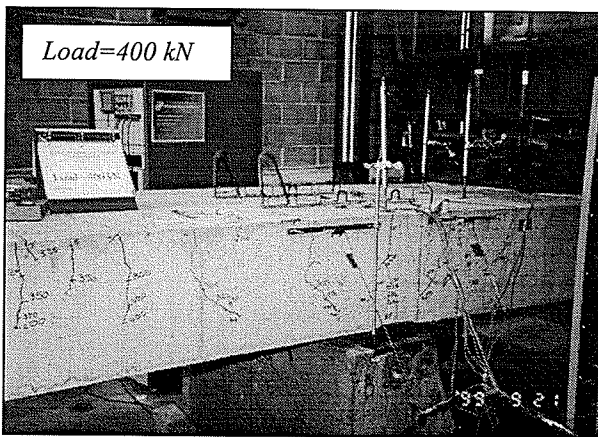
Fig. 4.14a Crack pattern at 400 kN for the unstrengthened cantilever
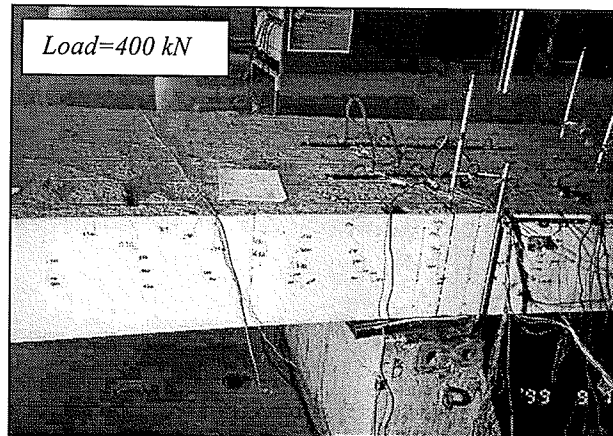
Fig. 4.14b Typical crack pattern at 400 kN for the strengthened cantilevers

The number of cracks, average spacing between the cracks and the loads corresponding to the stage of crack stabilization for all cantilever specimens are summarized in Table 4.1.

Table 4.1 Cracking behaviour of cantilever specimens

Specimen	No. of cracks	Average crack spacing (mm)	Stabilization load (kN), P_{st}	P_{st}/P_{HSS30} [*]	Crack width at failure (mm)
C1	9	155	350	2.5	3.14
C2	11	167	500	3.6	2.11
C3	8	160	450	3.2	4.50
C4	13	164	450	3.2	2.13
C5	13	170	500	3.6	1.80
C6	14	175	500	3.6	4.30

[*] P_{HSS30} is the AASHTO HSS30 truck design load.

4.2.2.5 Crack Width

The measured data from the PI gauges, mounted on the top surface of the cantilever specimens, was used to calculate the average crack width, w_{avg}, using Equation 4.1.

$$w_{avg} = \frac{\left(\Delta_h - L_g\, \varepsilon_{cr} \right)}{n} \qquad (4.1)$$

where Δ_h is the horizontal displacement measured by the PI gauge; L_g is the gauge length (L_g=200 mm); ε_{cr} is the maximum tensile strain of the concrete ($\varepsilon_{cr} = 0.13 \times 10^{-3}$); and n is the number of cracks passing through a PI gauge station. The applied load versus crack width relationships for cantilever specimens strengthened with near surface mounted CFRP reinforcement are shown in Fig. 4.15, compared to the control specimen.
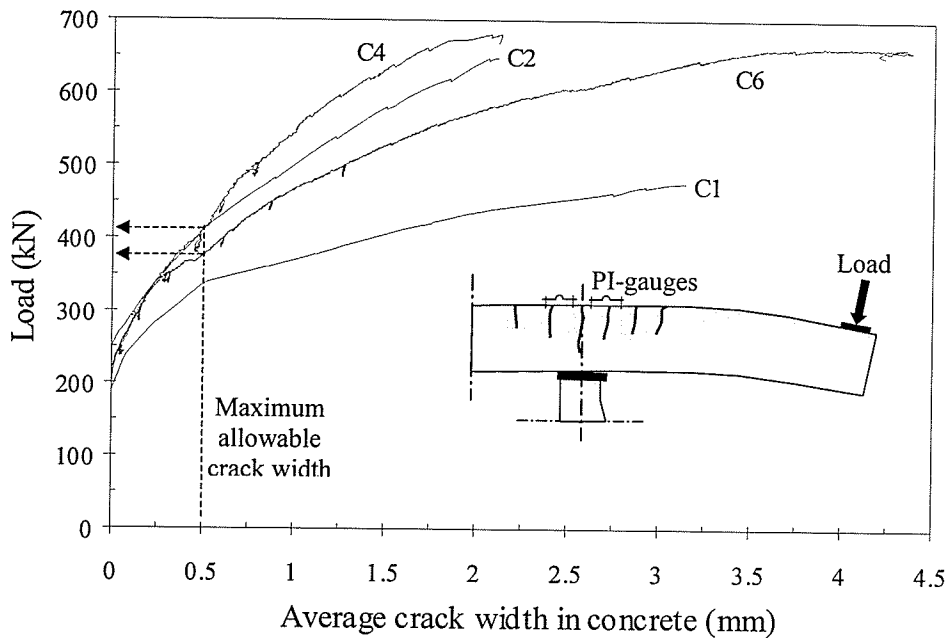
Fig. 4.15 Average crack width for cantilever specimens strengthened
with near surface mounted CFRP reinforcement

In general, strengthening using near surface mounted CFRP reinforcement decreased the crack width by a factor ranging between two and three. The figure clearly indicates that the average crack width is greatly influenced by the modulus of elasticity of the CFRP reinforcement. This was evident by the wider cracks observed for specimen C6, strengthened using C-Bars, in comparison to those observed for specimens C2 and C4, strengthened with Leadline bars and CFRP strips, respectively. Comparable crack widths were observed for specimens C2 and C4 up to failure.

Fig. 4.16 shows the applied load versus crack width relationships for the cantilever specimens, C3 and C5, strengthened with externally bonded CFRP strips and sheets, respectively.
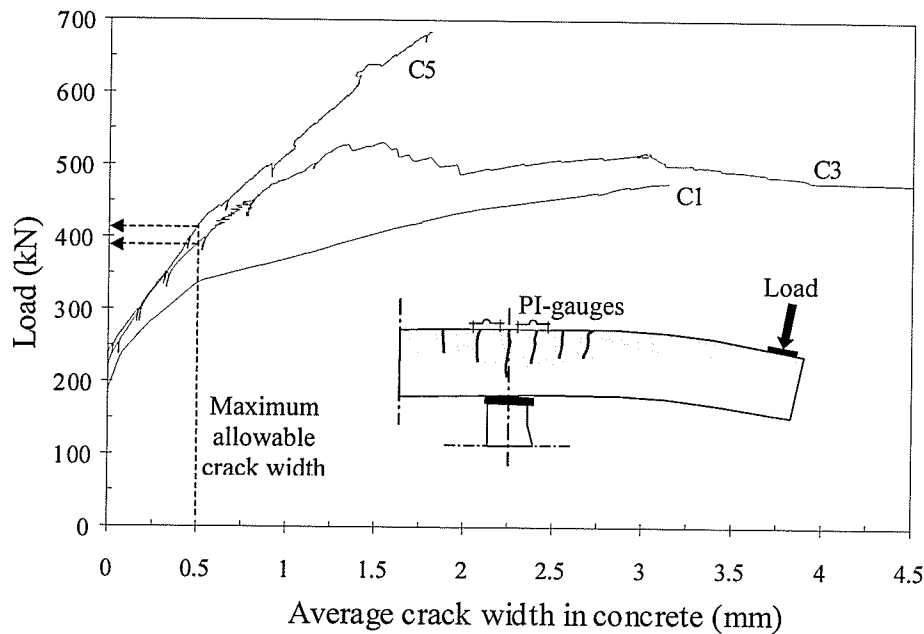
Fig. 4.16 Average crack width for cantilever specimens strengthened
with externally bonded CFRP reinforcement

Comparable crack widths were observed for specimens C3 and C5 until delamination of the CFRP strips occurred at a load level of 500 kN beyond which the crack width increased significantly.

The Japan Society of Civil Engineers (1997), The Canadian Highway Bridge Design Code (1996), and ACI-Committee 440 (2002), set the maximum allowable crack width to 0.5 mm for exterior exposure when FRP reinforcement is used. Using a criterion of maximum allowable crack width of 0.5 mm, the upgraded service load level for the strengthened cantilevers has a lower bound of 375 kN, which is 2.7 times the AASHTO HSS30 truck design load. Experimental results for the cantilever specimens are summarized in Table 4.2.

Table 4.2 Experimental results of cantilever specimens

Specimen	Strengthening technique	P_{cr} (kN)	Δ_{cr} (mm)	P_u (kN)	Δ_u (mm)	% Increase in ultimate capacity
C1	N.A (Control)	180	9.1	476	92.5	Control
C2	Near surface mounted Leadline bars	189	8.3	647	102	36
C3	Externally bonded CFRP strips	192	9.2	530[*]	39	11
C4	Near surface mounted CFRP strips	187	8.5	680	93	43
C5	Externally bonded CFRP sheets	194	9.1	683	112	44
C6	Near surface mounted C-BAR	197	8.3	663	100	39

[*] Specimen C3 failed due to delamination of CFRP strips, followed by crushing of concrete.

where P_{cr} is the cracking load; P_u is the ultimate failure load; Δ_{cr} is deflection at cracking and Δ_u is the deflection at failure.

4.2.3 Cost Analysis

One of the prime objectives of this study was to provide a cost-effective analysis for each strengthening technique considered in this investigation. It should be mentioned that all techniques were designed to increase the strength by 30 percent using the characteristics of each FRP material and applying a strain compatibility approach. The approximate cost calculation for each strengthening technique used for the cantilever specimens is given in Table 4.3. The total construction cost accounts for the cost of materials, equipment needed during construction and labour.

Table 4.3 Cost analysis for cantilever specimens

Specimen	Strengthening technique	Material cost/ ft	Total material cost	Epoxy cost	Labour hours [¥]	Equip. cost	Total cost
C2	NSM[+] Leadline bars	12.6	1058	150	7	67	1394
C3	EB[#] CFRP strips	17.0	1224	Included	5	None[*]	1309
C4	NSM CFRP strips	17.0	1224	Included	9	67	1444
C5	EB CFRP sheets	7.0	252	Included	4	34	354
C6	NSM C-BAR bars	3.5	336	150	9	100	739

. All costs are in US dollars.

[+] NSM: refers to near surface mounted.

[#] EB: refers to externally bonded.

[*] No especial equipment was used.

[¥] Labour cost was based on $17.0 U.S.D per hour [$25 CAD/hour].

The percentage increase in the flexural capacity and the construction cost for each of the strengthening techniques considered in this study for the cantilever specimens are shown in Fig. 4.17.
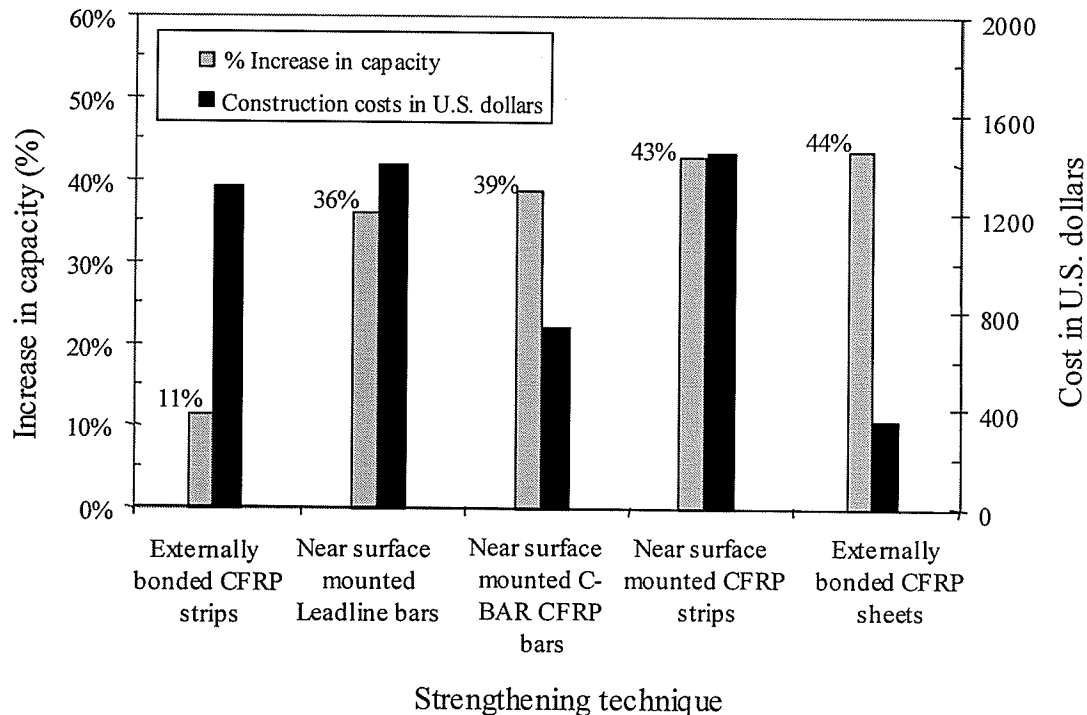
Fig. 4.17 Cost analysis of various strengthening techniques

The figure indicates that using near surface mounted CFRP strips and externally bonded CFRP sheets provided the maximum increase in strength. The construction cost of externally bonded CFRP sheets is only 25 percent in comparison to near surface mounted strips. Using either near surface mounted Leadline bars or C-Bars provided approximately the same increase in ultimate load carrying capacity. With respect to cost, strengthening using C-Bars bars is 50 percent less.

Using an efficiency scale, E, defined by Equation 4.2, the efficiency of each technique was evaluated as shown in Fig. 4.18.

$$E = \frac{\% \text{ Increase in strength}}{\text{Construction cost in USD}} \times 100 \qquad (4.2)$$
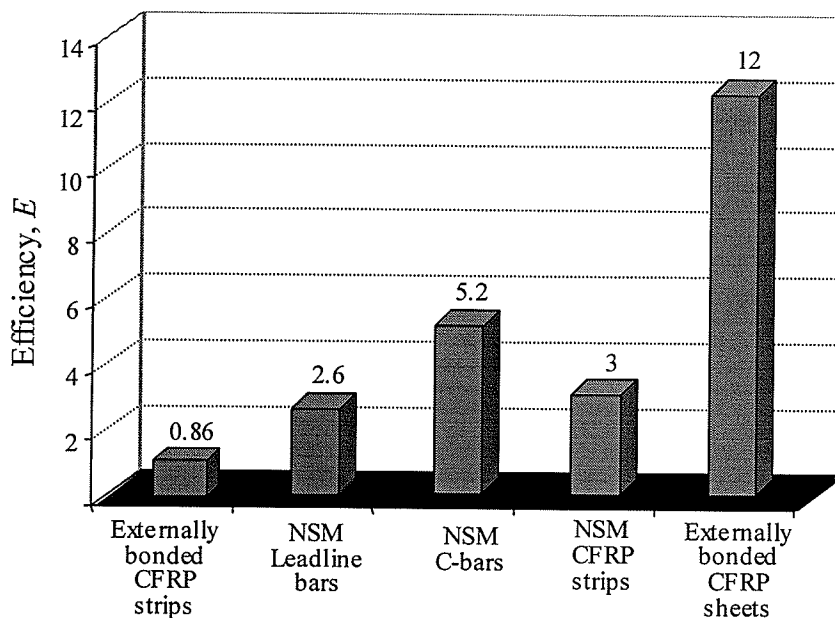
Fig. 4.18 Efficiency of various FRP strengthening techniques

The results show that strengthening using externally bonded CFRP sheets is the most efficient technique in terms of strength improvement and construction cost. The estimated cost of the rehabilitation work for the bridge under consideration in Winnipeg, Manitoba

using near surface mounted CFRP bars is approximately $1.6 million CAD, which is 60 percent of the cost of demolition and replacement of the existing structure [Hassan and Rizkalla, 2002].

4.2.4 Test Results of the Simply Supported Specimens

4.2.4.1 General

The cantilever test results showed that effective strengthening techniques could be used to increase the flexural strength of existing concrete bridges to withstand higher service loads. Test results provided sufficient evidence and confidence of the proposed strengthening technique using near surface mounting as a new and promising technology.

To duplicate and confirm the findings of this research program, the same specimens were tested in a simply supported configuration between the two tested cantilevers to examine the selected FRP strengthening techniques. The cracks resulted from the cantilever tests were injected and the specimen was simply supported between the two cantilevers. The simply supported spans of the three slabs were strengthened using near surface mounted Leadline bars (SS1), near surface mounted CFRP strips (SS2), and externally bonded CFRP sheets (SS3), respectively. The CFRP reinforcement was designed to achieve a 30 percent increase in the ultimate load carrying capacity of the slab. The slab was simply supported with a span of 4.90 meters and had double cantilever projections of 1.80 meters from each end. The load was applied at mid-span. To investigate different strengthening techniques, it was decided not to test a control specimen for the simply supported span and to rely on the results obtained from non-linear finite element analysis. The finite

element model was carefully calibrated to the behaviour of the unstrengthened cantilever specimen as will be explained later in this chapter.

4.2.4.2 Deflection

The load-deflection behaviour of the simply supported specimens strengthened with near surface mounted Leadline bars (SS1), near surface mounted CFRP strips (SS2) and externally bonded CFRP sheets (SS3) is shown in Fig. 4.19.
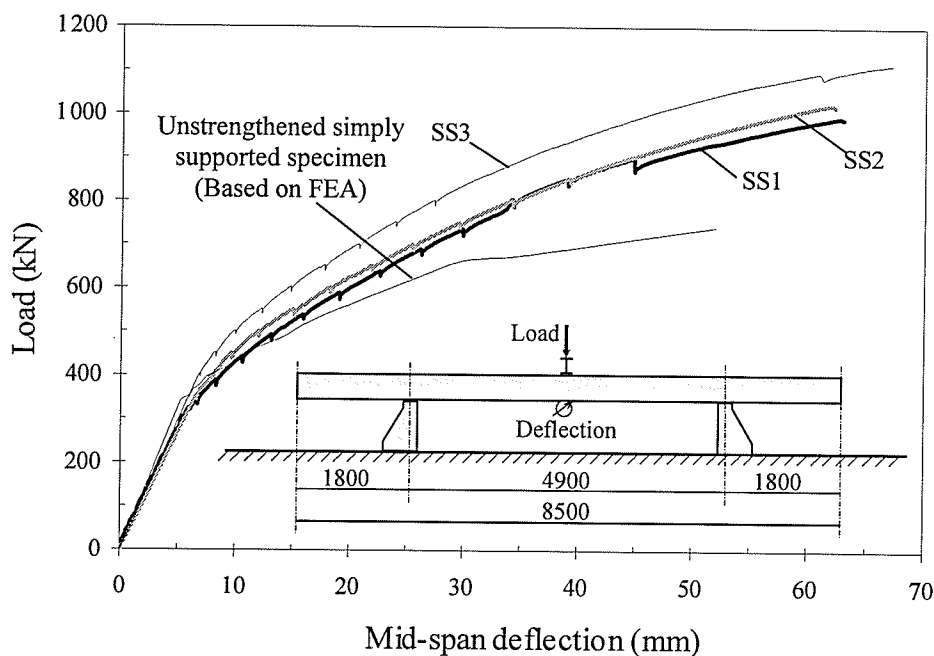
Fig. 4.19 Load-deflection behaviour of simply supported specimens

Strengthening of the specimens slightly increased the cracking load. However, this could be affected by the value of the tensile strength used for concrete in the finite element analysis for the unstrengthened specimen. Test results indicated a considerable increase in stiffnesses and ultimate loads with the addition of the CFRP reinforcement. Fig. 4.19 shows that CFRP reinforcement did not contribute greatly to an increase in stiffness in the elastic range of the slabs prior to cracking. However, the stiffnesses of the

154

strengthened slabs were significantly enhanced in the post-cracking region compared to the unstrengthened specimen. Identical behaviour was observed for all specimens until cracking occurred.

The mid-span deflection curves showed traditional non-linearities due to cracking of the concrete and yielding of the steel. Prior to yielding of the bottom tension steel reinforcement, the stiffnesses of all strengthened slabs were almost the same and were 1.5 times higher than the stiffness of the unstrengthened slab. Specimens SS1 and SS2, strengthened with near surface mounted Leadline bars and near surface mounted CFRP strips, respectively, showed comparable stiffnesses up to failure. After yielding of the tension steel reinforcement at a load level of 660 kN, the stiffnesses of specimens SS1 and SS2 were three times higher than that of the unstrengthened slab. Using externally bonded CFRP sheets in specimen SS3 increased the stiffness by an extra 25 percent. The area of the externally bonded sheets was calculated based on the manufacturer's guaranteed strength and modulus of elasticity, which are conservative values and resulted in a substantial increase of stiffness

4.2.4.3 Failure Modes

Traditional flexural failure due to crushing of the concrete at the mid-span section was observed for all three specimens. Failure occurred at the maximum moment zone at the face of the applied load. The concrete compressive strain, directly under the location of the applied load, was monitored during the tests using strain gauges as shown in Fig. 4.20.
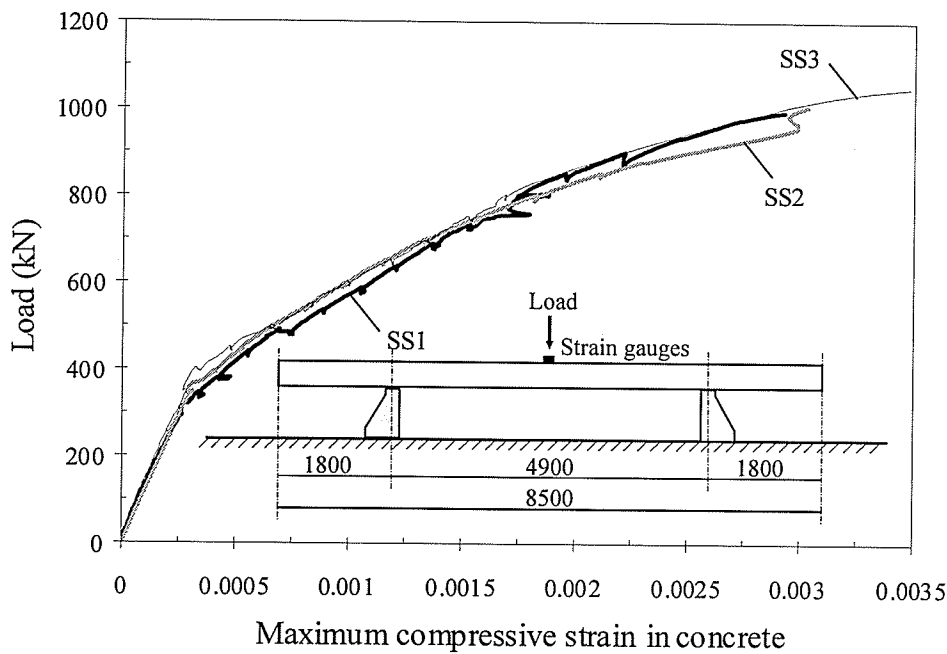
Fig. 4.20 Load-compressive strain behaviour of concrete for simply supported specimens

The ultimate concrete compressive strain at failure reached a value of 0.003 to 0.0035 for all specimens. At the onset of failure, the top steel bars were exposed and buckled as shown in Fig. 4.21.
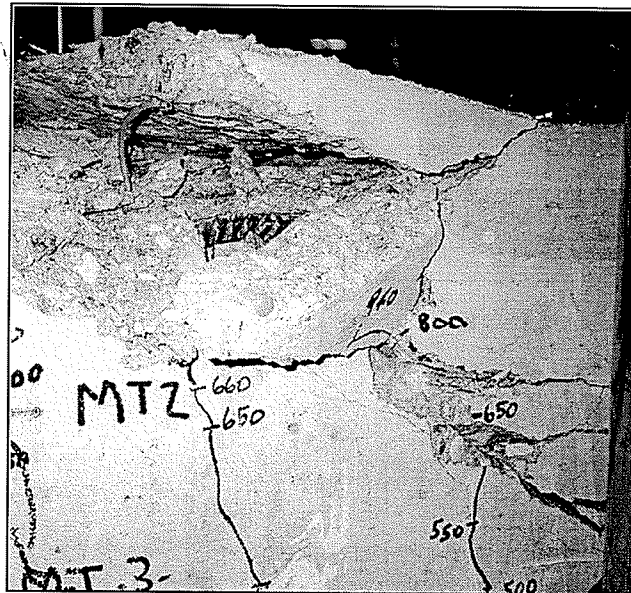
Fig. 4.21 Buckling of the top steel reinforcement

156

Typical failure due to crushing of concrete for the simply supported specimens is shown in Fig. 4.22.
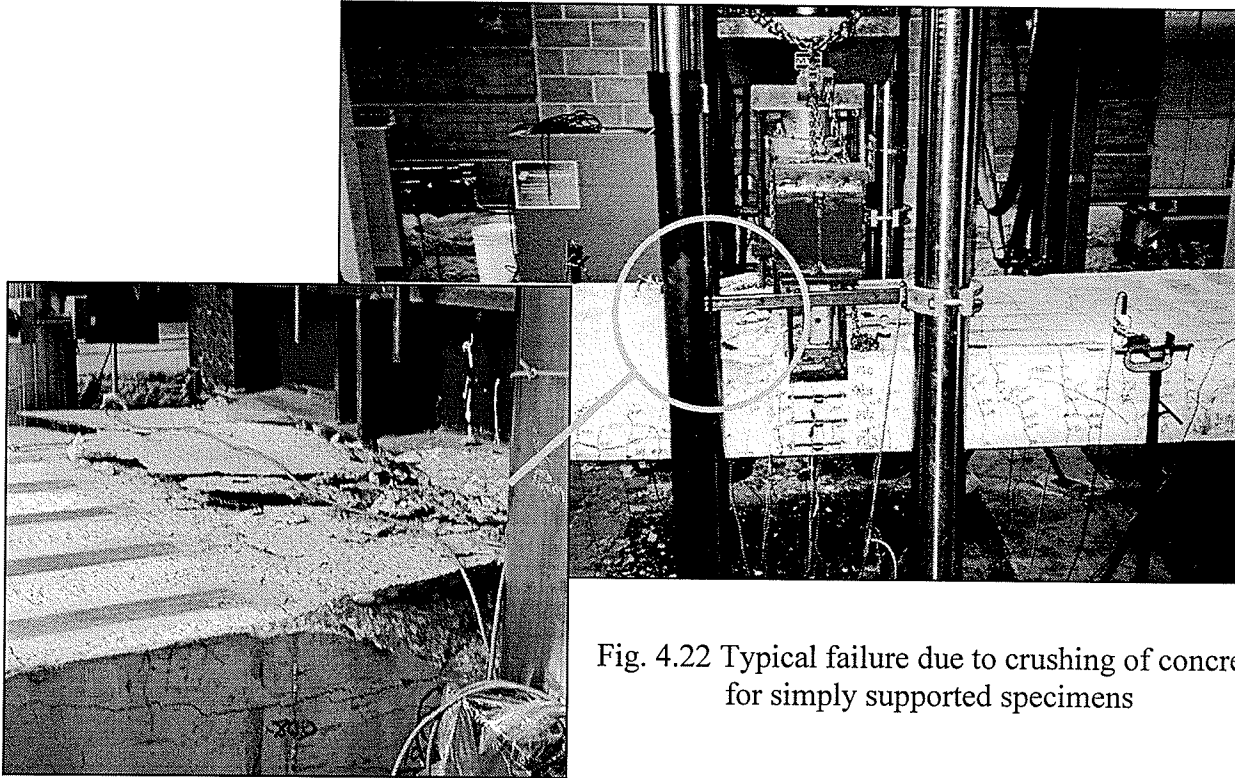
Fig. 4.22 Typical failure due to crushing of concrete
for simply supported specimens

The unstrengthened slab exhibited classical failure due to crushing of the concrete at a load level of 741 kN. Strengthening the slab using near surface mounted Leadline bars increased the strength by 34 percent in comparison to the design value of 30 percent. Using near surface mounted CFRP strips increased the strength by 38 percent. Using externally bonded CFRP sheets, provided the highest increase in strength by 50 percent [Hassan and Rizkalla, 2002].

4.2.4.4 Tensile Strains

The maximum tensile strain in the CFRP reinforcement at mid-span section was monitored during testing using strain gauges as shown in Fig. 4.23.
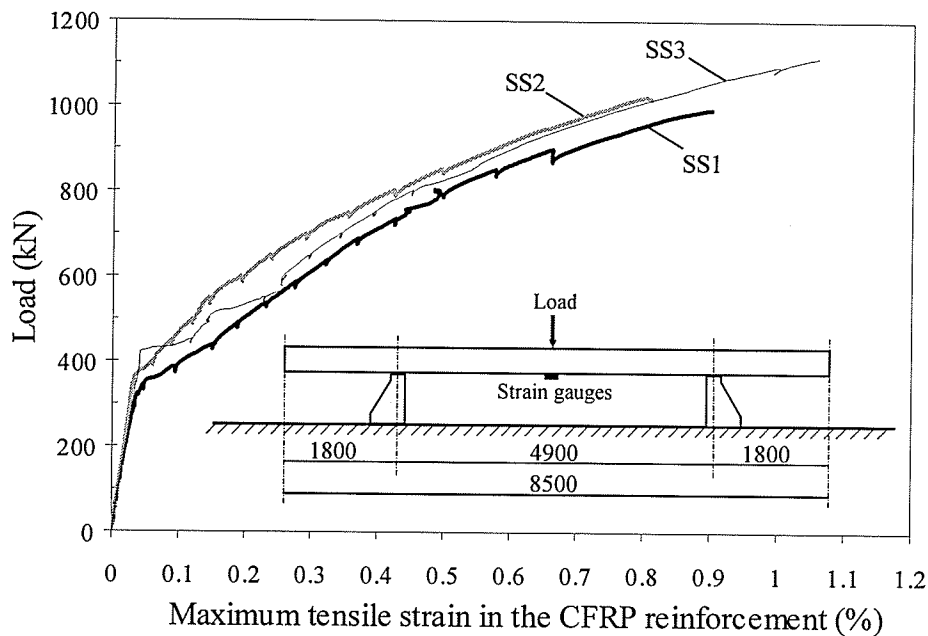
Fig. 4.23 Load-tensile strain behaviour of simply supported specimens

Full composite action was achieved between the CFRP reinforcement and concrete up to failure. This was evident by the considerable increase in the tensile strain of the CFRP reinforcement with increasingly load levels. The maximum tensile strain in the Leadline bars at failure was 0.9 percent, which is 67 percent of the ultimate strain of the bars. The maximum tensile strain in the CFRP strips at failure was 0.8 percent, which is equivalent to 60 percent of the rupture strain of the strips. No delamination was observed throughout the test between the CFRP sheets and concrete or within the plies of the CFRP sheets. The maximum tensile strain in the CFRP sheets at failure was 1.06 percent, which is 60 percent of the rupture strain of the sheets.

To evaluate the bond characteristics between the concrete and CFRP reinforcement, closely spaced strain gauges were placed along the length of the CFRP reinforcement. Figs. 4.24 to 4.26 show the strain distribution along the length of the Leadline bars, CFRP strips and CFRP sheets used for specimens SS1, SS2, and SS3, respectively. The

strain distributions are plotted at various levels of the applied load to illustrate the change

in the distribution with increasing load levels.
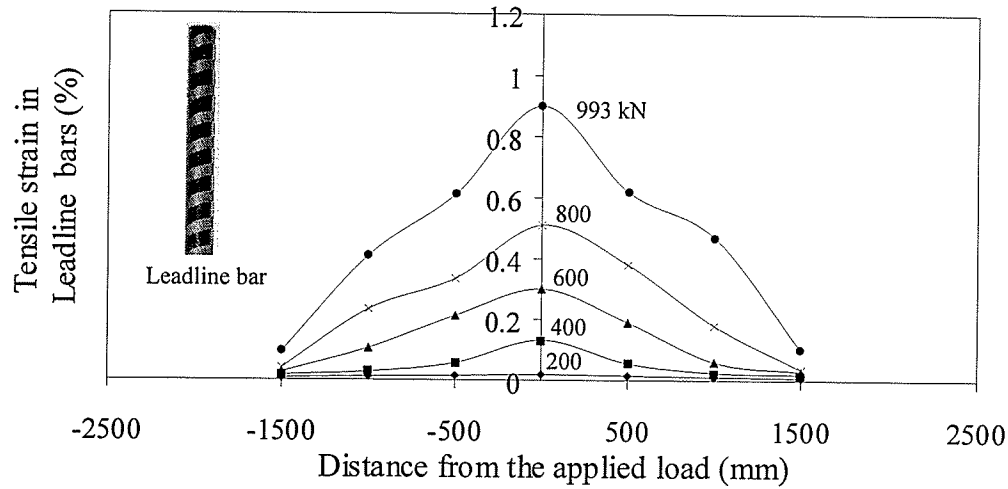
Fig. 4.24 Tensile strain distribution along the Leadline bars (specimen SS1)
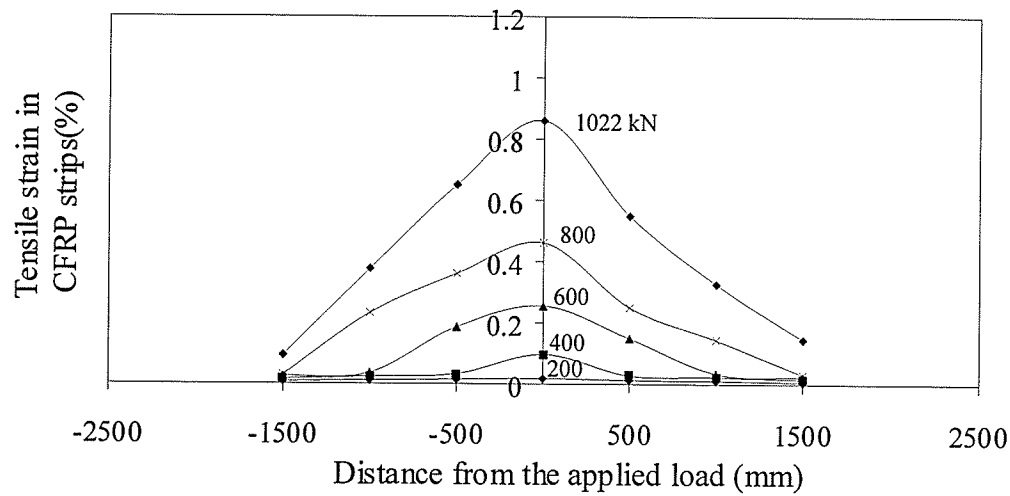
Fig. 4.25 Tensile strain distribution along the CFRP strips (specimen SS2)
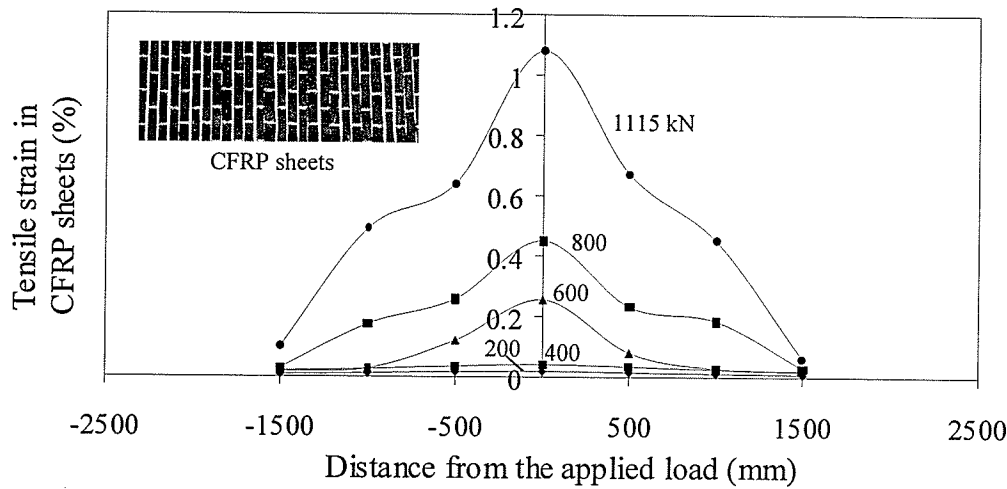
Fig. 4.26 Tensile strain distribution along the CFRP sheets (specimen SS3)

The shape of strain distribution was proportional to the moment diagram for all specimens. A comparison among Figs 4.24, 4.25 and 4.26 suggests that the strains in the near surface mounted Leadline bars or CFRP strips are typically lower than those measured in the externally bonded CFRP sheets. The Leadline bars and CFRP strips were located closer to the neutral axis in comparison to the CFRP sheets, which were bonded to the surface of the concrete. At the same load level, this arrangement resulted in lower strains in the near surface mounted reinforcement compared to externally bonded reinforcement.

A typical strain profile of the concrete, measured using PI gauges and demec points at both sides of the slab, is shown in Fig. 4.27.
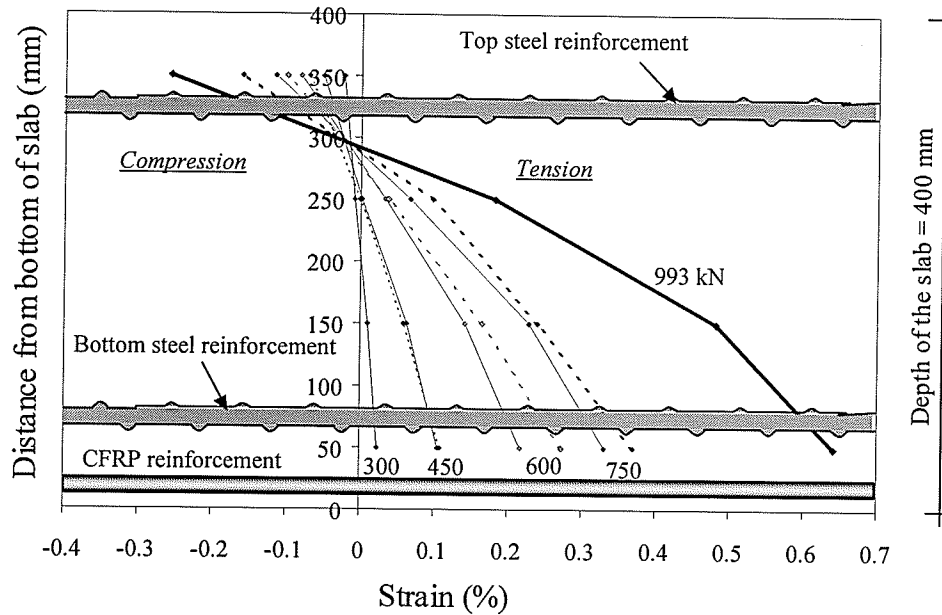
Fig. 4.27 Typical strain profile for simply supported slabs

The solid lines in the figure represent the measured values using PI gauges at one side of the slab. The dotted lines represent the measured values from the demec points on the other side of the slab. The figure reveals comparable strain values using either PI gauges or demec points. The neutral axis location was calculated based on the PI gauge readings at different load levels after cracking. The location of the neutral axis versus the applied load is shown in Fig. 4.28 for the simply supported specimens. It can be seen that the neutral axis depth decreases rapidly after cracking with increasing the applied load. The depth of the neutral axis tends to be stationary beyond a load level of 600 kN. The increase of the internal moment resistance was achieved by an increase in the tensile forces of the CFRP reinforcement and therefore, the neutral axis remains stationary up to failure of the slab.
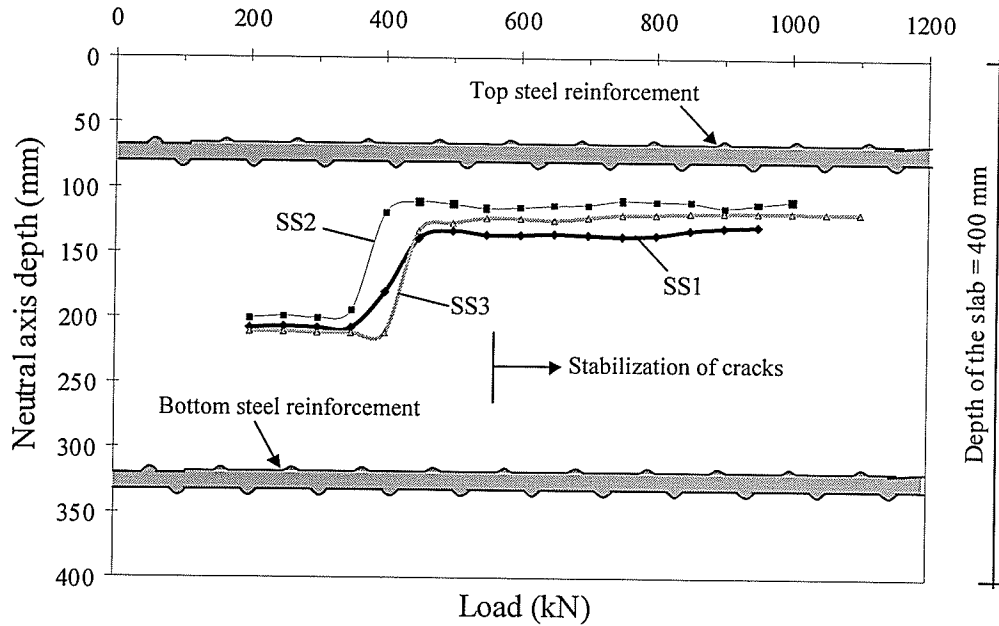
Fig. 4.28 Neutral axis depth vs. applied load for simply supported specimens

4.2.4.5 Crack Patterns

Cracking behaviour of the simply supported specimens strengthened with FRP systems was monitored within the maximum moment zone. The first crack was observed at load levels ranging between 350-370 kN for strengthened specimens. Cracks started perpendicular to the centre of the slab at the mid-span section and extended to the top surface. More than twenty cracks were observed throughout the length of the slab as shown in Fig. 4.29.
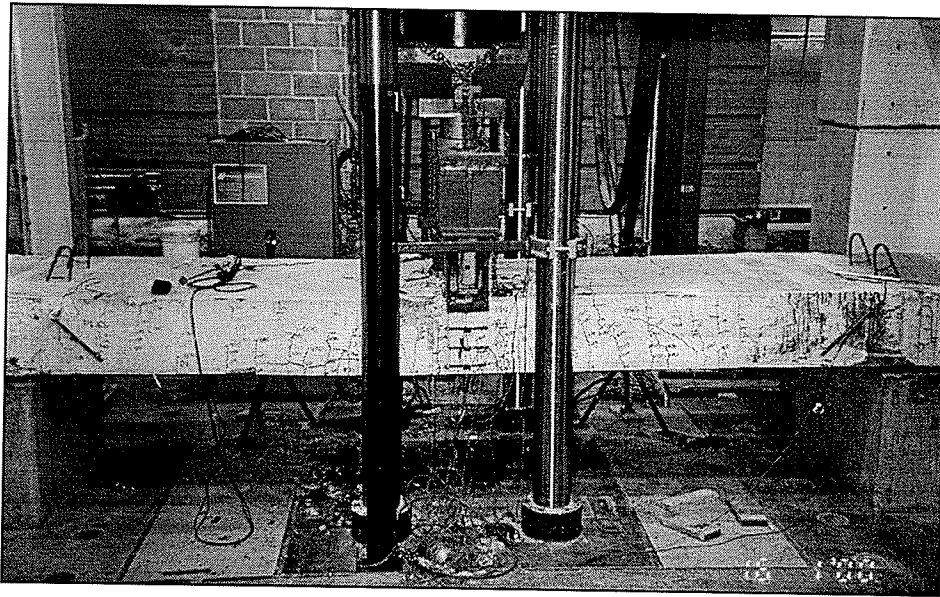
Fig. 4.29 Typical crack pattern for simply supported specimens

Test results indicated that stabilization of the flexural cracks occurred at a load level of 600 kN, which is 4.3 times the AASHTO HSS30 truck design load. The average crack width, measured at the extreme tension fibres, is shown in Fig. 4.30.
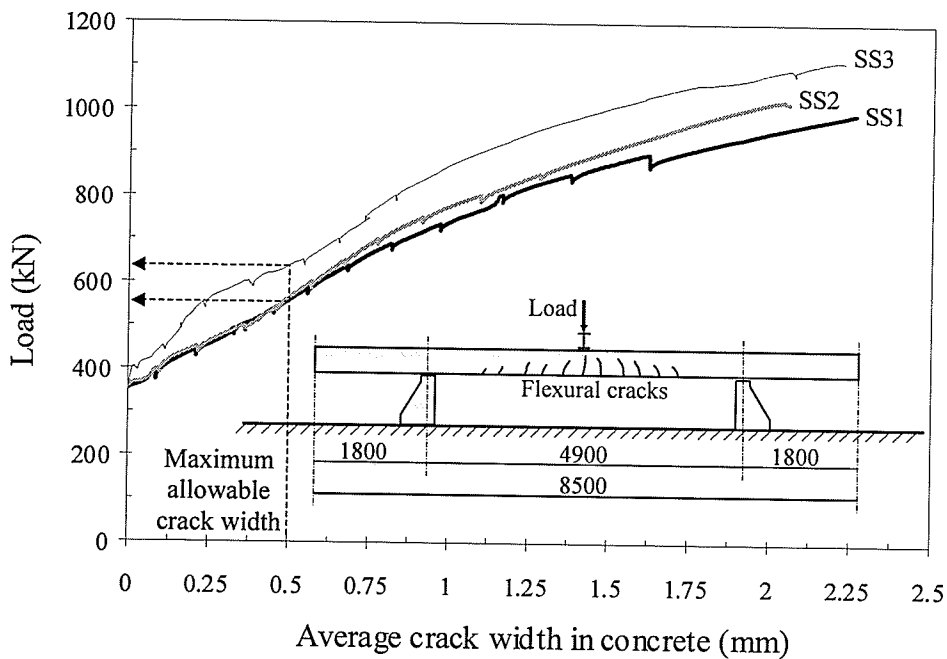
Fig. 4.30 Average crack width vs. applied load for simply supported specimens

The crack width increased non-linearly with the increase in the applied load. A comparable crack width was observed for specimens SS1 and SS2, strengthened with near surface mounted Leadline bars and CFRP strips, respectively. The location of externally bonded CFRP sheets with respect to the neutral axis provided additional constraints to the extreme fibre strains. Such a phenomenon was highly pronounced for externally bonded sheets in comparison to near surface mounted reinforcement. Consequently, strengthening using externally bonded CFRP sheets (SS3) reduced the average crack width by 25 percent compared to specimens SS1 and SS2. Using a criterion of maximum allowable crack width of 0.5 mm, the corresponding lower bound of the load for the strengthened simply supported specimens is 560 kN. This load is equivalent to four times the AASHTO HSS30 truck design load. Fig. 4.31 depicts a typical crack pattern development for strengthened slabs at three load levels.
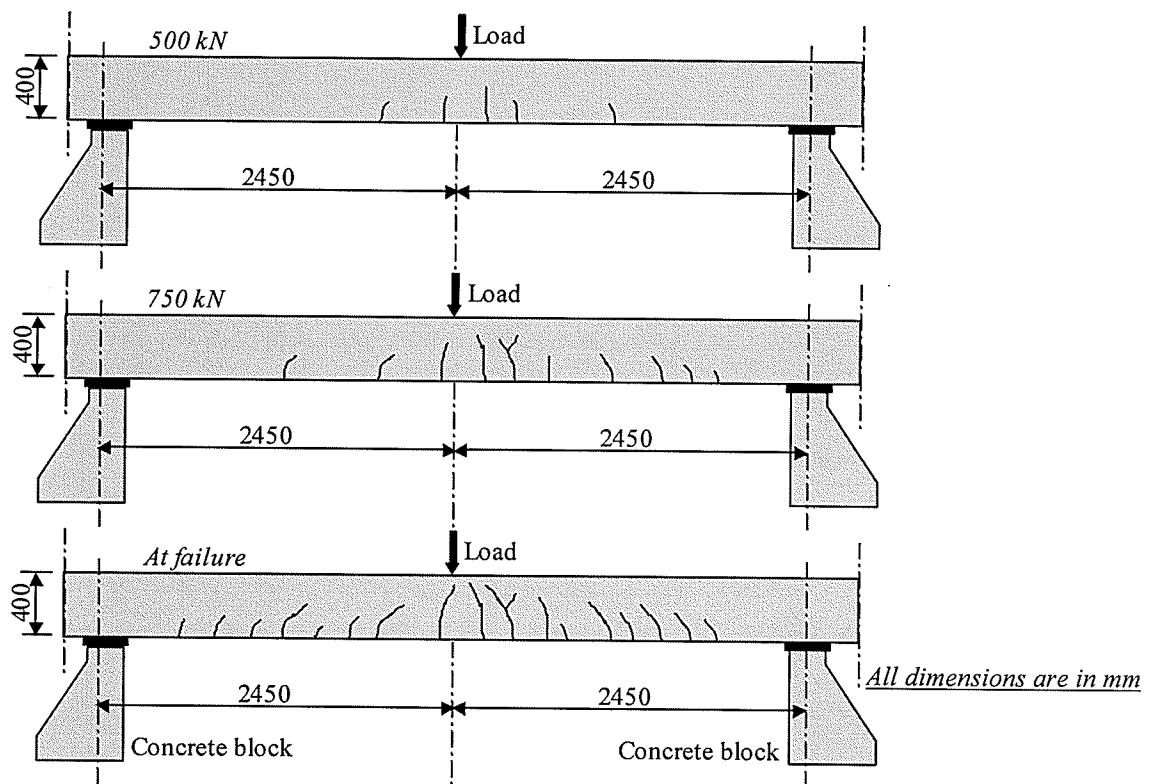
Fig. 4.31 Typical crack pattern development for simply supported slabs

The number of cracks, average crack spacing, and the load at which the cracks were stabilized, are given in Table 4.4.

Table 4.4 Cracking behaviour of simply supported specimens

Specimen	No. of cracks	Average crack Spacing (mm)	Stabilization Load (kN), P_{st}	P_{st}/P_{HSS30} *	Crack width at failure (mm)
SS1	21	144	650	4.6	2.30
SS2	18	120	600	4.3	2.10
SS3	18	150	650	4.6	2.22

* P_{HSS30} is the AASHTO HSS30 truck design load.

The crack width of the main flexural cracks at mid-span increased significantly as the curvature of the slab increased and plastic deformation took place at the central region of the slab. At the bottom of the slab, some of the small-width cracks above the level of the longitudinal reinforcement merged into a few wider cracks. The main cracks bifurcated near the neutral axis. At high load levels, cracks did not propagate vertically due to the presence of narrow and almost constant compression zone depth. Consequently, the cracks extended laterally in a forked configuration to release the tensile stresses at the tip of the cracks with increasing of the applied load. Flexural shear cracks were observed at a load level of 800 kN. These cracks remained small and did not affect the overall response. Experimental results of simply supported specimens are summarized in Table 4.5.

Table 4.5 Experimental results of simply supported specimens

Specimen	Strengthening technique	P_{cr} (kN)	Δ_{cr} (mm)	P_u (kN)	Δ_u (mm)	% Increase in ultimate capacity
SS0*	N.A	348	6.0	741	52	-
SS1	Near surface mounted Leadline bars	350	6.6	993	62.6	34
SS2	Near surface mounted CFRP strips	370	6.6	1022	62.0	38
SS3	Externally bonded CFRP sheets	362	6.8	1115	67.2	50

* SS0 is the unstrengthened simply supported span based on nonlinear finite element analysis.

4.2.5 Deformability

Deformability is a key issue related to the safety of concrete members prestressed or reinforced with FRP. Since FRP reinforcements do not exhibit ductility, care must be taken to ensure that sufficient warning is exhibited prior to failure of members prestressed or reinforced with FRP. The measured moment-curvature behaviour of FRP retrofitted concrete members is approximately linear up to failure and therefore cannot be characterized as ductile. Due to lack of ductility, the concept of deformability has been introduced by many researchers to quantify the performance of concrete members prestressed/reinforced with FRP [Jaeger et al., 1995; Naaman and Jeong, 1995; Abdelrahman 1995; and ACI 440, 2002].

Mufti et al. (1996) proposed a deformability index that could be quantified according to Equation 4.3. Mufti et al. recommended that the deformability index, D, should be greater than 4.0 for rectangular sections.

$$D = \frac{M_u \Delta_u}{M_s \Delta s}$$

(4.3)

where M_u is the maximum resisting moment at ultimate; Δ_u is the curvature or deflection at ultimate; M_s is the moment corresponding to a concrete compressive strain of 0.001; and Δ_s is the curvature or deflection corresponding to a concrete compressive strain of 0.001. The proposed equation was developed for reinforced concrete beams with rectangular cross-sections.

The deformability index as proposed by Mufti et al. (1996) was calculated for the tested specimens and given in Table 4.6.

Table 4.6 Deformability of large-scale slab specimens

Specimen	Strengthening technique	*Deformability index, D*
C1	N.A (Control)	4.62
C2	Near surface mounted Leadline bars	7.10
C3	Externally bonded CFRP strips	2.60 ←
C4	Near surface mounted CFRP strips	8.80
C5	Externally bonded CFRP sheets	9.60
C6	Near surface mounted C-BAR	8.00
SS0*	N.A	3.60
SS1	Near surface mounted Leadline bars	6.10
SS2	Near surface mounted CFRP strips	5.90
SS3	Externally bonded CFRP sheets	8.30

* SS0 is the unstrengthened simply supported span based on nonlinear finite element analysis.

It can be seen from the table that strengthening using externally bonded CFRP strips provided the least deformability index ($D=2.6$). This is attributed to the possible premature delamination of the strips at a considerably small deflection value. Near surface mounting technique and externally bonded sheets yielded satisfactory deformability indices in excess of the value recommended by Mufti et al. (1996).

4.3 Analytical Modelling

4.3.1 Introduction

Since concrete repair and rehabilitation using FRP systems has become quite common during the last decade, an understanding of the behaviour is urgently needed before design guidelines can be developed. The existing knowledge in this field is normally obtained from testing large-scale specimens in the laboratory and interpreting the results. However, it is impractical and costly to base the design entirely upon testing. Therefore, it is essential to develop analytical models capable of predicting the behaviour based on the measured data.

The analytical component of this thesis is mainly focusing on developing mathematical models to describe failure mechanisms of various FRP strengthening techniques, as will be discussed later in Chapter 5. This section discusses two different analytical approaches including a rational approach based on strain compatibility and a non-linear finite element approach to predict the behaviour of prestressed concrete members strengthened with near surface mounted FRP reinforcement. A comparison between analytical and experimental results is presented. Special emphasis was given to the behaviour prior to

cracking, after cracking, ultimate capacities and modes of failure. The finite element package could not predict delamination failures and therefore it was used primarily to predict the flexural behaviour of specimens strengthened with near surface mounted bars or strips. The following section emphasizes the applicability of the first approach based on strain compatibility in predicting the behaviour of FRP strengthened prestressed concrete members.

4.3.2 Cracked-Section Analysis

The cantilever slabs were analyzed using strain compatibility and internal force equilibrium procedures to predict the flexural response up to failure. This method is widely used for prestressed concrete members [Collins and Mitchell, 1991]. The concrete was assumed to be subjected to uniform uniaxial strains over the entire width of the slab. Strains were assumed to vary linearly over the depth of the section. The analysis was performed using the computer program, RESPONSE, version 1.0 [Collins and Mitchell, 1991]. The cantilever and the adjacent span were divided into 16 sections as shown in Fig. 4.32.
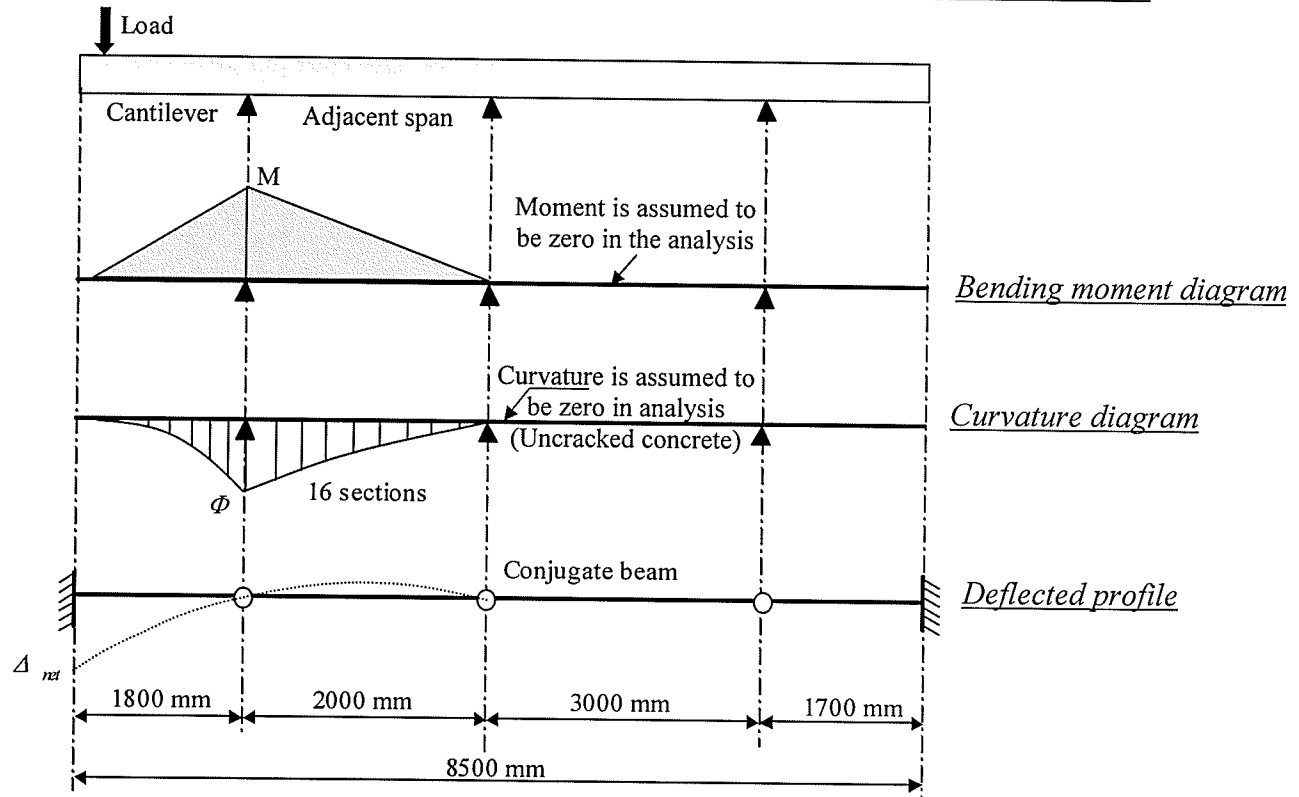
Fig. 4.32 Numerical integration of the curvature for deflection calculation

The moment-curvature relationship was determined at each section according to the following procedures:

a) Select a strain at the extreme compression fibre of the concrete.

b) Assume a neutral axis depth.

c) Determine the internal forces in compression and tension zones based on the tensile strains at every layer of the reinforcement as shown in Fig. 4.33.
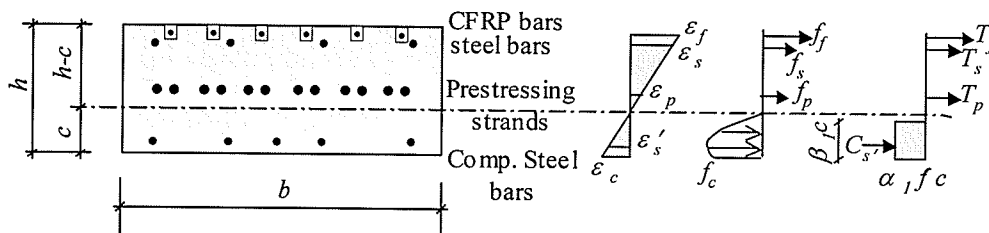
Fig. 4.33 Stress and strain distribution in a cantilever section at the ultimate-limit state.

d) Check the equilibrium of the section according to Equation 4.4, taking into account the initial strain in the prestressing reinforcement as given by Equation 4.5.

e) Revise the assumption of the neutral axis until equilibrium is satisfied.

f) Calculate the internal moment of the section according to Equation 4.6 and the curvature using Equation 4.7

g) Increase the concrete strain at the compression fibre and repeat steps b to f.

$$\int_{A_c} f_c \, dA_c + \int_{A_p} f_p \, dA_p + \int_{A_f} f_f \, dA_f + \int_{A_s} f_s \, dA_s + \int_{A_{s'}} f_{s'} \, dA_{s'} = 0 \qquad (4.4)$$

$$\varepsilon_p = \varepsilon_c \frac{d_p - c}{c} + \varepsilon_{ce} + \varepsilon_e \qquad (4.5)$$

$$M = \int_{A_c} f_c \, y \, dA_c + \int_{A_p} f_p \, y \, dA_p + \int_{A_f} f_f \, y \, dA_f + \int_{A_s} f_s \, y \, dA_s + \int_{A_{s'}} f_{s'} \, y \, dA_{s'} \qquad (4.6)$$

$$\varphi = \frac{\varepsilon_c}{c} \qquad (4.7)$$

where A_c is the area of concrete in compression; $A_{p,\,f,\,s,\,s'}$ are the areas of prestressed, CFRP, tension steel, and compression steel reinforcements respectively; f_c is the concrete stress in compression; $f_{p,\,f,\,s,\,s'}$ are the normal stresses in prestressed, CFRP, tension steel, and compression steel reinforcement respectively; y is the distance measured from the neutral axis; ε_p is the total strain in the prestressing steel; ε_c is the concrete strain at the extreme compression fibre; ε_{ce} is the concrete strain at the level of the prestressing steel due to the prestressing force; ε_e is the effective strain in the prestressing steel after losses; c is the neutral axis depth measured from the compression fibres; d_p is the depth of the prestressing steel from the compression fibre; $T_{p,\,f,\,s}$ are the tensile forces in the

prestressed, CFRP and tension steel reinforcement, respectively; $C_{s'}$ is the force in the compression steel reinforcement; α_1, β_1 are stress block parameters [Collins and Mitchell, 1991]; f'_c is the compressive strength of concrete after 28 days; h, b are the height and width of the concrete section, respectively; and ϕ is the curvature at a given strain increment.

The stress-strain relationship of the concrete was modelled using a parabolic relationship in compression. The internal compression force in the concrete was evaluated using the stress-block parameters introduced by Collins and Mitchell (1991). The stress-strain behaviour of the CFRP reinforcement was assumed to be linearly elastic up to failure. The modified Ramberg-Osgood function, given in Chapter 3, was used to model the behaviour of the steel strands.

Three failure modes were considered in the analysis:

a) crushing of concrete;

b) rupture of the CFRP reinforcement; and

c) simultaneous crushing of concrete and rupture of CFRP reinforcement *(balanced failure)*.

The moment-curvature relationship was determined at different sections along the entire length of the slab. The typical curvature distribution along the length of the cantilever slab at different load levels is shown in Fig. 4.34.
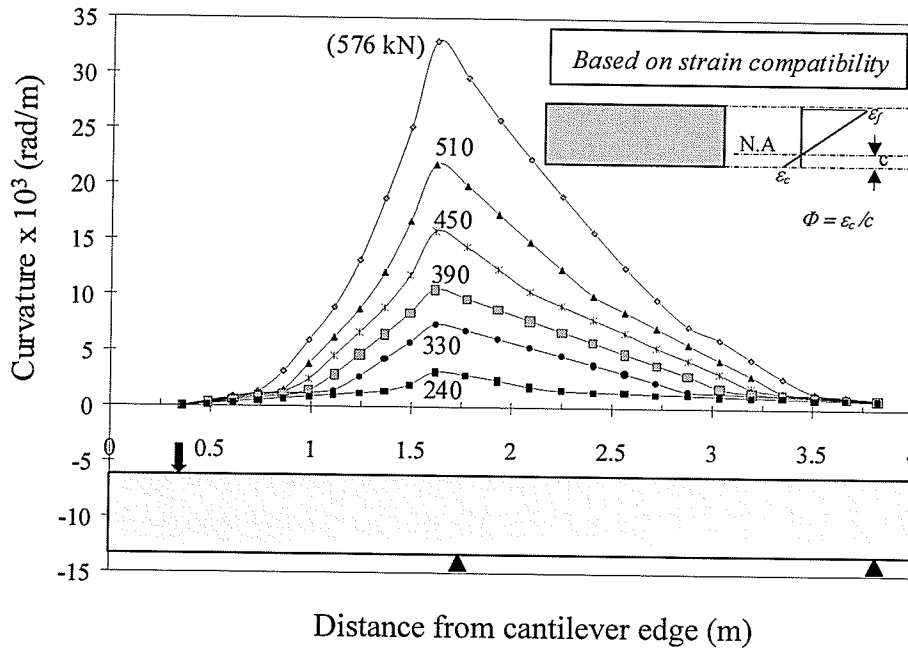
Fig. 4.34 Curvature distribution along the length of specimen C2

The deflection was calculated by integrating the curvature at each load increment. A spread sheet program was adopted to perform the numerical integration of the curvature along the span. The integration was performed at 16 sections for the cantilever specimens. A comparison between measured and predicted values will be presented in parallel with the results of the finite element analysis in section 4.3.4.

4.3.3 Finite Element Simulation

4.3.3.1 Background

The basic concept of the finite element method is described in Zienkiewicz (1967). The rapid development of computer technology permitted using sophisticated constitutive material models. The first introduction of a concrete material model into a finite element program was proposed by Ngo and Scordelis (1967). The model included a cracking capability so that the stress picture in the vicinity of cracking could be computed. This led

to the formulation of the discrete crack model. Soon thereafter, a basically different approach was proposed to assist in the design of a containment structure for a gas cooled nuclear reactor [Rashid, 1968]. Rashid's model addressed the problem in a more global sense. It was necessary to model a large segment of the concrete containment vessel and its reinforcement in order to study the overall behaviour of the structure. Therefore, the concrete model had to locate zones of cracking and investigate the influence of their development on the overall behaviour of the structure.

The consequence of these demands led to the development of a smeared crack model. Subsequent studies were undertaken predominantly to study the overall behaviour of special types of structures such as reinforced concrete plates and shells. In these studies, special emphasis was directed to the development of the smeared crack model [Hand et al., 1972; Darwin and Pecknold, 1974; Lin and Scordelis, 1975]. Over the past thirty five years, the distributed smeared crack model has been used for plane stress, plain strain and three dimensional solid systems [Scordelis, 1985].

4.3.3.2 Development of the Finite Element Model

Up-to-date, very limited research has been reported on the use of nonlinear finite element techniques to simulate the overall behaviour of prestresseed concrete members strengthened with FRPs. Some analyses have been reported on the normal and shear stress distributions at the end zones of the FRP strip/sheet. Non-linear simulations on strengthened concrete beams or slabs have been rarely performed.

Although carrying out experiments as well as numerical simulations is time-demanding, both studies are indispensable to gain insight into the failure mechanisms of a strengthened concrete member. By performing numerical simulations complementary to experiments, additional results were obtained and better-founded conclusions could be drawn. The prime objective in developing a finite element model is to examine the applicability of the non-linear finite element formulation in the global analysis of concrete members strengthened with FRP materials.

The finite element modelling described in this doctoral thesis was conducted using a commercially available program, ANACAP (Version 2.1). ANACAP is known for its advanced non-linear capabilities of the concrete material model [James, 1997]. The ANACAP software employs the classical incremental theory of plasticity that relates the increment of plastic strain to the state of stresses and stress increment. The formulation of the yield surfaces, loading, and failure surfaces takes into account the effect of a triaxial stress state on the concrete behaviour. The concrete material model is based on the smeared cracking methodology developed by Rashid (1968). The cracking criterion adopted is shown in Fig. 4.35. Within the concrete constitutive model, cracking and all other forms of material non-linearity are treated at the finite element integration points.
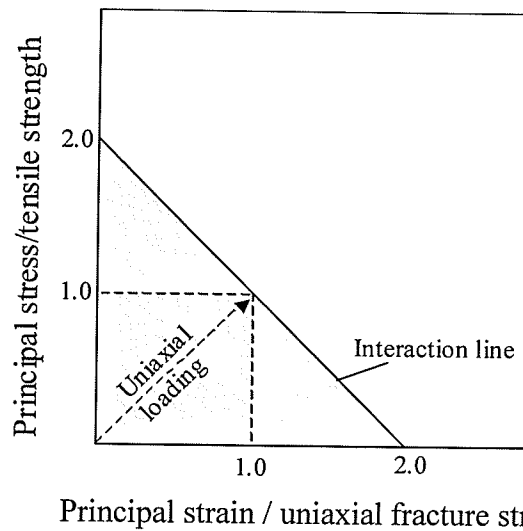
Fig. 4.35 Cracking criterion adopted in finite element analysis

Cracks are assumed to form perpendicular to the principal tensile strain direction in which the cracking criterion is exceeded. When cracking occurs, the stress normal to the crack direction is reduced to zero, which results in redistribution of stresses around the crack. The ability of cracked concrete to share the tensile forces with the steel/FRP reinforcement between cracks is modelled in ANACAP by means of a tension softening model as illustrated in Fig. 4.36.
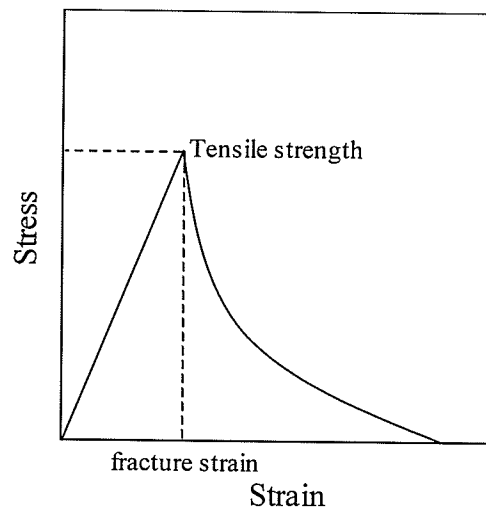
Fig. 4.36 Concrete uniaxial tensile stress-strain relationship

The descending branch of the tensile stress-strain curve is assumed to follow an exponential function. Cracks are allowed to form in the three principal directions, and once a crack forms it may close or reopen; this crack memory feature is essential for analysis involving load reversals. The modelling of concrete also includes residual tension stiffness for the gradual transfer of load to the reinforcement during crack formation. The program also accounts for the reduction in shear stiffness due to cracking and further decay as the crack opens [Gerstle, 1981].

The reinforcement is modelled as individual sub-elements within the concrete elements. Rebar sub-element stiffnesses are superimposed on the concrete element stiffness in which the rebar resides. The anchorage loss is modelled as an effective stiffness degradation of the rebar as a function of the concrete strain normal to the rebar. Interfacial failures are not considered in ANACAP. Consequently, delamination-type failures can not be predicted.

The non-linear relation between load and displacement requires an incremental-iterative solution procedure, in which the load is incrementally increased. Within each increment equilibrium is iteratively achieved. Iterations are repeated until internal equilibrium conditions are sufficiently fulfilled and convergence is obtained. In the ANACAP program, the regular Newton-Raphson iteration procedure is used, in which the tangential stiffness matrix is set up before each iteration. The regular Newton-Raphson iteration is illustrated graphically as shown in Fig. 4.37.
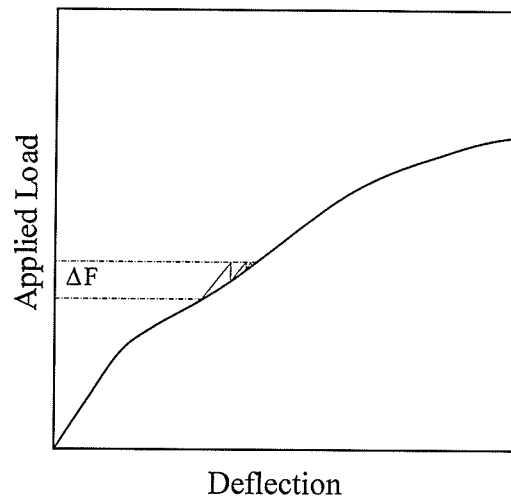
Fig. 4.37 Incremental-iterative solution using Regular Newton-Raphson method

At the end of each step, the ANACAP program adjusts the stiffness matrix to reflect the non-linear changes in the slab stiffness. Verification of the ANACAP program using independent experimental results can be found elsewhere (Megally and Ghali, 2000; Hassan et al., 2000; Mufti et al., 2001).

4.3.3.3 Modelling of the Cantilever Slabs

The cantilever slab and the adjacent panel were modelled to account for the continuity effect. Taking advantage of the symmetry of the cantilever slab, only one half of the slab in the longitudinal direction was modelled. The concrete was modelled using 20-node isoparametric brick elements with a 2x2x2 reduced Gauss integration scheme. Each node has three translational degrees of freedom. The slab was supported on elastic springs having the same axial stiffness of the neoprene pads, placed between the concrete slab and the supports during testing. The axial stiffness of the neoprene pads was determined experimentally by testing the pads in compression as shown in Fig. 4.38.
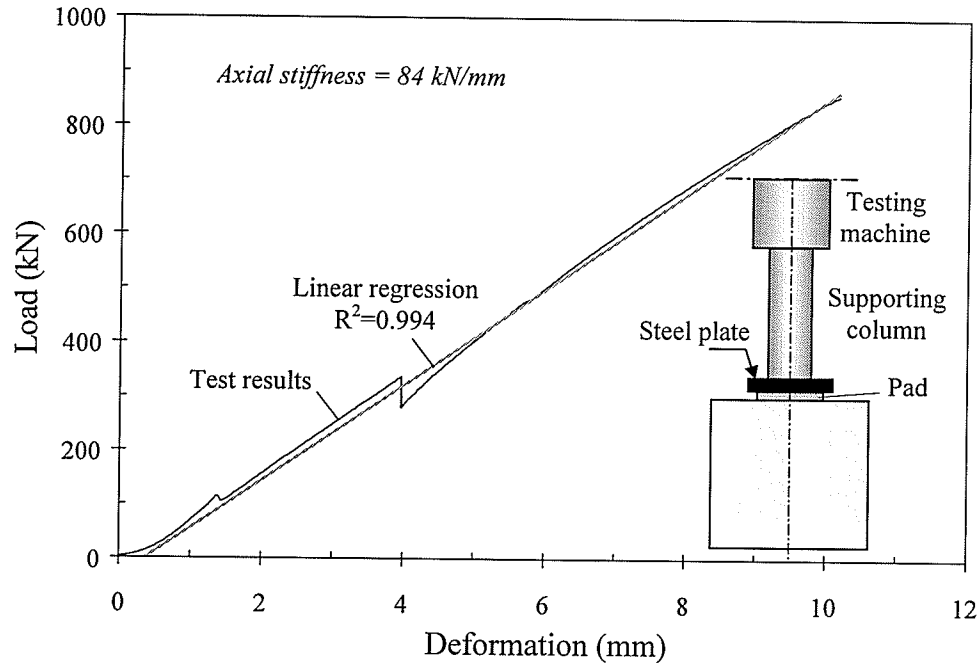
Fig. 4.38 Load-deformation response of neoprene pads

The load was applied as a uniform pressure acting on an area of 225x600 mm. The load was applied gradually using a step-by-step analysis. The number of load steps and step size were chosen based on the experience gained through different analytical simulations conducted on bridge deck slabs. The influence of the step size at failure is performed and reported elsewhere [Hassan, 1999].

Three analytical simulations were carried out by varying the size of the elements at the anticipated failure zone and the number of layers within the slab thickness. The number of elements varied from 324 elements in the first mesh to 924 elements in the third mesh for the unstrengthened specimen. Mesh dimensions for the three cases are shown in Fig. 4.39. The variation in element size was employed to provide a fine mesh around the area of maximum flexural and shear stresses.

MESH 1
(324 elements)

Load

Element size=100x150x133

Elevation

213 225   962.5   300 200 300   1700

Plane of symmetry

Plan

213 225   962.5   300 200 300   1700

MESH 2
(435 elements)

Load

Element size=75x120x133

Elevation

213 225   962.5   300 200 300   1700

Plane of symmetry

Plan

213 225   962.5   300 200 300   1700

MESH 3
(924 elements)

Load

Element size=50x100x100

Elevation

213 225   962.5   300 200 300   1700

Plane of symmetry

Plan

213 225   962.5   300 200 300   1700
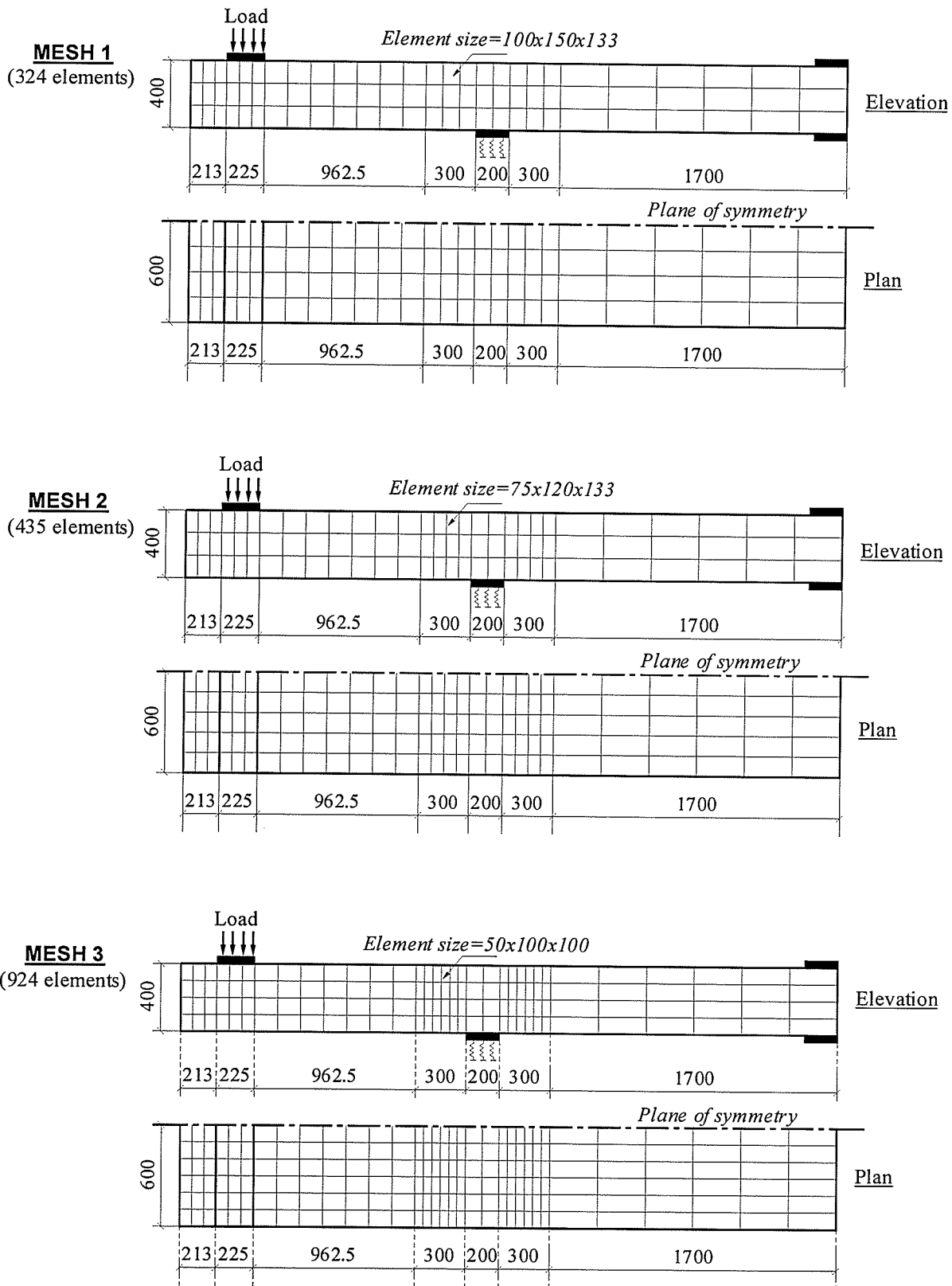
All dimensions are in mm

Fig. 4.39 Investigation of influence of mesh size

The predicted load-deflection behaviour of the three numerical simulations is shown in Fig. 4.40, where the results are compared to the measured values for the unstrengthened cantilever specimen, C1.
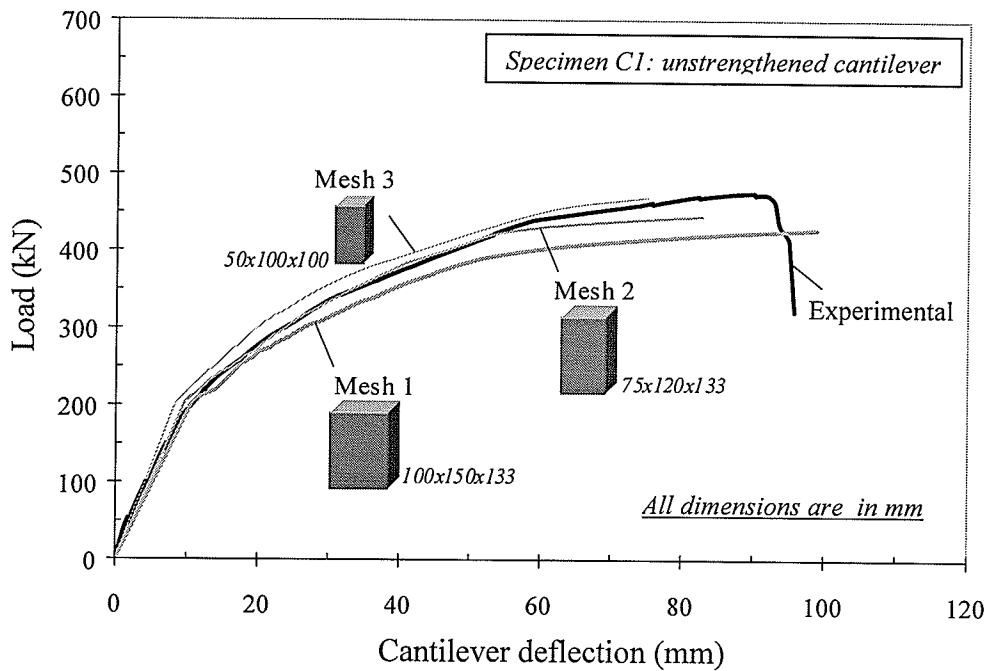
Fig. 4.40 Influence of mesh size on load-deflection behaviour

The response was relatively brittle when small size elements were used. Deformation at failure increased with the increase of the element size. As expected, the deformational behaviour was quite similar for the various simulations. The influence of the mesh size on the predicted failure loads was noticeable. The predicted failure load was 430 kN when the coarse mesh was used. Refining the finite element mesh resulted in an increase in the predicted failure loads. Compared to the test results, it emerged for the second mesh that the flexural stiffness was predicted with sufficient accuracy up to failure. Table 4.7 summarizes the results of the three numerical simulations.

Table 4.7 Influence of mesh size on predicted loads and deflections

		Experimental	Mesh 1	Mesh 2	Mesh 3
Load	Cracking (kN)	180	200	200	204
(kN)	Ultimate (kN)	476	430	445	470
Deflection	Cracking (mm)	9.1	10.5	9.5	8.7
(mm)	Ultimate (mm)	92.5	99	83	75

A comparison between flexural crack patterns at 350 kN *(stabilization load for the control specimen)* for the three simulations is shown in Fig. 4.41. Using the first mesh resulted in crack spacings wider than those observed in the laboratory. Identical crack patterns were observed for the second and the third mesh.
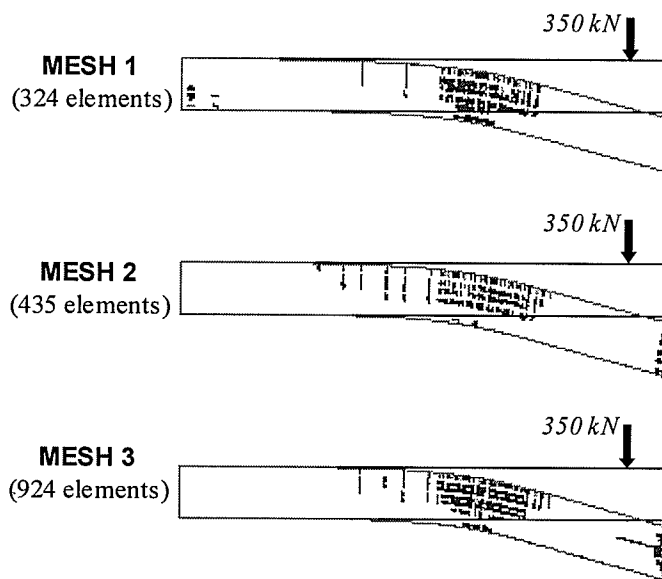
Fig. 4.41 Influence of mesh dimensions on crack patterns

From the above discussion, it is concluded that using the second mesh in modelling the cantilever specimens revealed sufficient accuracy. It should be mentioned that the corresponding execution time was 50 percent less than that of the third mesh.

4.3.3.4 Modelling of the Simply Supported Slabs

Taking advantage of the symmetry of the simply supported specimen, only one quarter of the slab was modelled using 20-node brick elements. To focus on the slab behaviour and to remain with a realistic computer execution time, the cantilevers were not included in the model since they were not loaded. The specimen was discretized into 255 elements as shown in Fig. 4.42. The element size at the anticipated failure zone was set to 75x120x133 mm, the same dimensions that were previously described in the cantilever model.
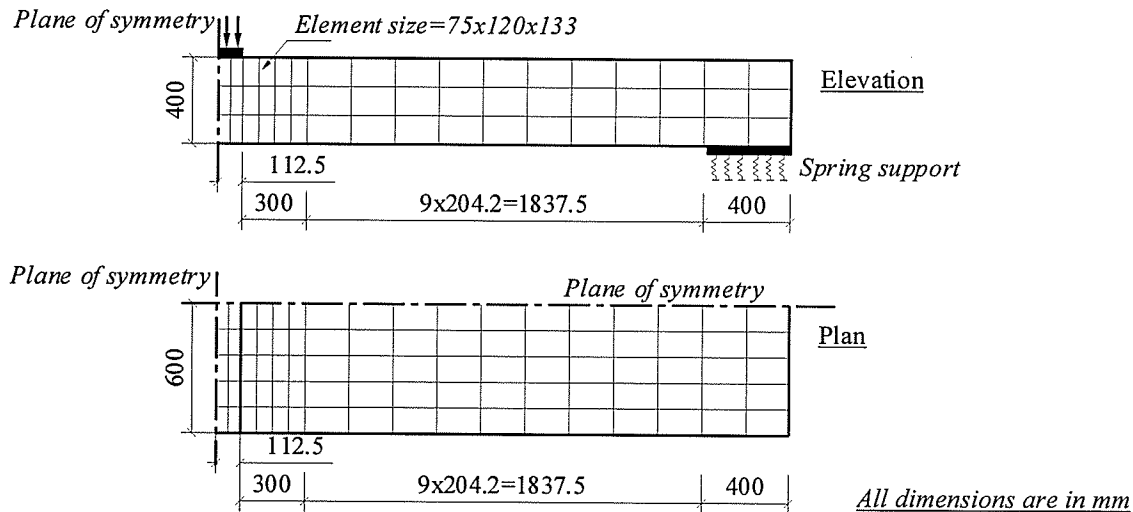
Fig. 4.42 Mesh dimensions for simply supported specimens

The slab was supported on spring elements in the vertical direction to simulate the neoprene pads. The stiffness of the springs matched the axial stiffness of the pads in compression. The springs did not have any stiffness in tension to simulate testing conditions. The load was applied as a uniform pressure acting on an area of 112.5x600 mm. The load was applied gradually using a step-by-step analysis.

4.3.3.5 Material Modelling

Concrete: Three basic features were incorporated in the concrete model:

a) a non-linear stress-strain relationship to allow for the softening of the material under increasing compressive stresses;

b) failure envelopes that define failure in tension and crushing in compression; and

c) a strategy to model the post-cracking and crushing behaviour of the material.

A modulus of elasticity of $4500\sqrt{f_c'}$ and a Poisson's ratio of 0.2 were assumed for the linear portion of the concrete model, where f_c' is the compressive strength of concrete after 28 days. The tensile behaviour of the concrete was modelled through a smeared crack continuum model. The stress-strain relationship accounts for stiffness degradation that accompanies cracking. Tensile failure occurs if the tensile stress in a principal direction exceeds the tensile failure stress ($0.60\sqrt{f_c'}$). Once this occurs, a plane of failure develops perpendicular to the corresponding principal stress direction.

Steel: An elastoplastic model was used for the steel reinforcement. A modulus of elasticity of 200 GPa and a Poisson's ratio of 0.3 were assumed for the linear portion of the stress-strain relationship. A yield stress of 400 MPa was used in the analysis

CFRP: Linear stress-strain behaviour was assumed for CFRP reinforcement and the Poisson's ratio was set to 0.30.

4.3.4 Results and Discussion

This section discusses the results of the two different analytical approaches undertaken to predict the behaviour of the tested specimens. A comparison among experimental results, the rational approach based on strain compatibility and the finite element analysis is presented.

4.3.4.1 Cantilever Specimens

To validate the finite element model, the unstrengthened cantilever was modelled first. Predicted load-deflection curves were compared to the experimental results as shown in Fig. 4.43.
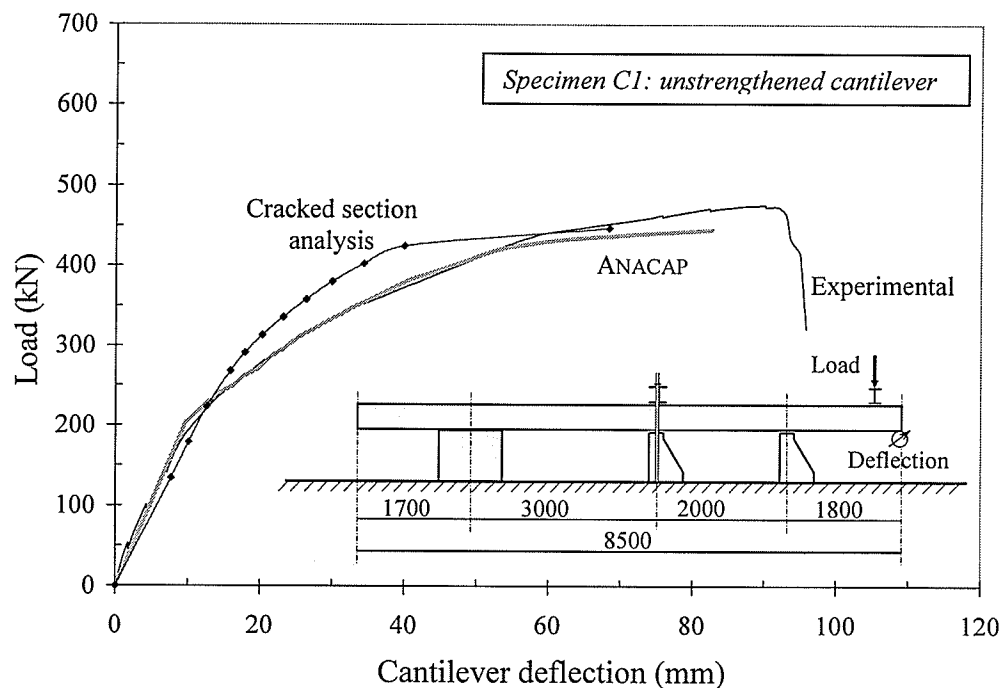
Fig. 4.43 Comparison of predicted load-deflection behaviour with laboratory results
(Specimen C1)

Cracked section analysis using strain compatibility underestimated the initial stiffness of the slab by 15 percent. Nevertheless, the cracking load and the yielding load of the cross-

section load agreed well with the measured values. The discrepancies could be attributed

to the assumption of a real hinged support at the end of the adjacent span to the cantilever

slab. Testing configurations suggested partial fixity conditions for this support. Other

assumptions such as neglecting the deformation of the neoprene pads, ignoring the width

of the supports and using limited number of sections along the cantilever span influenced

the integrated curvature and consequently, the deflections of the slab. However, the

overall predicted behaviour is satisfactory.

The predicted load-deflection behaviour using the finite element analysis compared very

well with the measured values. Comparison of cracking patterns, given in Fig. 4.44

shows similar patterns to those observed during testing.
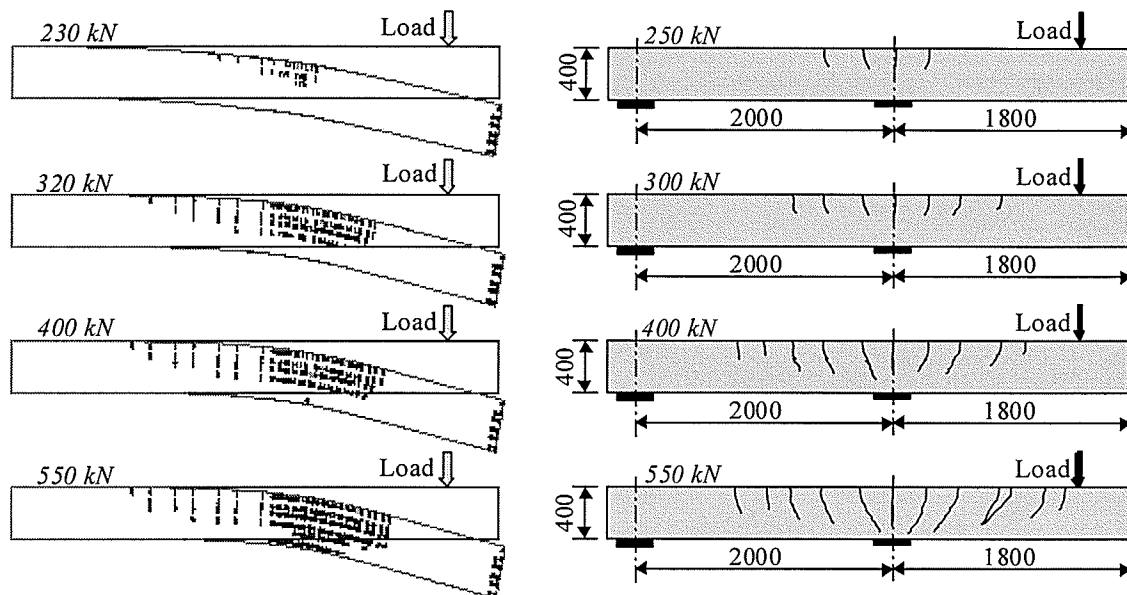
Fig. 4.44 Comparison of finite element cracking with laboratory results

Flexural cracks were initiated at the tension zone at the face of the support at a load level

of 200 kN. Cracks continued to propagate towards the end of the cantilever until failure

occurred. The predicted failure loads using the finite element analysis and strain compatibility approach underestimated the measured value by 7 percent and 6 percent, respectively. Failure was due to crushing of the concrete at the face of the support as is evident by the contours of the principal compressive strains shown in Fig. 4.45.
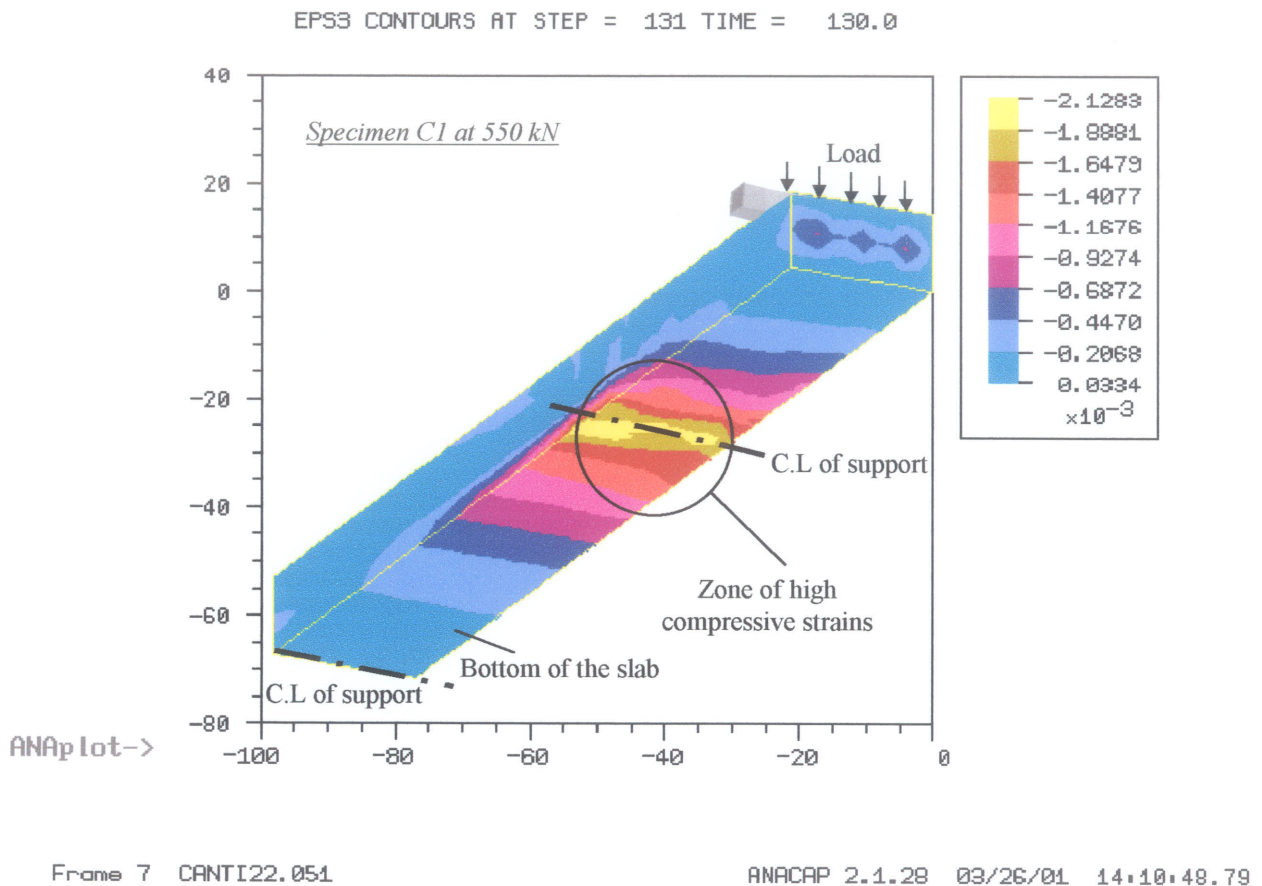
Fig. 4.45 Contours of principal compressive strains at 550 kN

The second stage of the model development involved the addition of CFRP reinforcement. Six 10 mm diameter Leadline bars were added to model the behaviour of specimen C2, which was strengthened with near surface mounted Leadline bars. The epoxy was not modelled in the analysis since no slip between the epoxy and the bars was

observed during the test. The CFRP bars were assumed to be fully bonded to the concrete. The predicted load-deflection behaviour is shown in Fig. 4.46.
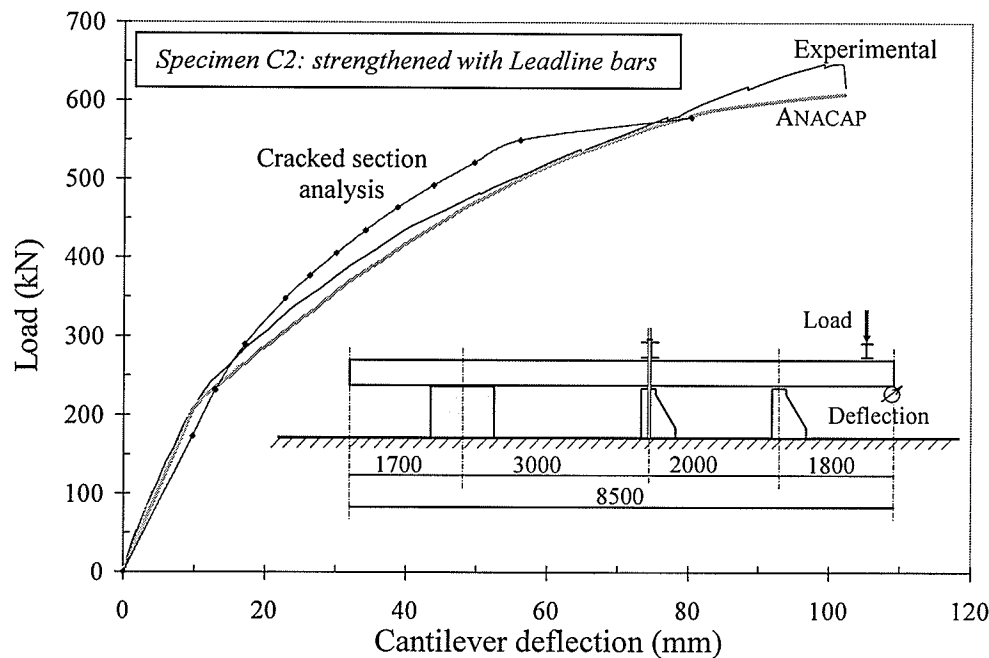
Fig. 4.46 Comparison of predicted load-deflection behaviour with laboratory results (Specimen C2)

Compared to the test results, the flexural stiffness of the cantilever slab was simulated with a very high accuracy using the finite element analysis. The cracked section analysis using strain compatibility underestimated the initial stiffness prior to cracking by 16 percent.

The maximum tensile strain in the CFRP reinforcement was predicted using the finite element analysis. The predicted behaviour is compared to the measured values as shown in Fig. 4.47. The predicted values are in a good agreement with the experimental results up to yielding of the steel reinforcement at a load level of 440 kN. At higher loads, the predicted strain is greater than the measured values. This is attributed to the assumption

188

of elastoplastic behaviour of steel reinforcement. Ignoring the increase in stress within the strain hardening zone resulted in higher strains at the steel reinforcement level and consequently in the CFRP bars.
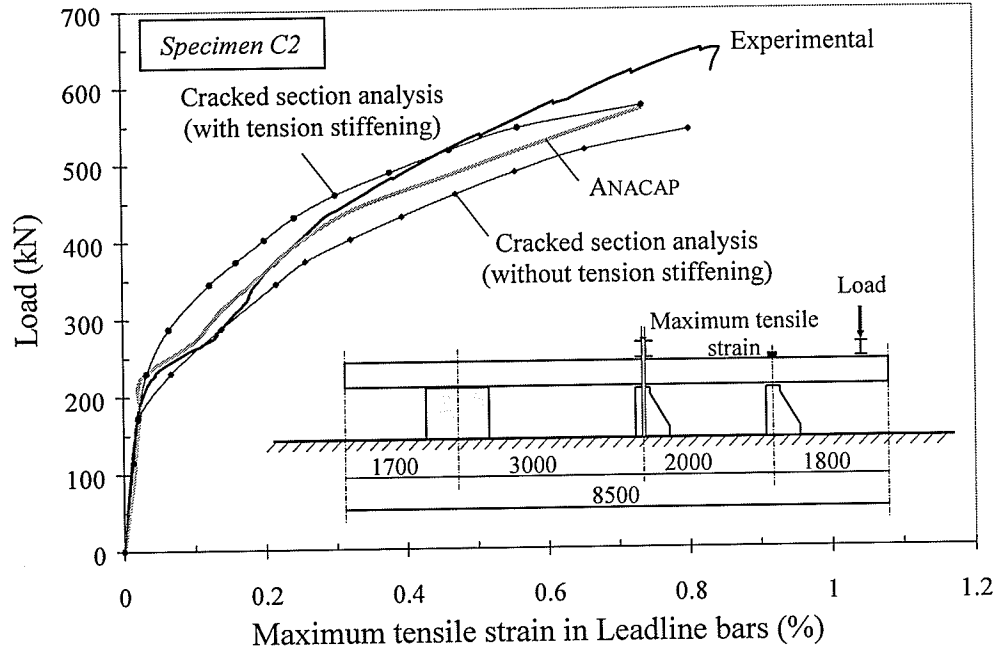
Fig. 4.47 Comparison of predicted load-tensile strain behaviour with laboratory results (Specimen C2)

The strain was also predicted using strain compatibility with and without accounting for tension stiffening of the concrete. The measured values lied in between these two extremes up to a load level of 500 kN. At higher loads the predicted strains were considerable greater than the measured values. The average tensile stress in concrete after cracking, f_t, is evaluated by Equation 4.8.

$$f_t = \frac{\alpha_1 \alpha_2 f_{ct}}{1 + \sqrt{500 \varepsilon_{ct}}} \quad \varepsilon_{ct} > \varepsilon_{cr} \qquad (4.8)$$

where f_{ct} is the tensile strength of concrete; ε_{ct} is the average tensile strain of concrete; ε_{cr} is the tensile strain at cracking; α_1 is a factor accounting for the bond characteristics of the reinforcement and is equal to 0.7 for Leadline bars as proposed by Abdelrahman

189

(1995); α_2 is a factor accounting for the type of loading and is equal to 1.0 for short term loading.

Failure was due to crushing of the concrete at the face of the support as observed in the experimental program. The predicted failure loads using the finite element analysis and strain compatibility approach underestimated the experimental value by 6 percent and 11 percent, respectively. Predicted loads and deflections at cracking and at failure compared to the measured values are given in Table 4.8.

Table 4.8. Predicted results for Specimens C1 and C2

Specimen	Method of analysis	P_{cr} (kN)	Δ_{cr} (mm)	P_u (kN)	Δ_u (mm)	P_u predicted / P_u experimental
C1	Experimental	180	9.1	476	92.5	-
	Finite element	200	9.5	445	83	0.93
	Strain compatibility	205	12	447	49	0.94
C2	Experimental	189	8.3	647	102	-
	Finite element	205	9.2	609	102	0.94
	Strain compatibility	210	11	579	65	0.89

Since the product of $(EA)_{CFRP}$ was kept constant for all cantilevers, the predicted load-deflection behaviour using either the finite element analysis or strain compatibility approach is anticipated to be identical for all strengthened specimens.

4.3.4.2 Simply Supported Specimens

The predicted load-deflection behaviour of specimen SS1, strengthened with near surface mounted Leadline bars is shown in Fig. 4.48, compared to the measured values.
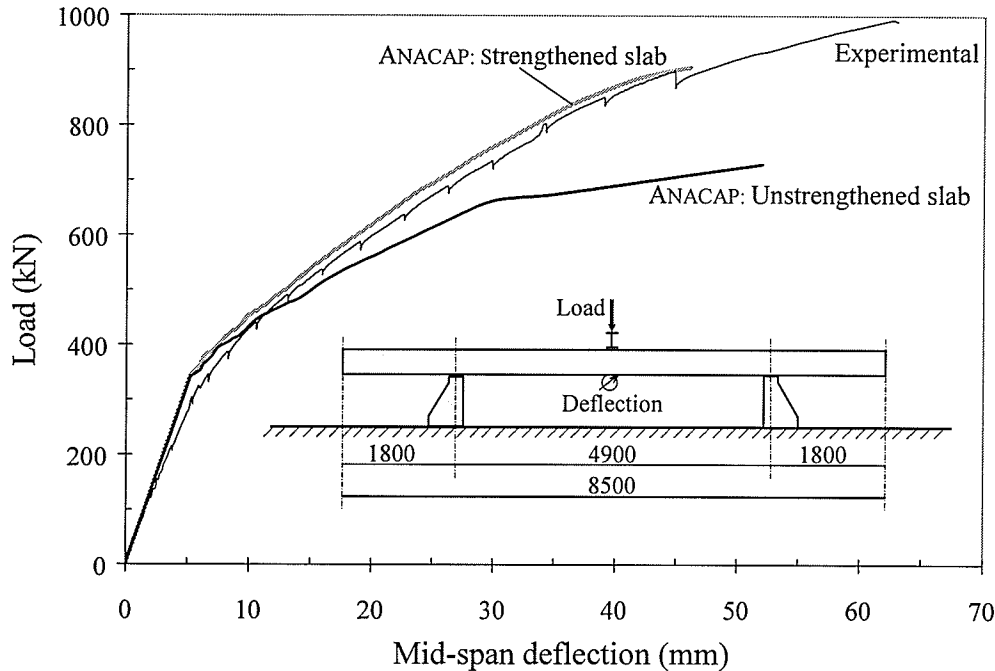
Fig. 4.48 Comparison of predicted load-deflection behaviour with laboratory results (Specimen SS1)

Although, the predicted behaviour was very satisfactory, the predicted initial stiffness overestimated the measured values by 11 percent. Such a phenomenon is a direct consequence of the previous bending tests conducted on the two cantilevers. In general, the predicted behaviour was in a good agreement in terms of cracking load, ultimate load and flexural stiffness after cracking of the concrete. Failure was due to crushing of the concrete at the location of the applied load. The analysis predicted a failure load of 907 kN, which is 9 percent less than the measured value. Compared to the experimental results, the overall behaviour is well simulated using the ANACAP program.

Fig. 4.49 depicts a typical crack pattern development for strengthened simply supported specimens using finite element analysis. It emerged that at a load of 350 kN flexural cracks were initiated under the location of the applied load. By increasing the applied load, cracks continued to propagate towards the top surface until crushing of the concrete occurred.
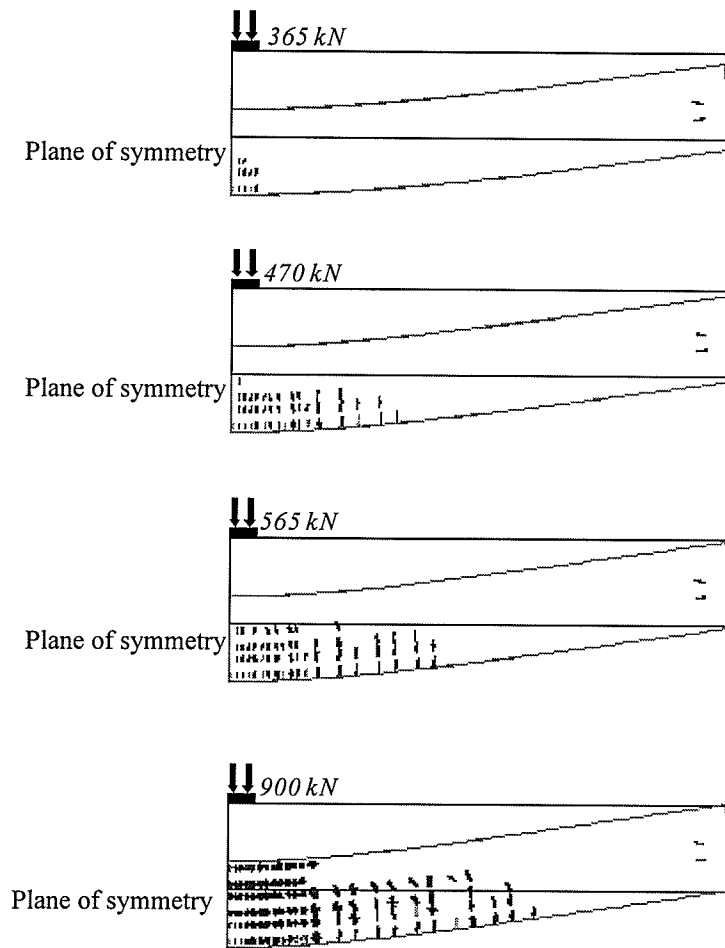
Fig. 4.49 Typical crack pattern development for simply supported slabs

Predicted loads and deflections at cracking and at failure compared to the measured values are given in Table 4.9.

Table 4.9 Observed and predicted loads and deflections for specimen SS1

		Experimental	**ANACAP**
Load	Cracking (kN)	350	350
(kN)	Ultimate (kN)	993	905
Deflection	Cracking (mm)	6.6	6.0
(mm)	Ultimate (mm)	62.6	46

From the above discussion, it is concluded that non-linear finite element modelling is a powerful predictive tool for the analysis of concrete members strengthened with near surface mounted FRP reinforcement. Failure loads as well as flexural failure mechanisms can be simulated with sufficient accuracy using cracked section analysis as well as non-linear finite element modelling. Various assumptions incorporated in the cracked section analysis could greatly influence the predicted response of FRP strengthened concrete members. However, the cracked section analysis is an excellent analysis tool and quite adequate for typical design and analysis due to its simplicity and validity for most engineers without the need for sophisticated finite element analysis.

Chapter 5

Experimental Results & Analytical Modelling:

Bond Specimens

This chapter presents both experimental and analytical investigations undertaken to evaluate bond characteristics of various FRP strengthening techniques. A total of 24 concrete bond specimens were constructed and tested under monotonic static loading. Different embedment lengths were studied to evaluate the development length needed for an effective use of near surface mounted C-Bars, CFRP strips and externally bonded CFRP sheets. A bond failure hypothesis for near surface mounted FRP bars is presented. Closed-form analytical solutions are proposed to predict the interfacial stresses for near surface mounted strips and externally bonded sheets. The proposed models are validated by comparing the predicted values with test results as well as non-linear finite element modelling. Quantitative criteria governing debonding failure of near surface mounted FRP bars and strips as well as externally bonded sheets are established.

5.1 Introduction

The bond of reinforcing FRP bars, strips and sheets to concrete is a critical factor that controls the structural performance of FRP retrofitted concrete members. Deformational capacity, cracking behaviour and tension stiffening are greatly influenced by the bond

characteristics of the FRP reinforcement. Up-to-date, limited research has been reported on the bond behaviour of FRP reinforcement. Lack of experimental data, design tools and analytical models concerning the bond characteristics of various FRP strengthening techniques introduce serious obstacles towards an efficient use of these materials. In general, debonding of the FRP reinforcement is a brittle phenomenon that, in most cases, occurs in an abrupt manner. In addition, these premature failures are generally associated with a considerable reduction in the deformability of the strengthened member. Therefore, a thorough understanding of the bond mechanisms is essential for the characterization of failure and for the realistic prediction of ultimate loads.

The previous chapter presented the effectiveness and feasibility of various FRP strengthening schemes. A cost analysis was performed to rank various techniques according to their efficiencies. Test results of the large-scale specimens provided sufficient evidence and confidence in near surface mounted C-Bars, CFRP strips and externally bonded CFRP sheets as innovative strengthening techniques. Excellent performance in terms of strength enhancement and overall cost of construction was observed. Nevertheless, fundamental understanding of the bond characteristics and load transfer mechanisms of these techniques are still challenging issues and require further investigation. Design guidelines are urgently needed to provide the current standards with the necessary tools to implement the proposed strengthening techniques.

To fully understand the behaviour of various FRP strengthening techniques, the research included a second phase to investigate the bond characteristics and load transfer mechanisms between FRP reinforcement and concrete.

A total of 24 simply supported T-beams with a span of 2.5 m and a depth of 300 mm were tested. Three series of beam specimens designated as A, B and C were strengthened using near surface mounted bars, strips and externally bonded sheets, respectively. The bond length was varied for each strengthening technique to examine its effects on the failure mode and the ultimate capacity of the strengthened beam. The T-section configuration was selected to avoid compression failure due to crushing of the concrete. The beams were adequately designed to avoid conventional shear failure. The selected configuration of the specimens allowed the FRP reinforcement to be in an area of flexural tension under a moment gradient and constant shear to simulate typical design stresses.

This chapter introduces three mathematical models for the interfacial shear stress and the minimum anchorage length required for near surface mounted FRP bars, strips and externally bonded FRP sheets. The analytical models are validated by comparing the predicted values with test results as well as non-linear finite element modelling. The influence of key parameters, believed to affect the bond behaviour of various FRP strengthening techniques is discussed.

5.2 Near Surface Mounted FRP Bars

5.2.1 Experimental Results (Series A)

A total of eight beams were tested from series A. One beam was tested as a control specimen while the other seven beams were strengthened with near surface mounted C-Bars, produced by Marshall Industries, USA. Each beam was strengthened using one bar inserted into a grove cut at the bottom surface of the beam. Complete details of the tested specimens were given in Chapter 3, section 3.3.3.

The load-deflection behaviour of the tested specimens is shown in Figs. 5.1a and 5.1b for two adhesives; Duralith-gel and Kemko040, respectively. In general, the behaviour for the two sets indicated that as the embedment length increased, the ultimate load increased up to a certain limit beyond which no significant increase in the ultimate load was measured.
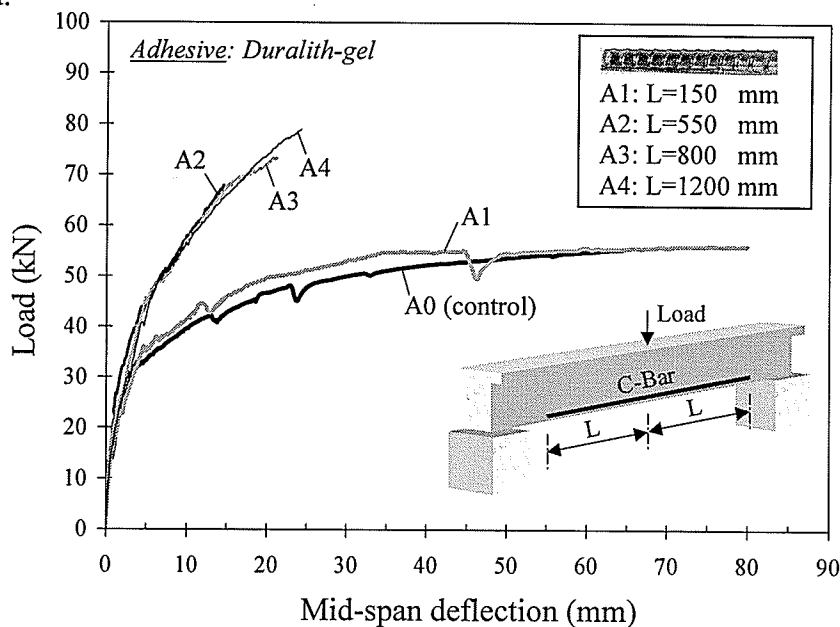
Fig. 5.1a Load-deflection behaviour of series A specimens using Duralith-gel as the bonding adhesive
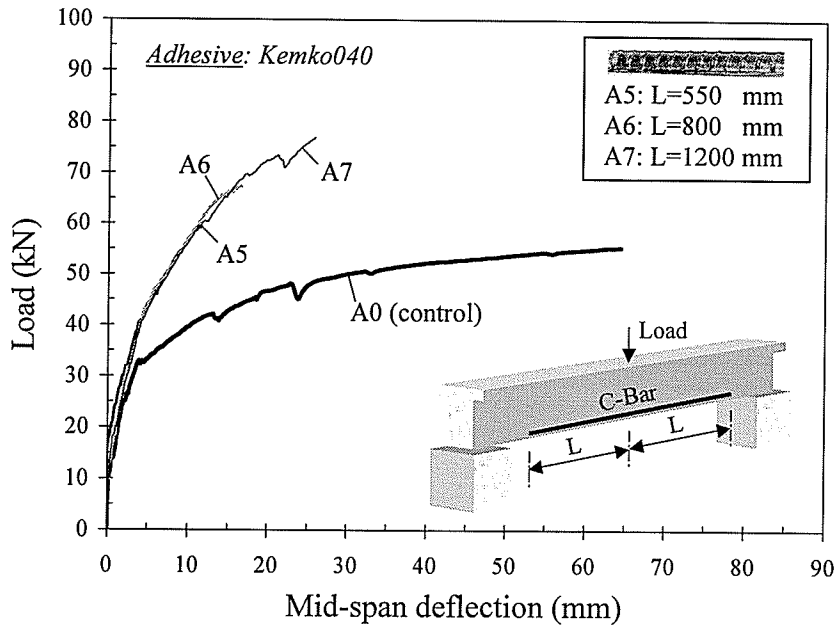
Fig. 5.1b Load-deflection behaviour of series A specimens using Kemko040 as the bonding adhesive

The control specimen, A0, failed due to crushing of concrete at a load level of 56 kN.

Using an embedment length of 150 mm (beam A1) provided insignificant increase in

stiffness or strength due to early debonding of the bar. Failure of beams A2, A3, and A4

with embedment lengths of 550, 800, and 1200 mm, respectively was due to debonding

of the CFRP bar. The ultimate loads for these beams ranged between 67 kN to 79 kN,

with an increase of 20 to 41 percent in comparison to the control specimen. Figs. 5.2a and

5.2b compare the load-deflection behaviour of the bond specimens strengthened using the

two sets of adhesives with embedment lengths of 800 and 1200 mm, respectively.
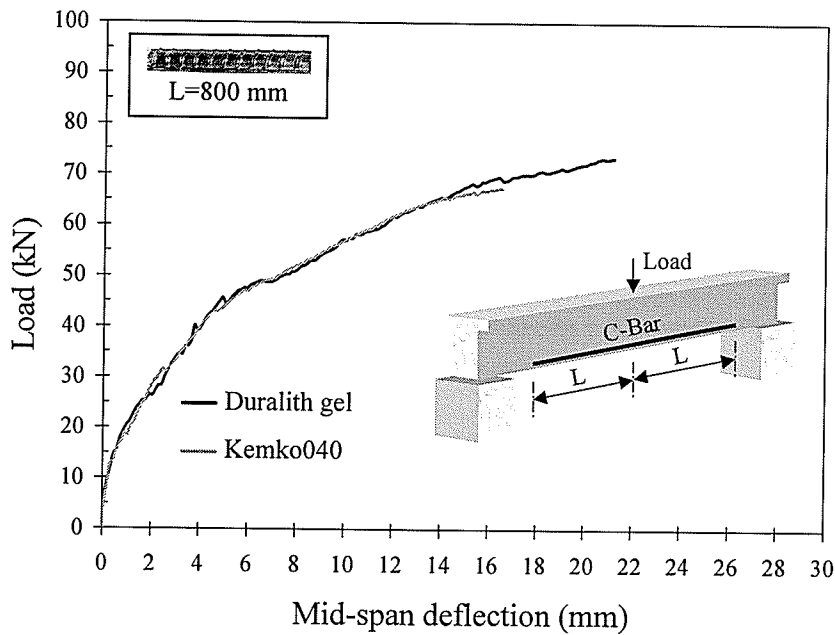
Fig. 5.2a Load-deflection behaviour of series A beams using different adhesives [L=800 mm]
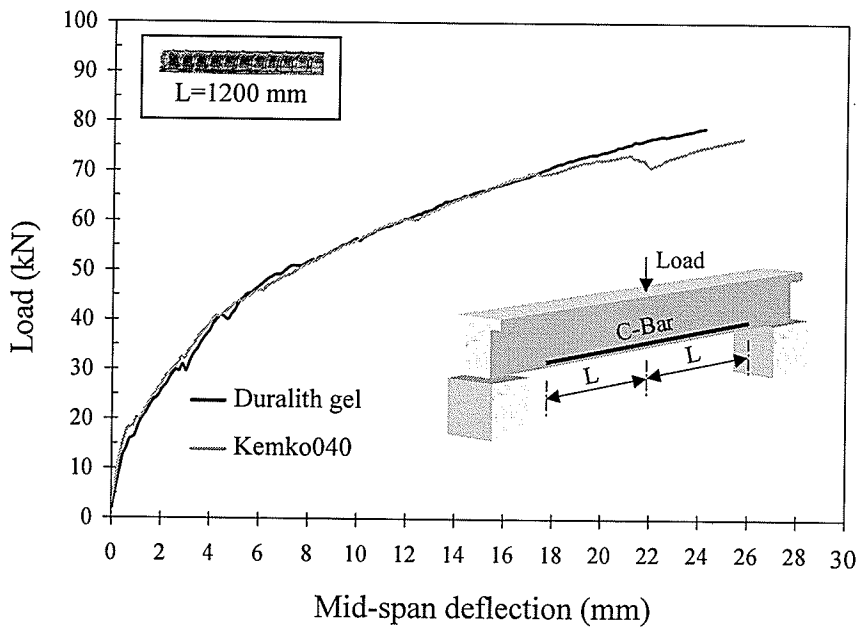
Fig. 5.2b Load-deflection behaviour of series A beams using different adhesives [L=1200 mm]

The comparison shown indicates identical behaviour for the beams strengthened with the two sets of adhesives up to failure. Altering the type of the epoxy adhesive had a negligible effect on the ultimate load carrying capacity of the strengthened beams. It

should be mentioned that both adhesives were originally used for bonding steel bars to concrete.

The observed mode of failure for all beams strengthened with CFRP C-Bars was due to cracking of the concrete surrounding the epoxy in the groove followed by complete debonding of the bars. After debonding failure, the beams behaved as conventional concrete beams reinforced with steel bars. The load dropped to a load level equivalent to the yielding moment of the cross-section and maintained until crushing of the concrete occurred. Debonding occurred at the location where the secondary bottom steel reinforcement was terminated due to high shear stress concentration in this zone as shown in Fig. 5.3
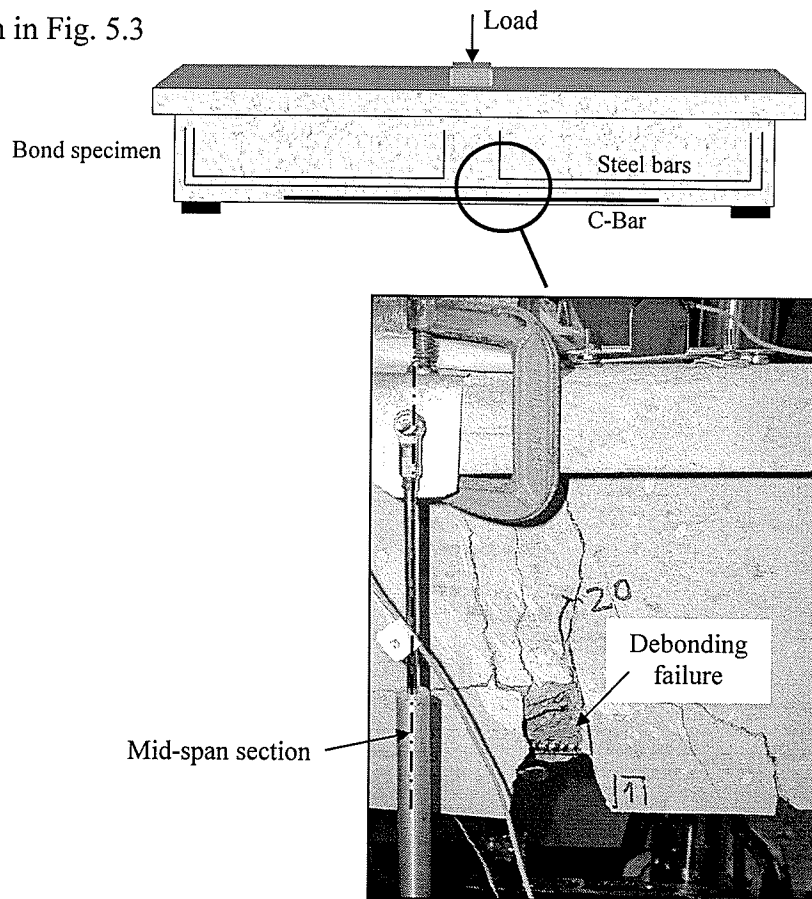
Fig. 5.3 Debonding of near surface mounted C-Bars

This finding is significant and has been confirmed by the finite element model described in section 5.2.2.8. Such a phenomenon indicates also that the configuration of the original steel reinforcement could influence the location where the debonding process can initiate.

Using an embedment length greater than 800 mm provided inconsiderable enhancement in the ultimate load carrying capacity of the strengthened beams. Test results indicated a failure load of 73 kN for an embedment length of 800 mm. Increasing the embedment length by 50 percent resulted in an increase in the ultimate load carrying capacity by only 8 percent. Flexural cracks were observed to be uniformly distributed within the bonded zone. The cracks were narrower in the strengthened beams compared to the control beam due to the presence of the CFRP bars. The maximum measured tensile strain in the C-bars was monitored during testing using electrical strain gauges as shown in Fig. 5.4.
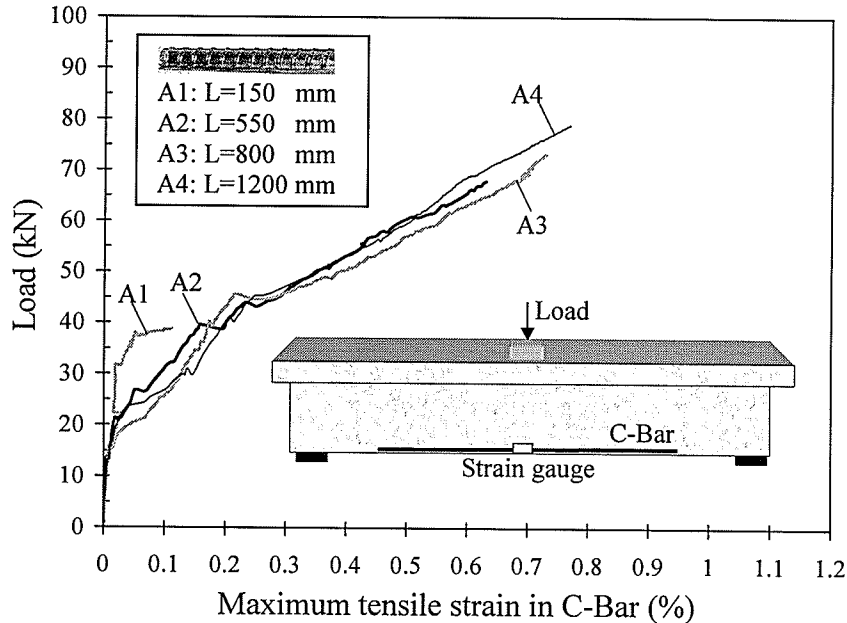
Fig. 5.4 Load-tensile strain behaviour of series A specimens

Debonding of the near surface mounted CFRP bar took place at a very early stage for beam A1, where the bond length was set to 15 times the diameter of the bar (*L=150 mm*). The composite action was completely lost at a strain level of 0.11 percent indicating that only 6 percent of the rupture strain of the bars was utilized prior to debonding. Consequently, the minimum embedment length recommended by the ACI 440 (2002) for FRP bars bonded to concrete (*L>4d*), is not applicable for near surface mounted FRP bars. This is primarily attributed to the distinct surface characteristics of the epoxy compared to concrete. Generally, the surface of the epoxy is smoother and requires relatively longer bond lengths to develop the same bond stresses as in the case of concrete. Comparable strains and consequently crack widths were observed for beams A2, A3, and A4 up to failure.

Test results showed that the maximum measured tensile strain in the CFRP bars at failure is in the range of 40 to 45 percent of the rupture strain of the bars, regardless of the embedment length used. De Lorenzis and Nanni (2002) reported a limiting strain value for near surface mounted C-Bars of 33 percent of the rupture strain. Such a limiting value is highly dependent on the configuration of the steel reinforcement inside the beam in the strengthened zone as well as on the stress level at the concrete-epoxy interface as will be emphasized later in this chapter (section 5.2.2.8).

Mathey and Watstein (1961) recommended using a free-end slip of 0.05 mm to define bond failure of steel bars in concrete. Test results indicated that bond stresses corresponding to this value of slip were considerably low and underestimating the bond

strength of near surface mounted C-Bars. Consequently, such a criterion could not be used for FRP bars. An examination of the bond stress-slip relationships shown in Fig. 5.5 indicates that bond failure can be better described in terms of bond strength rather than end slip values. The average bond stresses, τ, can be evaluated using Equation 5.1

$$\tau = \frac{d}{4} \frac{f_{FRP}}{L} \tag{5.1}$$

where d is the diameter of the bar (9.525 mm); L is the bond length and f_{FRP} is the maximum tensile stress in the bar based on strain gauge readings.
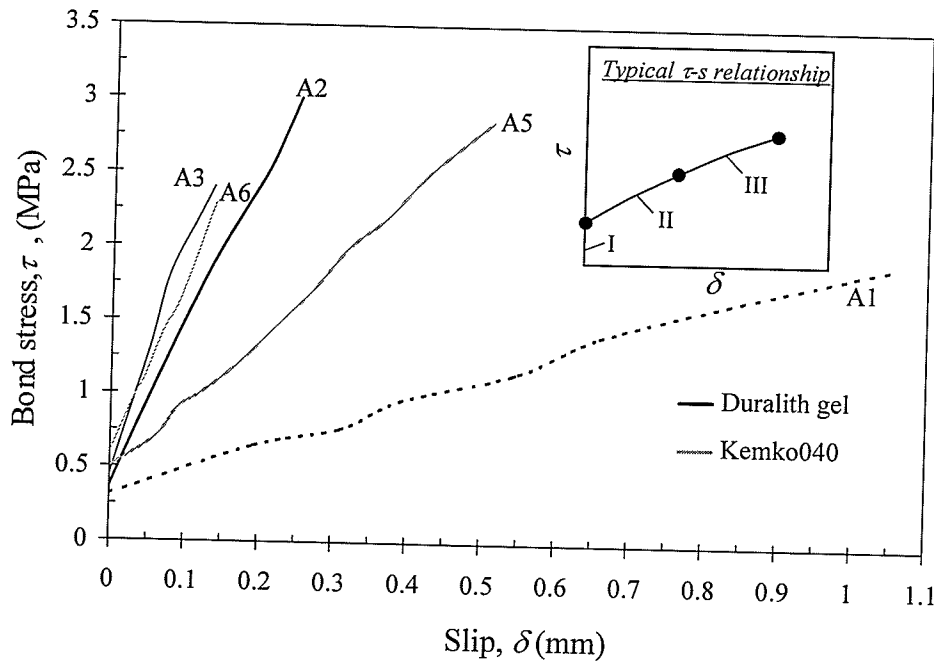
Fig. 5.5 Bond-slip relationship for near surface mounted C-Bars

As the embedment length increased, the induced tensile stresses in the bar increased up to an embedment length of 550 mm. Consequently, higher bond stresses were developed in beams A2 and A5 compared to beam A1. Further increase in the embedment length resulted in insignificant increase in the tensile stresses in the bars and lower bond stresses

were developed in beams A3 and A6 compared to beams A2 and A5. This behaviour was confirmed by the findings of Tepfers (1998).

Test results showed that bond stresses up to 3 MPa between the CFRP bars and epoxy could be developed prior to debonding of the C-Bars. No slip was observed for beams A4 and A7 where the embedment length was set to 1200 mm. Altering the type of the bonding adhesive had a negligible effect on the ultimate bond stresses. This was evident by comparing the ultimate bond stresses developed for beams A2 and A3 with those developed for beams A5 and A6, respectively.

Typical bond-slip relationship for near surface mounted C-Bars, shown in Fig. 5.5 suggested the following three main stages for the bond mechanism:

Stage I: represents the initial bond provided by the chemical adhesion. At this stage no slip occurs.

Stage II: represents break of the chemical adhesion and transfer of bond forces by the mechanical friction provided by the lugs of the bars. At this stage, bearing stresses in the concrete and epoxy are developed and induced transverse micro cracks at the tips of the lugs allowing the bar to slip.

Stage III: represents a significant increase of the bearing forces accompanied by numerous internal cracks around the deformed C-Bars causing debonding failure. Debonding could occur either at the FRP-epoxy interface or at the concrete-epoxy interface.

Modelling of the bond-slip relationship is of prime importance to conduct detailed theoretical or non-linear finite element analysis. Based on statistical evaluation of test results, a new model is proposed for the bond-slip relationship for near surface mounted CFRP bars.

$$\frac{\tau}{\tau_f} = 0.20 + 0.80\frac{\delta}{\delta_f} \tag{5.2}$$

where τ_f is the peak bond stress, δ_f is the slip at peak bond stress, τ is the average bond stress, δ is the slip at free end. The proposed model compared very well with the experimental results as shown in Fig. 5.6. The model represents a typical bond-slip relationship for near surface mounted FRP bars bonded to epoxy.
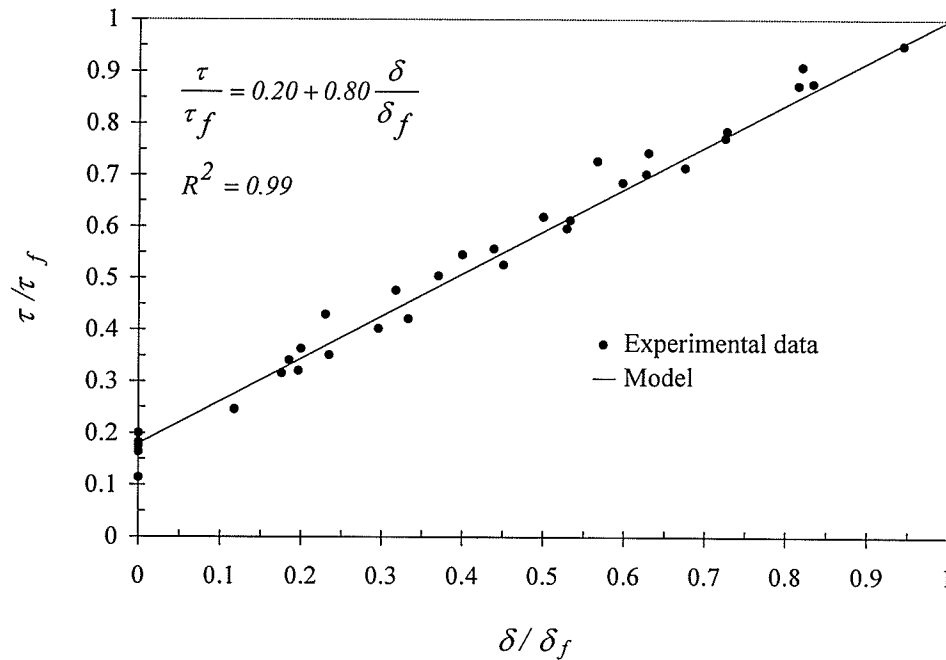
Fig. 5.6 Bond-slip model prediction compared to experimental results

Experimental results for the test specimens are summarized in Table 5.1.

Table 5.1 Summary of test results for series A

Beam No.	L (mm)	Epoxy used	P_u (kN)	Δ_u (mm)	ε_u (%)	τ_f (MPa)	Failure mode	% Increase in ultimate capacity
A0	N.A	N.A	56	64	-	-	C [+]	-
A1	150	Duralith-gel	56	78	0.11	1.93	D [*]	0.4
A2	550	Duralith-gel	67	15.3	0.63	3.0	D	20
A3	800	Duralith-gel	73	21.2	0.73	2.40	D	31
A4	1200	Duralith-gel	78.9	24.2	0.78	1.72	D	41
A5	550	Kemko 040	59	12	0.60	2.9	D	6
A6	800	Kemko 040	67	16.5	0.68	2.3	D	20
A7	1200	Kemko 040	76.8	25.8	0.73	1.61	D	37

[+] C refers to crushing of concrete and steel yielding

[*] D refers to debonding of CFRP bars.
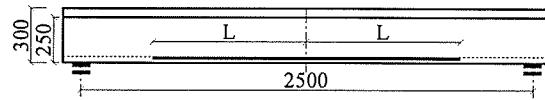
where L is the bond length; P_u is the ultimate failure load; Δ_u is the deflection at failure; ε_u is the maximum tensile strain in C-Bars at failure; and τ_f is the peak bond stress.

From the above discussion, it is concluded that the efficiency of using CFRP bars as near surface mounted reinforcement is controlled primarily by the bond characteristics of the bars as well as the bond between the adhesive material and the concrete. This behaviour has been confirmed and reported recently by other researchers [De Lorenzis and Nanni, 2002].

Test results demonstrated that rupture of near surface mounted C-Bars was not likely to occur regardless of the embedment length or the type of the epoxy adhesive used. Furthermore, the maximum allowable tensile strain should be limited to 40 percent of the

rupture strain of the bars. Test results suggested that the minimum development length for near surface mounted C-Bars with the given dimensions used in this program should not be less than 80 times the diameter of the bars.

5.2.2 Analytical Modelling

5.2.2.1 Significance of the Model

The following sections present a general methodology to evaluate the development length of near surface mounted FRP bars of different configurations. The model is based on equilibrium and displacement compatibility procedures using finite element analysis. The currently adopted ACI approach for evaluating the development length of steel bars was selected as a starting point for the proposed approach. The model accounts for distinct characteristics of concrete, epoxy and FRP materials. Design charts for calculating the development length of near surface mounted FRP bars are proposed. The influence of various parameters, believed to affect the development length of near surface mounted FRP bars, is discussed.

5.2.2.2 ACI Approach for Steel Bars

Thick-walled cylinder theory has been applied by many researchers to analyze the stresses in a concrete cylinder surrounding a single bar [Orangun et al., 1977; Mahmoud et al., 1999].

Ferguson and Briceno (1969) proposed a series of equations for calculating the development length of deformed steel bars. The equations served as the basis for the

development length provisions in the ACI codes since 1989. Thick-walled cylinder theory was adopted as a basis for the approach. Considering an effective cylindrical prism of concrete of diameter $2C$, affected by a given a steel bar of diameter, d, the radial components of the force on concrete cause a radial pressure on a portion of the cross-section of the prism as shown in Fig. 5.7.

Beam cross-section
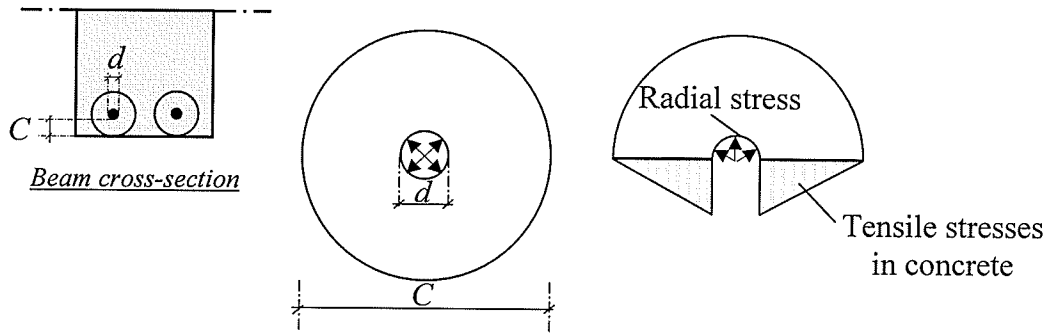
Fig. 5.7 Stresses in a concrete prism subjected to bond stresses

The radial pressure is equilibrated by the tensile stresses in concrete on either side of the bar. The distribution of these tensile stresses is based on the thick-walled cylinder theory and is approximated to a triangular shape as shown in Fig. 5.7. Equating the tensile strength of concrete to the splitting stresses, a relationship between material and geometrical properties of the spliced section can be established and the basic development length for steel bars can be determined.

5.2.2.3 Proposed Approach for NSM FRP Bars

The transfer of stresses from a deformed near surface mounted FRP rod to the concrete is assumed to be mainly through the mechanical interlocking of the lugs to the surrounding adhesive. Due to the shape of the lugs, the resultant force exerted by the lug to the epoxy is inclined with an angle β with respect to the axis of the bar as shown in Fig. 5.8, where $1/(\tan \beta)$ is the coefficient of friction between the bar and the adhesive, (μ).
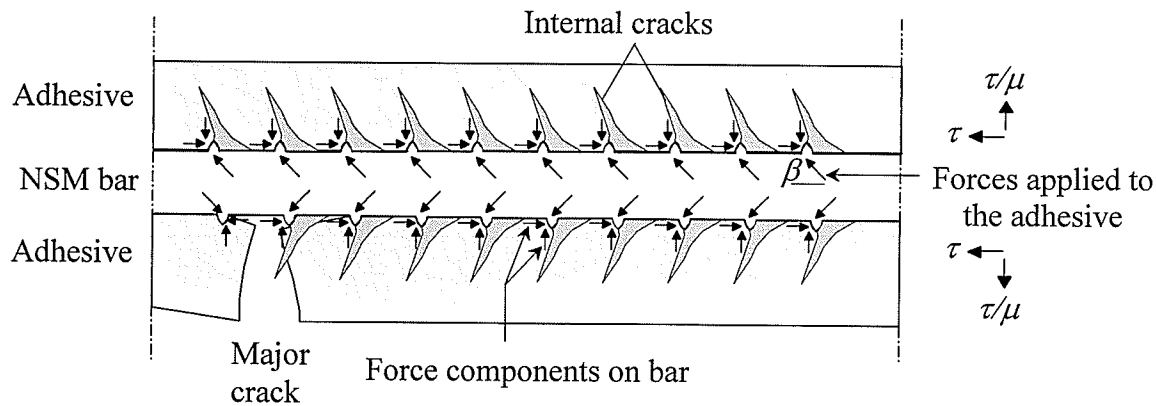
Fig. 5.8 Forces between near surface mounted FRP bar and epoxy

The radial component of the resultant force creates zones of high tensile stresses at the FRP-adhesive interface as well as at the concrete-adhesive interface. Lack of confinement, uneven distribution of bond stresses, edge effects and composite interaction between concrete, adhesive and FRP materials complicate the analysis of near surface mounted FRP bars. Consequently, thick-walled cylinder theory is no longer valid.

In this section finite element analysis is employed to provide in-depth understanding of the bond characteristics and load transfer mechanism between near surface mounted FRP bars and concrete. The finite element modelling described in this section was conducted

using ADINA program (Version 7.4). Fig. 5.9 shows the mesh dimensions used in modelling a portion of a concrete beam strengthened with a near surface mounted FRP bar using epoxy as an adhesive.
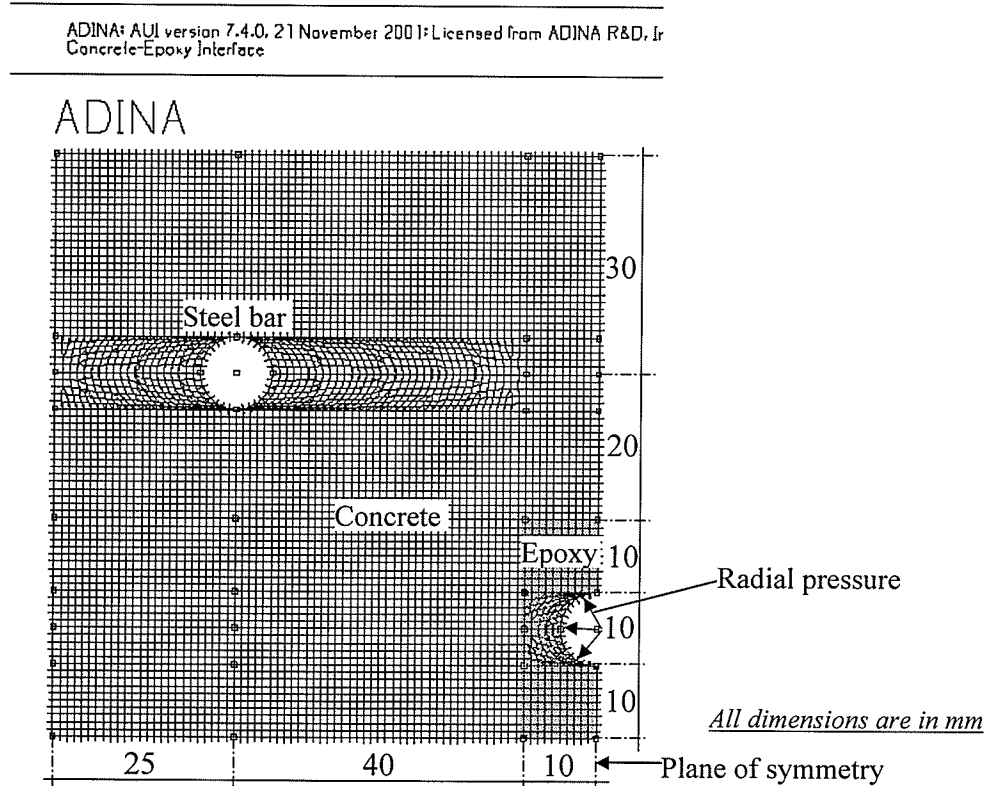
Fig. 5.9 Mesh dimensions for a portion of a concrete beam strengthened with a near surface mounted FRP bar

The concrete and the epoxy were modelled using eight-node plain strain elements with a 3x3 Gauss integration scheme. Groove dimensions, bar location and properties of concrete and epoxy were set identical to those used in the bond specimens. Radial pressure was applied at the bar location to simulate the bond stresses transferred from the bar to the surrounding epoxy. Typical principal tensile stress distribution around the FRP bar is shown in Fig. 5.10.
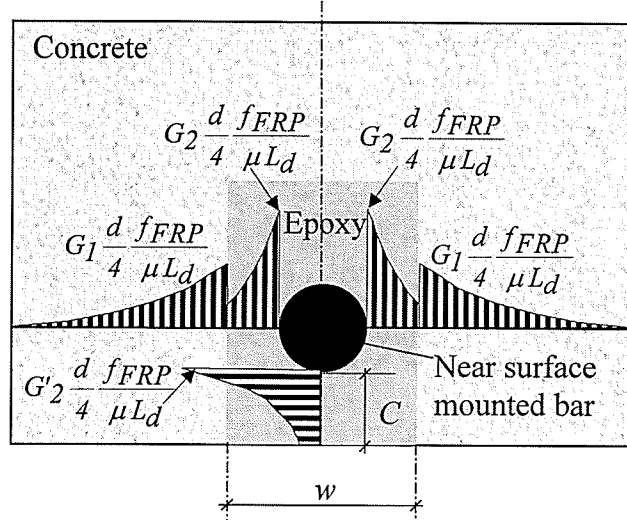
Fig. 5.10 Typical stress distribution around near surface mounted bar

It should be noted that the elastic modulus of the adhesive is generally less than that of the concrete. Such a phenomenon results in a stress discontinuity at the concrete-epoxy interface as shown in Fig. 5.10. High tensile stresses are observed at the concrete-epoxy interface as well as at the FRP-epoxy interface. Two different types of debonding failures can occur for near surface mounted FRP bars. The first mode of failure is due to splitting of the epoxy cover as a result of high tensile stresses at the FRP-epoxy interface, and is termed "epoxy split failure". Increasing the thickness of the epoxy cover reduces the induced tensile stresses significantly. Furthermore, using adhesives of high tensile strength delays epoxy split failure. This type of debonding failure forms with longitudinal cracking through the epoxy cover. The second mode of failure is due to cracking of the concrete surrounding the epoxy adhesive and is termed "concrete split failure". This mode of failure takes place when the tensile stresses at the concrete-epoxy interface reach the tensile strength of the concrete. Widening the groove minimizes the induced tensile stresses at the concrete-epoxy interface and increases the debonding loads of near surface mounted bars. Concrete split failure was the governing mode of failure for the bond

specimens reported in this investigation. Large epoxy cover and high tensile strength of the epoxy adhesive provided high resistance to epoxy split failure and shifted the failure to occur at the concrete-epoxy interface [Rizkalla and Hassan, 2002].

Measurements of bar strains along the embedment length of near surface mounted FRP bars shows linear strain distribution at high load levels. Therefore, the tangential bond stress, τ, can be estimated with an average value of:

$$\tau = \frac{d}{4} \frac{f_{FRP}}{L_d} \tag{5.3}$$

where d is the diameter of the bar, and L_d is the embedment length needed to develop a stress of f_{FRP} in the near surface mounted bar. The maximum tensile stress in near surface mounted FRP bars, f_{FRP}, will be discussed in detail in section 5.2.2.8. If the coefficient of friction between the bar and the epoxy is μ, the radial stresses, σ_{radial}, can be expressed as:

$$\sigma_{radial} = \frac{\tau}{\mu} = \frac{d}{4} \frac{f_{FRP}}{\mu L_d} \tag{5.4}$$

The tensile stresses at the concrete-epoxy interface, $\sigma_{con-epoxy}$, and at the FRP-epoxy interface, $\sigma_{FRP-epoxy}$, shown in Fig. 5.10 can be expressed in terms of the radial stress as follows:

$$\sigma_{con-epoxy} = G_1 \frac{d}{4} \frac{f_{FRP}}{\mu L_d} \tag{5.5}$$

$$\sigma_{FRP-epoxy} = G_2 \text{ or } G'_2 \left[\frac{d}{4} \frac{f_{FRP}}{\mu L_d} \right] \tag{5.6}$$

where G_1, G_2 and G'_2 are coefficients determined from the finite element analysis based on a unit radial pressure applied at the bar location and using specified groove dimensions, concrete and adhesive properties. The maximum tensile stress at the FRP-epoxy interface, $\sigma_{FRP\text{-}epoxy}$, depends on the coefficients G_2 and G'_2, whichever is greater as shown in Fig. 5.10. Equating the tensile strength of concrete to Equation 5.5, the minimum embedment length needed for near surface mounted FRP bars to prevent concrete split failure can be expressed as:

$$L_d = G_1 \frac{d}{4} \frac{f_{FRP}}{\mu f_{ct}} \qquad (5.7)$$

Equating the tensile strength of the adhesive to Equation 5.6, the minimum embedment length needed for near surface mounted FRP bars to avoid epoxy split failure shall not be less than:

$$L_d = G_2 \text{ or } G'_2 \left[\frac{d}{4} \frac{f_{FRP}}{\mu f_{epoxy}} \right] \qquad (5.8)$$

where f_{ct} and f_{epoxy} are the tensile strength of concrete and epoxy, respectively. Increasing the stiffness of concrete by using high strength concrete increases the tensile stresses at the concrete-epoxy interface. This is evident by the considerable increase in the value of G_1 by increasing the modular ratio, n as shown in Fig. 5.11. Furthermore, increasing the stiffness of the adhesive increases the tensile stresses at the FRP-epoxy interface. This is evident by the increase in the values of G_2 and G'_2 by decreasing the modular ratio as shown in Fig. 5.12.

$$n = \frac{E_c}{E_a} \qquad (5.9)$$

where E_c and E_a are the modulus of elasticity of concrete and adhesive, respectively.
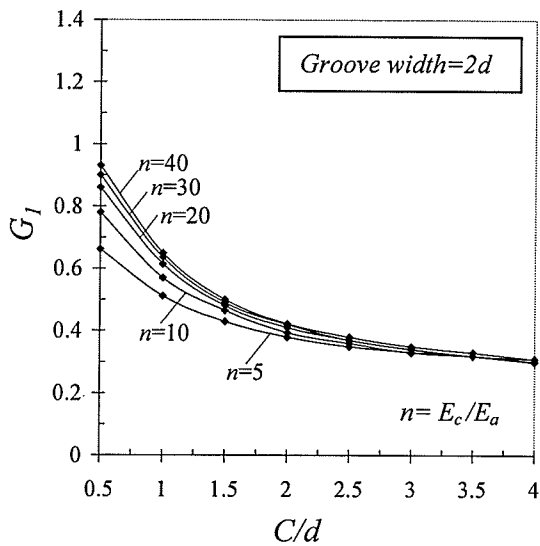
Fig. 5.11 Influence of concrete and adhesive properties on tensile stresses at concrete-epoxy interface
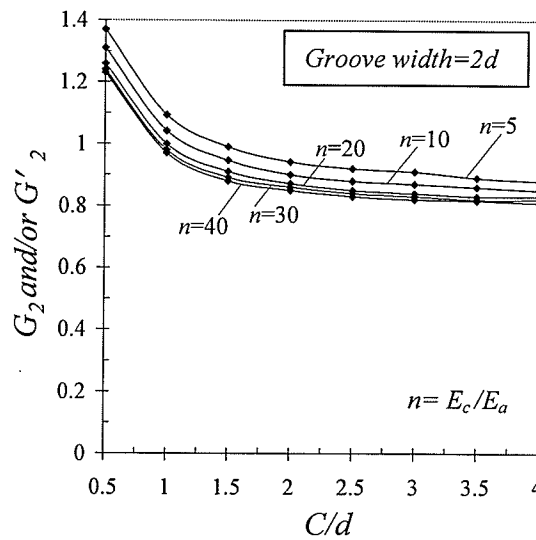
Fig. 5.12 Influence of concrete and adhesive properties on tensile stresses at FRP-epoxy interface

It should be noted that neighbouring steel bars have no adverse effect on the induced tensile stresses in concrete and adhesive. Practical values of the modular ratio, n, can vary between 5 and 40. This range covers various types of concrete and adhesives that are commonly used in concrete structures. Fig. 5.13 shows a proposed design chart for the development length of near surface mounted FRP bars. To simulate the most critical conditions for design purposes, the coefficient G_1 was evaluated for a modular ratio of 40, which represents the case of high strength concrete and low stiffness adhesive. The coefficients, G_2 and G'_2 were evaluated for a modular ratio of 5 to simulate the case of low strength concrete and high stiffness adhesive. The curves represent the greater of the two coefficients G_2 and G'_2. The chart covers a wide range of possible epoxy covers, C/d, and accounts for three different groove sizes, w.
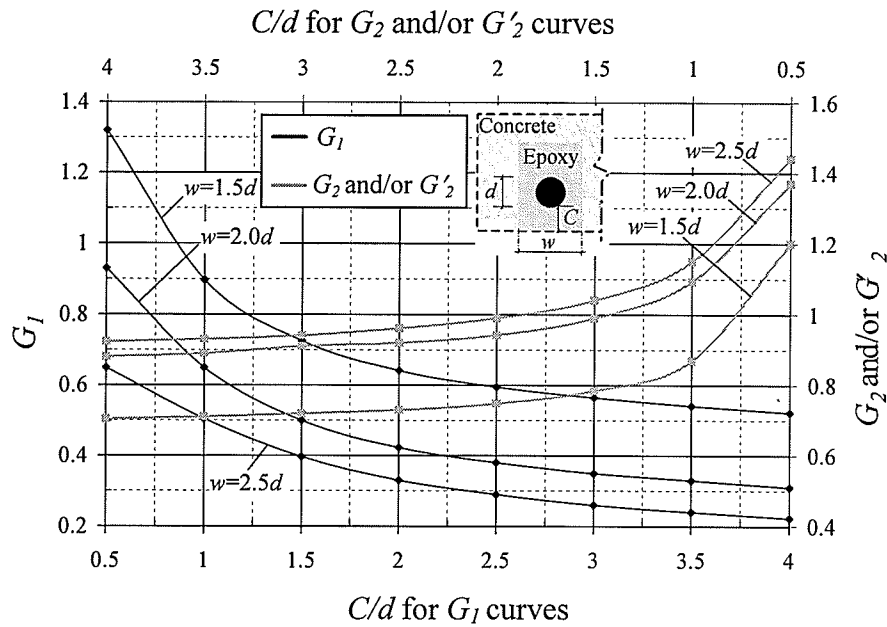
Fig. 5.13 Design chart for the development length of near surface mounted FRP bars

The chart clearly indicates that increasing the thickness of the epoxy cover, C/d, reduces the tensile stresses in both concrete and adhesive as is evident by the reduction of G_1, G_2 and G'_2 with the increase of C/d. Furthermore, using wider grooves, w, increases the tensile stresses at the FRP-epoxy interface (G_2 and/or G'_2) due to the substantial increase in the area of adhesive and consequently in its stiffness. Therefore, the tensile stresses at the concrete-epoxy interface (G_1) decrease by increasing the groove width. Using the proposed design chart, the coefficients G_1 and the greater value of either G_2 or G'_2 could be evaluated for a given groove width, w, and using a specified clear cover to the bar diameter ratio (C/d). The governing development length for near surface mounted FRP bars could be predicted using the greater of Equations 5.7 and 5.8.

5.2.2.4 Coefficient of Friction (μ)

The coefficient of friction between the FRP reinforcement and adhesive is a critical parameter in the theoretical analysis. Fig. 5.14 shows the test setup used to determine the coefficient of friction between C-Bars and different adhesives used in this investigation.
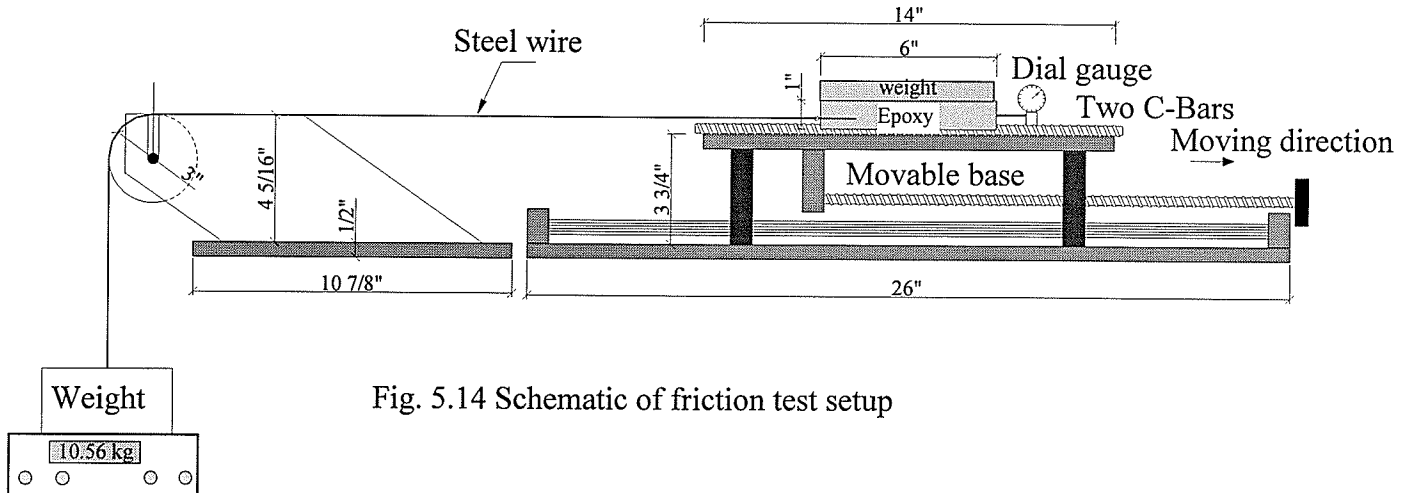
Fig. 5.14 Schematic of friction test setup

The coefficient of friction was determined according to the ASTM, G115-98. Both smooth- and rough-surface adhesives were examined as shown in Fig. 5.15. The rough-surface topography was accomplished by printing the lugs' pattern of the C-Bar in the adhesive prior to hardening.
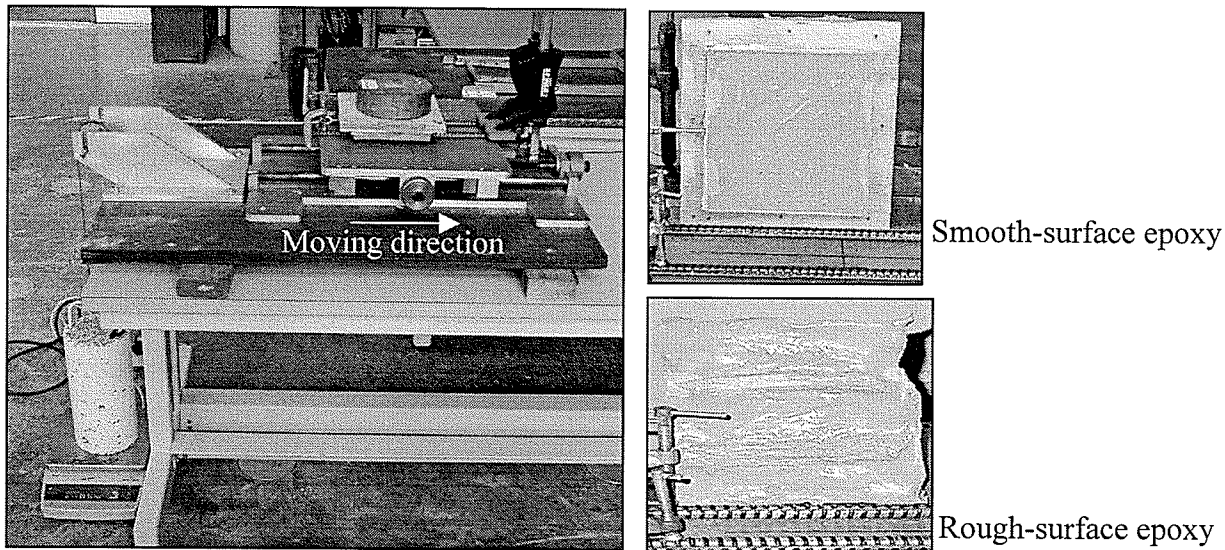
Fig. 5.15 Friction test setup [ASTM G115-98]

The bottom surface of the adhesive was placed to bear on two pieces of C-Bars. Force was applied through a horizontal steel wire attached to the adhesive block at the level of the FRP-epoxy interface. The relative movement between the reinforcement and the adhesive was monitored using a mechanical dial gauge. Force was applied to the steel wire by gradual movement of the steel base in the direction shown in Fig. 5.15. The maximum load was measured by an electronic scale at impending motion and was equal to the friction force. The test was repeated twelve times. The static coefficient of friction was calculated by dividing the friction force by the known weight, placed on the top of the adhesive. Test results showed that the coefficient of friction between C-bars and different epoxy adhesives used in this investigation has lower and upper bound values of 0.33 and 0.66, respectively with an average value of 0.5.

5.2.2.5 Comparison with Experimental Results

Using a groove width equal to twice the diameter of the bar ($w=2d$), a coefficient of friction of 0.33 and a clear cover to bar diameter ratio of one ($C/d=1.0$), the coefficients G_1 and the greater of G_2 and G'_2 for the bond specimens reported in this investigation are 0.65 and 1.1, respectively. The diameter of the bar is 9.525 mm. The average tensile strength of the concrete and epoxy used in the bond specimens are 4.3 MPa and 48 MPa, respectively. Using Equations 5.7 and 5.8, the minimum embedment length needed to develop 40 percent of the ultimate strength of the bars shall not be less than 834 mm, which coincides with the measured value of 800 mm [Rizkalla and Hassan, 2002].

5.2.2.6 Comparison with ACI—440

The draft report of the ACI-440 (2002) suggests the following expression for the development length, L_d, of FRP reinforcing bars:

$$L_d = 0.028 \frac{\pi d^2 f_u}{4\sqrt{f'_c}} \qquad (5.10)$$

where, d is the diameter of the bar; f_u is the tensile strength of the bar and f'_c is the concrete compressive strength after 28 days. Using the stress limit of 40 percent of the tensile strength of the C-Bars as observed in the experimental program, d=9.525 mm, f'_c =48 MPa, the development length according to the ACI-440, Equation 5.10, is equal to 221 mm. This value is equivalent to 28 percent of the value measured when the same bars were used for strengthening the beam in near surface mounted configuration. The results suggest that the ACI expression is not adequate for near surface mounted FRP bars. The significant discrepancy could be attributed to the following reasons:

a) The ACI expression is developed to characterize the bond of FRP bars to concrete. In near surface mounted FRP bars, the bond is primarily governed by the surface characteristics of the adhesive, which is considerably smoother than concrete and requires longer development length to achieve the same bond stress compared to concrete.

b) The ACI expression assumes a coefficient of friction between FRP bars and concrete equal to 1.0. This value is typically used for steel bars bonded to concrete and has been confirmed by many researchers [Goto 1971]. The coefficient of friction between FRP bars and epoxy is lower and ranges between

30 to 60 percent of the value used by the ACI. Consequently, a longer development length is needed for near surface mounted FRP bars.

c) The ACI-expression is designed for concrete structures reinforced with FRP bars where large concrete covers are typically used. For near surface mounted FRP bars, the thickness of the clear epoxy cover is greatly influenced by the location of the internal steel reinforcement. Therefore, the thickness of the epoxy cover is always limited. This type of configuration induces high tensile stresses at both the concrete-epoxy and the FRP-epoxy interface and consequently requires a longer development length.

d) The ACI expression assumes full confinement of the FRP bars by steel and/or FRP stirrups. Lack of such confinement in near surface mounted FRP bars results in higher bond stresses and consequently, a longer development length is needed.

Replacing f_u with the limited stress level observed in the experimental results, f_{FRP}, in Equation 5.10 and using $f_{ct} = 0.6\sqrt{f'_c}$, d=9.525 mm, Equation 5.10 can be rewritten as:

$$L_d = 0.5027\frac{d f_{FRP}}{4 f_{ct}}$$
(5.11)

Using a typical coefficient of friction between FRP bars and adhesives of 0.5, Equation 5.11 can be expressed by:

$$L_d = 0.25\frac{d f_{FRP}}{4\mu f_{ct}}$$
(5.12)

Equation 5.12 modifies the ACI expression to account for the distinct material characteristics of adhesives compared to concrete. Comparing Equations 5.7 and 5.12, it

can be concluded that the coefficient G_l is constant and equal to 0.25 regardless of the clear cover to bar diameter ratio, C/d as shown in Fig. 5.16.
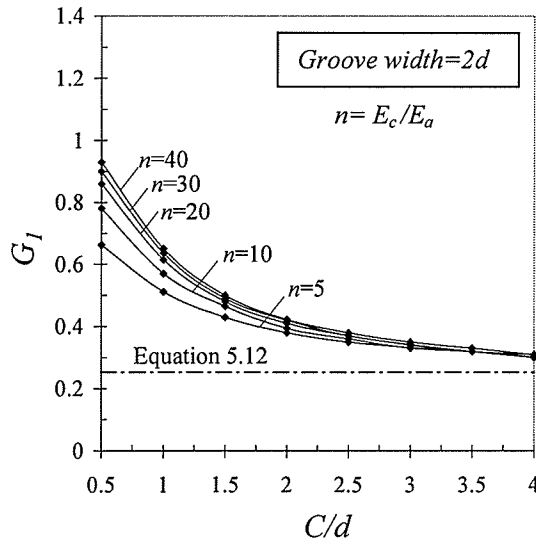
Fig. 5.16 Comparison of proposed approach with Equation 5.12

The constant value of G_l compares well only for the case of relatively large clear cover to bar diameter ratios ($C/d > 4.0$). *From the above discussion*, it is obvious that the influence of the C/d ratio affects the development length for near surface mounted FRP bars and should be considered in future design guidelines.

5.2.2.7 Detailing Guidelines

The previous sections have demonstrated the applicability of the proposed approach to evaluate the development length of near surface mounted FRP bars. Detailing provisions are urgently needed to ensure uniform distribution of stresses among the bars. Closely spaced arrangement of near surface mounted bars could magnify the tensile stresses at the concrete-epoxy interface and expedite concrete split failure. In this section, the finite element model was used to investigate the influence of the clear groove spacing, s, as

well as the edge distance, *e,* on interfacial stresses as shown in Fig. 5.17. The clear

spacing between the grooves of near surface mounted bars was varied from $0.25d$ to $2.0d$,

where d is the diameter of the bar. The groove width was also varied from $1.5d$ to $2.5d$ to

examine its effect on the induced stresses.
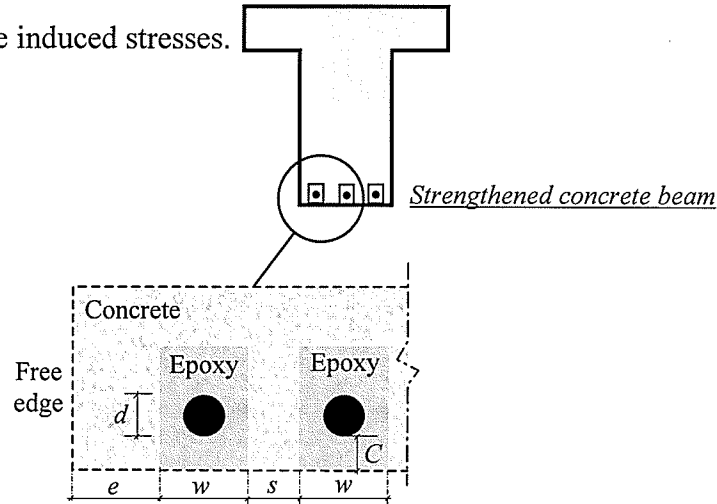
Fig. 5.17 Detailing parameters

The maximum tensile stress at the concrete-epoxy interface due to a unit radial pressure

applied at the location of FRP bars (coefficient G_1) is shown in Fig. 5.18 for various clear

groove spacing to bar diameter ratios (s/d). The modular ratio, n, was set to 40 to

simulate the most critical conditions for the tensile stresses at the concrete-epoxy
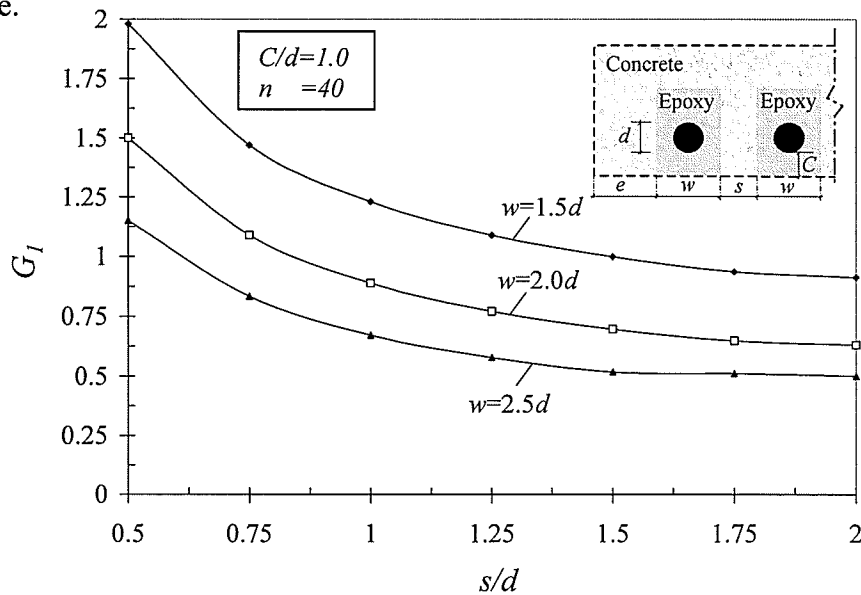
interface.

Fig. 5.18 Influence of groove spacing on tensile stresses at the concrete-epoxy interface

The analysis indicates that the tensile stress at the concrete-epoxy interface is greatly influenced by the clear spacing between the grooves of near surface mounted FRP bars. Increasing the clear groove spacing to bar diameter ratio reduces the tensile stress considerably up to a clear groove spacing of 2.0*d*, where *d* is the diameter of the bars. Increasing the clear groove spacing beyond this limit has a negligible effect on the induced tensile stresses. The limiting value of the clear spacing of 2*d* is independent of the groove width.

Fig. 5.19 shows the tensile stress at the FRP-epoxy interface, (coefficient G_2 and/or G'_2) due to a unit radial pressure applied at the locations of FRP bars. The modular ratio, *n*, was set to 5 to simulate the most critical conditions for the tensile stresses at the FRP-epoxy interface. The figure clearly indicates that the clear spacing between the grooves of near surface mounted bars has a negligible effect on the induced tensile stresses at the FRP-epoxy interface. These stresses are influenced by the groove width rather than the clear spacing between the grooves as shown in Fig. 5.19.
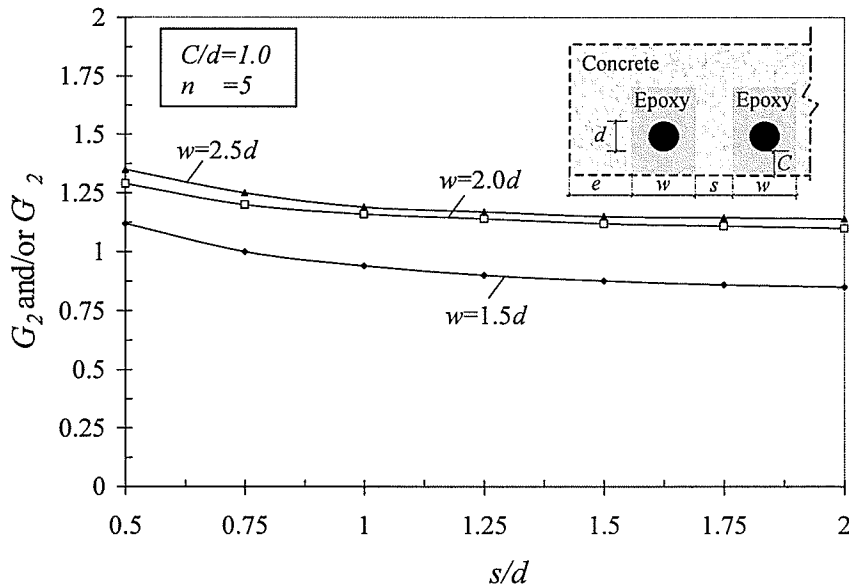
Fig. 5.19 Influence of groove spacing on tensile stresses at the FRP-epoxy interface

Fig. 5.20 depicts contours of principal tensile stresses for various groove spacing to bar diameter ratios. It should be noted that the proposed design chart, shown in Fig. 5.13 is applicable for $s/d \geq 2.0$.

a) $s/d=0.25$

b) $s/d=1.0$

c) $s/d=1.50$

d) $s/d=2.0$
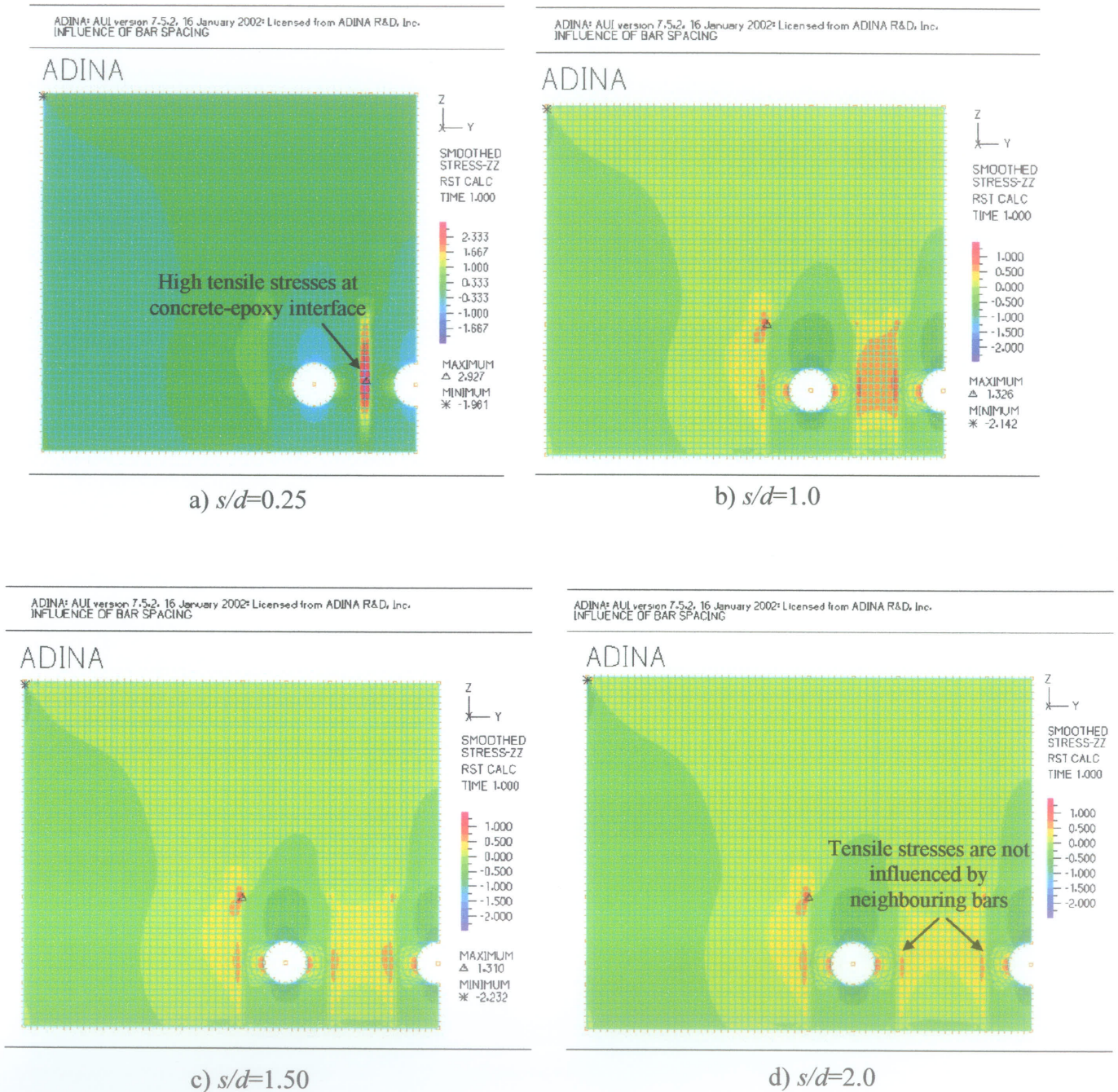
Fig. 5.20 Tensile stress distribution surrounding near surface mounted bars due to unit radial pressure

From the above discussion, it is concluded that the minimum clear spacing between the grooves of near surface mounted FRP bars should not be less that two times the diameter of the bars regardless of the groove width. Using a clear groove spacing to bar diameter ratio less than the proposed value results in overlapping of the tensile stresses at the concrete-epoxy interface and should be accounted for in design.

Placing a near surface mounted FRP bar close to the edge of a concrete beam introduces additional tensile stresses at the concrete-epoxy interface. Such a phenomenon is termed "edge effect". To determine the minimum edge distance required for near surface mounted FRP bars, the edge distance, *e*, was varied from 2*d* to 6*d*, where *d* is the diameter of the bar as shown in Fig. 5.21.
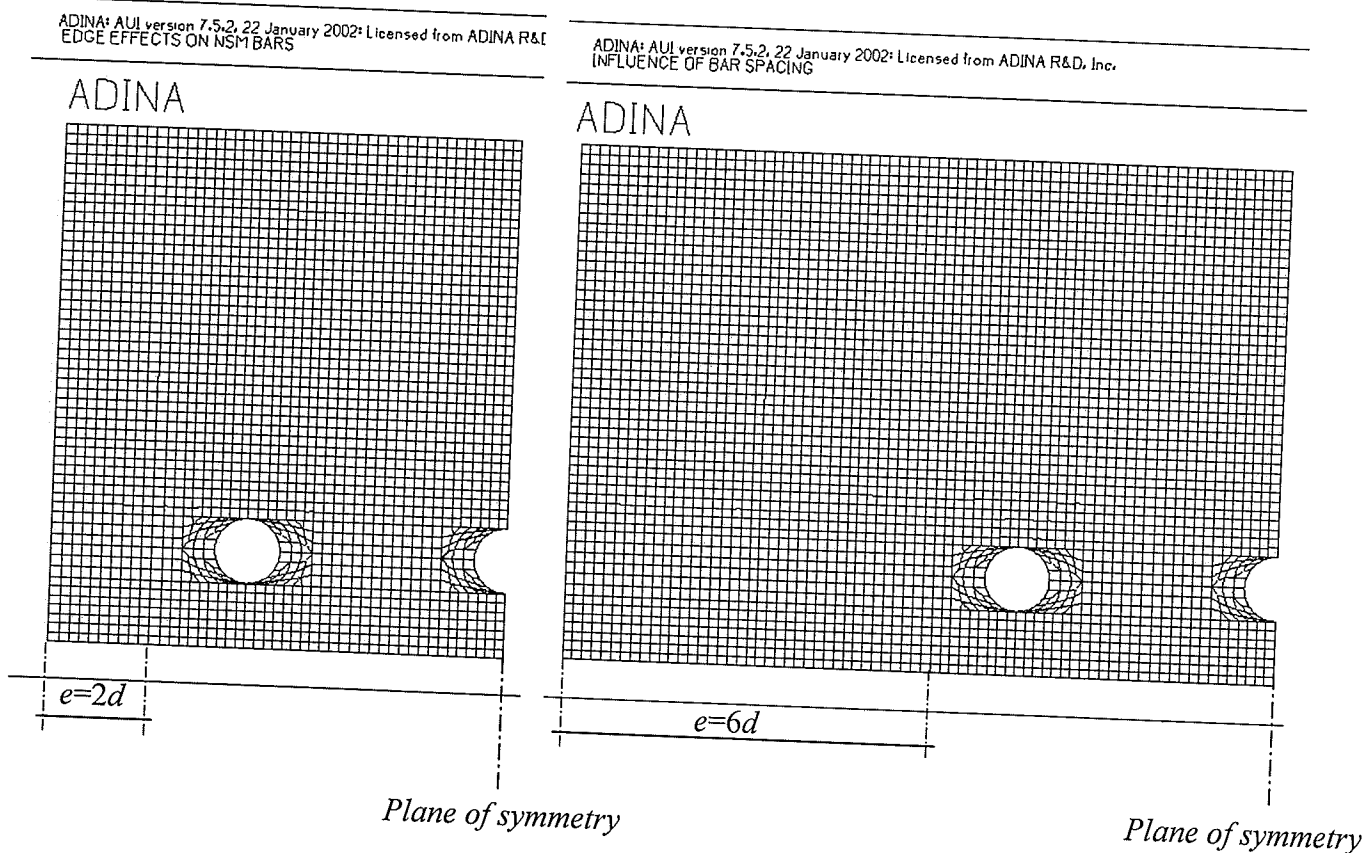
Fig. 5.21 Mesh dimensions used in ADINA for various edge distances

The maximum tensile stress at the concrete-epoxy interface due to a unit radial pressure applied at the location of FRP bars (coefficient G_1) is shown in Fig. 5.22 for various edge distances. In general, increasing the edge distance reduces the induced tensile stresses considerably regardless of the groove width. The analysis suggests a minimum edge distance of four times the diameter of the bars to minimize the edge effect and permit using the proposed design chart, shown in Fig. 5.13.
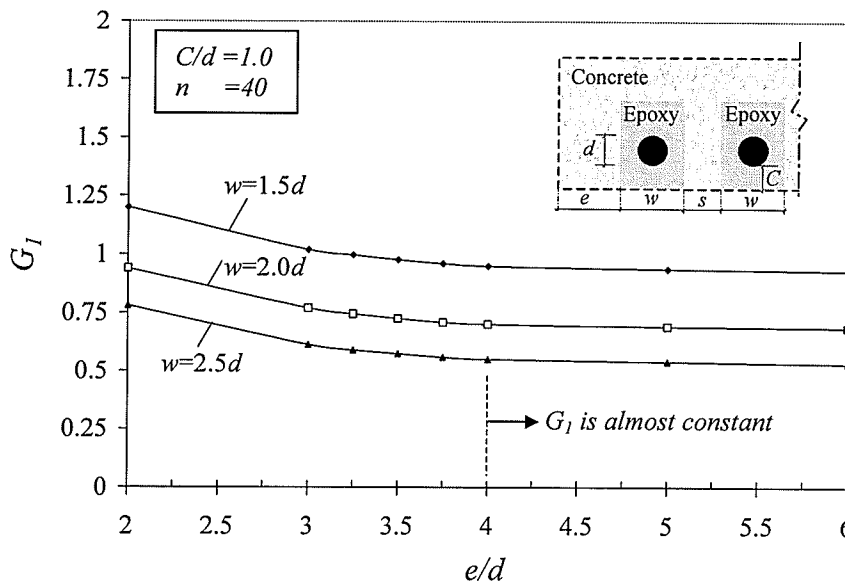
Fig. 5.22 Influence of edge distance on tensile stresses at the concrete-epoxy interface

5.2.2.8 Maximum Stresses in NSM Bars (f_{FRP})

Test results showed that the maximum tensile stress in near surface mounted CFRP bars at the onset of debonding did not exceed 43 percent of the tensile strength of the bars regardless of the embedment length used. Initiation of the debonding failure was observed at the concrete section where the secondary bottom steel reinforcement was terminated as shown in Fig. 5.3.

This section investigates the influence of various configurations of the bottom steel reinforcement on the behaviour based on a non-linear finite element modelling. Termination of the bottom steel reinforcement in the maximum moment region simulates cases where the bottom steel reinforcement is corroded or damaged. Consequently, evaluation of the existing concrete structure and identifying the conditions as well as the configuration of the internal steel reinforcement is essential prior to strengthening using near surface mounted FRP bars. Taking advantage of the symmetry of the bond specimens, only one quarter of the beams was modelled by ANACAP using 20-node brick element. Full description of the finite element model as well as the analysis procedures using ANACAP were reported in Chapter 4, section 4.3.3.2. In the analysis, the embedment length of near surface mounted C-Bars was set to 550 mm to develop the maximum bond stresses as observed in the experimental program for beams A2 and A5. Four different configurations for the bottom steel reinforcement were examined as shown in Fig. 5.23a.
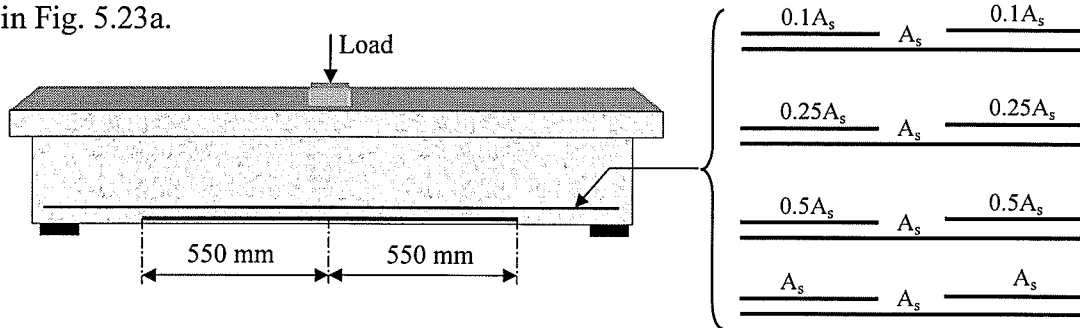
Fig. 5.23a Various configurations for the bottom steel reinforcement

Using Equations 5.3 and 5.7 and rearranging, the bond strength of near surface mounted FRP bars, τ_{max}, can be expressed as:

$$\tau_{max} = \frac{\mu f_{ct}}{G_1}$$

(5.13)

where μ is the coefficient of friction between the FRP bars and bonding adhesives; f_{ct} is the tensile strength of concrete and G_l is a coefficient determined using the proposed design chart given in Fig. 5.13 for specified groove dimensions. Using an average coefficient of friction between C-Bars and the adhesive of 0.5, tensile strength of concrete of 4.3 MPa and G_l of 0.65 for the bond specimens reported in this investigation, the bond strength was calculated and is equal to 3.3 MPa, which is 10 percent higher than the measured value, reported in Table 5.1. Equation 5.13 was adopted in the finite element analysis as a criterion for debonding failure at the concrete-epoxy interface.

A typical bond stress distribution, at failure, is shown in Fig. 5.23b. In general, terminating the bottom steel reinforcement at the maximum moment region creates zones of high stresses and therefore, accelerates debonding failure. Increasing the area of the terminated steel reinforcement results in a proportional increase in the axial stiffness of the bars and consequently, high tensile stresses are developed in the bars. Equilibrium and compatibility provisions require full transmission of the tensile stresses in the terminated steel bars to neighbouring steel and FRP bars. Such a phenomenon results in a significant increase in the bond stress and a corresponding decrease in the loads initiating debonding of the FRP bars.
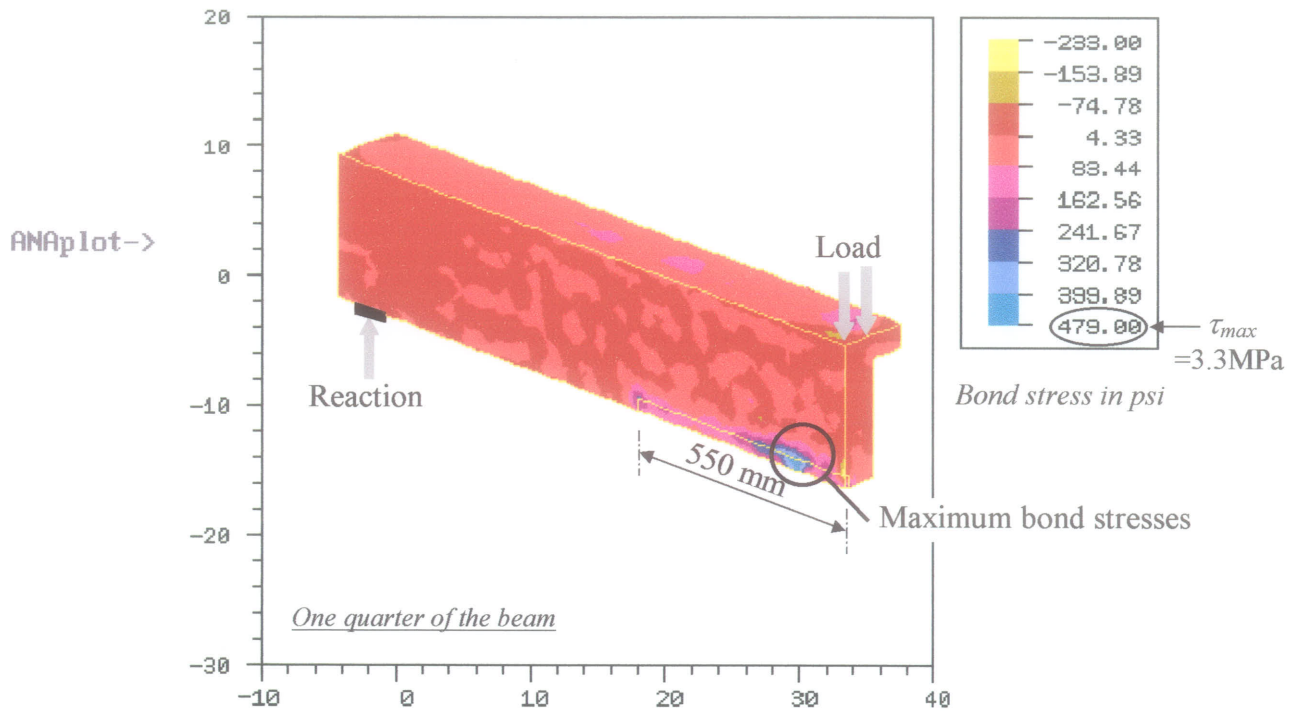
Fig. 5.23b Typical bond stress distribution at failure

The maximum tensile strain in near surface mounted C-bars at the onset of debonding failure for various configurations of the bottom steel reinforcement considered in this study, is given in Table 5.2.

Table 5.2 Results of numerical simulations

Bottom reinforcement configuration		P_d^* (kN)	ε_u (%)	$\varepsilon_u/\varepsilon_{fu}$ x 100
$0.1A_s$ $\quad$ A_s $\quad$ $0.1A_s$		113	1.04	60
$0.25A_s$ $\quad$ A_s $\quad$ $0.25A_s$		105	0.80	46
$0.5A_s$ $\quad$ A_s $\quad$ $0.5A_s$		99	0.71	41
A_s $\quad$ A_s $\quad$ A_s		99	0.7	40

* Failure is due to concrete split failure.

where P_d is the predicted debonding load; ε_u is the ultimate strain in near surface mounted C-Bars at the onset of debonding and ε_{fu} is the rupture strain of the bars. The analysis indicated that terminating 10 percent of the main bottom steel reinforcement allowed the CFRP bars to utilize 60 percent of its tensile strength prior to debonding. It should be noted that terminating 50 percent or more of the main bottom steel reinforcement had a negligible effect on the tensile strain of the CFRP bars at debonding failure. In these cases, extremely high bond stresses were developed and the maximum induced tensile stresses in CFRP bars did not exceed 40 percent of the tensile strength of the bars, which coincided with the measured values as reported in section 5.2.1. It should be noted that the numerical simulations were conducted using a steel reinforcement ratio at mid-span section of 1.0 percent, which simulates most of the commonly used reinforcement ratios for flexural members. High bond stresses in near surface mounted FRP bars are developed due to transfer of tensile stresses from the terminated steel reinforcement to the FRP reinforcement. Such a phenomenon normally takes place after yielding of the main bottom steel reinforcement. Therefore, doubling the reinforcement ratio has no effect on the maximum utilized strain in the near surface mounted bars. This behaviour was confirmed through a set of numerical simulations using a steel reinforcement ratio of 2.0 percent at the mid-span section.

Using GFRP as near surface mounted bars is likely to alter the maximum allowable tensile stresses in the bars due to distinct mechanical properties of both CFRP and GFRP materials. To determine the maximum tensile stresses in near surface mounted GFRP bars, f_{FRP}, the same analysis procedures as outlined above were conducted. The GFRP

bars were assumed to have a typical modulus of elasticity of 40 GPa and an ultimate

tensile strength of 700 MPa. A typical coefficient of friction of 0.5 was assumed in the

analysis. The ultimate bond strength, given by Equation 5.13 was set to 3.3 MPa and was

used as a failure criterion in the finite element modelling. The analysis suggested that the

full tensile strength of GFRP bars could be utilized prior to debonding. Rupture of the

GFRP bars was the governing mode of failure for all the numerical simulations regardless

of the configuration of the bottom steel reinforcement. This is primarily attributed to the

relatively low modulus of elasticity of GFRP compared to CFRP bars.

Based on the reported experimental and analytical investigations, typical procedures to

evaluate the development length of any configuration of near surface mounted FRP bars

can be summarized as follows:

a) Determine the material characteristics of FRP bars, concrete and adhesive.

b) Determine the coefficient of friction between the FRP bar and the bonding
   adhesive according to the ASTM G115-98 or based on information provided by
   the manufacturer.

c) Select groove dimensions, thickness of the clear epoxy cover and use the
   proposed design chart, given in Fig. 5.13 to determine the coefficients G_1 and the
   greater of coefficients G_2 and/or G'_2.

d) Determine the maximum allowable tensile stress in near surface mounted FRP
   bars in light of the outlined analytical approach or based on laboratory testing.

e) Calculate the development length using the greater of Equations 5.7 and 5.8.

f) Reselect groove dimensions if necessary and repeat steps (c) to (e).

5.3 Near Surface Mounted CFRP Strips

5.3.1 Experimental Results (Series B)

A total of nine beams were tested from series B. One beam was tested as a control specimen while the other eight beams were strengthened using near surface mounted CFRP strips. Each beam was strengthened using one strip (25 x 1.2 mm) inserted into a groove cut at the bottom surface of the beam. Complete details of the tested specimens were reported in Chapter 3, section 3.3.3.

The sequence of testing started by testing specimens B1, B2, B3, and B4 with embedment lengths of 150, 250, 500, and 750 mm, respectively. Based on the results of these tests, specimens B5 to B8 with embedment lengths ranged from 850 mm to 1200 mm were tested. The load-deflection behaviour of the control specimen, B0, and the eight strengthened specimens is shown in Fig. 5.24.

(a)

231

(b)
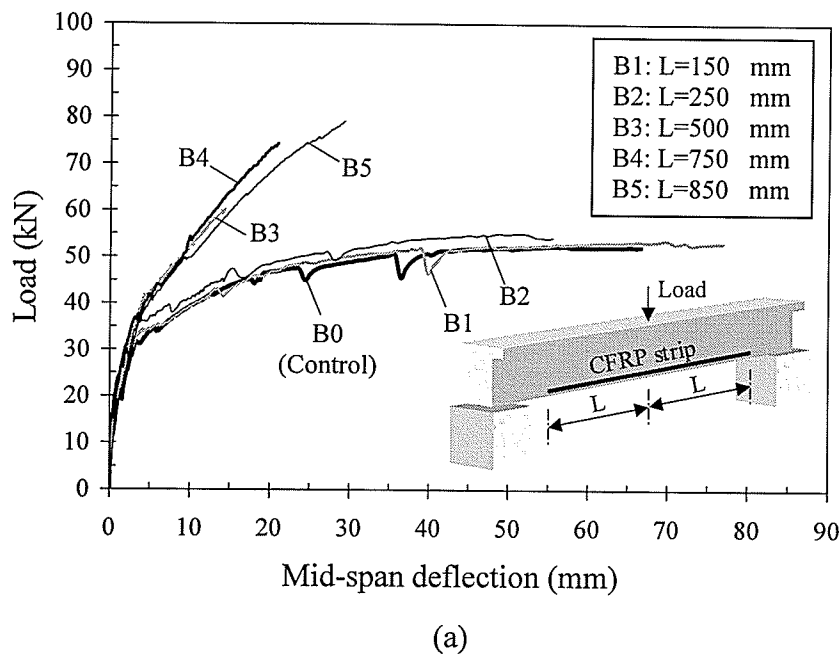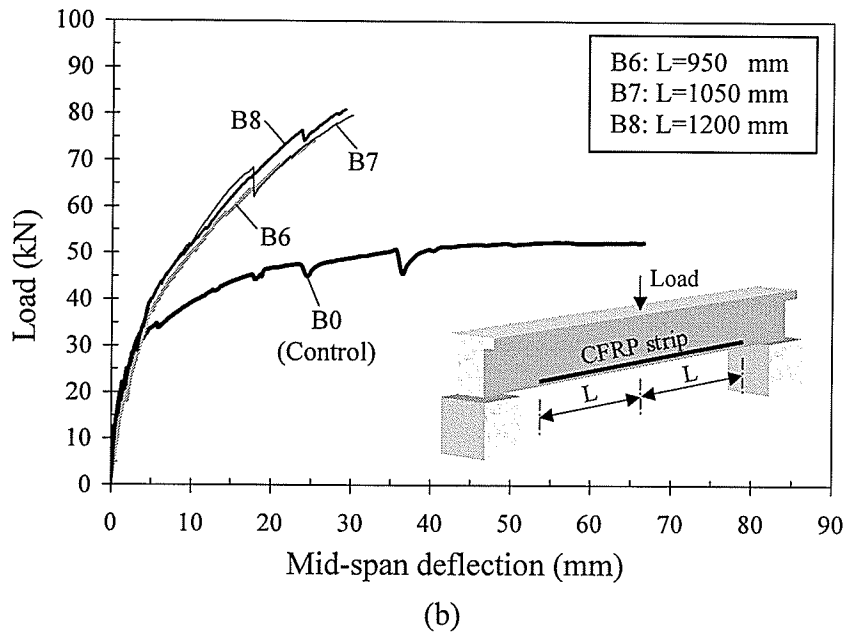
Fig. 5.24 Load-deflection behaviour of series B specimens

The control specimen, B0, failed due to crushing of concrete at a load level of 52 kN. The figure clearly indicates that using embedment lengths up to 250 mm provided insignificant improvement in strength. This is attributed to the early debonding of the CFRP strips.

A considerable enhancement in strength was observed for embedment lengths greater than 250 mm. Specimens B3 and B4 with embedment lengths of 500 mm and 750 mm, respectively failed also due to debonding of the CFRP strips. Debonding was observed at both ends of the strips as well as at mid-span. This is attributed to high shear stress concentrations at cutoff point as well as at the vicinity of flexural cracks. Debonding was observed to occur at the concrete-epoxy interface with failure in the concrete in all cases. The failure loads for both beams were 60 kN and 74 kN, respectively. This indicates that full composite action has not yet been developed and therefore, the measured ultimate load was increasing with the increase of the embedment length.

232

Beams B5, B6, B7, and B8 were strengthened using embedment lengths ranging from 850 mm to 1200 mm. The failure of these beams was due to rupture of the CFRP strips as shown in Fig. 5.25.
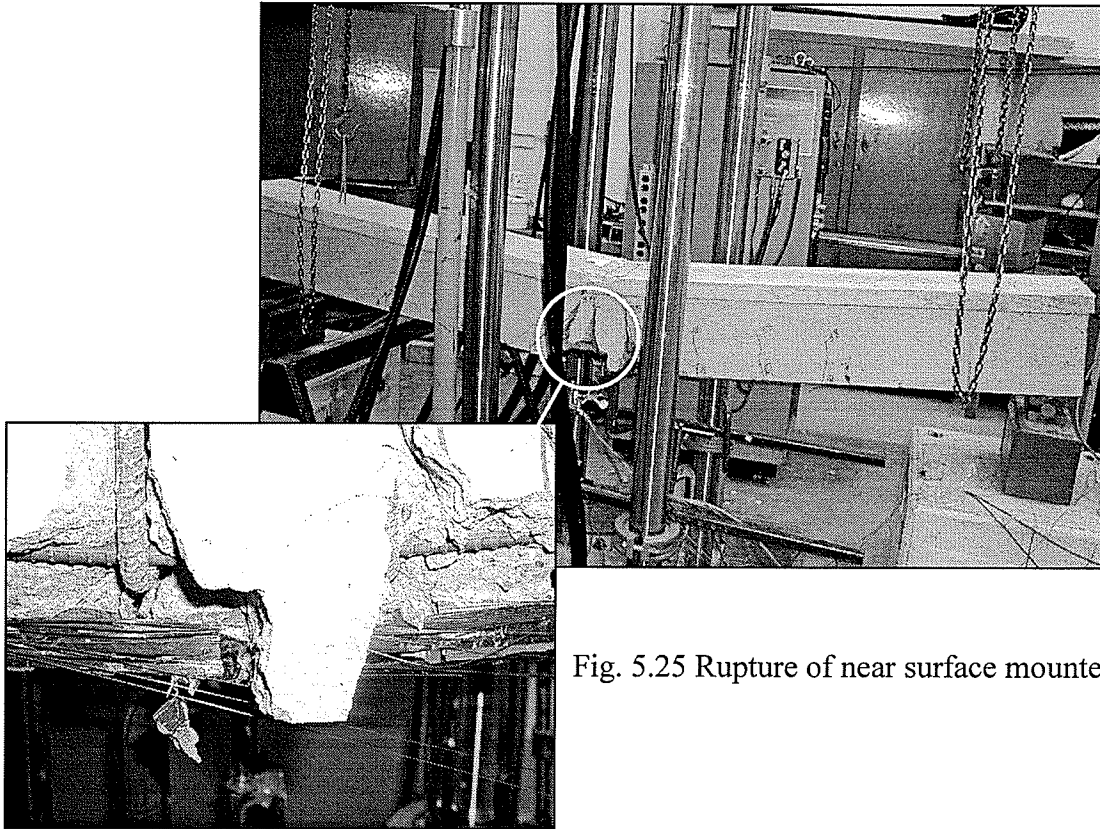
Fig. 5.25 Rupture of near surface mounted strips

The maximum measured tensile strain in the CFRP strips used for specimens B5, B6, B7 and B8 was approximately 1.3 percent. The measured failure loads for the four beams were almost identical and ranged from 75 kN to 80 kN. Shear cracks were observed to appear at relatively high load levels, but they did not extend to the compression face. At the onset of rupture of the strips, the load dropped to the yielding load of the cross-section until crushing of concrete occurred. Test results suggest that the minimum embedment length needed to rupture the near surface mounted CFRP strips, with the

given dimensions used in this program is 850 mm. Experimental results for the test specimens are summarized in Table 5.3.

Table 5.3 Summary of test results for series B

Beam No.	L (mm)	P_u (kN)	Δ_u (mm)	ε_u (%)	Failure mode	% Increase in ultimate capacity
B0	N.A	52	66.6	-	C [+]	-
B1	150	53	76.8	0.049	D [*]	1.9
B2	250	54	56	0.17	D	3.8
B3	500	60	14.4	0.71	D	15.4
B4	750	74	21	1.18	D	42.3
B5	850	79	29	1.27	R [Π]	52
B6	950	75	25	1.28	R	44
B7	1050	80	30	1.29	R	54
B7	1200	80	29	1.31	R	54

[+] C refers to crushing of concrete with steel yielding

[*] D refers to debonding of CFRP strips.

[Π] R refers to rupture of near surface mounted strips
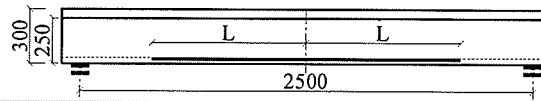
where L is the bond length; P_u is the ultimate failure load; Δ_u is the deflection at failure and ε_u is the maximum tensile strain in the CFRP strips at failure. It should be noted that rupture of near surface mounted CFRP strips can be achieved provided that the bond length is greater than the development length. However, rupture of near surface mounted CFRP bars is not likely to occur regardless of the bond length. This is primarily attributed to the distinct nature of the bond stresses at the concrete-adhesive interface as well as to the differences in shape and configuration of the FRP reinforcement.

5.3.2 Analytical Modelling

5.3.2.1 General

The proposed model is based on the combined shear-bending model introduced by Malek et al. (1998) for externally bonded FRP plates. The model is modified to account for the double bonded area of near surface mounted strips. The model accounts also for the continuous reduction in flexural stiffness due to cracking of the concrete. The derivation of the model is based on the assumption that shear and bending stresses can be investigated separately. Debonding of near surface mounted strips is assumed to occur as a result of the high shear stress concentration at the cutoff point.

5.3.2.2 Derivation of the Model

5.3.2.2.1 Simply Supported Beam Subjected to a Concentrated Load

Considering the equilibrium of an infinitesimal portion of the strengthened concrete beam, shown in Fig. 5.26, the shear stress, τ along a length of dx can be derived in terms of the incremental normal stress in the CFRP strip, $d\sigma_f$, and the thickness of the CFRP strip, t_f, as follows:

$$\tau = \frac{1}{2}\frac{d\sigma_f}{dx}t_f \tag{5.14}$$

Assuming a linear shear stress-strain relationship for the adhesive:

$$\tau = G_a\gamma \tag{5.15}$$

where G_a and γ are the shear modulus and shear strain of the adhesive, respectively. Assuming linear strain-displacement relationships for the adhesive:

$$\gamma = \frac{\partial u}{\partial z} + \frac{\partial w}{\partial x} \tag{5.16}$$

where u and w are the longitudinal and transverse displacements of the adhesive, respectively.

$$\sigma_c + \frac{d\sigma_c}{dx}\,dx \qquad \sigma_f + \frac{d\sigma_f}{dx}\,dx \qquad \sigma_c + \frac{d\sigma_c}{dx}\,dx$$

Adhesive   CFRP   Adhesive
                  Strip

300

Near surface mounted strip

Sec (A-A)

300

X

Y

Z   Global axes

u

v

w   Displacements

All dimensions are in mm

Cutoff point

Near surface mounted strip
(Length = 2*L*)

A   A

2700 mm

Portion under consideration

dx

x
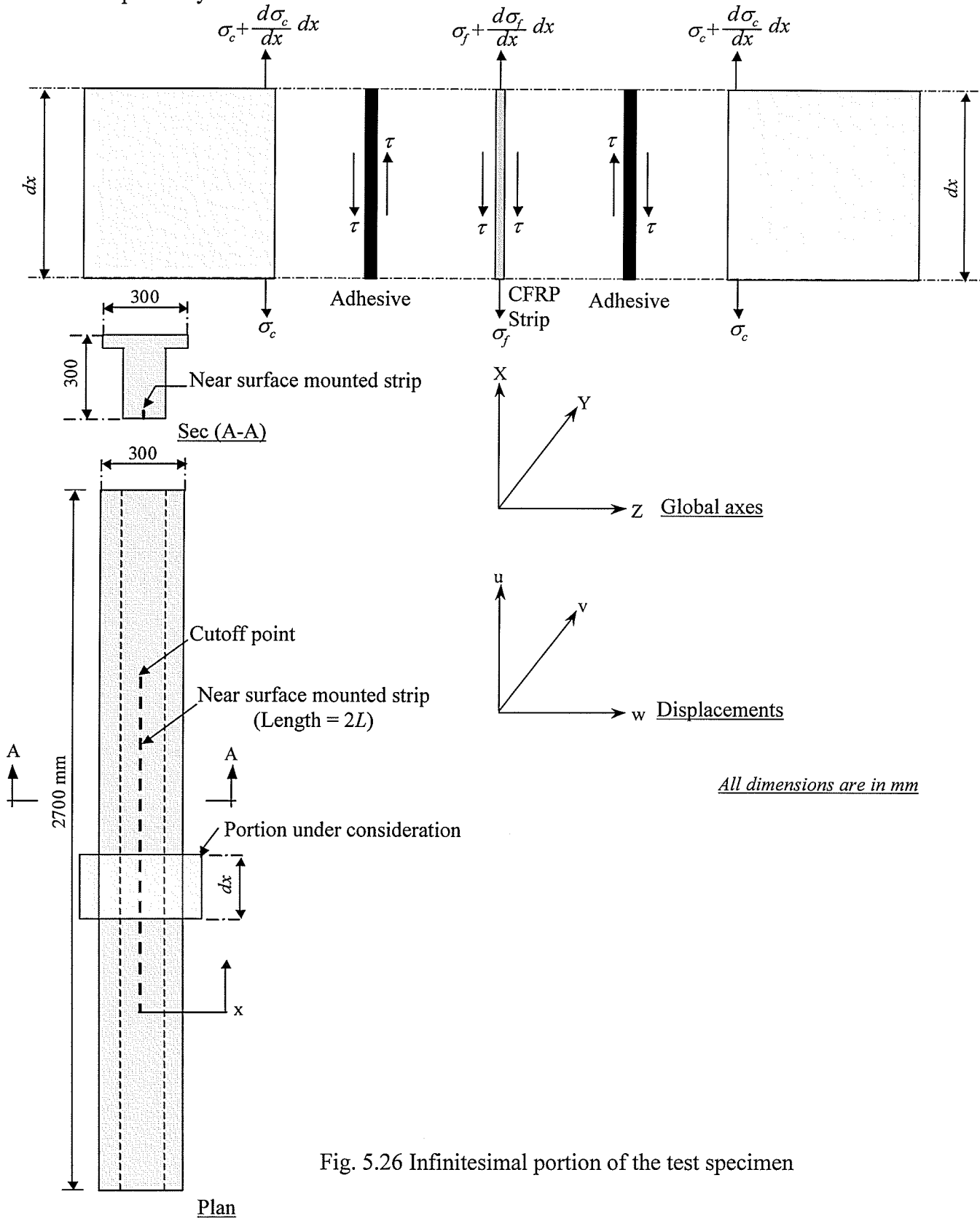
Fig. 5.26 Infinitesimal portion of the test specimen

Plan

Using (5.14), and differentiating with respect to x results in:

$$\frac{d^2\sigma_f}{dx^2} = \frac{2G_a}{t_f}\left(\frac{\partial^2 u}{\partial x\,\partial z} + \frac{\partial^2 w}{\partial x^2}\right)$$

(5.17)

$\partial^2 u/\partial x\,\partial z$ can be expressed as:

$$\frac{\partial^2 u}{\partial x\,\partial z} = \frac{\partial}{\partial z}\left(\frac{\partial u}{\partial x}\right) = \frac{\partial}{\partial z}\left(\varepsilon_f - \varepsilon_c\right) = \frac{1}{t_a}\left(\varepsilon_f - \varepsilon_c\right) = \frac{1}{t_a}\left(\frac{\sigma_f}{E_f} - \frac{\sigma_c}{E_c}\right)$$

(5.18)

where ε_f and ε_c are the interfacial strain of the CFRP strip and concrete, respectively; E_f and E_c are the modulus of elasticity of the CFRP strip and concrete, respectively; t_a is the thickness of the adhesive layer; σ_f and σ_c are the normal stress in the CFRP strip and concrete, respectively.

From symmetry:

$$\frac{\partial^2 w}{\partial x^2} = 0$$

(5.19)

The governing differential equation for the tensile stress in near surface mounted CFRP strips can be expressed as:

$$\frac{d^2\sigma_f}{dx^2} - \frac{2G_a}{t_a t_f E_f}\sigma_f = -\frac{2G_a}{t_a t_f E_c}\sigma_c$$

(5.20)

Rewriting Equation 5.20:

$$\frac{d^2\sigma_f}{dx^2} - \omega^2\sigma_f = -\omega^2 n\sigma_c$$

(5.21)

where,

$$\omega^2 = \frac{2G_a}{t_a t_f E_f} \qquad (5.22)$$

$$n = \frac{E_f}{E_c} \qquad (5.23)$$

For simply supported beams subjected to a concentrated load at mid-span, the normal stress in the concrete, σ_c, can be expressed in terms of the effective moment of inertia, I_{eff} as follows:

$$\sigma_c = \frac{P l_o y_{eff}}{2 I_{eff}} + \frac{P y_{eff}}{2 I_{eff}} x \qquad (5.24)$$

where P is the applied concentrated load; l_o is the unbonded length of the CFRP strip; x is the longitudinal coordinate starting from the cutoff point; and y_{eff} is the distance from the CFRP strip to the neutral axis of the section. The above expression is conditioned by the loading configuration and can be easily formulated for other load cases as will be given in the next sections. To account for the continuous reduction in flexural stiffness due to the cracking of concrete, I_{eff} can be expressed as:

$$I_{eff} = \left(\frac{M_{cr}}{M_a}\right)^3 I_{g\,(transformed)} + \left(1 - \left(\frac{M_{cr}}{M_a}\right)^3\right) I_{cr\,(transformed)}$$

$$\text{[Branson and Trost, 1982]} \quad (5.25)$$

where M_{cr} and M_a are the cracking and applied moments on a concrete section, respectively; I_g and I_{cr} are the gross and cracked moment of inertia of the transformed strengthened section, respectively.

The corresponding neutral axis depth can be expressed as:

$$c_{eff} = \left(\frac{M_{cr}}{M_a}\right)^{2.5} c_g + \left(1 - \left(\frac{M_{cr}}{M_a}\right)^{2.5}\right) c_{cr}$$

[Branson and Trost, 1982]   (5.26)

where c_g and c_{cr} are the neutral axis depth for the gross and cracked transformed strengthened sections, respectively.

$$y_{eff} = d_f - c_{eff}$$

(5.27)

where d_f is the depth of near surface mounted strips from the compression fibre.

Rewriting Equation 5.21:

$$\frac{d^2\sigma_f}{dx^2} - \omega^2 \sigma_f = -\omega^2 n \left(\frac{P l_o y_{eff}}{2 I_{eff}} + \frac{P y_{eff}}{2 I_{eff}} x\right)$$

(5.28)

The general solution for Equation 5.28 can be expressed as:

$$\sigma_f = C_1 e^{\omega x} + C_2 e^{-\omega x} + \frac{n P y_{eff}}{2 I_{eff}} x + \frac{n P l_o y_{eff}}{2 I_{eff}}$$

(5.29)

where C_1 and C_2 are constants. The solution represents a characteristic solution for σ_f as:

$$\sigma_{f_{chracteristic.}} = C_1 e^{\omega x} + C_2 e^{-\omega x}$$

(5.30)

and a particular solution for σ_f as:

$$\sigma_{f_{particular}} = \frac{n P y_{eff}}{2 I_{eff}} x + \frac{n P l_o y_{eff}}{2 I_{eff}}$$

(5.31)

The shear stress can be expressed as:

$$\tau = \frac{t_f}{2}\left[C_1 \omega e^{\omega x} - C_2 \omega e^{-\omega x} + \frac{n P y_{eff}}{2 I_{eff}}\right]$$

(5.32)

Constants C_1 and C_2 can be evaluated using the following boundary conditions:

$$\sigma_f = 0 \qquad\qquad \text{at } x = 0 \qquad\qquad (5.33)$$

$$\tau = 0 \qquad\qquad \text{at } x = L \qquad\qquad (5.34)$$

where L is the embedment length of the CFRP strip. Using the above boundary conditions, the following expressions for C_1 and C_2 are derived:

$$C_1 = \frac{-n\,P\,y_{eff}}{4\,\omega\,I_{eff}\,\cosh(\omega L)}\left[1 + \omega l_o\,e^{-\omega L}\right] \qquad\qquad (5.35)$$

$$C_2 = -C_1 - \frac{n\,P\,l_o\,y_{eff}}{2\,I_{eff}} \qquad\qquad (5.36)$$

Using practical values for ω and L, $\cosh\,(\omega L)$ is always a very large number compared to other terms. Therefore, the constant C_1 can be ignored. Rewriting Equation 5.32, the shear stress can be expressed as:

$$\tau = \frac{t_f}{2}\left[\frac{n\,P\,l_o\,y_{eff}}{2\,I_{eff}}\,\omega\,e^{-\alpha x} + \frac{n\,P\,y_{eff}}{2\,I_{eff}}\right] \qquad\qquad (5.37)$$

Debonding will occur when the shear stress reaches a maximum value, which depends on the concrete properties [Hassan and Rizkalla, 2002b].

5.3.2.2.2 Simply Supported Beam Subjected to a Uniform Load

Using the same procedures as outlined above, the induced shear stress, τ, in a simply supported beam of a span L', subjected to a uniform load, q, can be expressed as:

$$\tau = \frac{t_f}{2}\left[a\,x + b + c\,\omega\,e^{-\omega x}\right] \qquad\qquad (5.38)$$

where,

$$a = -\frac{q\,n\,y_{eff}}{2I_{eff}};$$ (5.39)

$$b = \frac{q\,n\,y_{eff}}{2I_{eff}}\left(L'-2l_o\right); \text{ and}$$ (5.40)

$$c = -\frac{q\,n\,y_{eff}}{\omega^2 I_{eff}} + \frac{q\,n\,y_{eff}\,l_o}{2I_{eff}}\left(L'-l_o\right)$$ (5.41)

5.3.2.2.3 Simply Supported Beam Subjected to Two Concentrated Loads

For a simply supported beam subjected to two equal concentrated loads, $2P$, placed symmetrically about the centre line of the beam, the induced shear stress, τ, can be expressed as:

$$\tau = \frac{t_f}{2}\left[\frac{n\,P\,y_{eff}}{I_{eff}} + \frac{n\,P\,y_{eff}\,l_o}{I_{eff}}\omega\,e^{-\omega x}\right]$$ (5.42)

where, t_f is the thickness of the strip; n is defined by Equation 5.23; P is the concentrated load; l_o is the unbonded length of the strip; ω is defined by Equation 5.22; y_{eff} is the distance from the strip to the neutral axis of the section and I_{eff} is the effective moment of inertia of the transformed section.

5.3.2.3 Failure Criterion

Premature debonding of near surface mounted CFRP strips is governed by the shear strength of the concrete. Test results showed that other components of the system such as the epoxy adhesive and the CFRP strips have superior strength and adhesion properties

compared to concrete. Knowing the compressive and tensile strength of concrete, the Mohr-Coulomb line, which is tangential to both Mohr's circles for pure tension and pure compression, can be represented as shown in Fig. 5.27.
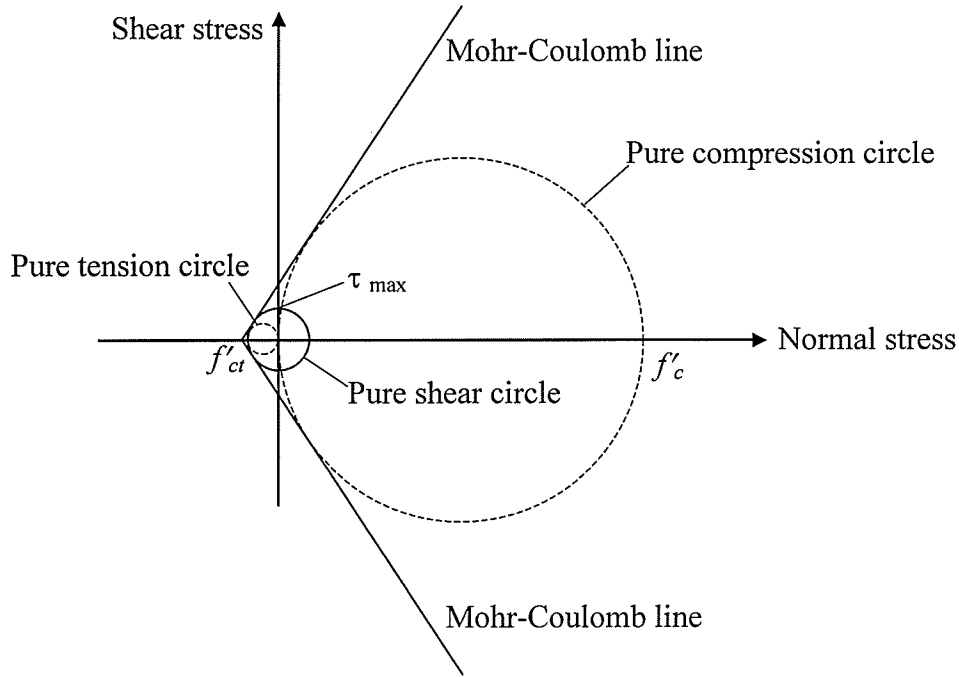
Fig. 5.27 Mohr-Coulomb failure criterion

All circles tangential to the Mohr-Coulomb line represent a critical stress combination. The maximum critical shear stress for the pure shear circle is given by:

$$\tau_{max} = \frac{f'_c \, f_{ct}}{f'_c + f_{ct}} \qquad (5.43)$$

where f'_c is the compressive strength of concrete after 28 days and f_{ct} is the tensile strength of concrete. Equating the shear strength proposed in Equation 5.43 to the shear stress given in Equations 5.37, 5.38 and 5.42, debonding loads for near surface mounted CFRP strips can be determined for various loading cases and embedment lengths [Hassan and Rizkalla, 2002b].

5.3.2.4 Verification of the Analytical Model

The analytical model is verified by comparing the calculated shear stress from Equation 5.37 to that obtained from the finite element analysis at the cutoff point. The finite element modelling described in this section was conducted using the ANACAP program (Version 2.1). It is well established by many researchers that mesh size is a key parameter that influences the shear stress distribution in externally bonded FRP reinforcement especially at cutoff points [Malek et al., 1998]. Consequently, the first step towards developing a reliable finite element model is to determine the optimum size of elements that should be used in the analysis.

5.3.2.4.1 Modelling of Test Specimens

Two test specimens, B3 and B4, were selected from the experimental program to be modelled using finite element analysis. Failure of both beams was due to debonding of the near surface mounted CFRP strips at the cutoff points. Taking advantage of the symmetry of the specimens, only one quarter of the beams was modelled. The concrete, epoxy and the CFRP strip were modelled using 20-node isoparametric brick elements with a 2x2x2 reduced Gauss integration scheme. Each node has three translational degrees of freedom. The load was applied as a uniform pressure acting on an area of 100x150 mm.

Various numerical simulations were conducted by varying the size of the brick elements around the strip cutoff point in the longitudinal as well as in the vertical directions. One

element was used within the thickness of the CFRP strip and the adhesive as shown in Fig. 5.28.
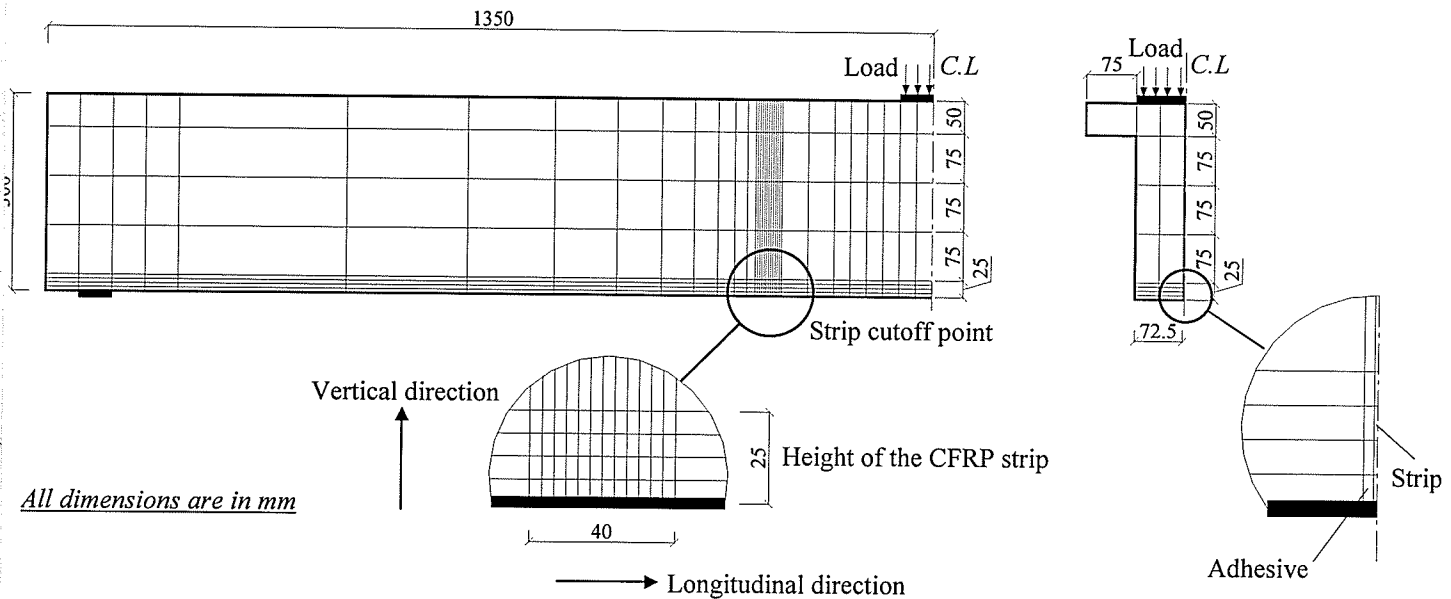
Fig. 5.28 General mesh dimensions of the test specimens

The influence of the mesh size on the predicted shear stress at the cutoff points was noticeable. In general, increasing the size of the elements results in a proportional increase in the distances among the integration points within the element. Therefore, the induced shear stresses at the strip cutoff points are averaged over a large distance and are considerably less than the true values. Decreasing the size of the elements results in a substantial increase in the maximum shear stress up to a certain limit beyond which no further increase in the shear stresses is observed. The size of the elements at this transition stage is termed the "optimum size".

The optimum size of the elements in the longitudinal as well as in the vertical directions was determined as shown in Fig. 5.29 and 5.30, respectively. Further refinement of the

mesh around the cutoff points increased the predicted shear stress by less than 0.5 percent.
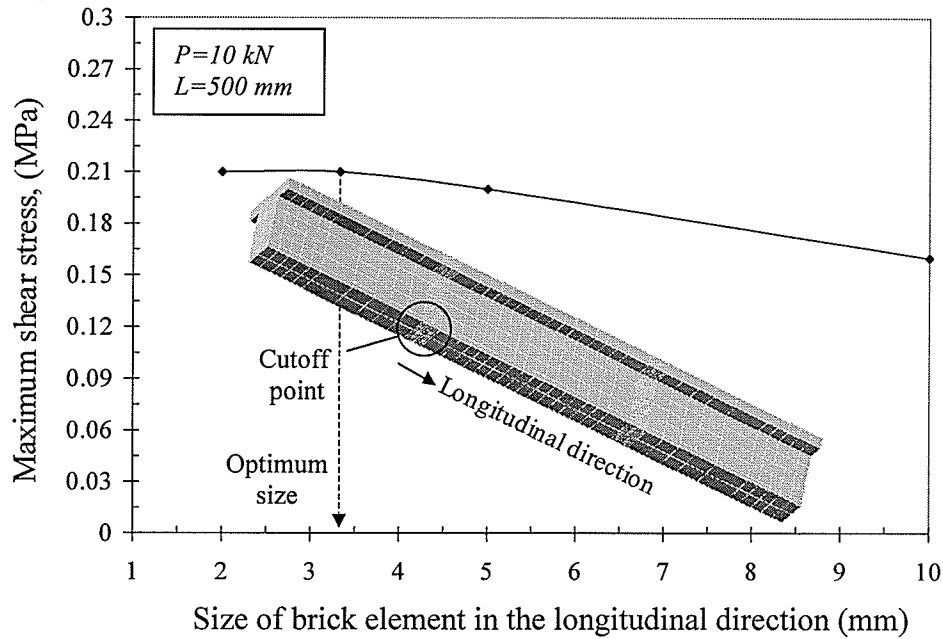
Fig. 5.29 Influence of element size in the longitudinal direction on maximum shear stress at cutoff point
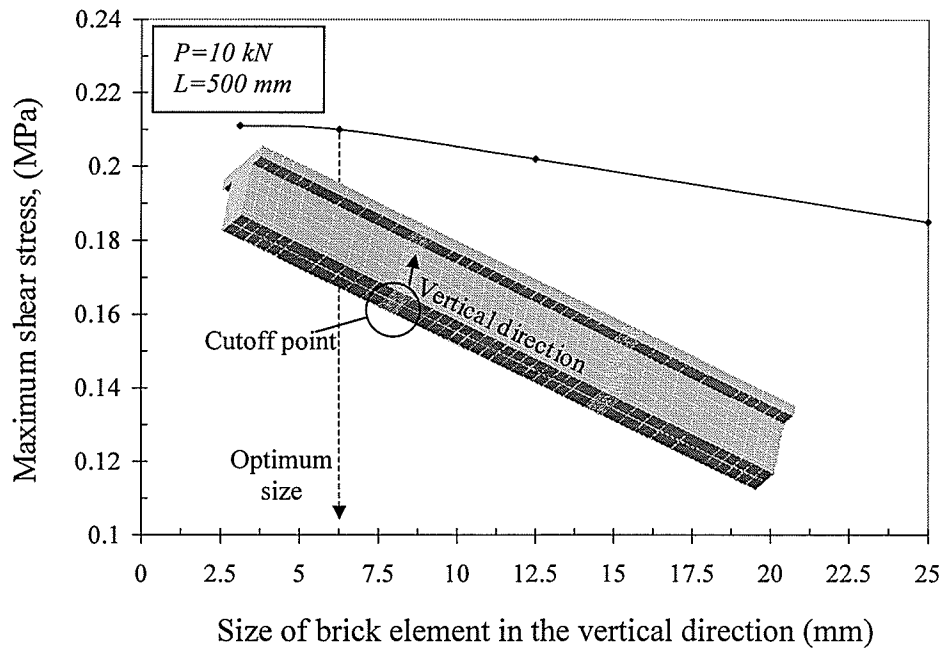
Fig. 5.30 Influence of element size in the vertical direction on maximum shear stress at cutoff point

The final mesh dimensions used for test specimens B3 and B4 with embedment lengths of 500 mm and 750 mm, respectively are shown in Fig. 5.31.
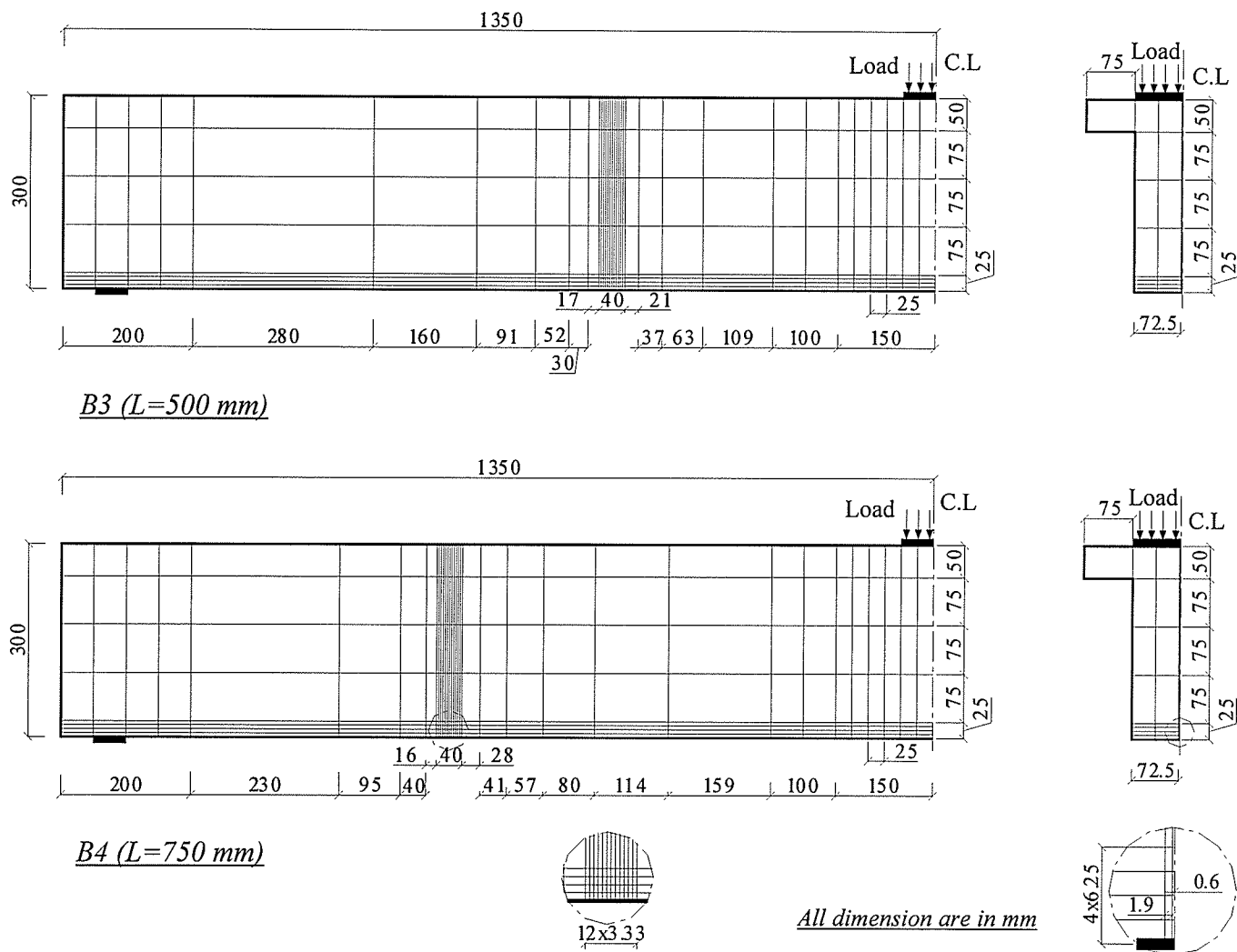
Fig. 5.31 Mesh dimensions used in finite element analysis

5.3.2.4.2 Comparison with Finite Element Analysis

The interfacial shear stress distributions for specimens B3 and B4 are calculated at two different load levels and compared to those predicted using finite element analysis. The first selected load level was less than the cracking load of the test specimens to validate the analytical model at the elastic stage. The second selected load level matched the cracking load at cutoff points for specimens B3 and B4. The shear modulus of the epoxy adhesive was set to 1230 MPa as reported by the manufacturer. Based on a groove width of 5 mm, the thickness of the epoxy adhesive used in the analysis was set to 1.9 mm. The results of the finite element analysis together with the proposed analytical model are shown in Fig. 5.32 at the elastic stage. The results, at the onset of cracking are shown in Fig. 5.33.
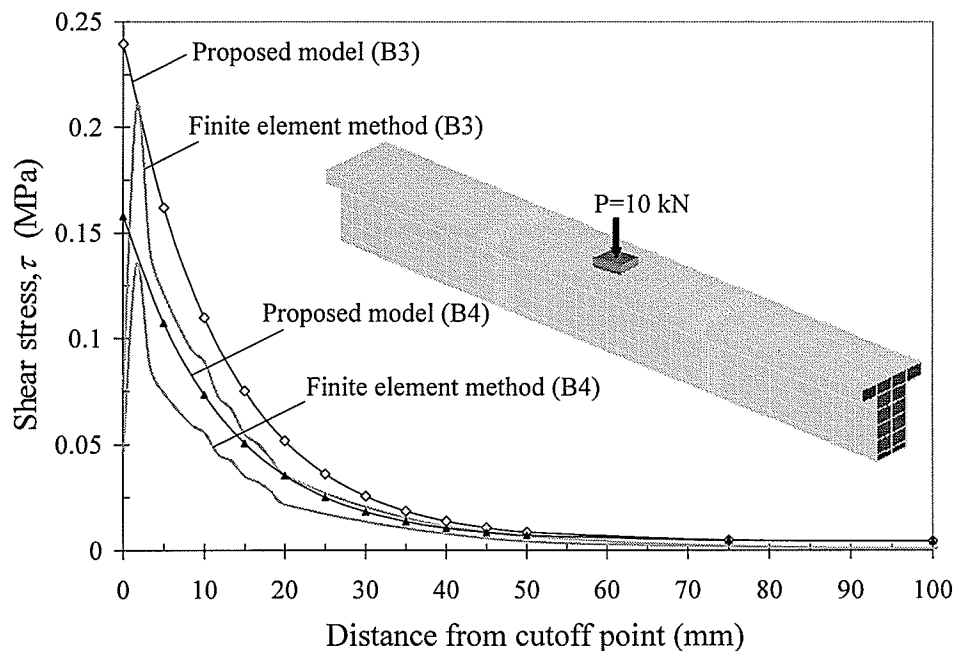
Fig. 5.32 Comparison of the proposed model to finite element method
before cracking of the concrete at cutoff point

The interfacial shear stress distribution, predicted using the analytical model, is in a good agreement with the results of the finite element analysis before cracking of the concrete.
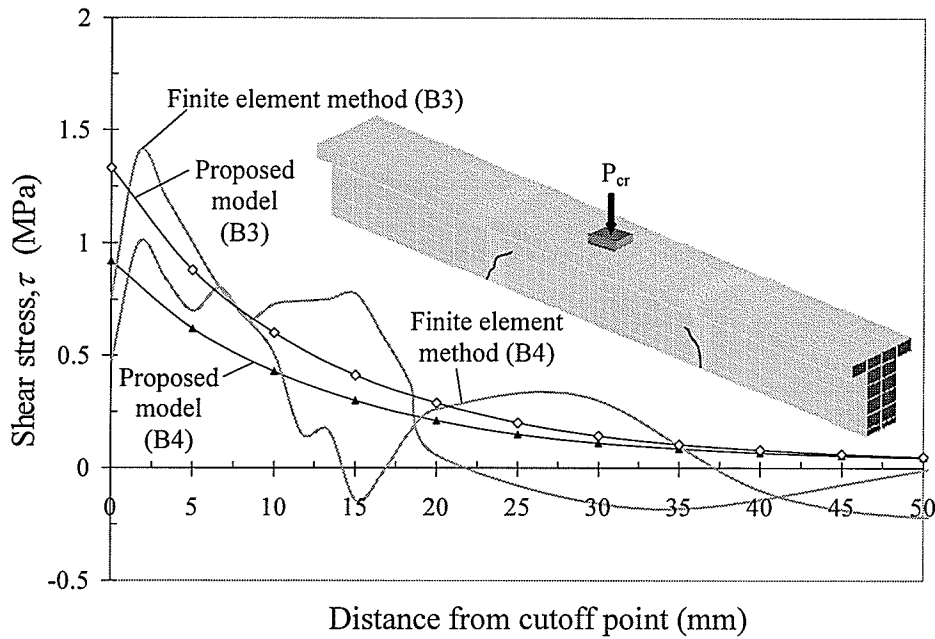
Fig. 5.33 Comparison of the proposed model to finite element method
at the onset of cracking of the concrete at cutoff point

At the onset of cracking of the concrete at the cutoff points, the calculated shear stress distribution deviates from the finite element results. This behaviour is attributed to the possible redistribution of shear stresses around the cracks. Such a phenomenon is accounted for in the finite element analysis and not considered in the proposed model. However, the maximum shear stress calculated using the analytical model is in a good agreement with the finite element results. Using the proposed model for the effective transformed moment of inertia showed good agreement in predicting the maximum interfacial shear stresses at the cutoff points.

5.3.2.4.3 Comparison with Experimental Results

Debonding loads are predicted using the proposed analytical model (Equations 5.37 and 5.43) for different embedment lengths of the CFRP strips as shown in Fig. 5.34.
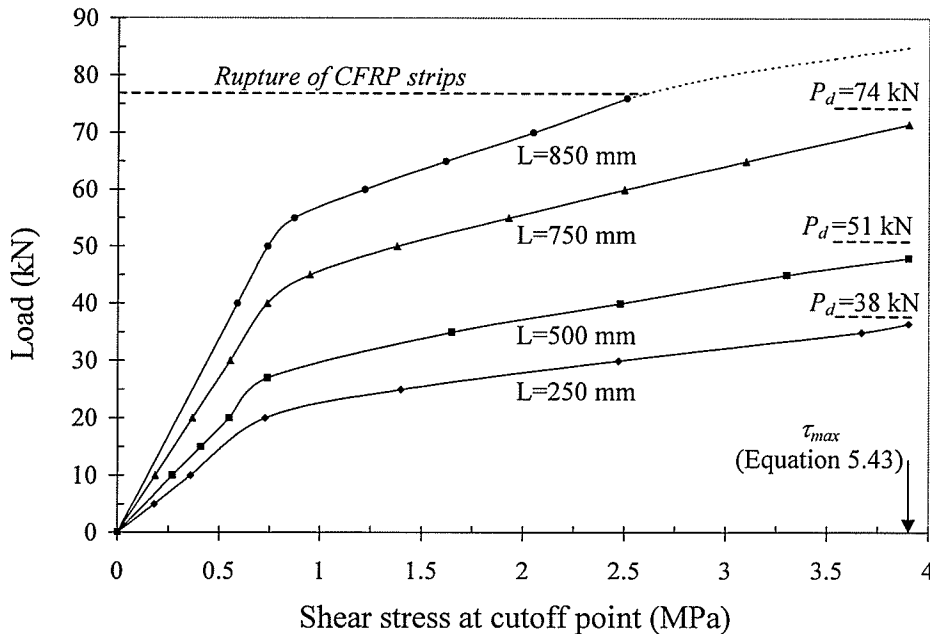
Fig. 5.34 Maximum shear stress at cutoff point vs. applied load

The measured debonding loads for different embedment lengths are also shown in Fig. 5.34. In general, the predicted loads at the maximum shear stress for each length are in a good agreement with the measured debonding loads. The predicted debonding loads for specimens B2, B3 and B4 underestimated the measured values by less than 7 percent. The mid-span section of the test specimen was analyzed using a strain compatibility approach to predict the flexural behaviour up to failure. The predicted failure load due to rupture of the CFRP strip is 76 kN. Failure of specimen B5, with an embedment length of 850 mm was due to rupture of the CFRP strip at a load level of 79 kN, which is 4 percent higher than the predicted value. Fig. 5.34 shows also that the minimum embedment

length needed to rupture the CFRP strips used in this program is greater than 750 mm and less than 850 mm, which coincides with the experimental results.

The development length is highly dependent on the dimensions of the strips, concrete properties, adhesive properties, internal steel reinforcement ratio, reinforcement configuration, type of loading, and groove width. The proposed model in Equations 5.37 and 5.43, can be used to estimate the development length of near surface mounted strips of any configuration as follows:

1. Use the proposed Equations 5.37 and 5.43 to determine the debonding load of the strip for different embedment lengths as shown in Fig. 5.35. The resulting curve represents a failure envelope due to debonding of the strip at cutoff point.
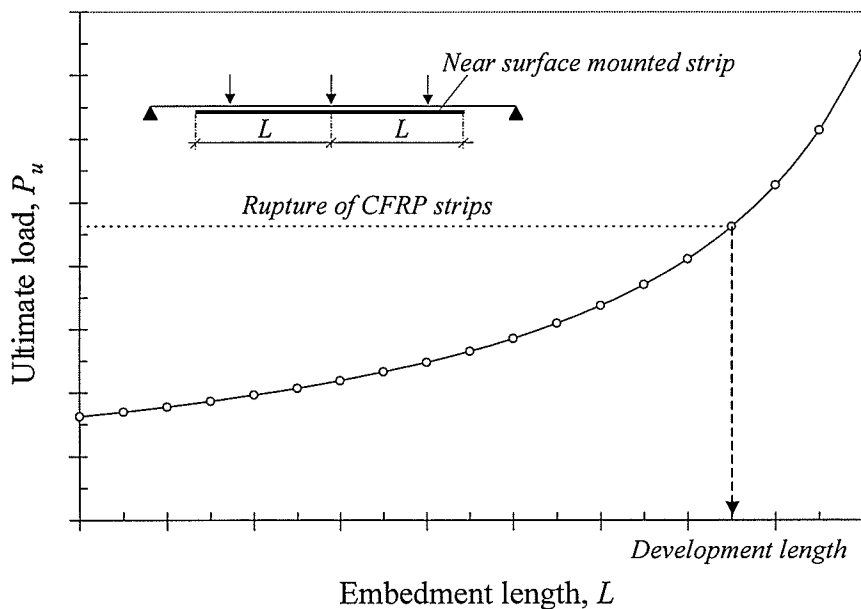
Fig. 5.35 General procedures to calculate the development length for near surface mounted strips

2. Use a cracked section analysis at sections of maximum induced normal stresses and determine the ultimate load required to rupture the strip as shown in Fig. 5.35.

3. Determine the development length at the intersection of the line corresponding to flexural failure of the strip with the curve representing debonding failure at the cutoff point.

The calculated development length will preclude brittle failure due to debonding of the strips and will ensure full composite action between the strip and concrete up to failure.

5.3.2.5 Parametric Study

Based on the confidence established in the analytical model, the analysis was extended to investigate the influence of various parameters, believed to affect the development length of near surface mounted CFRP strips. The key parameters considered in this section are the internal steel reinforcement ratio, concrete compressive strength and groove width. In the following analysis, tension stiffening of the concrete was not considered to simplify the procedure. Fig. 5.36 shows the influence of the internal steel reinforcement ratio on the development of near surface mounted CFRP strips. Two different sizes of the CFRP strip were considered in the analysis. The first strip had a height of 25 mm. The strip could be easily inserted in typical concrete covers. The height of the second strip was 50 mm and was selected to accommodate typical bridge members normally provided with large concrete covers. The thickness of the CFRP strips was set to 1.2 mm in both cases.
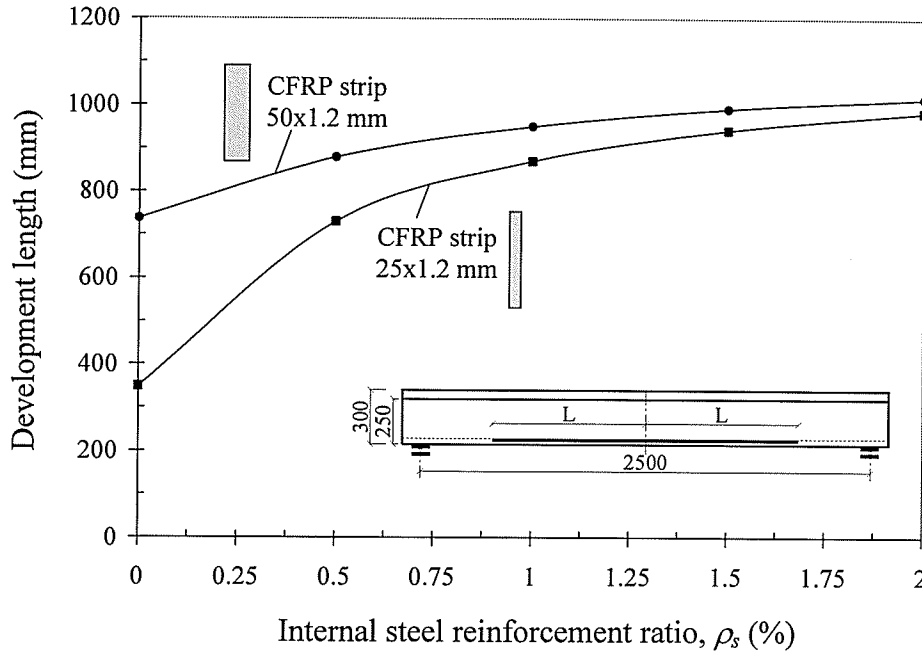
Fig. 5.36 Influence of internal steel reinforcement ratio

In general, for the given flexural member, increasing the internal steel reinforcement ratio results in a significant increase in the development length of near surface mounted CFRP strips. The ultimate moment capacity of the concrete section at mid-span due to rupture of near surface mounted CFRP strips can be expressed by:

$$M_u = A_f f_u \left(d_f - \frac{\beta_1 c}{2} \right) + \rho_s b d_s f_y \left(d_s - \frac{\beta_1 c}{2} \right) \qquad (5.44)$$

where A_f is the area of the CFRP strip; f_u is the tensile strength of the CFRP reinforcement; f_y is the yield stress of the steel reinforcement; d_f and d_s are the depths of the CFRP and steel reinforcement from the extreme compression fibres, respectively; ρ_s is the reinforcement ratio of the steel reinforcement; b is the width of the concrete section; c is the neutral axis depth from the extreme compression fibres; and β_1 is the stress block parameter. For plain concrete members where the internal steel reinforcement ratio, ρ_s, is zero, doubling the area of the near surface mounted CFRP

strips doubles the ultimate moment needed to rupture the strips. Consequently, the development length required to rupture the CFRP strips is longer as shown in Fig. 5.36. It should be noted that the internal steel reinforcement ratio has a negligible effect on the debonding loads of the strips.

At high internal steel reinforcement ratios, the second term in Equation 5.44 becomes the dominant factor for the ultimate moment capacity of the strengthened member and the contribution of the CFRP reinforcement becomes less pronounced. Therefore, the influence of doubling the area of the CFRP strip becomes less dominant on the development length by increasing the internal steel reinforcement ratio as shown in Fig. 5.36.

The influence of the concrete compressive strength and the groove width is illustrated in Figs. 5.37a and 5.37b, respectively.
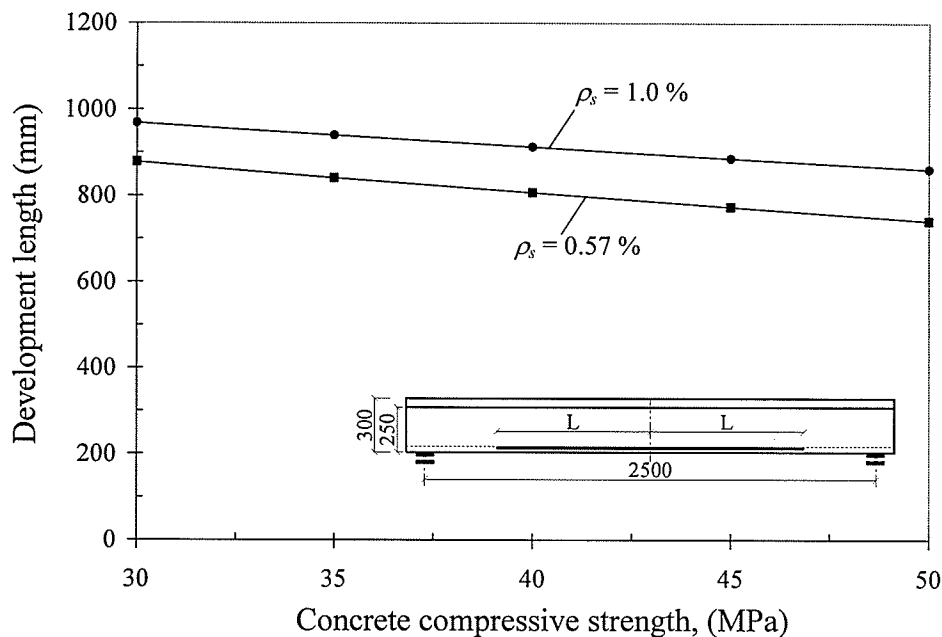
Fig. 5.37a Influence of concrete compressive strength
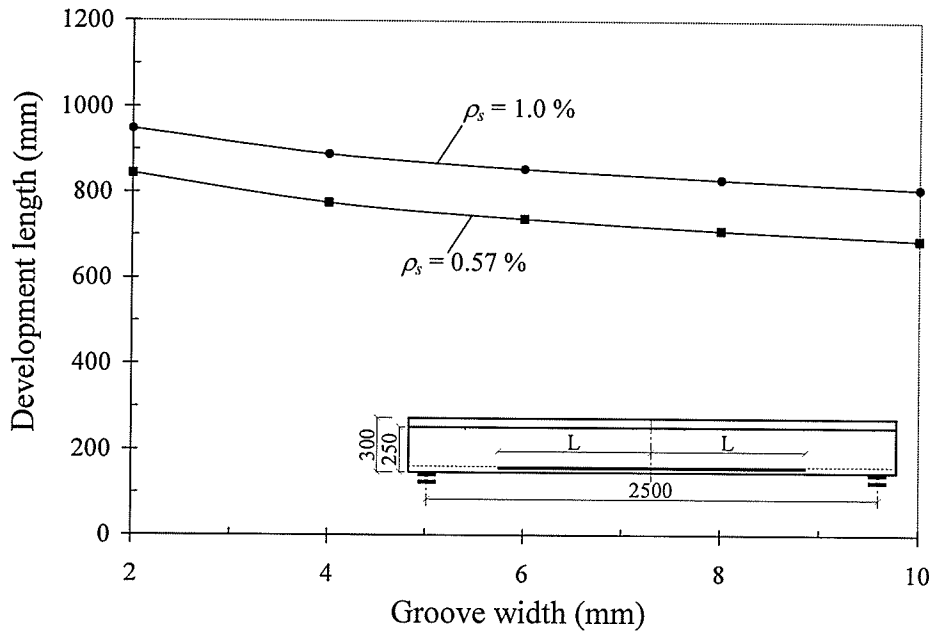
Fig. 5.37b Influence of groove width

The analysis was performed using two different internal steel reinforcement ratios. The first reinforcement ratio was set to 0.57 percent to match the steel reinforcement ratio at mid-span section of the test specimens. The second reinforcement ratio was set to 1 percent to simulate the most commonly used reinforcement ratio in flexural members.

Generally, increasing the concrete compressive strength and/or the groove width reduces the development length required to rupture the CFRP strips. The development length depends primarily on the predicted debonding load using Equations 5.37 and 5.43 as well as on the rupture load of the CFRP strips as shown in Fig. 5.35. The analysis indicated that failure loads due to rupture of the CFRP strips were trivially changed with the variation of either the concrete compressive strength or the groove width. However, increasing the concrete compressive strength results in a significant increase in the shear strength, τ_{max} given by Equation 5.43. Consequently, the failure envelope due to

debonding of the CFRP strips is shifted as shown in Fig. 5.38 and the development lengths needed to rupture the CFRP strips is reduced.

Increasing the thickness of the adhesive reduces the shear deformation within the adhesive layer. Such a phenomenon results in a significant increase in debonding loads and consequently reduces the development length as shown in Figs. 5.37b and 5.38 [Hassan and Rizkalla, 2002b].
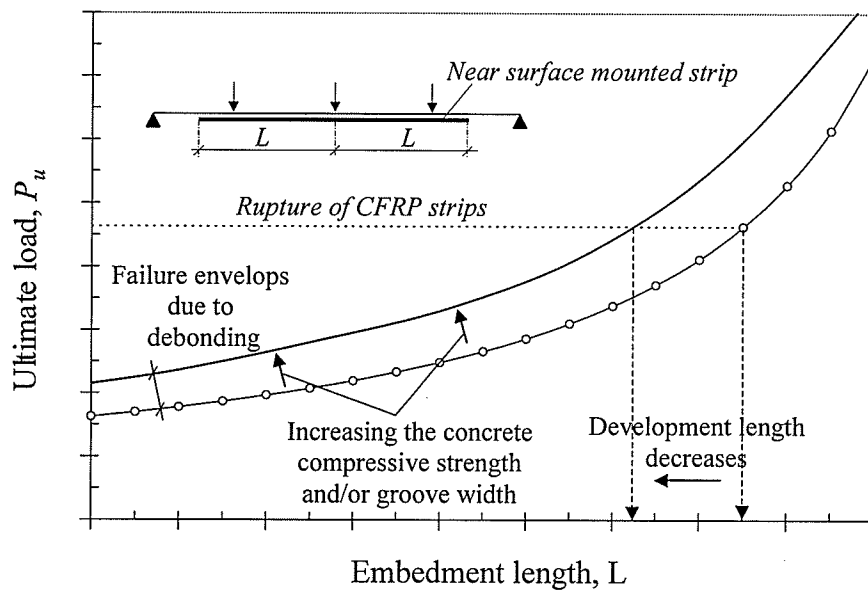
Fig. 5.38 Influence of concrete compressive strength and/or groove width on development length

5.4 Externally Bonded CFRP sheets

5.4.1 Experimental Results (Series C)

A total of seven beams were tested from series C. One beam was tested as a control specimen, while the other six beams were strengthened with various lengths of externally bonded CFRP sheets. The bond length of the sheets was varied from 150 mm to 750 mm. Complete details of the tested specimens were given in Chapter 3, section 3.3.3. The objectives of this experimental program were to isolate and monitor the development of the delamination process and also to investigate the influence of the bond length on the behaviour. The load-deflection behaviour of series C beams is shown in Figs. 5.39a and 5.39b.

(a)

(b)
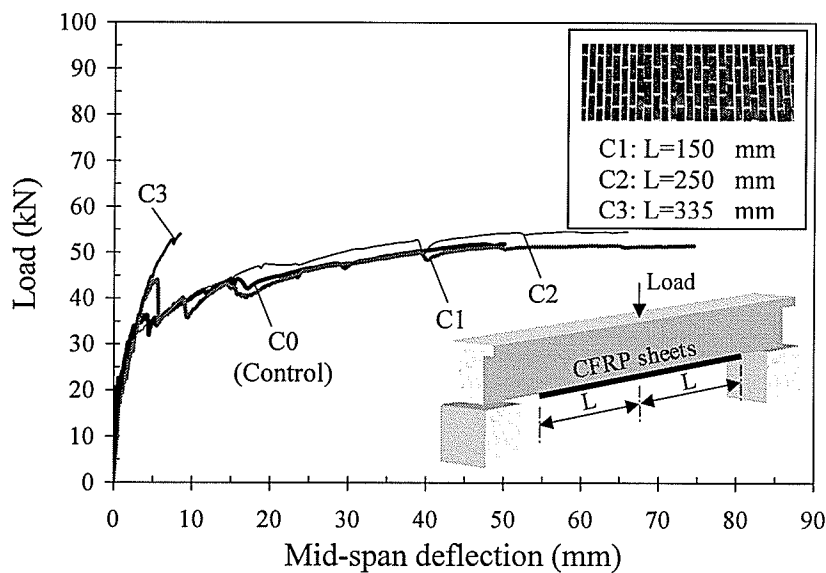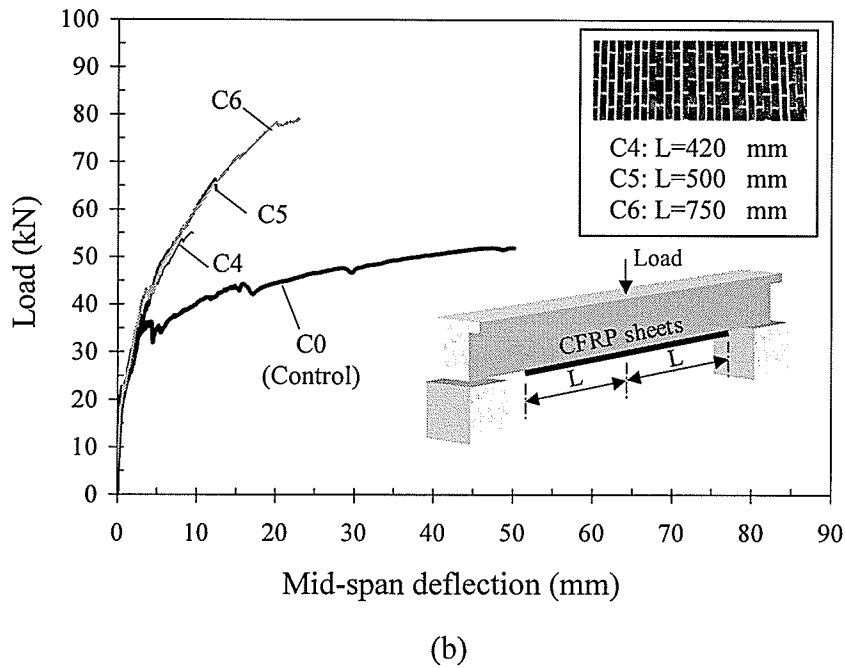
Fig. 5.39 Load-deflection behaviour of series C specimens

The strengthened beams exhibited a higher concrete cracking load level than the control specimen. The control specimen, C0, showed traditional non-linear behaviour after cracking of the concrete and yielding of the internal steel reinforcement. The failure of the control specimen was due to crushing of the concrete at the top surface at a load level of 52 kN. Specimens C1 and C2, with bond lengths of 150 mm and 250 mm, respectively showed identical behaviour to the control specimen. The beams experienced no enhancement in either stiffness or strength as was evident by the failure loads of both specimens, which were almost identical to the control specimen. For these two specimens, delamination initiated well before yielding of the internal steel reinforcement at the end of the sheet and propagated toward the mid-span of the beam. This process continued until the tensile strains in the CFRP sheet were reduced to zero and failure

occurred when complete delamination took place resulting in peeling of the sheet, adhesive and the concrete cover as shown in Fig. 5.40.
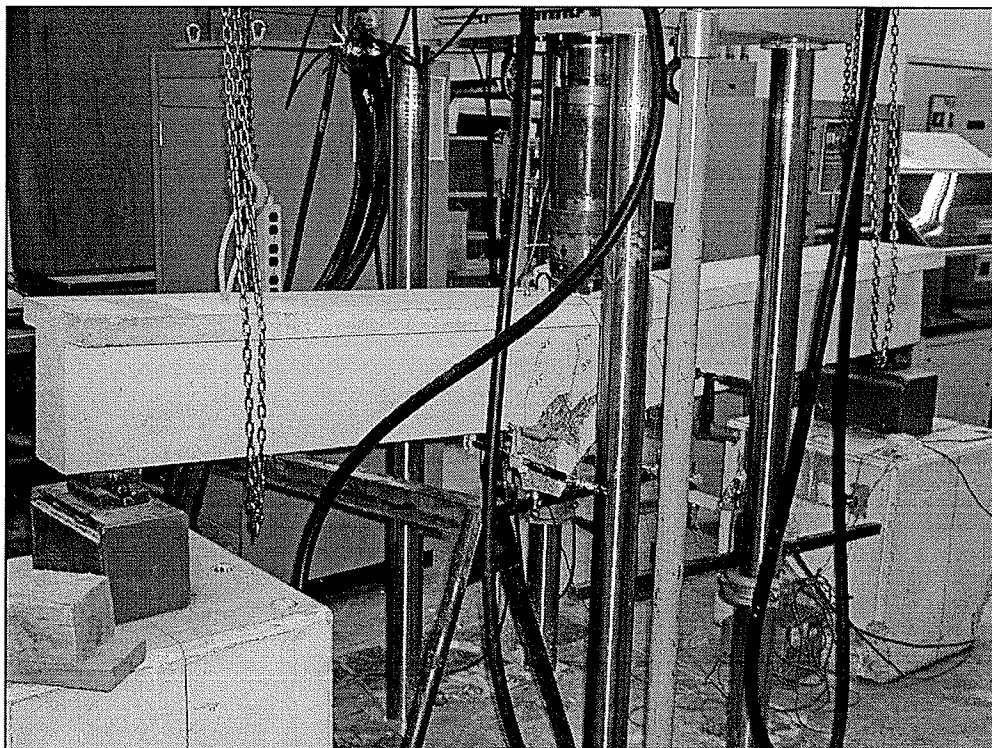
Fig. 5.40 Typical delamination failure of CFRP sheets

Beams with longer sheets demonstrated more brittle failure with sudden delamination along the entire span. Test resulted showed that beams with longer sheets had less delay between the first signs of delamination and ultimate loads. Shorter sheets were observed to peel at lower loads with less brittleness characteristics.

In general, delamination loads for the tested specimens were found to increase by increasing the bond length. For specimens C3, C4, C5 and C6, cracking in the concrete substrate was typically observed after yielding of the internal steel reinforcement. Consequently, Significant improvement in strength and stiffness were observed for these

258

beams compared to the control specimen. Initial cracks at the concrete substrate were often accompanied by audible noises. Changes in the stiffness were also observed in the mid-span deflection curves.

The maximum measured tensile strain in the CFRP sheets used for specimen C6, was approximately 1.96 percent, indicating that the full tensile strength of the CFRP sheets was utilized prior to delamination of the sheets. Shear cracks were observed to appear at relatively high load levels, but they did not extend to the compression face. At the onset of delamination of the sheets, the load dropped to the yielding load of the cross-section until crushing of concrete occurred. Test results suggest that the minimum bond length needed to utilize the full strength of externally bonded CFRP sheets used in this program is 750 mm. Extending the CFRP sheets beyond this value would not provide extra strength for the retrofitted beam. Experimental results for the test specimens are summarized in Table 5.4.

Table 5.4 Summary of test results for series C

Beam No.	L (mm)	P_u (kN)	P_d (kN)	Δ_u (mm)	ε_u (%)	Mode of failure	% Increase in ultimate capacity
C0	N.A	52	N.A	52	-	C +	-
C1	150	51	35	74.5	0.042	P *	0
C2	250	52	42	66.0	0.44	P	0
C3	335	54	52	8.4	0.67	P	4
C4	420	55.2	54	9.5	1.00	P	6
C5	500	66	61	12.3	1.30	P	48
C6	750	79	79	23	1.96	P	52

+ C refers to crushing of concrete with steel yielding

* P refers to Peeling of CFRP sheets
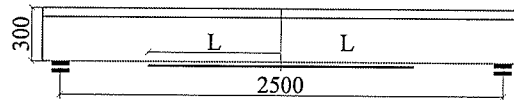
where L is the bond length; P_u is the ultimate failure load; P_d is load at which delamination process started (delamination load); Δ_u is the deflection at failure and ε_u is the maximum tensile strain in the CFRP sheets at failure.

5.4.2 Analytical Modelling

5.4.2.1 Background

Malek et al. (1998) developed a closed form analytical solution for calculating the shear and normal (peeling) stresses at the ends of externally bonded FRP reinforcement. The predicted stresses showed good agreement with the results of the finite element analysis. A gross moment of inertia for the transformed section, I_{gtr}, was assumed in the derivation of the model for the concrete section at the sheet/strip cutoff points. Therefore, the model is applicable only prior to cracking of the concrete at the cutoff points. Brosens and Van

Gemert (2001) modified Malek's approach and proposed using the cracked moment of inertia, I_{crtr}, after cracking of the concrete at cutoff points as shown in Fig. 5.41. Brosens and Van Gemert's model showed satisfactory agreement with test results. However, the modified model did not account for the continuous reduction in flexural stiffness due to cracking of the concrete. For concrete beams with slight cracking intensities at cutoff points, the modified model is too conservative.
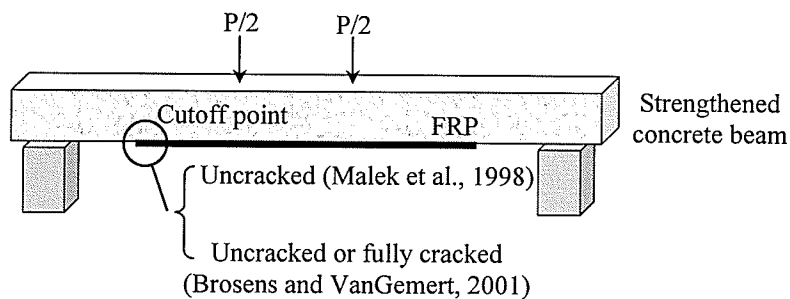
Fig. 5.41 Different approaches for predicting interfacial stresses at cutoff points

This section examines the applicability of both approaches to predict delamination failure loads of the tested specimens and proposes a new approach that accounts for the state of stresses as well as the cracking intensity of the concrete at cutoff points.

5.4.2.2 Proposed Approach for Externally Bonded FRP Reinforcement

The proposed approach modifies Malek's model by introducing new expressions for the moment of inertia and the neutral axis depth of the concrete section at cutoff points. An effective moment of inertia, I_{eff} (Equation 5.25), and an effective neutral axis depth, y_{eff} (Equations 5.26 and 5.27), are proposed to account for the continuous degradation in stiffness as cracking progresses. Both expressions were originally developed by Brosens and Trost (1982) to predict the deflections of concrete members after cracking. Fig. 5.42

261

shows the shear and normal stresses acting on an infinitesimal portion of a concrete beam strengthened with externally bonded FRP reinforcement. Derivation of Malek's model including various loading cases can be found in Malek et al. (1998).
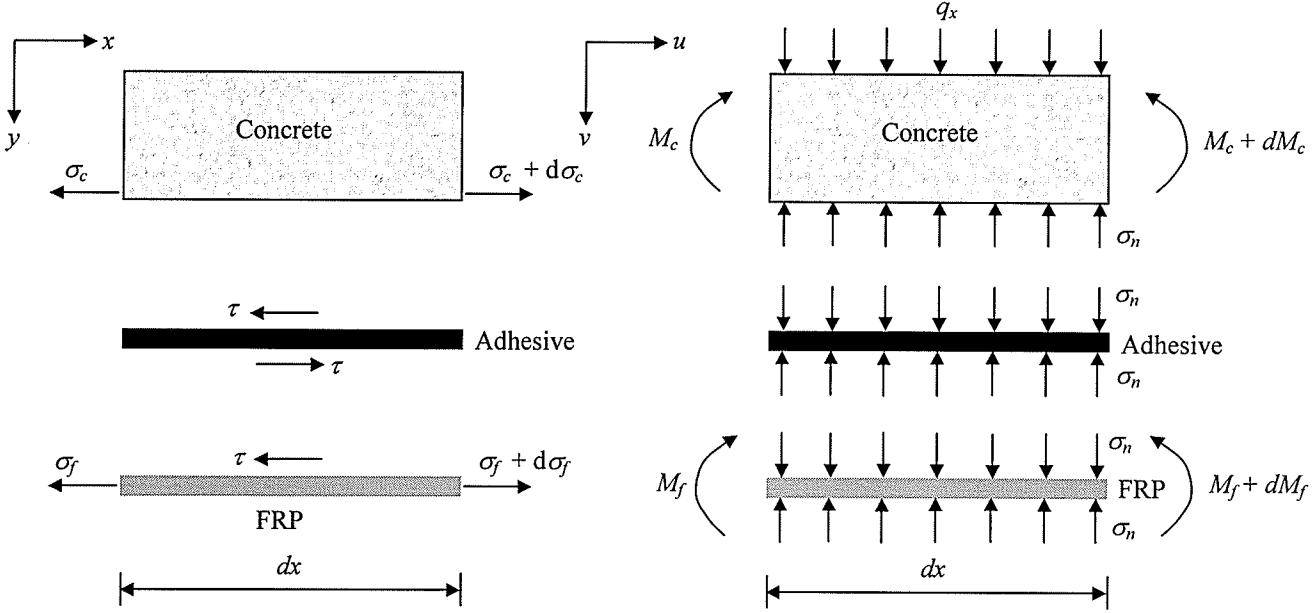
Fig. 5.42 Shear and normal stress distribution on an infinitesimal portion of a strengthened concrete beam [Malek et al., 1998]

For simply supported beams subjected to a concentrated load at mid-span, the shear stress, τ, and the normal stress, σ_n, at the ends of the externally bonded FRP reinforcement can be expressed by:

$$\tau = t_f \left[\frac{n P l_o y_{eff}}{2 I_{eff}} \omega' + \frac{n P y_{eff}}{2 I_{eff}} \right] \tag{5.45}$$

$$\sigma_n = \frac{k_n}{2\beta^3} \left(\frac{V_f}{E_f I_f} - \frac{V_c + \beta M_a}{E_c I_{eff}} \right) \tag{5.46}$$

$$\omega'^2 = \frac{G_a}{t_a t_f E_f} \tag{5.47}$$

$$k_n = \frac{E_a}{t_a} \tag{5.48}$$

$$\beta = \left(\frac{k_n b_f}{4 E_f I_f} \right)^{0.25} \qquad (5.49)$$

$$V_c = V_o - b_f y_{eff} t_f \left(\frac{n P l_o y_{eff}}{2 I_{eff}} \omega' + \frac{n P y_{eff}}{2 I_{eff}} \right) \qquad (5.50)$$

$$V_f = -\frac{1}{2} b_f t^2 {}_f \left(\frac{n P l_o y_{eff}}{2 I_{eff}} \omega' + \frac{n P y_{eff}}{2 I_{eff}} \right) \qquad (5.51)$$

where t_f is the thickness of the FRP sheets; t_a is the thickness of the adhesive; n is defined by Equation 5.23; P is the applied concentrated load; l_o is the unbonded length of the FRP sheets; y_{eff} is the effective distance from the sheet to the neutral axis of the section; I_{eff} is the effective moment of inertia of the transformed section; I_f is the moment of inertia of the FRP sheets; E_a, E_c, E_f and are the modulus of elasticity of the adhesive, concrete and FRP, respectively; G_a is the shear modulus of the adhesive; b_f is the width of the FRP reinforcement; M_a is the applied moment on the concrete section at cutoff points; and V_o is the shear force in the concrete beam at the sheet cutoff point.

5.4.2.3 Failure Criterion

Delamination of externally bonded FRP reinforcement can be determined using a critical combination of both normal and shear stresses at cutoff points. The critical combination of these two stresses was established by Brosens and Van Gemert (2001) using a delamination circle shown in Fig. 5.43.
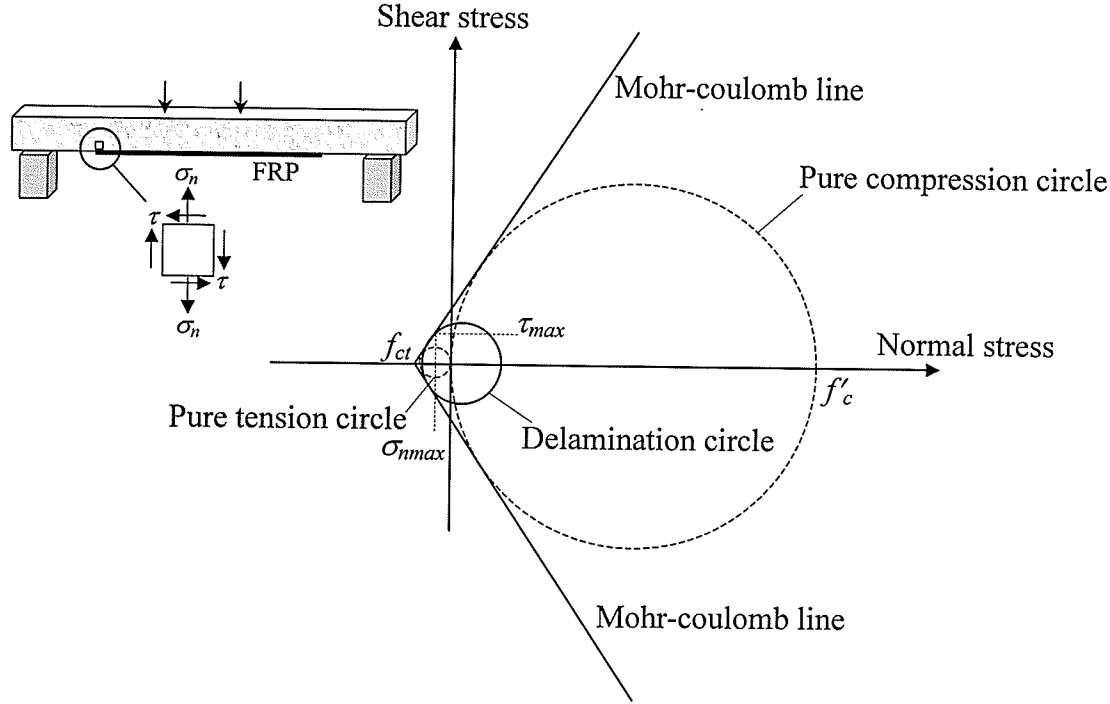
Fig. 5.43 Failure criterion for delamination of externally bonded FRP reinforcement [Brosens and Van Gemert, 2001]

The delamination circle provides a relationship between the shear strength, τ_{max}, and the normal strength, σ_{nmax}. This relationship can be expressed in terms of the concrete compressive strength, f'_c and the concrete tensile strength, f_{ct} as follows:

$$\tau^2_{max} = \left(\frac{f'_c\, f_{ct}}{f'_c + f_{ct}}\right)^2 - \frac{f'_c\, f_{ct}}{\left(f'_c + f_{ct}\right)^2}\left(f'_c - f_{ct}\right)\sigma_{n\,max} - \frac{f'_c\, f_{ct}}{\left(f'_c + f_{ct}\right)^2}\sigma^2_{n\,max}$$

$$(5.52)$$

The delamination circle is always located between the pure shear and pure tension circles. The following section examines the applicability of the Mohr-Coulomb failure criterion in light of the proposed modifications to Malek's model.

5.4.2.4 Comparison with Experimental Results

In this section, the maximum normal and shear stresses are evaluated for specimens C1,
C2, C3, C4, C5 and C6 using the proposed approach (Equations 5.45 and 5.46).
Delamination failure loads are predicted using Mohr-Coulomb failure criterion developed
by Brosens and Van Gemert, 2001 (Equation 5.52). The analysis is extended further to
include specimens F1, C2 and G1 tested by Brosens et al. (2001) as well as specimens
S1.0, S1.2 and S1.4 tested by Hearing and Buyukozturk (2000) to examine the validity of
the proposed approach. All the selected specimens experienced concrete cracking with
various intensities at the sheets' cutoff points prior to delamination.

Fig. 5.44 shows the predicted delamination loads using the proposed approach compared
with the experimental results. The predicted delamination loads using Malek's model as
well as those predicted using Brosens and Van Gemert's model are also shown for
comparison.
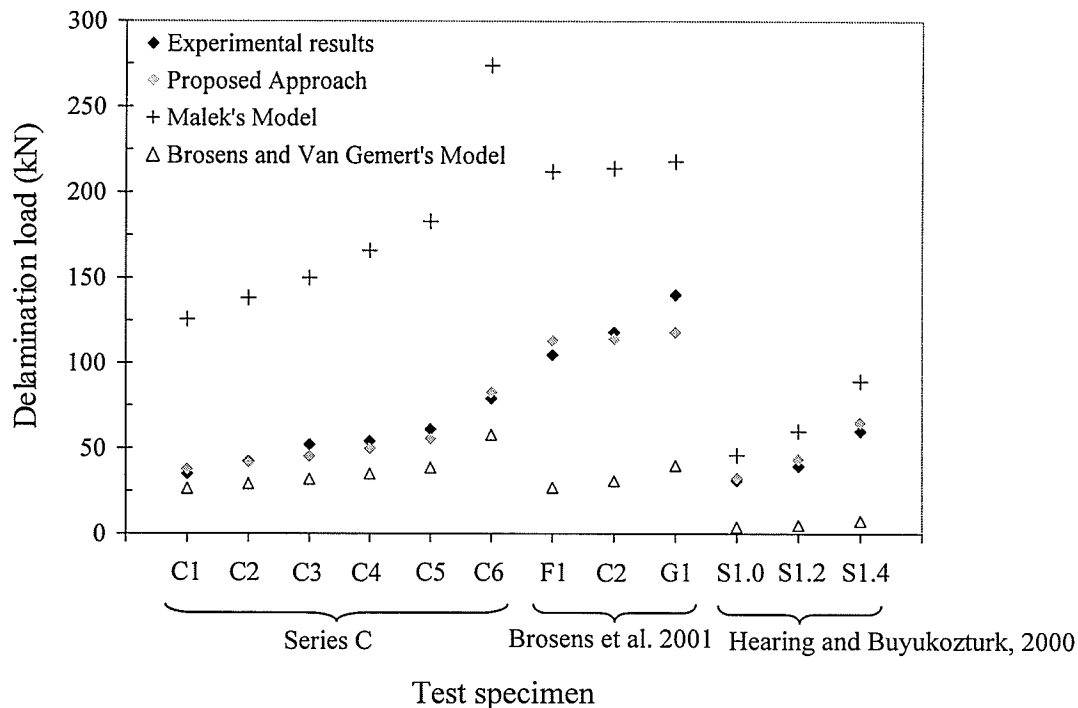
Fig. 5.44 Experimental results compared with the proposed approach

The figure clearly indicates that delamination loads can be predicted with a sufficient accuracy using the proposed approach. Assuming uncracked concrete sections at the sheets' cutoff points (Malek's model) overestimated the strength of the beams considerably and led to huge errors. Furthermore, using fully cracked concrete sections at cutoff points (Brosens and Van Gemert's model) provided very conservative delamination loads.

The average thickness of the epoxy adhesive was measured after delamination of the CFRP sheets as shown in Fig. 5.45 and was set in the analysis to 0.77 mm. Calculation results are summarized in Table 5.5.
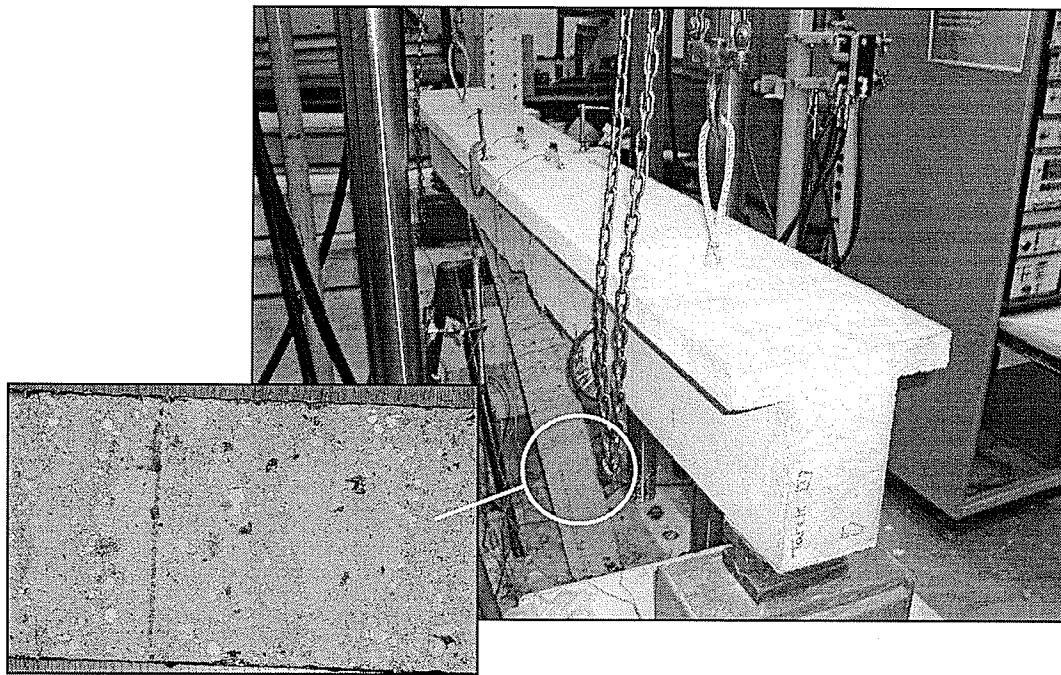
Fig. 5.45 Peeling of CFRP sheets

Table 5.5 Experimental results compared to the proposed approach

Test specimen	Reference	l_o (mm)	f'_c (MPa)	E_c (GPa)	E_{FRP} (GPa)	E_a (GPa)	G_a (GPa)	t_a (mm)	t_{FRP} (mm)	M_{cr} (kN.m)	τ_{max} (MPa)	σ_{max} (MPa)	$P_{exp}*$ (kN)	P_{del} (kN)	$\dfrac{P_{exp}}{P_{del}}$
C1		1100	57	33.97	228	1.85	0.64	0.77	0.165	10.9	3.74	1.0	35	37.7	0.93
C2		1000	57	33.97	228	1.85	0.64	0.77	0.165	10.9	3.74	1.0	42	41.5	1.01
C3	Bond specimens Series C	915	57	33.97	228	1.85	0.64	0.77	0.165	10.9	3.74	1.0	52	45.3	1.15
C4		830	57	33.97	228	1.85	0.64	0.77	0.165	10.9	3.74	1.0	54	49.9	1.08
C5		750	57	33.97	228	1.85	0.64	0.77	0.165	10.9	3.74	1.0	61	55.3	1.10
C6		500	57	33.97	228	1.85	0.64	0.77	0.165	10.9	3.74	1.0	79	82.7	0.96
F1		100	43	32.49	235	3.16	0.93	0.77	0.334	4.7	3.09	1.12	104.8	113.2	0.93
C2	Brosens et al. 2001	100	43	32.49	235	3.16	0.93	0.77	0.334	4.7	3.09	1.12	118.1	114.2	1.03
G1		100	43	32.49	235	3.16	0.93	0.77	0.334	4.7	3.09	1.12	140.1	118.1	1.19
S1.0		400	20.5	25.4	155	2.70	1.0	1.0	1.0	6.0	1.98	0.94	31.1	32.6	0.95
S1.2	Hearing & Buyukozturk, 2000	300	20.5	25.4	155	2.70	1.0	1.0	1.0	6.0	1.98	0.95	39.6	43.5	0.91
S1.4		200	20.5	25.4	155	2.70	1.0	1.0	1.0	6.0	1.98	0.95	60	64.9	0.92
														$Avg.=$	1.01
														$S.D=$	9 %

* Failure of all specimens was due to delamination of the externally bonded FRP reinforcement at the concrete-epoxy interface.
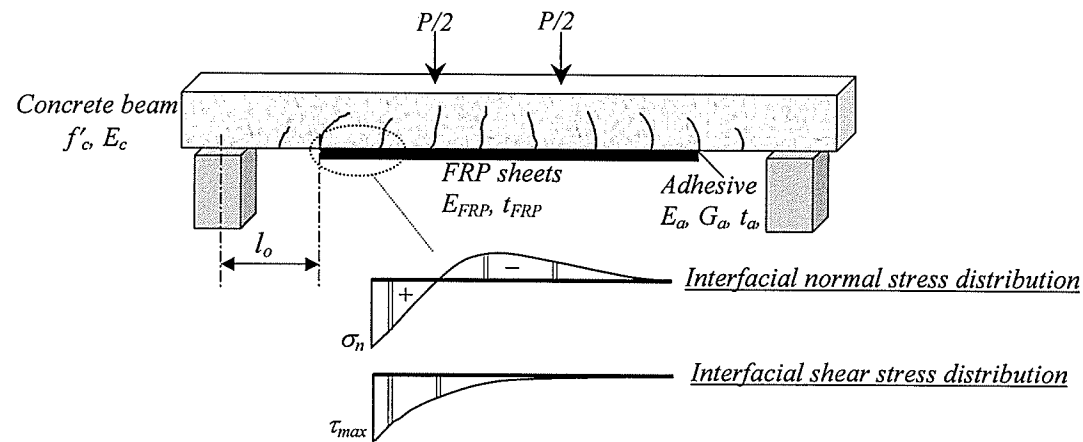
5.4.2.5 Parametric Study

In this section a parametric study is performed using the proposed model. The influence of the number of plies of externally bonded FRP sheets, thickness of the adhesive, and concrete compressive strength on the development length is investigated. A standard concrete beam having the same dimensions and the same loading configuration as the tested specimens was selected to perform the analysis.

Fig. 5.46 shows the influence of the number of plies of the CFRP sheets as well as the bond length on the maximum predicted tensile strain in the CFRP sheets prior to delamination.
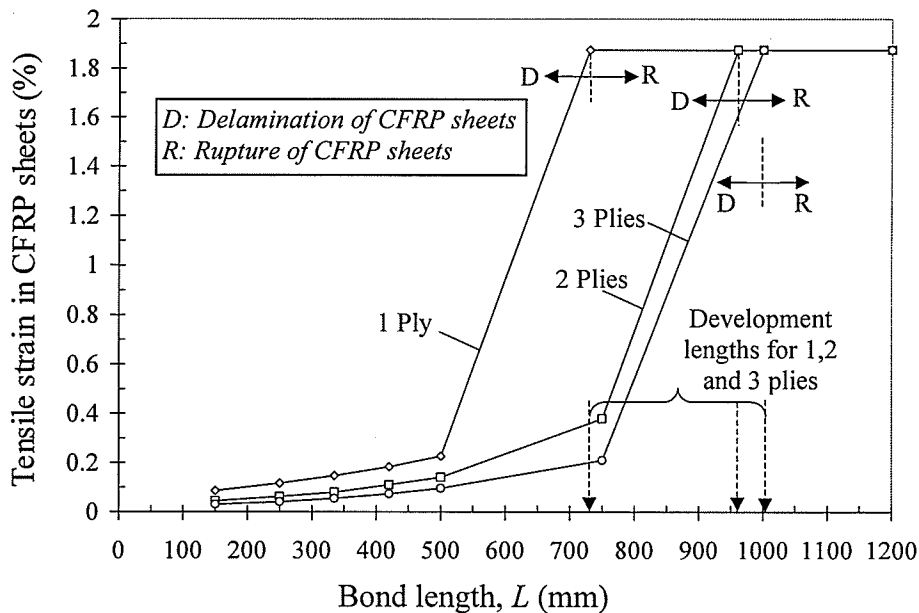
Fig. 5.46 Influence of number of plies of externally bonded FRP reinforcement

The mid-span section of the concrete beam was analyzed using a strain compatibility approach to predict the flexural behaviour up to failure. The predicted failure loads due to rupture of the CFRP sheets ranged from 80 kN to 164 kN depending on the number of

plies considered in Fig. 5.46. Increasing the bond length of the FRP sheets increases in the maximum tensile stresses developed in the FRP reinforcement prior to delamination. Therefore, the effectiveness of using externally bonded FRP reinforcement is substantially improved by the increasing the bond length. The analysis indicated that the minimum bond length needed to utilize the full strength of one ply of CFRP sheets used in this program is 730 mm which is 3 percent less than the measured value. Increasing the thickness of the sheets results in an increase in the development length. Nevertheless, the increase in the development length is not directly proportional to the increase in thickness. Increasing the thickness of the sheets by a factor of three resulted in an increase in the development length by 33 percent.

For the same bond length, increasing the thickness of the CFRP sheets results in a proportional increase in the interfacial shear stress (Equation 5.45). Therefore, the predicted delamination loads as well as the tensile strains in the CFRP sheets at the onset of delamination are decreased.

Fig. 5.47 shows the influence of the adhesive thickness on the development length of externally bonded FRP sheets. The development length decreases by increasing the thickness of the adhesive. Increasing the thickness of the adhesive reduces the shear deformation within the adhesive layer. Consequently, the interfacial shear stresses as well as the development lengths are reduced.
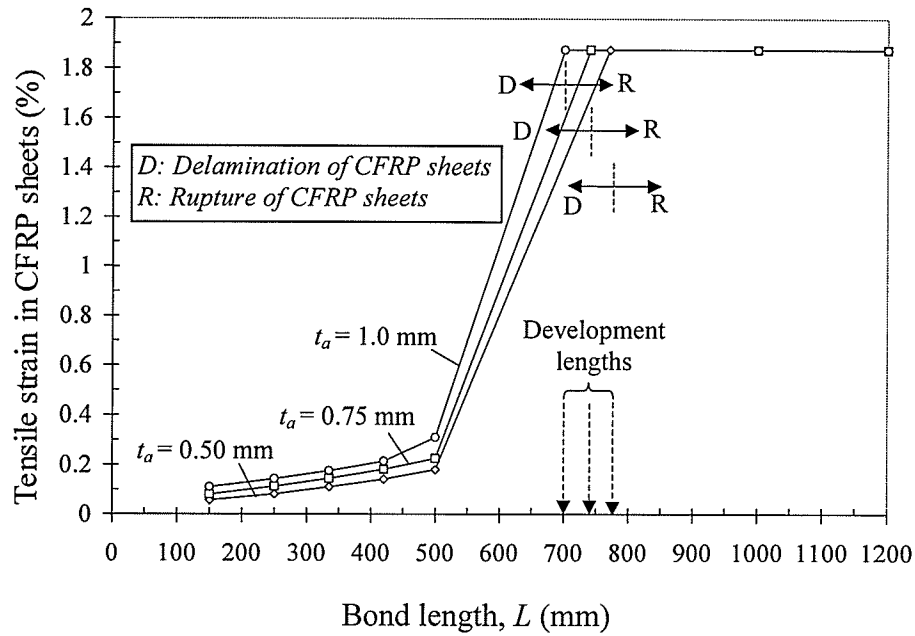
Fig. 5.47 Influence of adhesive thickness

The influence of the concrete compressive strength on the development length of externally bonded FRP sheets is shown in Fig. 5.48.
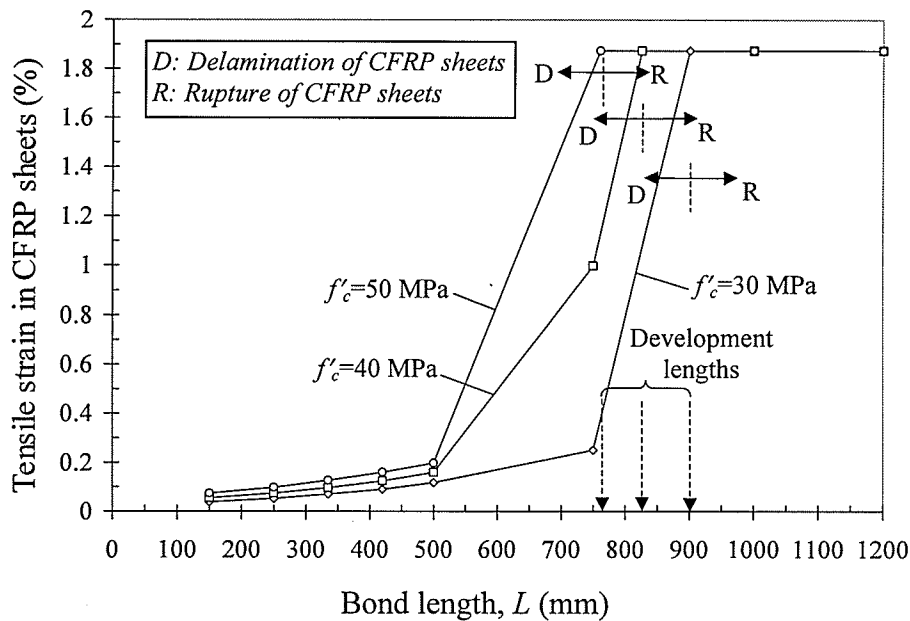
Fig. 5.48 Influence of concrete compressive strength

The development length decreases by increasing the concrete compressive strength. Equation 5.52 demonstrates that increasing the concrete compressive strength results in a significant increase in the shear strength, τ_{max}. Consequently, the delamination loads are increased and the development lengths are reduced.

Chapter 6

Summary & Conclusions

This last chapter summarizes the research performed in this thesis. The main findings of the various phases considered in this investigation are outlined. Recommendations for practical design and strengthening procedures using FRP are highlighted. Finally, some suggestions for future research topics are made.

6.1 General

Understanding of the fundamental behaviour of various strengthening schemes using FRP materials is essential to performing successful repairs of concrete structures and bridges. This thesis investigates the flexural performance of five different FRP strengthening systems. The research focuses on the bond characteristics of the FRP reinforcement to concrete. The study provides a significant contribution to the current knowledge towards feasible restorative procedures of concrete structures to prevent their replacement and to ensure public safety. The information presented in this thesis is applicable to repair damaged or deteriorated concrete structures, to overcome design or structural deficiencies as well as to increase the capability of structures to accommodate new uses beyond the original design. In principle, the findings of this research program will enable engineers to make more informative decisions regarding the repair and/or strengthening of flexural

members and will assist in developing reliable design procedures for concrete structures strengthened with near surface mounted FRP reinforcement.

6.2 Summary

6.2.1 Experimental Investigation

To understand the fundamental flexural performance of reinforced and/or prestressed concrete structures strengthened with various FRP systems, a two-phase experimental program was conducted. In Phase I, three half-scale models of a typical concrete bridge slab were constructed and tested to failure. The model consisted of one simple span and two overhanging cantilevers. Each specimen was tested at three different locations. The first and second tests were performed on the two cantilevers with the load applied at the edge of each cantilever, while the third test was conduced on the mid-span. Therefore, a total of nine tests were conducted in this phase. Five different strengthening techniques were investigated including near surface mounted Leadline bars, C-Bars, CFRP strips and externally bonded CFRP sheets and strips. The structural performance of each technique was examined using the test results of the experimental program. To study the effectiveness of the various systems, a cost analysis of each of the FRP strengthening techniques considered in this study was performed.

Phase II of the experimental program was conducted to study the bond characteristics and load transfer mechanisms of the FRP systems to the concrete surfaces. A total of 24 concrete bond specimens were constructed and tested to characterize the bond of various FRP strengthening systems. Based on the test results, different failure modes of concrete

members strengthened with FRP reinforcement were studied. Composite action between the FRP and concrete for different bond lengths was investigated and development lengths for various FRP strengthening techniques were proposed.

6.2.2 Analytical Phase

The applicability of a cracked section analysis to predict the behaviour of concrete structures strengthened with FRP reinforcement is examined. A smeared crack model has been developed using non-linear finite element analysis. The model was applied to analyze concrete members strengthened with near surface mounted FRP reinforcement. Predictions according to the modelling techniques confirmed the experimental observation in terms of strength, stiffness and crack pattern. Through cracked section analysis and finite element modelling, it was concluded that the global behaviour of concrete members strengthened with near surface mounted FRP reinforcement could be predicted with sufficient accuracy.

Three different analytical models were developed to predict debonding and/or delamination of near surface mounted FRP bars, strips and externally bonded FRP sheets, respectively. The analytical models were verified by comparing the predicted behaviour with test results as well as with non-linear finite element modelling. The mathematical models were used to investigate the influence of key parameters believed to affect the behaviour of FRP strengthened concrete structures. Design guidelines are provided to assist in establishing specifications on the use of near surface mounted FRP reinforcement for strengthening concrete structures.

6.3 Conclusions

6.3.1 Effectiveness of FRP systems

Based on the experimental program and analysis of the test results of the large-scale slab specimens, the following conclusions could be drawn:

1. Failure modes of reinforced and/or prestressed concrete structures strengthened with FRP materials are brittle and include possible separation of the FRP material from the concrete substrate.

2. Strengthening of concrete structures using near surface mounted FRP reinforcement is effective, fast, feasible and cost effective. Nevertheless, caution should be exercised in view of the possible brittle failure modes.

3. Preliminary analysis of FRP strengthened concrete members using strain compatibility and equilibrium of internal forces provides good estimation of the ultimate load carrying capacity of the strengthened system.

4. Both the stiffness and strength of concrete slabs strengthened with CFRP materials can be substantially increased. The ultimate load carrying capacity of the slabs tested in this research program increased by as much as 50 percent in comparison to the control specimens.

5. The strength increase is influenced by the type and configuration of the CFRP materials. In general, near surface mounted CFRP strips and externally bonded CFRP sheets provide the highest strength increase for the same axial stiffness. The cost of strengthening flexural members using externally bonded CFRP sheets could be as low as 25 percent of the cost of strengthening using near surface mounted CFRP strips to achieve the same nominal strength increase.

6. Serviceability could not be used as a criterion to compare the efficiency of the various strengthening schemes used in this investigation since negligible differences were observed among the various techniques at the elastic stage.

7. For the same axial stiffness of CFRP reinforcement, strengthening using either near surface mounted Leadline bars or C-Bars provides approximately the same increase in strength. With respect to cost, strengthening using C-Bars is about 50 percent less.

8. Reducing the spacing between near surface mounted CFRP reinforcement results in a more uniform distribution of stresses, provides additional constraints to opening of the cracks and increases the stiffness of the strengthened member considerably.

9. Strengthening using externally bonded CFRP strips provided the least increase in strength by 11 percent due to peeling of the strips from the concrete surface. Using the same amount of strips but as near surface mounted reinforcement enhanced the ultimate load carrying capacity by about 40 percent.

10. Delamination of externally bonded CFRP strips occurs at a tensile strain of 0.5 to 0.55 percent, which is equivalent to 40 percent of the rupture strain of the strips as reported by the manufacturer. The delamination strain is about 20 percent less than the value recommended by the draft of the ACI-Committee 440 (2002).

11. The number of cracks in a concrete slab strengthened with externally bonded CFRP strips is less than that in a comparable slab strengthened with near surface mounted CFRP strips with the same axial stiffness due to the lower flexural bond strength of the externally bonded strips. Consequently, the crack width and the crack spacing are typically larger at any given load level.

12. Using near surface mounted CFRP strips or externally bonded CFRP sheets for flexural strengthening reduces the cracks width by 50 to 70 percent compared to the unstrengthened specimen. The crack width is directly proportional to the elastic modulus and bond characteristics of the CFRP reinforcement

13. Using epoxy adhesives that are commonly used for bonding steel rebars into concrete is very efficient in bonding near surface mounted CFRP bars to the surrounding concrete.

14. Full composite action between near surface mounted CFRP reinforcement and concrete was achieved throughout the tests since no slip was observed for the different cases examined in this investigation.

15. Using a maximum allowable crack width of 0.5 mm as a criterion for serviceability requirements, the upgraded service load of the strengthened specimens is equivalent to at least three times the ASSHTO HSS 30 truck design load.

16. Strengthening using externally bonded CFRP strips provides the least deformability index among the investigated techniques. Near surface mounted bars and strips as well as externally bonded sheets provide satisfactory deformability indices in excess of the minimum value recommended by other researchers.

17. Various assumptions incorporated in the cracked section analysis can influence the predicted response of FRP strengthened concrete structures. However, cracked section analysis is an excellent analysis tool and quite adequate for typical design and analysis due to its simplicity and validity for most engineers without the need for sophisticated finite element analysis.

18. The predicted results using non-linear finite element analysis are in excellent agreement with the experimental results. The error involved in the analysis was less than 10 percent.

6.3.2 Bond Characteristics of FRP Strengthening Systems

Based on the second phase of the experimental program and analysis of test results of the bond specimens, the following conclusions could be drawn:

6.3.2.1 General Conclusions

19. The test procedure used to evaluate bond characteristics of various FRP strengthening techniques is simple, easy to perform and provides reliable data while maintaining a manageable specimen size. It is recommended to adopt this procedure as an ASTM Standard test method. The configuration of the specimens allowed the FRP reinforcement to be in an area of flexural tension under a moment gradient and constant shear to simulate typical design stresses.

20. Debonding/delamination loads increase by increasing the bond length. For every strengthening technique, there is a certain bond length beyond which no further increase in the ultimate capacity of the strengthened beam can be obtained. At this stage, full composite action between the FRP and concrete is achieved.

21. The development length of near surface mounted FRP reinforcement is highly dependent on the dimensions of the bars/strips, concrete properties, adhesive properties, internal steel reinforcement ratio, reinforcement configuration, type of

loading, and groove width. Consequently, complete evaluation of the existing structures is compulsory prior to any strengthening application.

6.3.2.2 Near Surface Mounted CFRP Bars

22. The mode of failure for all beams strengthened with near surface mounted C-Bars and tested in this program was due to cracking of the concrete surrounding the epoxy paste followed by complete debonding of the bars. The failure mode is greatly influenced by the groove dimensions as well as by the mechanical characteristics of the materials.

23. Rupture of near surface mounted C-Bars is not likely to occur regardless of the embedment length used. The efficiency of using CFRP bars as near surface mounted reinforcement is controlled primarily by the bond characteristics of the bars as well as by the bond between the adhesive material and the concrete. Adhesion and mechanical friction are the main factors that control the bond strength of near surface mounted FRP bars.

24. The development length of near surface mounted C-Bars tested in this investigation should not be less than 80 times the diameter of the bars. The minimum embedment length recommended by the ACI 440 (2002) for FRP bars bonded to concrete is not applicable for near surface mounted FRP bars due to distinct surface characteristics of concrete compared to adhesives.

25. An analytical model is developed for the bond-slip behaviour of near surface mounted CFRP bars. The model can be easily incorporated to commercially available finite element programs to perform detailed theoretical analysis.

26. The maximum measured tensile strain in the CFRP bars at failure is in the range of 40 to 45 percent of the rupture strain of bars, regardless of the embedment length used. Such a limiting value is highly dependent on the configuration of the bottom steel reinforcement inside the beam as well as on the stress level at the concrete-epoxy interface.

27. The slip failure hypothesis used for reinforcing steel bars bonded to concrete can not be adopted as a failure criterion for near surface mounted FRP bars. An examination of the bond stress-slip relationships for the tested specimens indicates that debonding failure can be better described in terms of bond strength rather than end slip values.

28. The proposed design chart in this thesis can be used to determine the development length of near surface mounted FRP bars accurately. The chart is also easy to use and provides excellent correlation to experimental results.

29. Two different types of debonding failures can occur for near surface mounted FRP bars. The first mode of failure is due to splitting of the epoxy cover as a result of high tensile stresses at the FRP-epoxy interface, and is termed "epoxy split failure". The second mode of failure is due to cracking of the concrete surrounding the epoxy adhesive and is termed "concrete split failure".

30. Increasing the groove width and/or using high strength concrete, increases the resistance to concrete split failure. Using high strength adhesives and/or increasing the epoxy cover layer delays epoxy split failure for near surface mounted FRP bars.

31. The recommended minimum clear spacing between the grooves of near surface mounted FRP bars is twice the diameter of the bars regardless of the groove width. Using a clear groove spacing to bar diameter ratio less than the proposed value results

in overlapping of the tensile stresses at the concrete-epoxy interface and should be accounted for in design.

32. A minimum edge distance of four times the diameter of the bars is recommended to diminish edge effect for near surface mounted FRP bars and permit using the proposed design chart.

33. Termination or damage of the internal steel reinforcement creates zones of high bond stresses and accelerates debonding failure. Increasing the reinforcement ratio of the terminated and/or damaged steel reinforcement results in a proportional increase in the bond stress and a corresponding decrease in debonding loads.

34. Using GFRP as near surface mounted bars increases the maximum allowable tensile stresses in the bars prior to debonding. The full tensile strength of GFRP bars could be utilized prior to debonding due to the relatively low modulus of elasticity of GFRP compared to CFRP bars.

6.3.2.3 Near Surface Mounted CFRP Strips

35. Use of near surface mounted CFRP strips substantially increases both the stiffness and strength of concrete beams. The ultimate load carrying capacity of the beams can be increased by as much as 55 percent for the specimens used in this program. The minimum embedment length needed to rupture the near surface mounted CFRP strips, with the given dimensions used in this program is 850 mm.

36. The proposed analytical model is capable of predicting the interfacial shear stress distribution, ultimate load carrying capacity and mode of failure of concrete beams strengthened with near surface mounted CFRP strips. Excellent agreement was

established between the calculated values using the proposed model and those predicted using finite element analysis.

37. The proposed failure criterion for debonding of near surface mounted CFRP strips provides sufficient evidence and confidence in predicting debonding loads.

38. Debonding loads increase by increasing the embedment length of CFRP strips, concrete compressive strength and/or groove width.

39. The development length of near surface mounted CFRP strips increases by increasing the internal steel reinforcement ratio. The development length decreases with the increase of either the concrete compressive strength and/or the groove width.

6.3.2.4 Externally Bonded CFRP Sheets

40. Failure of all concrete beams strengthened with externally bonded CFRP sheets is due to delamination of the sheets at cutoff points. The bond length of the CFRP sheets has a significant effect on the load at which the delamination process is initiated. Beams with longer sheets had less delay between the first signs of delamination and ultimate loads. Shorter sheets were observed to peel at lower loads with less brittleness.

41. The minimum bond length needed to fully utilize the strength of the externally bonded CFRP sheets used in this investigation is 750 mm. Extending the CFRP sheets beyond this value would not provide additional strength to the retrofitted beam.

42. Using the proposed approach for the effective transformed moment of inertia showed good agreement in predicting delamination loads within a range of 20 percent.

43. Increasing the thickness of externally bonded sheets results in an increase in the development length. Nevertheless, the increase in the development length is not

directly proportional to the increase in thickness. Furthermore, the development length decreases by increasing the thickness of the adhesive and/or the concrete compressive strength.

6.4 Recommendations for Future Research Areas

While the objectives of this research study are achieved, it is recognized that much more work is still needed to fully characterize the behaviour of FRP retrofitted concrete structures. Future research should concentrate on the following topics:

1. Evaluation of the effectiveness of different mechanical anchorage systems and their design procedures, for both near surface mounted and externally bonded FRP reinforcement.

2. Durability of various FRP strengthening techniques under harsh environmental conditions with or without sustained stress levels.

3. Prestressing of near surface mounted CFRP bars to fully utilize the strength of the materials.

4. Fire resistance of various FRP strengthening techniques as well as fire protective measures that should be accounted for.

5. Development of an internationally accepted standard regarding the design of FRP retrofitted concrete structures including various FRP strengthening techniques.

References

1. Abdelrahman, A.A. (1995) "Serviceability of concrete beams prestressed by fibre reinforced plastic tendons", Doctoral Thesis, The University of Manitoba, Canada, 331p.

2. Achillides, Z., Pilakoutas, K., and Waldron, P., (1997) "Modeling of FRP rebar bond behavior", Proceedings, Non-metallic Reinforcement for Concrete Structures, Supporo, Japan, Japan Concrete Institute, Vol. 2, pp. 423-430.

3. ACI Committee 440F, (2002) "Guide for the design and construction of externally bonded FRP systems for strengthening concrete structures", Draft report, American Concrete Institute, Framington Hills, MI.

4. ACI Committee 318, (1999), "Building code requirements for structural concrete and commentary", ACI 318M-99, American Concrete Institute, Framington Hills, MI.

5. ADINA (2001) "Theory and modeling guide", ADINA R&D Inc. MA, USA.

6. Ahmed, O., (2000) "Strengthening of R.C beams by means of externally bonded CFRP laminates-Improved model for plate end shear", Doctoral Thesis, K.U.Leuven.

7. Arduini, M., D'ambrisi, A., and Di Tommaso, (1994), "Shear failure of concrete beams reinforced with FRP plates", New materials and Methods of Repair, Proceedings of the Materials Engineering Conference, San Diego, CA, pp.123-130.

8. Arduini, M., Di Tommaso, A., and Nanni, A., (1997), "Parametric study of beams with externally bonded FRP reinforcement", ACI Structural Journal, V.94 No.5, pp. 493-501.

9. Asplund, S. O., (1949), "Strengthening bridge slabs with grouted reinforcement", ACI Structural Journal V.20, No. 4, pp.397-406.

10. Baumert, M.E., Green, M.F, and Erki, M.A., (1996) "Low temperature behavior of concrete beams strengthened with FRP sheets", Proceedings of the CSCE Annual Conference, Canadian Society for Civil Engineers, Montreal, Quebec.

11. Beber, A. J., Filho, A. C., and Campagnolo, (2001), "CFRP in the strengthening of reinforced concrete beams", Proceedings of the International Conference on FRP Composites in Civil Engineering, Hong Kong, China, pp. 391-398.

12. Beeby, A., (1979), "Prediction of crack widths in hardened concrete", The Structural Engineer Journal, Vol. 57, No. 1 pp. 9-17.

13. Benmokrane, B., Tighiouart, B., and Chaallal, O., (1996) "Bond strength and load distribution of composite GFRP reinforcing bars in concrete", ACI Materials Journal, Vol. 93, No. 3.

14. Benmokrane, B., and Wang, P., (2001), "Durability of FRP composites in civil engineering infrastructure applications", Draft of the State-of-the-Art Report, American Concrete Institute, Framington Hills, MI.

15. Bizindavyi, L., and Neale, K.W., (1999) "Transfer lengths and bond strengths for composites bonded to concrete", Journal of Composites for Construction, ASCE, Vol. 3, No. 1, 153-160.

16. Blaschko, M., and Zilch, K., (1999), "Rehabilitation of concrete structures with strips glued into slits", Proceedings of the 12th International conference on Composite Materials, Paris.

17. Branson, D. E., and Trost, H. (1982). "Unified procedures for predicting the deflection and centrodal axis location of partially cracked nonprestressed and prestressed concrete members", ACI Structural Journal, Vol. 79, No. 2, pp. 119-130.

18. Bresson, J., 1971, "Nouvelles recherches et applications concernant l'utillisation des collages dans les structures", Annales de l'ITBTB, serie BBA/116.

19. Brosens, K., and Van Gemert, D., (1998) "Plate end shear design for external CFRP laminates", Fracture Mechanics of Concrete Structures, Proceedings FRAMCOS-3, Germany, pp.1793-1804.

20. Brosens, K., (2001) "Anchorage of externally bonded steel plates and CFRP laminates for the strengthening of concrete elements", Ph.D. Thesis, K. U. Leuven, Belgium, 225p.

21. Brosens, K., and Van Gemert, D., (2001) "Anchorage of externally bonded reinforcements subjected to combined shear/bending action", Proceedings of the International Conference on FRP Composites in Civil Engineering, Hong Kong, China, pp. 589-596.

22. Canadian Standards Association, CSA, (1994), "Design of concrete structures for buildings", CAN-A23.3-94, Rexdale, Ontario, 220 p.

23. Canadian Prestressed Concrete Institute, CPCI, (1996), "Design manual, precast and prestressed concrete", Ottawa, Canada, 340 p.

24. Canadian Standards Association, (1996) "Canadian Highways Bridge Design Code", Section 16, Fiber Reinforced Structures, 28 pp.

25. Chajes, M.J., Januszka, T.F., Mertz, D.R., Thomson, T.A., and Finch, W.W., (1995) "Shear strengthening of reinforced concrete beams using externally applied composite fabrics", ACI structural Journal, Vol. 92, No. 3, pp.295-303.

26. Chajes, M.J., Thomson, T.A., and Farschman, C.A., (1995) "Durability of concrete beams externally reinforced with composite fabrics", Construction and Building Materials, Vol. 9, No. 3, pp.141-148.

27. Chajes, M.J., Finch, W.W., Januszka, T.F., and Thomson, T.A., (1996), "Bond and force transfer of composite material plates bonded to concrete", ACI Structural Journal, V.93, No. 2, pp.208-217.

28. Chen, J.F., and Teng, J.G., (2001) "Anchorage strength models for FRP and steel plates attached to concrete", Journal of Structural Engineering, ASCE, Vol. 127, No. 7, pp. 784-791.

29. Collins, M., and Mitchell, D., (1991) "Prestressed Concrete Structures", Prentice Hall, Englewood Cliffs, New Jersey, 766 p.

30. Corry, R. and Dolan, C. W., (2001) "Strengthening and repair of a column bracket using carbon fibre reinforced polymer (CFRP) fabric", PCI Journal, Vol. 46, No. 1, pp. 54-63.

31. Cosenza E., Manfredi, G., and Realfonzo, R., (1997) "Behavior and modeling of bond of FRP rebars to concrete", Journal of Composites for Construction, Vol. 1, No. 2, pp.40-51.

32. Cosenza, E., Manfredi, G., Pecce, M., and Realfonzo, R., (1999) "Bond between glass fibre reinforced plastic reinforcing bars and concrete – experimental analysis", Proceedings of the Fourth International Symposium on Fibre Reinforced Polymer Reinforcement for Reinforced Concrete Structures, Dolan et al. Eds, ACI SP-188, pp. 347-358.

33. Darwin, D., and Pecknold, D. A., (1974), "Inelastic model for cyclic biaxial loading for reinforced concrete", Civil Engineering Studies, SRC No. 389, University of Illinois, Urbana, Illinois.

34. De Lorenzis, L., Nanni, A., and La Tegola, A., (2000) "Flexural and shear strengthening of reinforced concrete structures with near surface mounted FRP rods", proceeding of the 3rd ACMBS conference, August 2000, pp.521-528.

35. De Lorenzis L. and Nanni, A., (2001) "Shear strengthening of reinforced concrete beams with near-surface mounted fibre reinforced polymer rods", ACI Structural Journal, Vol. 98, No. 1, pp.60-68.

36. De Lorenzis L. and Nanni, A., (2002) "A bond between near-surface mounted FRP rods and concrete in structural strengthening", ACI Structural Journal, Vol. 99, No. 2, pp. 123-132.

37. Deuring, M., (1993) "Verstarken von stahlbeton mit gespannten faser-verbundwerstoffen", Ph.D. Thesis, EMPA, Switzerland.

38. Dutta, P.K., (1988) "Structural fibre composite materials for cold regions", Journal of Cold Regions Engineering, Vol. 2, No. 3, pp. 124-135.

39. Eligehausen, R., Popove, E.P., and Bertero, V.V., (1983) "Local bond stress slip relationships of deformed bars under generalized excitation", Report No. 82/23, Earthquake Engineering Research Center, EERC, University of California, Berkeley.

40. Faoro, M. (1992) "Bearing and deformation behavior of structural components with reinforcements comprising resin bonded glass fibre bars and conventional ribbed steel bars", Proceedings of the International Conference on Bond in Concrete.

41. Ferguson, P.M., and Briceno, A., (1969) "Tensile lap splices-Part 1: Retaining wall type, varying moment zone", Research Report No. 113-2, The university of Texas, Austin, USA.

42. Ferrier, E., Lagarde, D., and Hamelin, P.P., (1998) "Durability of reinforced concrete beams repaired by composites", Durability of Fibre Reinforced Polymer (FRP) Composites for Construction, CDCC 98, pp.217-228.

43. Ferrier, E., and Hamelin, P., (1999) "Influence of time-temperature loading on carbon epoxy reinforcement for concrete structures," The Fourth International Symposium: Fibre Reinforced Polymer Reinforcement for Reinforced Concrete Structures, SP-188, pp. 491 – 500.

44. Fleming, C.J., and King G.E.M., (1967), "The development of structural adhesives for three original uses in South Africa", RILEM International Symposium, Synthetic Resins in Building Construction, Paris, pp.75-92.

45. Focacci, F., Nanni, A., and Bakis, C.E., (2000), "Local bond-slip relationship for FRP reinforcement in concrete", Journal of Composites for Construction, Vol. 4, No. 1, pp. 24-31.

46. Gentile, C. and Rizkalla, S., (1999), "Flexural strengthening of timber beams using FRP", Technical Progress Report, ISIS Canada.

47. Gerstle, K. H., (1981), "Material Modelling of Reinforced Concrete", IABSE Colloquium on Advanced Mechanics of Reinforced Concrete, Introductory Report, Delft.

48. Goland, M., and Reissner, E., (1944), "The stresses in cemented joints", Journal of Applied Mechanics, No. 66.

49. Goto, Y., (1971) "Cracks formed in concrete around deformed tension bars", ACI Structural Journal, Vol. 68, No. 4, pp.244-251.

50. Green, M.F, Bisby, L.A, Beaudoin, Y., and Labossiere, P., (1998) "Effects of freeze-thaw action to the bond of FRP sheets to concrete", Durability of Fibre Reinforced Polymer (FRP) Composites for Construction, CDCC 98, pp. 179-189.

51. Green, M.F., Bisby, L.A., Beaudoin, Y., and Labossiere, P., (2000) "Effect of freeze-thaw cycles on the bond durability between fibre reinforced polymer plate reinforcement and concrete", Canadian Journal of Civil Engineering, Vol. 27, No. 5, pp.949-959.

52. Hamada, H., Nakai, A., Urai, S., and Yokoyama, A., (1997) "Experimental and analytical studies of adhesives property for rehabilitation of concrete structures by using composite materials", Proceedings of the International Composites Expo '97, Nashhville, Tennessee, January 1997.

53. Hamoush, S.A., and Ahmad, S.H., (1990) "Debonding of steel plate-strengthened concrete beams", ASCE Journal of Structural Engineering, 116(2) pp.356-371.

54. Hand, F. R., Pecknold, D. A., and Schnobrich, W. C., (1972), "A layered finite element nonlinear analysis of reinforced concrete plates and shells", Civil Engineering Studies, SRC No. 389, University of Illinois, Urbana, Illinois.

55. Hankers, C., (1997), Technical report, Beuth Verlag GmbH, Berlin.

56. Hassan, T., (1999), "Behaviour of concrete bridge decks reinforced with FRP", M.Sc. Thesis, University of Manitoba, Canada, 226 p.

57. Hassan, T., Abdelrahman, A., Tadros, G., and Rizkalla, S., (2000) "FRP reinforcing bars for bridge decks", Canadian Journal for Civil Engineering, Vol. 27, No. 5, pp. 839-849.

58. Hassan, T., Horeczy, G., Svecova, D., Rizkalla, S., Shehata, E., and Stewart, D., (2000) "Flexural strengthening of post-tensioned bridge slab using FRP", Proceedings of the 3rd International Conference on Advanced Composite Materials for Bridges and Structures (ACMBS-III) Ottawa, Ontario, July, 2000.

59. Hassan, T., Mohamedien, M., Hassan, N., and Rizkalla, S., (2001) "Bond performance of different FRP strengthening systems", P.S. Engineering Research Journal, Vol. 5, No.2.

60. Hassan, T., and Rizkalla, S., (2002) "Flexural strengthening of prestressed bridge slabs with FRP systems", PCI Journal, Vol. 47, No. 1, pp. 76-93.

61. Hassan, T., and Rizkalla, S., (2002b) "Investigation of bond in concrete structures strengthened with near surface mounted CFRP strips", Journal of Composites for Construction, ASCE, Accepted for Publication.

62. Hattori, A., Inoue, S., Miyagawa, T., and Fujii, M., (1995) "A study on bond creep behavior of FRP rebars embedded in concrete", Proceedings of the second international RILEM Symposium (FRPRCS-2), L. Taerwe, ed.

63. Hearing, B. and Buyukozturk, O., (2000) "Delamination in reinforced concrete retrofitted with fibre reinforced plastics", Doctoral thesis, MIT, January 2000, 287pp.

64. Hiroyuki, Y. and Wu. Z., (1997) "Analysis of debonding fracture properties of CFS strengthened member subject to tension", Non-metallic (FRP) Reinforcement for Concrete Structures, Proceedings of the Third International Symposium, Sapporo, Japan, pp. 287-294.

65. Holzenkampfer, O. (1994) "Ingenieurmodelle des verbunds geklebter bewehrung fur betonbauteile" Dissertation, TU, Braunschweig.

66. Honma, M., and Maruyama, T., (1989) "Study on bond characteristics of deformed fiber reinforced plastics rod at elevated temperature," Architecture Institute of Japan Convention, Vol. C (Oct.), pp. 443 – 444.

67. Horiguchi, T., and Saeki, N., (1997), "Effect of test methods and quality of concrete on bond strength of CFRP sheet", Proceedings of the Third International Symposium on Non-Metallic FRP Reinforcement for Concrete Structures, Sapporo, Japan, October 1997, Vol 1, pp. 265-270.

68. Hussain, M., Sharif, A., Basunbul, I.A., Balunch, M.H., and Al-Sulaimani, G.J., (1995) "Flexural behavior of precracked reinforced concrete beams strengthened externally by steel plates", ACI Structural Journal, Vol. 92, No. 1, pp. 14-22.

69. ISIS Canada Design Manuals, (2001) "Strengthening reinforced concrete structures with externally-bonded fibre reinforced polymers". Editors: Neale et al.

70. Jaeger L.G., Tadros, G., and Mufti, A.A., (1995) "Balanced section, ductility and deformability in concrete with FRP reinforcement", Research report No. 2, Nova Scotia CAD/ACM Centre, 30 p.

71. James, R.G., (1997) "ANACAP Concrete Analysis Program Theory Manual", Version 2.1, Anatech Corp., San Diego, CA, September 1997.

72. Jansze, W., (1997), "Strengthening of reinforced concrete members in bending by externally bonded steel plates", Ph.D. thesis, Delft University of Technology.

73. Japan Society of Civil Engineers (JSCE), (1997), "Recommendation for design and construction of concrete structures using continuous fiber reinforcing materials," Concrete Engineering Series, No. 23, 325 pp.

74. Joh, O., Wang, Z., and Goto, Y., (1997), "Experimental study on bond cracking performance of FRP reinforced concrete", Proceedings of the Third International Symposium on Non-Metallic FRP Reinforcement for Concrete Structures, Sapporo, Japan, Vol. 2, pp. 431-438.

75. Johnson, R.P., and Tait, C.J., (1981) "The strength in combined bending and tension of concrete beams with externally bonded reinforcing plates", Building Environment, 16(4) pp.287-299.

76. Jones, R., Swamy, R.N., and Charif, A., (1988) "Plate separation and anchorage of reinforced concrete beams strengthened by epoxy-bonded steel plates", Structural Engineering, 66(5), pp.85-94.

77. Kaiser, H.P., (1989), "Strengthening of reinforced concrete with epoxy-bonded carbon fibre plastics", Doctoral Thesis, Switzerland, 224 p.

78. Kanakubo, T., Yonemaru, K., Fukuyama, H., Fujisawa, M., and Sonobe, Y., (1993) "Bond performance of concrete members reinforced with FRP bars", Proceedings of Fibre Reinforced Plastic Reinforcement for Concrete Structures, ACI Special Publication, SP-138, pp. 767-788.

79. Karam, G. N., (1992), "Optimal design for prestressing with FRP sheets in structural members", Advanced Composite Materials in Bridges and Construction, CSCE Conference Proceedings, 277-285.

80. Karbhari, V.M., Engineer, M., and Eckel, D.A., (1997) "On the durability of composite rehabilitation schemes for concrete: Use of a peel test", Journal of Materials Science, 32(1), pp.147-156.

81. Katz, A. (2001) "Bond to concrete of FRP rebars and tendons", Proceedings of the International Workshop, Capri, Italy, pp. 121-129.

82. Kelly, P.L., Brainerd, M.L., and Vatovec, M., (2000) "Design philosophy for structural strengthening with FRP" Concrete International Magazine, Vol. 22, No. 2, pp. 77-82.

83. Klaiber, F.W., Dunker, K.F., Wipf, T.J., and Sanders, W.W. (1987) "Methods of strengthening existing highway bridges" Technical Report, Transportation Research Board, NCHRP Research Report No. 293.

84. Kobotake, Y., Kimura, K., and Katsumata, H., (1993) "A retrofitting method for reinforced concrete structures using carbon fibre", Journal of Composites for Construction, Vol. 2, No. 4, pp.195-203.

85. Kumahara, S., Masuda, Y., and Tanano, Y., (1993) "Tensile strength of continuous fiber rebar under high temperature," Proceeding of Fiber-Reinforced Plastic Reinforcement For Concrete Structures, Eds. Nanni, A., and Dolan C.W. American Concrete Institute, Detroit, pp. 731 – 742.

86. Ladner, M., (1983), "Reinforced concrete members with subsequently bonded steel plates", printed in Strengthening of Building Structures, Iabse Symposium, pp.203-210.

87. Larralde, J., and Silva, R., (1993) "Bond and slip of FRP rebars in concrete", Journal of Materials in Civil Engineering, ASCE, Vol. 5, No. 1.

88. L'Hermite, R.L., and Bresson, J., (1967), "Beton arme par collage des armateures", RILEM International Symposium, Synthetic Resins in Building Construction, Paris, pp.175-203.

89. Leonhardt, F., (1977), "Crack control in concrete structures", IABSE Surveys No. S-477, Zurich, 26 p.

90. Lercehntal, C.H., (1967) "Bonded steel reinforcement for concrete slabs", Materials and Structures, Vol. 37, pp.263-269.

91. Leung, H.Y., Balendran, R.V., and Lim, C.W., (2001) "Flexural capacity of strengthened concrete beam exposed to different environmental conditions", Proceedings of the International Conference on FRP Composites in Civil Engineering, Hong Kong, China, pp. 1597-1606.

92. Lin, C. S., and Scordelis, A., (1975), "Nonlinear analysis of RC shells of general form", ASCE Journal of Structural Engineering, Vol. 101, No. ST3, pp. 523-538.

93. Macdonald, M.D., and Calder, A.J.J., (1982), "Bonded steel plating for strengthening concrete structures", International Journal of Adhesion and Adhesives, pp.119-127.

94. Maeda, T., Asano, Y., Sat, Y., Ueda, T., and Kakuta, Y., (1997), "A study on bond mechanism of carbon fibre sheet", Proceedings of the Third International Symposium on Non-Metallic FRP Reinforcement for Concrete Structures, Sapporo, Japan, October 1997, Vol. 1, pp.279-286.

95. Mahmoud, Z., Rizkalla, S.H., and Zahgloul, E., (1999) "Transfer and development lengths of carbon fibre reinforced polymers prestressing reinforcement", ACI Structural Journal, Vol. 96, No. 4.

96. Malek, A., Saadatmanesh, H., and Ehsani, M., (1998), "Prediction of failure load of R/C beams strengthened with FRP plate due to stress concentration at the plate end", ACI Structural Journal, Vol. 95, No. 1, pp.142-152.

97. Malvar, L.J., (1994) "Bond stress-slip characteristics of FRP rebars" Report TR-2013 SHR, Naval Facilities and Engineering Services, California, USA.

98. Mathey, R.G., and Watstein, D., (1961) "Investigation of bond in beam pull-out specimens with high yield strength deformed bars", ACI Structural Journal, Vol. 57, No. 9, pp.1071-1090.

99. Mattock, A. H., (1979), "Flexural strength of prestressed concrete sections by programmable calculator", PCI Journal, Vol. 24, No.1 pp. 32-54.

100. Matthys, S. et al. (1996) "Influence of transverse thermal expansion of FRP reinforcement on the critical concrete cover," Proceeding of the 2nd International Conference on Advanced Composites Materials for Bridge and Structure, Canadian Society for Civil Engineering, Montreal, pp. 665 – 672.

101. Mays G.C., and Hutchinson, A.R., (1992) "Adhesives in civil engineering" Cambridge University Press.

102. Megally, S. and Ghali, A., (2000) "Punching of concrete slabs due to column moment transfer", Journal of Structural Engineering, Vol., 126, No. 2, pp. 180-189.

103. Meier, U., (1987), "Bridge repair with high performance composite materials", Material und Technik, V. 4 pp. 125-128.

104. Meier, U., and Kaiser, H.P., (1991), "Strengthening of structures with CFRP laminates", Advanced Composite Materials in Civil Engineering Structures", ASCE Specialty Conference, pp.224-232.

105. Meier, U., (1992), "Carbon fibre-reinforced polymers: Modern materials in bridge engineering", Structural Engineering International, Vol. 2, No. 1, pp.7-12.

106. Meier, U., Deuring, M., Meier, H., and Schwegler, G., (1995) "Strengthening of structures with CFRP laminates: Research and applications in Switzerland", Advanced Composite Materials in Bridges and Structures, CSCE, Sherbrooke, Canada, pp.243-251.

107. Mosallam, A., and Dutta, P.K., (2001) "Behavior of epoxy adhesives for repair and rehabilitation of concrete structures under extreme temperature environments", Proceedings of the International Conference on FRP Composites in Civil Engineering, Hong Kong, China, pp. 1559-1568.

108. Mufti, A. A., Erki, M. A., and Jaeger, L. G., (1991), "Advanced composite materials with applications to bridges", State-of-the-Art-Report, Canadian Society of Civil Engineering, CSCE, 350 p.

109. Mufti, A.A., Newhook, J., and Tadros, G. (1996) "Deformability versus ductility in concrete beams with FRP reinforcement" Proceedings of the Advanced Composite Materials in Bridges and Structures, ACMBS-II, pp. 189-199.

110. Mukhopadhyaya, P., Swamy, R.N., and Lynsdale, C.J., (1998) "Durability of adhesive bonded concrete-GFRP joints", Durability of Fibre Reinforced Polymer (FRP) Composites for Construction, CDCC 98, pp.373-380.

111. Mufti, A. A., Hassan, T., Memon, A., and Tadros, G., (2001) "Analytical study of punching shear strength of restrained concrete slabs", Proceedings of the Canadian Society of Civil Engineering (CSCE) Annual Conference, Victoria, British Colombia, CD-Rom.

112. Naaman, A., and Jeong, S., (1995) "Structural ductility of concrete beams prestressed with FRP tendons", Non-metallic (FRP) Reinforcement for Concrete Structures, FRPRCS-2, Belgium, pp. 379-386.

113. Nanni, A., (1995), "Concrete repair with externally bonded FRP reinforcement", Concrete International, Vol. 17 No.6, pp.22-26.

114.   Neubauer, U. and Rostasy, F. S., (1997), "Design aspects of concrete structures strengthened with externally bonded CFRP-plates", Proceedings of the 7th International Conference on Structural Faults and Repairs, pp. 109-118.

115.   Neville, A.M., (1995) "Properties of concrete", John Wiley & Sons, Inc., New York, NY, USA.

116.   Ngo, D. and Scordelis, A. C., (1967) "Finite element analysis of reinforced concrete beams", ACI Structural Journal, Vol. 64, No.3, pp.152-163.

117.   Niedermeier, R., (1996) Report No. 139, Munchen, Germany.

118.   Nordin, H., Taljsten, B., and Carolin, A., (2001) "Concrete beams strengthened with prestressed near surface mounted reinforcement", Proceedings of the International Conference on FRP Composites in Civil Engineering, Hong Kong, China, pp. 1067-1075.

119.   Oehlers, D.J., (1988), "Reinforced concrete beams with steel plates glued to their soffits: Prevention of plate separation induced by flexural peeling", Report No. 80, Department of Civil Engineering, The University of Adelaide, Australia.

120.   Oehlers, D.J., and Moran J.P., (1990) "Premature failure of externally plated reinforced concrete beams", ASCE Structural Journal, Vol. 116, No. 4 pp.978-995.

121.   Oehlers, D.J., Mohamed Ali, M.S., and Luo, W., (1998), "Upgrading continuous reinforced concrete beams by gluing steel plates to their tension faces", Journal of Structural Engineering, ASCE, Vol. 124 No. 3, pp. 224-232.

122.   Ong, K.C.G., and Cuesens, A.R. (1982) "Flexural tests of steel-concrete open sandwiches", Magazine of Concrete Research, V.34, No.120, pp.130-138.

123. Orangun, C.O., Jirsa, J.O., and Breen, J.E., (1977) "A reevaluation of test data on development length and splices", ACI Structural Journal, Vol. 74, No. 3, pp.114-122.

124. Plevris, N., Triantafillou, T.C., and Veneziano, D., (1995) "Reliability of R/C members strengthened with CFRP laminates", ASCE Journal of Structural Engineering, 121(7) pp.1037-1044.

125. Quantrill, R.J., Hollaway, L.C., and Thorne, A.M., (1996), "Experimental and analytical investigation of FRP strengthened beam response: Part I", Magazine of Concrete Research, V.48, No.177, pp.331-342.

126. Quantrill, R. J., Holloway, L. C., Thorne, A. M., and Park, G. A. R., (1995) "Preliminary research on the strengthening of reinforced concrete beams using GFRP" Proc. Of the 2nd Int. Symp., Non-Metallic (FRP) reinforcement for concrete structures London pp. 542-550.

127. Quantrill, R.J., Hollaway, L.C., and Thorne, A.M., (1996), "Predictions of the maximum plate end stresses of FRP strengthened beams: Part II", Magazine of Concrete Research, V.48, No.177, pp.343-351.

128. Rabinovich, O. and Frostig, Y., (2000) "Closed-form high order analysis of RC beams strengthened with FRP strips" ASCE, Journal of composites for construction, Vol. 4 No. 2, pp. 65-74.

129. Rashid, Y. R., (1968) "Analysis of prestressed concrete pressure vessles", Nucl. Eng. Design, Vol. 7, No. 4, pp.334-344.

130. Raithby, K.D., (1980) "External strengthening of concrete bridges with bonded steel plates" Transport and Road research Laboratory, Crowthorne, SR612.

131.   Ritchie, P.A., Thomas, D.A., Lu, L., and Connelly, G.M., (1991), "External reinforcement of concrete beams using fibre reinforced plastics", ACI Structural Journal, V.88, No.4, July-Aug., pp. 490-500.

132.   Rizkalla, S., and Hassan T., (2002) "Effectiveness of FRP techniques for strengthening concrete bridges", Journal of the International Association for Bridge and Structural Engineering, IABSE, Vol. 12, No.2, SEI. 2 (May 2002).

133.   Roberts, T.M., (1988), "Plate separation and anchorage of reinforced concrete beams strengthened by epoxy-bonded steel plate", The Structural Engineer, V.67, No.12, pp.187-188.

134.   Roberts, T.M., and Haji-Kazemi, H., (1989) "Strengthening of under-reinforced concrete beams with mechanically attached steel plates", The International Journal of Cement Composites and Light weight Concrete, Vol. 11, No. 1, pp. 21-27.

135.   Rostasy, F., Hankers, C., and Ranisch, E., (1992), "Strengthening of R/C and P/C structures with bonded FRP plates", Advanced Composite Materials in Bridges and Structures, Canadian Society for Civil Engineers, pp.253-263.

136.   Rubinsky, I.A., and Rubinsky, A., (1954), "An investigation into the use of fibre-glass for prestressed concrete", Magazine of Concrete Research, V.6.

137.   Rutz, J., (1995) Kantons St. Gallen.

138.   Saadatmanseh , E., and Ehsani, M. R., (1989), "Application of fibre-composites in civil engineering", Proceedings of the 7th ASCE Structures Congress, pp. 526-535.

139.   Saadatmanesh, H., and Ehsani, M.R., (1990) "Fibre composite plates can strengthen beams", Concrete International V.12, No. 3, pp.65-71.

140. Saadatmanesh, H., and Ehsani, M.R., (1991), "RC beams strengthened with GFRP plates, I: Experimental Study", Journal of Structural Engineering, ASCE, V.117, No.11, pp.3417-3433.

141. Scordelis, C. A., (1985) "Past, Present and Future Development", Seminar on Finite Element Analysis of Reinforced Concrete Structures, Japan Concrete Institute, V.1, pp.203-212.

142. Shahawy, M., and Beitelman, T. E. 1998 "Fatigue performance of RC beams strengthened with CFRP laminates," Durability of Fiber Reinforced Polymer (FRP) Composites For Construction, CDCC98, Sherbrooke, Canada, pp. 169 – 173.

143. Sharif, A., Al-Sulaimani, G. J., Basunbul, I. A., Baluch, M.H., and Ghaleb, B.N., (1994), "Strengthening of initially loaded reinforced concrete beams using FRP plates", ACI Structural Journal, 91 (2) pp.160-168.

144. Sharif, A., Al-Sulaimani, G.J., Basunbul, I.A., Balucn, M.H., and Husain, M., (1995), "Strengthening of shear-damaged RC beams by external bonding of steel plates", Magazine of Concrete Research, V.47, No.173, pp.329-334.

145. Swamy, R.N., Jones, R., and Bloxham, J.W., (1987), "Structural behaviour of reinforced concrete beams strengthened by epoxy-bonded steel plates", The Structural Engineer, V.65A, No.2, pp.59-68.

146. Swamy, R.N., Jones, R.., and Charif, A., (1989), "The effect of external plate reinforcement on the strengthening of structurally damaged RC beams", The Structural Engineer, V.67, No.3, pp.45-56.

147.   Taljsten, B., (1994) "Strengthening of existing concrete structures with externally bonded steel or fibre reinforced plastics", Doctoral Thesis, Lule, University of Technology.

148.   Taljsten, B., (1996) "Strengthening of concrete prisms using the plate bonding technique", International Journal of Fracture Mechanics, V.82 pp.253-266.

149.   Taljsten, B., (1997) "Defining anchor lengths of steel and CFRP plates bonded to concrete", International Journal of Adhesion and Adhesives, Vol. 17, No. 4, PP. 319-327.

150.   Tanaka, T. (1997) "Shear resisting mechanism of reinforced concrete beams with CFS as shear reinforcement" Graduation Thesis, Hokkaido University.

151.   Tann, D. B. and Delpark, R., (1999), "Experimental investigation of concrete beams reinforced with narrow carbon strips", Proc. Int. Conf. Structural Faults & Repair-99. CD-Rom.

152.   Teng, J.G., Chen, J.F., Smith, S.T., and Lam, L., (2002) "FRP strengthened RC structures", John Wiley & Sons Ltd, England.

153.   Tepfers, R., (1998) " Bond of FRP reinforcement in concrete: A state-of-the-art in preparation", Bond and Development of Reinforcement, ACI SP180-22, pp.493-508.

154.   Toutanji, H., and Ortiz, G., (1997) "Durability characteristics of concrete columns wrapped with FRP plates", Proceedings of the International Conference on Rehabilitation and Development of Civil Engineering Infrastructure Systems, Vol. 2, Beirut, Lebanon, pp.25-29.

155.   Tysl, S.R., Imrogno, M., and Miller, B.D., (1998) "Effect of surface delamination on the freeze-thaw durability of CFRP-reinforced concrete beams", Durability of Fibre Reinforced Polymer (FRP) Composites for Construction, Quebec, pp.317-324.

156. U.S. Department of Transportation (DOT), (1997), "Bureau of Transportation Statistics", Transportation Statistics Annual Report.

157. Van Gemert, D.A. (1980), "Force transfer in epoxy bonded steel-concrete joints", International Journal of Adhesion and Adhesive, No. 2, pp.67-72.

158. Van Gemert, D.A., (1981) "Repairing of concrete structures by externally bonded steel plates", Proc. of the Int. Symm. for Plastics in Materials and Structural Engineering, Czechoslovakia, pp.519-526.

159. Van Gemert, D., and VandenBosch, M., (1985), "Repair and strengthening of reinforced concrete structures by means of epoxy bonded steel plates", International Conference on Deterioration, Bahrain, pp. 181-192.

160. Van Gemert, D., (1990) "The plate bonding technique for solving concrete deterioration", International Seminar on structural repairs/strengthening by the plate bonding technique, Sheffield, England.

161. Wang, Z., Goto, Y., and Joh, O., (1999) "Bond strength of various types of fiber reinforced plastic rods", Proceedings of the fourth International Symposium on Fibre Reinforced Polymer Reinforcement for Concrete Structures, Dolan et al. Eds, ACI SP-188, pp. 1117-1130.

162. Wines, J.C., et al., (1996), "Laboratory investigation of plastic-glass fibre reinforcement for reinforced and prestressed concrete", United States Army Corps. Of Engineers, WES, V.1&2, Vicksburg, MS, 228.

163. Wu, Z., Matsuzaki, T., and Tanabe, K., (1997) "Interface crack propagation in FRP-strengthened concrete structures", Non-metallic FRP Reinforcement for Concrete Structures, Vol. 1, pp.319-326.

164.   Wu, Z., and Niu, H., (2000) "Study on debonding failure load of RC beams strengthened with FRP sheets", Journal of Structural Engineering, V.46A, pp.1431-1441.

165.   Yaun, H., Wu, Z.S., and Yoshizawa, H., (2001) "Theoretical solutions on interfacial stress transfer of externally bonded steel/composites laminates", Journal of Structural Mechanics and Earthquake Engineering, JSCE, No. 675/1-55, pp. 27-39.

166.   Yoshizawa, H., Myojo, T., Okoshi, M., Mizukoshi, M., and Kilger, H.S., (1996), "Effect of sheet bonding condition on concrete members having externally bonded carbon fibre sheet", Proceedings of the 4th Materials Engineering Conference, ASCE Annual Convention, Washington D.C.

167.   Zienkiewicz, O. C., (1967), "The finite element method in engineering science", Mcgraw-Hill.

168.   Ziraba, Y. N., Baluch, M. H., Basunbal, I. A., Sharif, A. M., and Al-Sulaimani, G. H., (1994) "Guidelines toward the design of reinforced concrete beams with external plates", ACI Structural Journal, Vol. 91, No. 6, pp. 639-646.